AFWAL-TR-82-4172

AD A 1 29817

ADHESIVE LAYER THICKNESS AND POROSITY CRITERIA FOR BONDED JOINTS

L. J. Hart-Smith, Ph.D.

Douglas Aircraft Company
McDonnell Douglas Corporation
Long Beach, California 90846

December 1982

Final Report for Period August 1980 — September 1982

MATERIALS LABORATORY
AIR FORCE WRIGHT AERONAUTICAL LABORATORIES
AIR FORCE SYSTEMS COMMAND
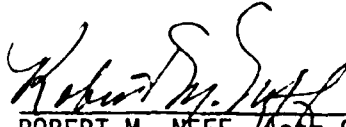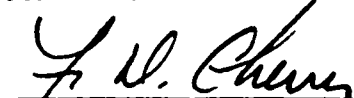WRIGHT-PATTERSON AIR FORCE BASE, OHIO 45433

DTIC
ELECTE
JUN 2 7 1983

E

83

HERBERT S. SCHWARTZ, Matls Rsch Engr
Composites, Adhesives & Fibrs Matls Br
Nonmetallic Materials Division

ROBERT M. NEFF, Actg Chief
Composites, Adhesives & Fibrs Matls Br
Nonmetallic Materials Division

FOR THE COMMANDER

FRANKLIN D. CHERRY, Chief
Nonmetallic Materials Division

SECURITY CLASSIFICATION OF THIS PAGE *(When Data Entered)*

REPORT DOCUMENTATION PAGE		READ INSTRUCTIONS BEFORE COMPLETING FORM
1 REPORT NUMBER AFWAL-TR-82-4172	2. GOVT ACCESSION NO.	3. RECIPIENT'S CATALOG NUMBER
4 TITLE *(and Subtitle)* Adhesive Layer Thickness and Porosity Criteria for Bonded Joints		5. TYPE OF REPORT & PERIOD COVERED Final Report August 1980 - September 1982
		6. PERFORMING ORG. REPORT NUMBER
7 AUTHOR*(s)* L. J. Hart-Smith, Ph.D.		8. CONTRACT OR GRANT NUMBER*(s)* F33615-80-C-5092
9 PERFORMING ORGANIZATION NAME AND ADDRESS Douglas Aircraft Company McDonnell Douglas Corporation Long Beach, California 90846		10. PROGRAM ELEMENT, PROJECT, TASK AREA & WORK UNIT NUMBERS P.E. 62102F Project 2419 02 14
11 CONTROLLING OFFICE NAME AND ADDRESS Materials Laboratory (AFWAL/MLBC) AF Wright Aeronautical Laboratories Wright-Patterson AFB, Ohio 45433		12. REPORT DATE December 1982
		13. NUMBER OF PAGES 161
14 MONITORING AGENCY NAME & ADDRESS*(if different from Controlling Office)*		15. SECURITY CLASS. *(of this report)* Unclassifed
		15a. DECLASSIFICATION/DOWNGRADING SCHEDULE

16 DISTRIBUTION STATEMENT *(of this Report)*

Approved for public release; distribution unlimited.

17 DISTRIBUTION STATEMENT *(of the abstract entered in Block 20, if different from Report)*

18 SUPPLEMENTARY NOTES

19. KEY WORDS *(Continue on reverse side if necessary and identify by block number)*

Adhesive Bonded Joints   Repairs
Porosity   Peel Stresses
Flaws
Variable-Thickness Bonds

20 ABSTRACT *(Continue on reverse side if necessary and identify by block number)*

This investigation is concerned with two aspects of the effects of imperfections in adhesive bonds. These imperfections are nonuniform thickness and porosity (or, in the extreme case, flaws). Both cause redistribution of the load transfer with rrespect to that for nominally perfect bonds. A thorough treatment of induced peel stresses in structural joints and test coupons is included because the growth of bond flaws is known to be associated more with peel stresses than shear stresses in the adhesive. The report covers both the

DD $_{1 \text{ JAN } 73}^{\text{FORM}}$ 1473   EDITION OF 1 NOV 65 IS OBSOLETE

ductile adhesives most suitable for subsonic transport aircraft and the brittle adhesives needed for supersonic military aircraft. The first major section of the report discusses the effects of adhesive layer thickness variation, with particular emphasis on the ends of bonded overlaps where peak load transfer inevitably occurs. The second major topic is that of flaws and porosity; and it is shown that adhesive bonded joints are far more tolerant of such naturally occurring imperfections than is generally recognized. The final subject is that of peel stresses induced in the adhesive layer due to eccentricities in load path. While it is known that such peel stresses can be very detrimental to the life of bonded joints, it is shown here that it is often quite simple to eliminate them from structurally proportioned joints.

Accession For	
NTIS GRA&I	☒
DTIC TAB	☐
Unannounced	☐
Justification	
By	
Distribution/	
Availability Codes	
Dist	Avail and/or Special
A	

SUMMARY

This report covers two primary aspects of the effects of imperfections in adhesive-bonded joints. These are the effects of nonuniform thickness and of porosity and flaws. In each case, the consequences are a redistribution in the load transfer with respect to nominally perfect bonds. Because the growth of bond flaws is known to be associated more with peel stresses than with shear stresses in the adhesive, a thorough treatment of induced peel stresses in structural joints and test coupons is included. The report is divided into three major sections.

The first section covers two related topics: (1) the loss of adhesive-bonded joint strength due to pinch-off at the ends of the overlap and to squeeze-out during cure, and (2) deliberate thickening of the adhesive layer locally to nullify the pinch-off effect or even to increase the joint strength above the strength that can be obtained with uniform adhesive layers. The unacceptable level of adhesive pinch-off is easily established as the point at which the adhesive becomes weaker than the adherends. However, the problem is quite complex, and there are several factors which decrease the amount of acceptable pinch-off. These include the stress concentrations induced in the adherends outside the joint area by the pinch-off in the adhesive and the greatly increased cost of inspecting and justifying the acceptance of a marginal bonded joint after it has been manufactured. Two simple procedures for elimination of the pinch-off problem are discussed. These are: (1) thickening the adhesive locally up to 0.020 inch, and (2) tapering the splice plates over the outermost 0.25 to 0.50 inch down to a thickness of 0.030 ± 0.010 inch. These techniques, used alone or in conjunction, restrict the need for the more complex stepped-lap joints to greater adherend thicknesses. No such modifications are needed for lightly loaded minimum gage secondary structure. The pinch-off problem involves consideration of induced adhesive peel stresses as well as of the applied shear stresses. In fact, the modifications made to alleviate the pinch-off problem are vital for thicker adherends if the joint strength is not to be degraded by premature peel-stress failures. Specific calculations are provided for aluminum adherends and both ductile and brittle adhesives. In addition to explaining the various factors involved, acceptance criteria for the pinch-off problem are established.

The second section addresses the effects of adhesive porosity as a particular case of flaws and disbonds in structural bonded joints. Thin structures are shown to have a remarkable tolerance for quite large bond imperfections. The complex joints associated with the bonding of thicker structures, however, exhibit a sensitivity to both large voids and porosity. Flaws in thin bonded structures can usually be ignored or, at most, just be sealed at the edges to prevent corrosion. Simple analysis methods and acceptance criteria are provided for flaws and porosity in thin bonded structures. Flaws of any kind in thick bonded structures could propagate catastrophically, so mechanical fasteners are needed as a fail-safe load path. Because porosity is usually confined to thickened adhesive layers away from the overlap edges (where the great majority of the load is transferred), porous bonds are thicker and softer than adjacent flawless bonds rather than weaker. Thus a porous bond area is more likely to overload adjacent flawless bond areas than to fail itself.

The third section addresses the peel stresses induced by primary and secondary eccentricities in the load paths in adhesive-bonded joints and test coupons. The primary applied loads cause a shear load transfer through the adhesive. Three specific joint configurations are analyzed: single-lap joints with moderate induced peel stresses, single-strap (flush) joints with severe induced peel stresses, and double-lap joints with the least peel stresses. Examples are presented to show how an adequate overlap (for the first two classes of joints) can reduce peel stresses to below the intensity at which they would otherwise cause a premature failure. Furthermore, de-

tailed modifications at the ends of the overlap are shown to be capable of reducing the peel stresses to a level of insignificance, at least for structurally preportioned joints. An analysis is included for the peel stress distribution between skins and stiffeners, as between fuselage skins and frame outer tees. Comparative tests have been run between single-strap (flush) joints with square-cut ends and with tapered ends to thicken the glue layer locally. This modification increased the fatigue life substantially.

FOREWORD

CONTENTS

SECTION 1

INTRODUCTION

Assessing the implications of the various imperfections that occur in adhesive bonds has been more of an art than a science. During the Primary Adhesively Bonded Structure Technology (PABST) program, U.S. Air Force Contract No. F33615-75-C-3016, considerable progress was made in improving this situation, both in the basic program (References 1 to 4) and in some of the associated contracts. A very clear conclusion was reached: it is exceedingly difficult to make flaws in bonded joints grow if the structure tested bears a close resemblance to well-designed aircraft structural details. The controlled growth of flaws in test coupons required the use of artificial and obviously impractical configurations (see for example the thick square-cut plate specimens in Reference 5), which even those with a modest understanding of the load transfer in bonded joints would not be tempted to use on real structures.

It is clear that adhesively bonded structure exhibits considerable tolerance to bond flaws, porosity, and even highly variable thicknesses of the adhesive layer. The objectives of this investigation are twofold. First, for obvious safety reasons, one needs to establish an upper bound on the application of adhesively bonded structure to prevent its misapplication in circumstances in which there is no tolerance to even the slightest bond imperfection. Second, and more importantly, within the regime of practical application of adhesive bonding, one should establish realistic accept/reject criteria for the various bond imperfections such as porosity and variable thickness. The prevailing criteria, which at first seem to be overly conservative, are actually detrimental because they mandate the unnecessary repair of structurally adequate bonded structure which repair, in turn, decreases the safe life of such structure by breaking the surface protection (anodized or etched) against the environment.

In retrospect, it is fortuitous that the PABST full-scale demonstration component (FSDC) (Reference 6) — a 42-foot-long forward fuselage section 216 inches in diameter — was not of a higher quality than it was. There were innumerable small bond flaws that were correctly judged to be harmless and a few flaws of sufficient size that it was deemed prudent to monitor them closely during test. Some such flaws that were left unrepaired were so large that, on a production aircraft, they would have been repaired without question. They were deliberately left unrepaired to learn as much as possible about the effects of such flaws. The test record was a sound endorsement for adhesively bonded structure — the adhesively bonded fuselage structure outperformed conventional riveted structure both in the tremendous reduction in the incidence of fatigue cracks in the metal (see Figure 1) and in the benign failure mode from deliberately induced skin cracks (compare Figures 2 and 3). Very few of the bond flaws grew at all, and no such growth ever imposed a structural problem. Ironically, had the correct manufacturing method been agreed to earlier, it is possible that the quality of the FSDC would have been so good that the remarkable tolerance to bond flaws might never have been demonstrated.

A similar tolerance to flaws was demonstrated by the slow-cycle testing of flawed coupons. A word of explanation about the "slow" cycle is appropriate here. Adhesives are significantly viscoelastic, and their responses to the various loads to which they are subjected are influenced by the duration of the load cycles. This was demonstrated most convincingly at the start of the PABST program by the testing of short-overlap thick-adherend test coupons. When tested at the high frequencies typical of metal fatigue tests (30 cycles per second), the test coupons would show no indication of the slightest damage at 10^7 cycles. Yet the very same specimens, when tested more slowly (one or two cycles per hour) to approximate the real-time service exposure in a pressurized fuselage, would fail after the application of only a few hundred load cycles of the same intensity. The reason for this vast difference is that, during the high-frequency testing, the load was being removed again so rapidly that there was no time for any creep to occur and accumulate. This phenomenon applies equally to flawed and unflawed adhesive bonds. It is fair to

2

110 X 168 IN. CURVED PRESSURE PANEL
TEST RESULTS
METAL AND FASTENER OR BOND FAILURES

PRESSURIZATION CYCLES
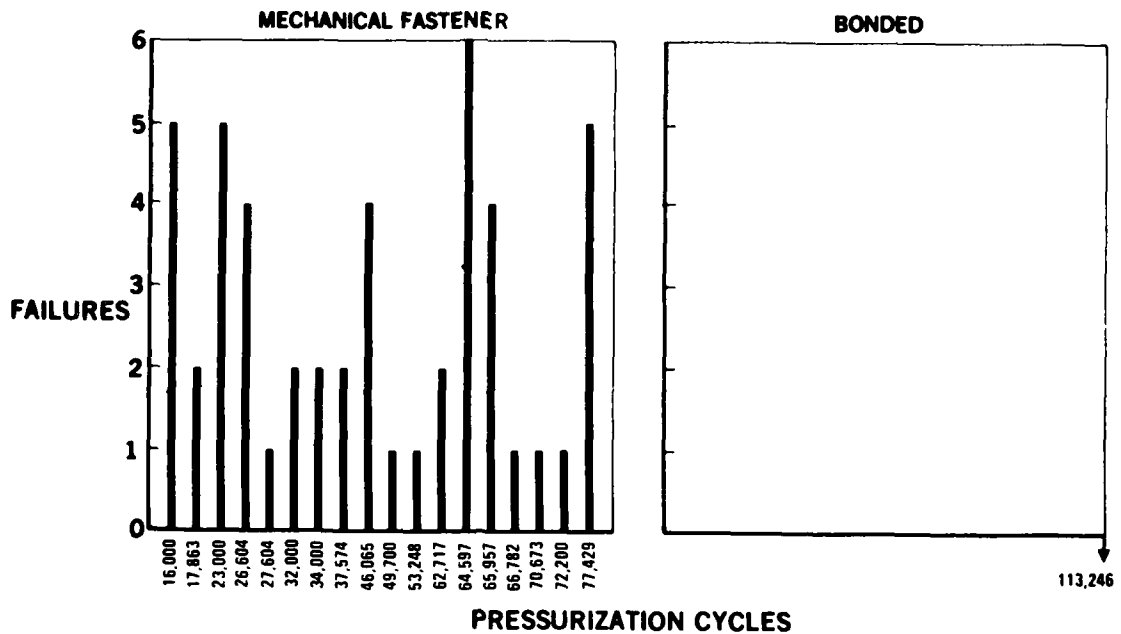
FULL-SCALE FUSELAGE TEST RESULTS
METAL AND FASTENER OR BOND FAILURES
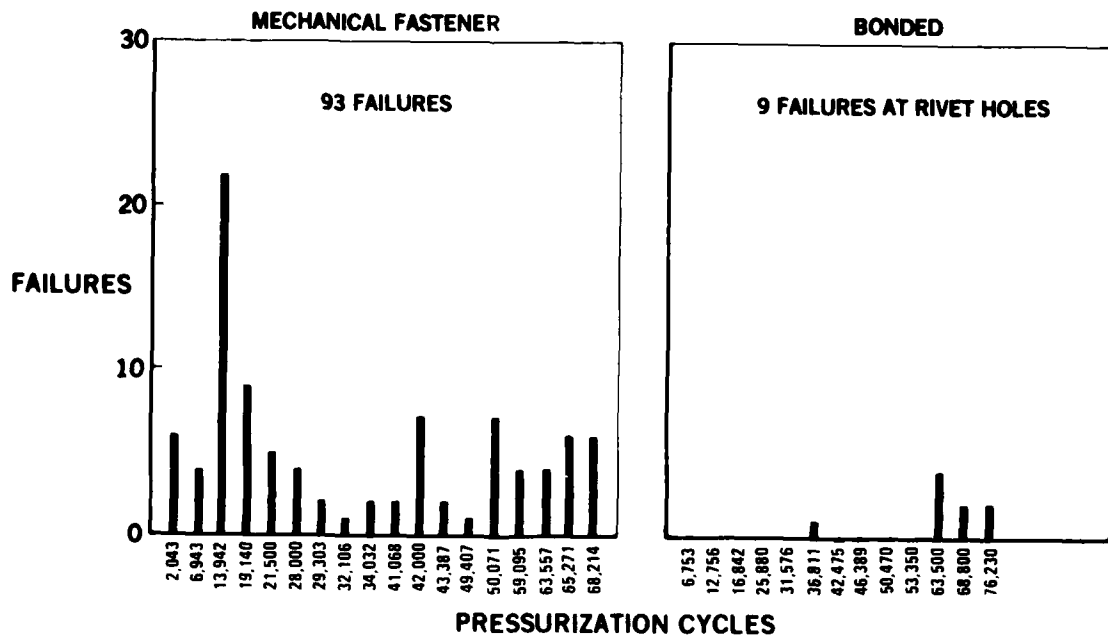

PRESSURIZATION CYCLES

FIGURE 1. COMPARISON BETWEEN FATIGUE TESTING OF MECHANICALLY FASTENED AND
ADHESIVELY BONDED STRUCTURES

3

FIGURE 2. RIVETED, CURVED PANEL CRACK PROPAGATION. CRACK GREW OVER FRAMES
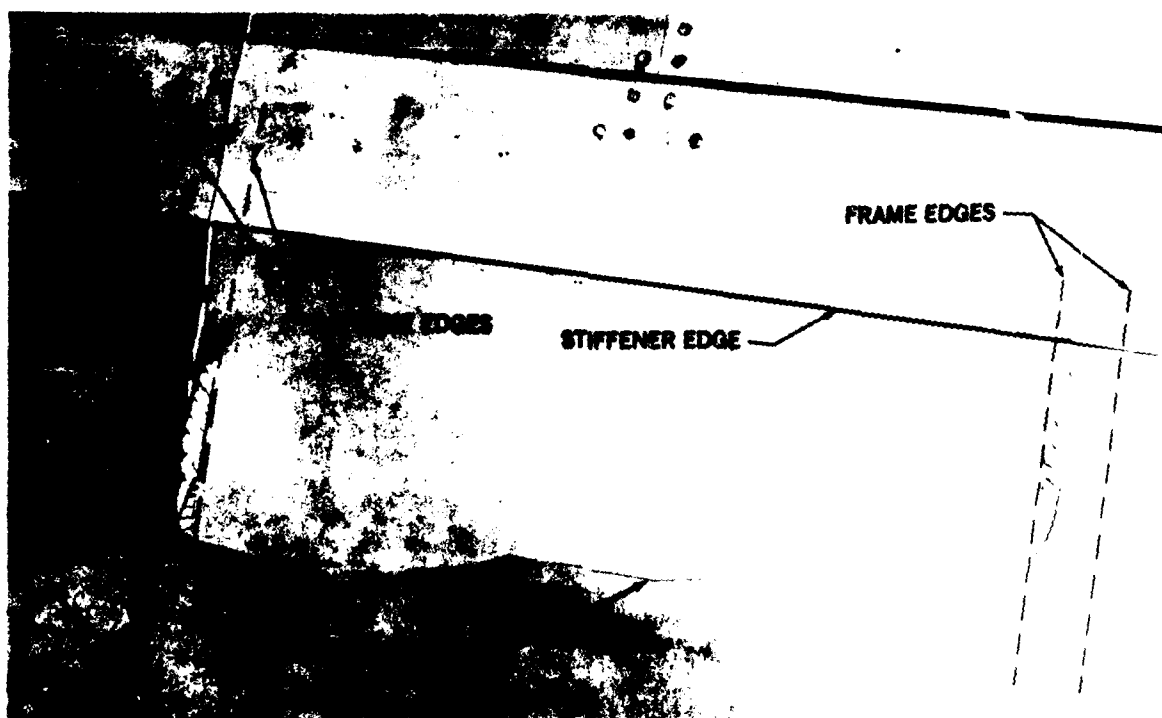

FIGURE 3. BONDED, CURVED PANEL CRACK PROPAGATION. CRACK TURNED AT FRAME AND STIFFENER EDGE

4

state that the testing conducted on the PABST program makes it clear that high-frequency fatigue testing of adhesive bonds is misleading and a waste of time and effort. The considerable time and expense of performing such tests properly, with slow-cycle testing, must be borne if meaningful results are to be obtained.

The effects of defects program of PABST bears directly on the objectives of this investigation. Even with deliberate flaws, the environmentally resistant adhesive/primer/surface preparation combinations resulted in far more metal-fatigue failures than the solitary flawed-adhesive failure.

This demonstrated insensitivity to bond flaws for structurally configured joints is a strong contrast to the behavior of some of the thick-adherend test coupons, which sometimes did not even require flaws to initiate failure of the adhesive in an unacceptably low number of cycles to failure. The technical discussions in this report offer a plausible explanation of this dichotomy.

A significant highlight of the testing performed under PABST and related contracts is that, even with artificial joint geometries to preclude premature fatigue failures in the metal rather than the adhesive, it was impossible to initiate or grow cracks in adhesive bonds under shear loads alone. A significant peel stress was a prerequisite to the fatigue of the adhesive bond itself (Reference 7). This report shows how those peel stresses can be eliminated by design relatively easily in most instances; when they cannot, one should use mechanical fasteners instead of bonding. The only occurrence of adhesive peel stresses as a problem during the PABST testing was in a panel to represent a flush (single-strap) circumferential bond splice. The adhesive disbonded throughout a small band of very high peel stresses immediately adjacent to the seam where the skin panels butted together. Yet, even so, the failure in the adhesive stabilized, and the panel ripped apart from a small fatigue crack in the splice plate that had been induced by the same eccentricity in the load path that had partially parted the adhesive. Even then, the adhesive was still stronger than the pieces bonded together.

The above outline highlights some of the prior effort pertaining to the subject of this investigation, which builds directly on the work reported in Reference 7. It is significant that, in the service record of adhesively bonded structures, it has been the inadequate surface preparation or the use of environmentally sensitive adhesives without corrosion-inhibiting primers that has led to problems, not the incidence of various flaws in the bonds. It should be noted at this point that the accept/reject criteria established by this investigation refer specifically to the mechanical damage of environmentally resistant systems. The criteria are not directly applicable to service problems involving disbonding due to environmental attack, associated with the problems identified just above. Because the growth of such disbonds has no threshold size and is essentially independent of the load history, the best that can be achieved in that context is the identification of the extent of disbonding that could be tolerated before a complete rebuild of the part (with new adhesive bonding systems) to prevent a static failure.

This brief outline of the prior knowledge on the subject of the effects of imperfections in adhesive bonds indicates that adhesive bonded structures are far more tolerant of flaws than is generally recognized. However, much of that information is of an empirical nature rather than scientifically based. The purpose of this investigation is to examine these issues from a largely theoretical viewpoint, to be able to access the issues parametrically and establish the tolerable levels of imperfections and identify those imperfections which are unacceptable. Because of the known association of delamination growth with peel stresses in the adhesive, analyses have also been performed for the induced peel stresses in both structural joints and coupons used to test adhesive shear properties.

This report is divided into three major sections which, while they rely on common theory, discuss separate aspects of this investigation and are largely self contained. These topics are: (1) the effects of adhesive layer edge thickness on the strength of adhesive-bonded joints, (2) the effects of flaws and porosity on the strength of adhesive-bc 'ed joints, and (3) the induced peel stresses in a variety of structurally different adhesive-bor ued joints. These three sections are essentially updates of three of the quarterly reports published during the course of this investigation — MDC-J4675, MDC-J4699, and MDC-J9422A, respectively.

REFERENCES

1. Thrall, E. W., Jr., et al, Primary Adhesively Bonded Structure Technology, Phase Ib: Preliminary Design Report (Douglas Aircraft Company Report MDC-J6070), Air Force Flight Dynamics Laboratory Technical Report No. AFFDL-TR-76-141, December 1976.

2. Thrall, E. W., Jr., et al, Primary Adhesively Bonded Structure Technology, Phase II: Detail Design Report (Douglas Aircraft Company Report MDC-J6073), Air Force Flight Dynamics Laboratory Technical Report No. AFFDL-TR-77-135, August 1977.

3. Thrall, E. W., Jr., et al, Primary Adhesively Bonded Structure Technology: Design Handbook for Adhesive Bonding (Douglas Aircraft Company Report MDC-J6076), Air Force Flight Dynamics Laboratory Technical Report No. AFFDL-TR-79-3129, November 1979.

4. Shannon, R. W., et al, Primary Adhesively Bonded Structure Technology: General Material Property Data (Douglas Aircraft Company Reports MDC-J6065 and MDC-J6065A), Air Force Flight Dynamics Laboratory Technical Report No. AFFDL-TR-77-107, Vol. I, September 1978 and Vol. II, August 1982.

5. Brussat, T. R., Chiu, S. T., and Mostovoy, S., Fracture Mechanics for Structural Adhesive Bonds, USAF Technical Report AFML-TR-77-163, October 1977.

6. Potter, D. L., et al, Primary Adhesively Bonded Structure Technology: Full-Scale Test Report (Douglas Aircraft Company Report MDC-J6077), Air Force Flight Dynamics Laboratory Technical Report No. AFWAL-TR-80-3112, November 1980.

7. Clark, H. T., Definition and Non-Destructive Detection of Critical Adhesive Bond-Line Flaws (McDonnell Aircraft Company), USAF Technical Report AFML-TR-78-108, July 1978.

SECTION 2

EFFECTS OF ADHESIVE LAYER EDGE THICKNESS
ON STRENGTH OF ADHESIVE-BONDED JOINTS

CONTENTS

INTRODUCTION

All of the classical analyses of adhesive-bonded joints modeled the adhesive as being of uniform thickness and properties throughout (References 1 to 3). Yet experience has shown that this is usually not the case. The exposed fillet of adhesive is either moistening or drying out with respect to the interior. Most porosity and voids occur in the interior of the overlap, where it is harder for air and volatiles to escape. Further, the adhesive is often thinnest at the edges because it is easiest for the adhesive to be squeezed out or flow away from there. This last variation in adhesive-bonded joints forms the basis of this report. The report explains how pinch-off occurs and how it can be prevented; explains and quantifies the strength losses associated with the pinch-off; establishes criteria for acceptable pinch-off when the bond remains stronger than the adherends; and explains how the adhesive can be slightly thickened at the ends of the overlap to enhance the bonded-joint strength.

The basic elastic-plastic adhesive analysis for bonded joints with variable adhesive properties was developed during the Primary Adhesively Bonded Structures Technology (PABST) program and has since been improved (Reference 4). A computerized analysis of the insensitivity of the PABST bonded splices to quite large bond flaws is presented in Reference 5, based on the analysis program A4EI. These two references contain all the derivatives of the load transfer in the specific adhesive-bonded joints examined in this report. An explanation of the governing phenomena, which are examined here comprehensively for the first time, is also presented.

9

ADHESIVE SHEAR STRESSES AND STRAIN DISTRIBUTIONS IN BONDED JOINTS

The various analyses of adhesively bonded joints typically show sharp peaks in the adhesive shear stresses at one or both ends of the overlap which surround a lightly loaded elastic trough, as shown in Figure 1. The severity of the peaks depends on the properties of both the adherend and the adhesive. The effect of the adhesive properties is more pronounced, with the softer, more ductile adhesives used for subsonic aircraft structure having less of a stress concentration for a given load than the brittle adhesives used for the high-temperature applications associated with supersonic flight or engine cowlings. This difference is also shown in Figure 1.

Figure 2 compares the typical adhesive shear stress-strain curves for ductile and brittle adhesives at room temperature. Figure 3 shows how these characteristics vary with temperature for ductile adhesives. While the elevated-temperature condition is usually found to be most severe for ductile adhesives, the subzero environment is usually most severe for brittle adhesives because they become more ductile at higher temperatures. A closed-form solution shows that the strength of structural bonded joints is defined uniquely by the adhesive strain energy in shear, not by any of the individual properties like the failure stress alone (Reference 3). That is why it can be deduced from Figure 3 that the joint strength of a real structural joint will not be sensitive to the environment unless the joint is improperly proportioned so that the failure mode changes with environment. There might also be a change in joint strength of brittle adhesives at subzero temperatures because of a change in failure mode of the adhesive from shear to peel. This should be avoided by careful design, as discussed below, since it is always associated with a loss of joint strength and life with respect to shear-dominated behavior.
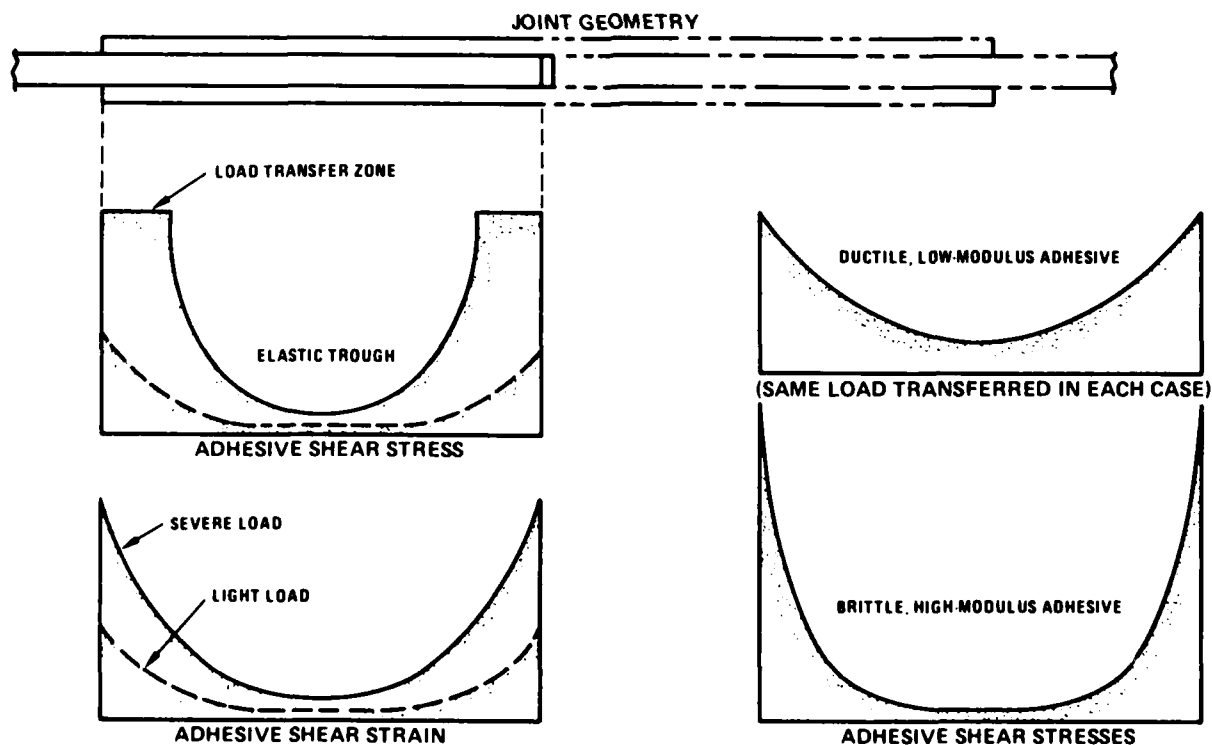
FIGURE 1. NONUNIFORM ADHESIVE SHEAR STRESSES AND STRAINS IN BONDED JOINTS

10
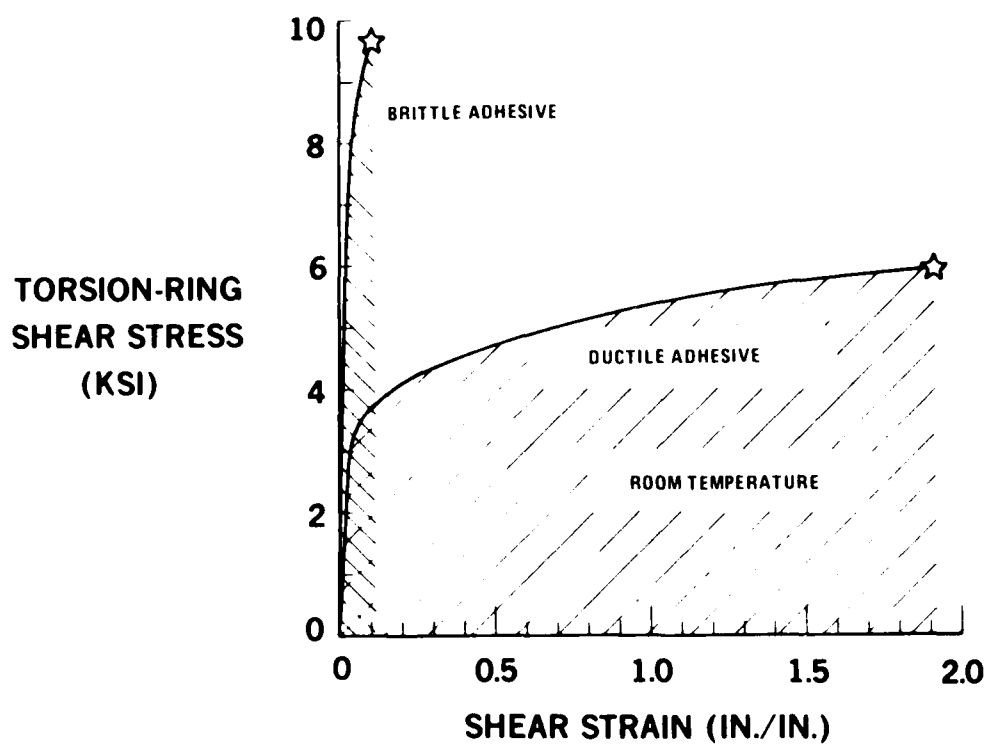
FIGURE 2. ADHESIVE STRESS-STRAIN CURVES IN SHEAR
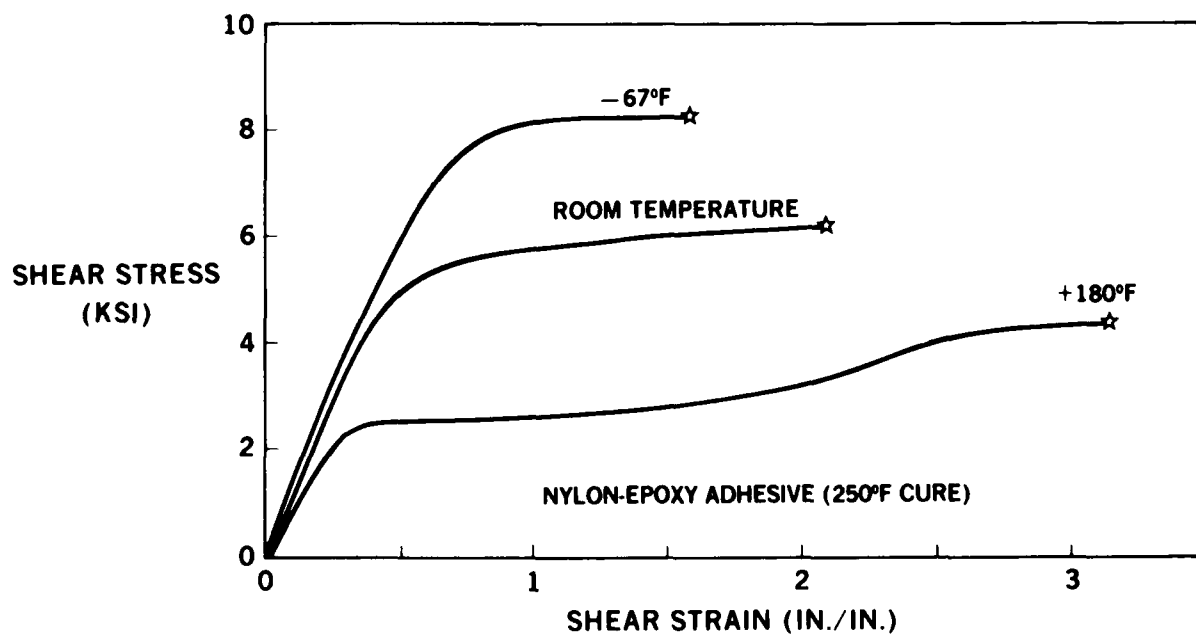
FIGURE 3. EFFECT OF TEMPERATURE ON ADHESIVE STRESS-STRAIN CURVES IN SHEAR

11

Since the critical conditions in adhesive bonds develop at the ends of the overlap, some more refined analyses have been derived that account for variation in stress across the thickness of the adhesive layer. Specifically, this has been done for elastic behavior to satisfy the condition of zero stress on the exposed edges of the adhesive, as shown in Figure 4. It appears that because of the mathematical complexities, this refinement has not yet been combined with analyses accounting for nonlinear adhesive behavior. However, the improvement in accuracy associated with the refined analysis becomes less significant as the adhesive is loaded beyond the knee in the stress-strain curve, since the peak stress immediately inboard of the edge of the overlap is then defined independently of the precise load level. Even the peak adhesive shear strain is defined. It follows from the width of the plastic zones which must balance the applied load. More importantly, the distinction between the refined and basic elastic analyses is defined only for the artificially square cut (fillet-less) adhesive test coupons shown in Figure 4. It is probable that the fillet that forms on structural adhesive-bonded joints actually makes the approximate solution the more accurate because the stress-free surface is moved outboard, as shown in Figure 4. Test coupons often, but not always, have square-cut ends on the adhesive to ensure a lower bound result and to avoid the ambiguity that accompanies different fillet sizes. But in all cases, the presence of the fillet is beneficial since it provides an area of reduced stress and strain beyond the peak values at the end of the overlap. As mentioned in Reference 6, the presence of a good fillet, with evidence of wetting the surface and adhesive flow, is the most important indication of a quality bond. It is also best from the structural viewpoint. One should not try to rework or eliminate this fillet to save weight.

It can be seen from the above discussion that the most critical location within an adhesive-bonded joint is at the ends of the overlap.
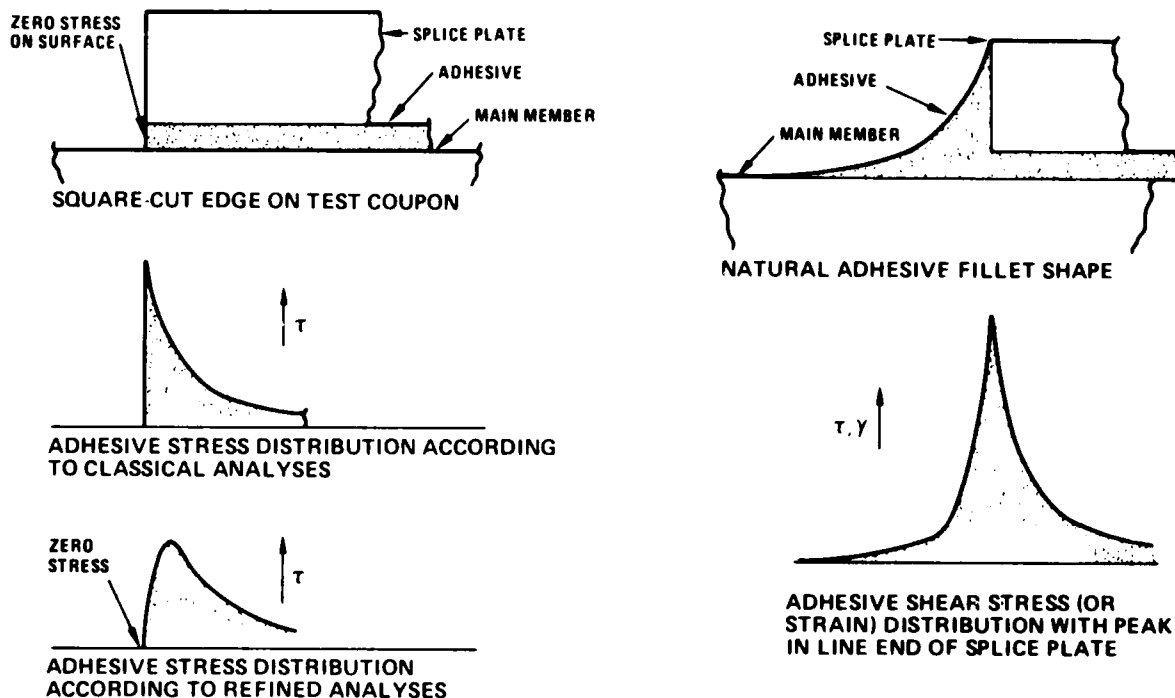
FIGURE 4. ADHESIVE STRESSES AT ENDS OF OVERLAPS

EFFECT OF BONDED OVERLAP AND ADHEREND THICKNESS ON JOINT STRENGTH

The strength of adhesive-bonded joints is influenced not only by the adhesive properties, but also by the adherend properties. A systematic survey of these effects is presented in Figures 6 to 8 of Section 3. The basic influence of the adherend geometry on joint strength can be characterized approximately by two straight lines, as shown in Figure 5. For short overlaps, the bond strength is proportional to the bond area (and hence the overlap) while for long overlaps, the joint strength is constant regardless of the overlap. The short-overlap area is used for test coupons to force a failure in the adhesive, while the long-overlap area is used for structural joints to prevent a failure of the adhesive. The strength plateau for the adhesive bond strength is

$$P_b = 2\tau_{av}\ell = \sqrt{4\eta\tau_p(1/2\gamma_e + \gamma_p) \cdot 2Et} \quad , \tag{1}$$

the derivation of which is given in Reference 3. In this equation, the term $\eta\tau_p(1/2\gamma_e + \gamma_p)$ represents the adhesive shear strain energy per unit bond area. The bond shear strength is proportional to the square root of the adherend thickness. This thickness influences the adhesive behavior in another way because the load that can be transferred through the bond is limited by the strength of the adherends, which are proportional to the first power of that thickness. Thus, to the bond strength plateau in Figure 5 must be added another cutoff — the adherend strength, which might lie above or below the bond strength. For any properly proportioned structural bonded joint, this adherend strength must lie below the bond shear strength to prevent the bond becoming a weak-link fuse. This adherend strength is given by

$$P_a = F_y t \tag{2}$$

in which F_y is the adherend yield strength. When the load is thus restricted to $P_a < P_b$, the maximum induced adhesive strain is also reduced, to a maximum plastic value of

$$\gamma_{max} = \frac{1}{2}\gamma_e + \frac{F_y^2 t}{8E\eta\tau_p} \qquad (\gamma_{max} \geqslant \gamma_e) \tag{3}$$

or if the load is so light as to not exceed the adhesive elastic capability,

$$\gamma_{max} = \frac{F_y}{2}\sqrt{\frac{t}{EG\eta}} \qquad (\gamma_{max} \leqslant \gamma_e) \tag{4}$$

13
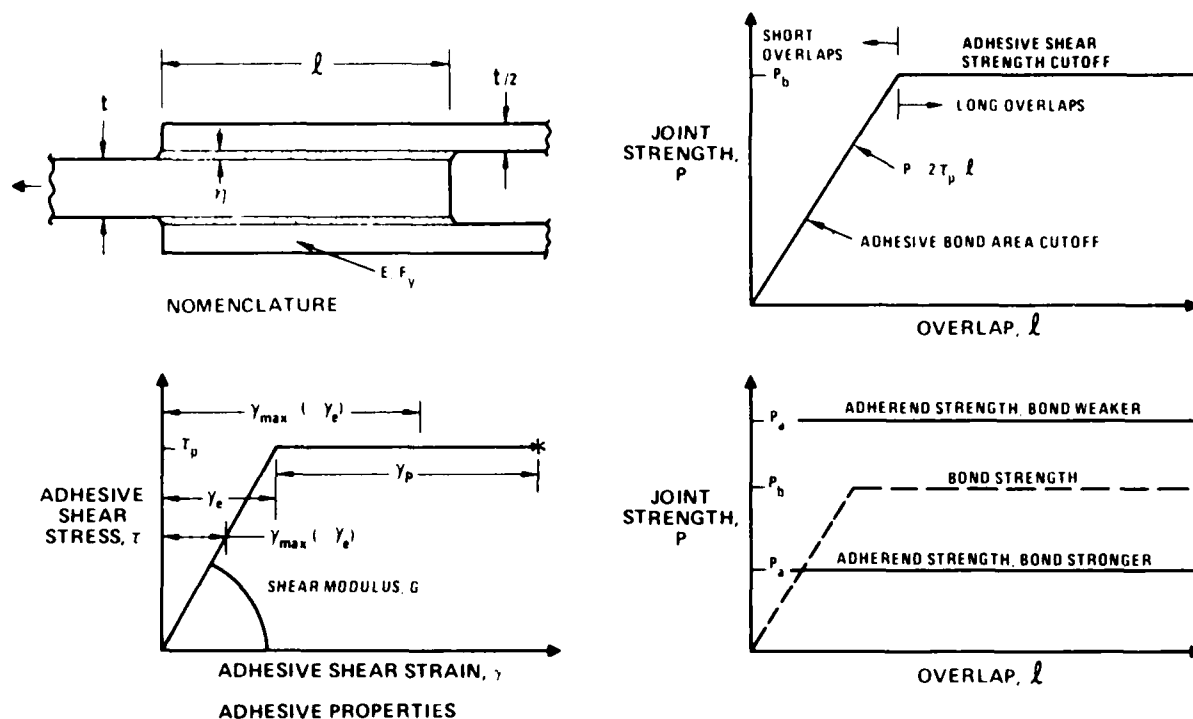
FIGURE 5. INFLUENCE OF JOINT GEOMETRY ON ADHESIVE BOND STRENGTH

Since most long-life adhesively bonded structure does not load the adhesive beyond the knee in the stress-strain curve, it follows from Equation (4) that the maximum adhesive shear strain induced is inversely proportional to the square root of the thickness of the adhesive layer. Further, the thickness of the adhesive layer at one or both ends of the bond determines the peak adhesive shear strain because that is where most of the load is transferred. Thus, Equation (4) explains why pinch-off of the adhesive layer at the ends of the overlap is important. It can be seen that a thickness reduction by a factor of 2 translates into either a strength loss or an aggravated peak shear strain about 30 percent higher. A pinch-off down to 0.001 inch from a typical basic thickness of 0.005 inch would thus correspond with a strength reduction by a factor of just over 2. However, that might not be evident if the reduction factor were applied to a bond strength P_b which was considerably in excess of the adherend strength P_a, as would be the case for much bonded thin secondary structure.

Apart from indicating the need for concern about pinch-off at the edges of adhesive-bonded joints, Equation (4) also suggests that the joint strength or life can be enhanced by deliberately thickening the adhesive layer with the very simple technique shown in Figure 6. Such modifications, of course, modify the distribution of the load transfer across the splice. Before discussing that in detail, it will first be explained how, for balanced joints, the total load transferred at each end is not influenced by such modifications.

14
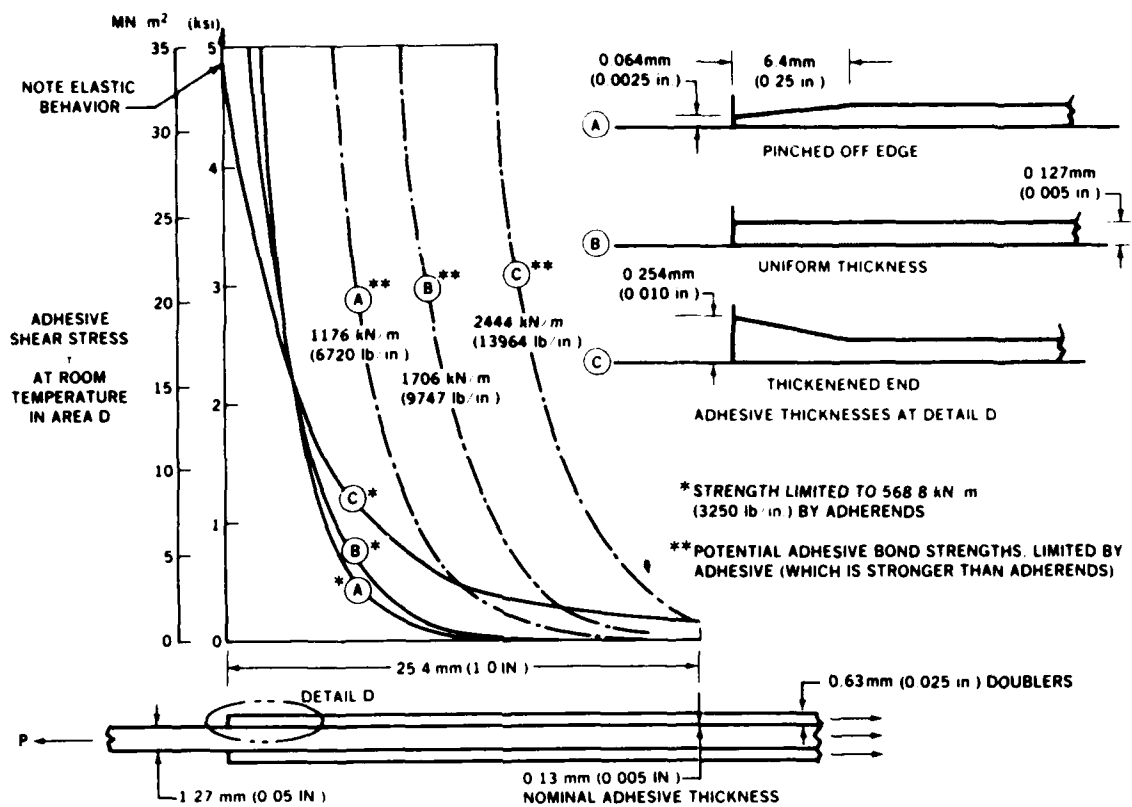
FIGURE 6. VARIATION OF PEAK INDUCED SHEAR STRESS WITH THICKNESS OF ADHESIVE AT ENDS OF OVERLAP

15

EQUALITY OF LOAD TRANSFER AT EACH END OF BALANCED JOINTS

The same load is transferred at each end of the joint shown in Figure 5 because the adherend stiffness Et at the left end is equal to the sum of the two stiffnesses Et/2 at the right end. Also, the adhesive shear stress distribution, as shown in Figure 1, would be precisely symmetrical. An imbalance in adherend stiffness or thermal mismatch would upset this symmetry, as is explained in Reference 7, but those effects are omitted here to simplify the discussion. Figure 7 compares the load transfer through adhesive bonds in joints and in doublers. Where the total doubler stiffness equals that of the skin, the load transfer through the adhesive bond is precisely the same in each case. In fact, the adhesive strain distribution is also the same. The reason for this is that the uniformity of adherend stress σ/2 halfway along the joint and at the right end of the doubler is necessarily associated with an absence of adhesive shear stress at these points. Similarly, the load transferred into each doubler, σt/4 where t is the basic sheet thickness, equals the load transferred into each splice plate halfway along the joint.

● SAME ADHESIVE STRESSES IN EACH CASE
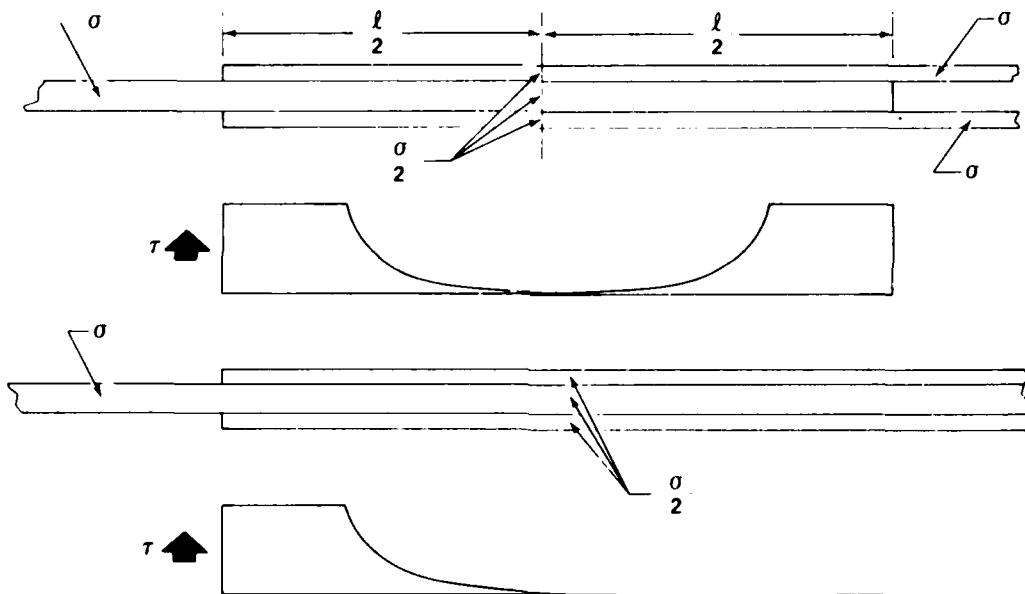
● SAME MAXIMUM ADHESIVE SHEAR STRAIN FOR SAME ADHERENDS
AND METAL STRESSES

FIGURE 7. SIMILARITY OF BOND STRESSES IN JOINTS AND DOUBLERS

Figure 7 has been prepared for a bonded joint in which the adherend details are the same at each end of the overlap. Yet the equality of load transfer extends to quite different end conditions, provided that the stiffnesses are still matched. This is shown in Figure 8, based on the uniformity of adherend stresses halfway along the joint. The difference between Figures 7 and 8 is that when the end details of the joint are not the same, one end of the adhesive is more critical. Thus, pinch-off is doubly harmful because it weakens the load transfer at the end at which it occurs, and strain compatibility then prevents the other, stronger end from developing its full bond strength before failure of the adhesive at the other, more critical end.

16

The refinements shown on the left of Figure 8 should be used as standard design techniques to increase the thickness of members that can be adhesively bonded together reliably. Specifically, for very thin adherends, the induced adhesive peel stresses are so small as to be negligible. As the thickness of the adherends is increased, the peel stresses become significant, as shown in Figure 9, until they actually detract from the shear strength of the adhesive bond.

LOCAL THICKENING OF ADHESIVE
TO REDUCE ADHESIVE SHEAR STRAIN
IN AREA OF INDUCED PEEL STRESSES

ADHESIVE BOND WITH PINCHED-OFF ENDS

LOCAL TAPERING OF ADHERENDS
TO REDUCE ADHESIVE PEEL STRESSES
AT ENDS OF OVERLAP

ADHESIVE SHEAR STRESS DISTRIBUTION

ADHESIVE SHEAR STRESS DISTRIBUTION

ADHESIVE SHEAR STRAIN DISTRIBUTION
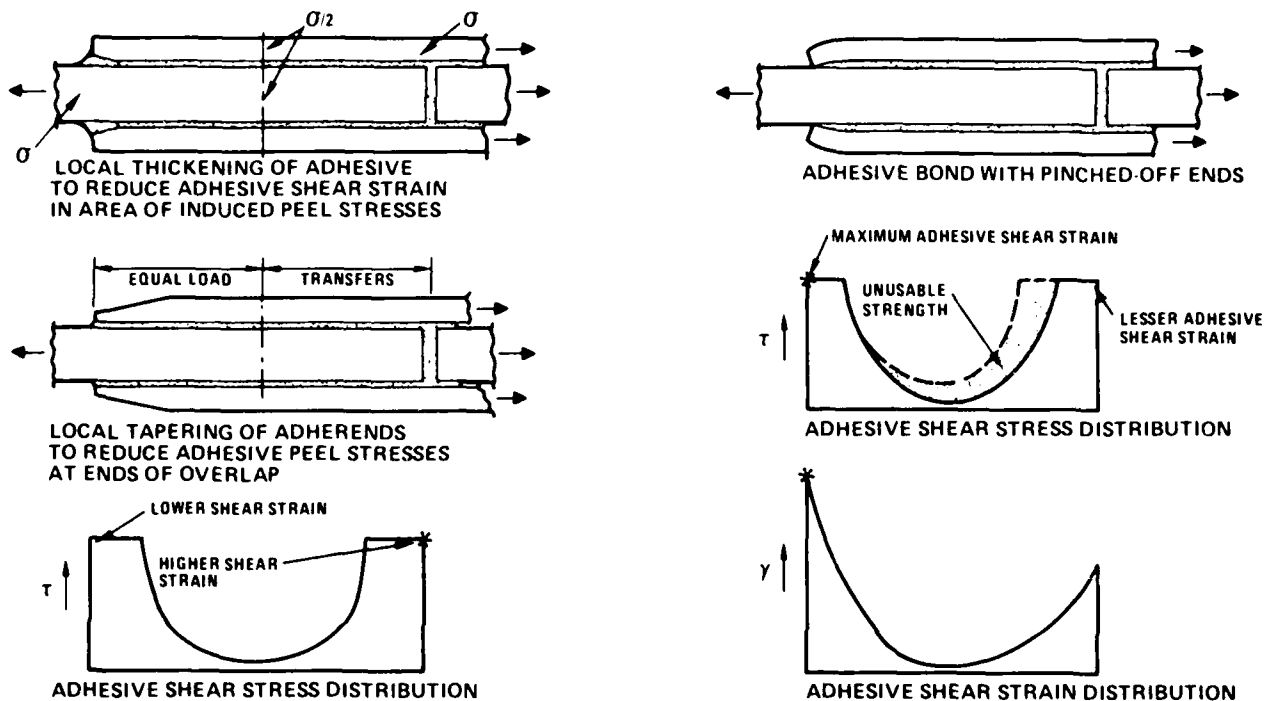
FIGURE 8. EQUALITY OF LOAD TRANSFER AT EACH END OF BALANCED BONDED JOINTS

STRESSES ACTING ON OUTER ADHEREND

B.

A.

C.
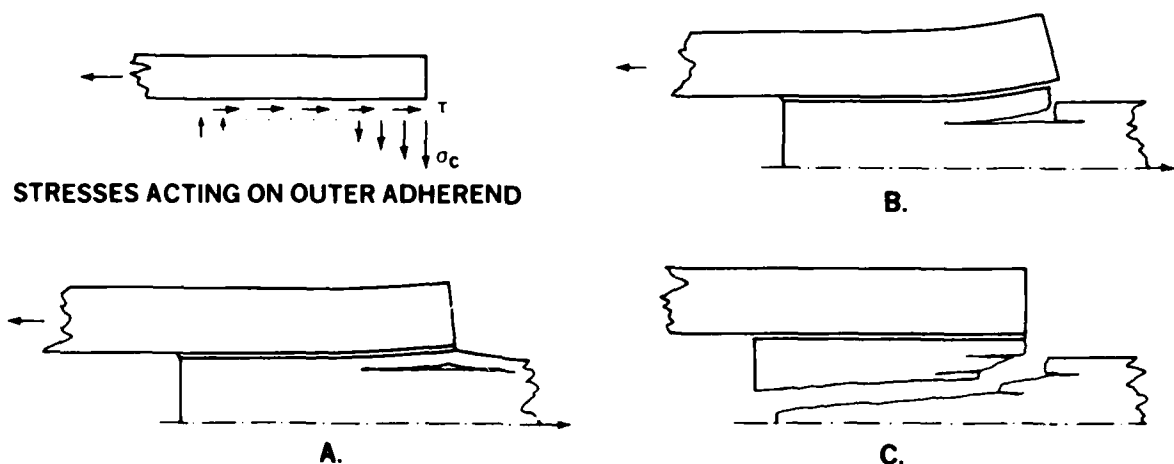
A, B, AND C INDICATE FAILURE SEQUENCE

FIGURE 9. PEEL STRESS FAILURE OF THICK COMPOSITE JOINTS

17

Some adhesive bond analysts have attempted to promote the philosophy of accepting this loss of strength by developing a combined-stress failure criterion for the adhesive under simultaneous shear and peel loads. The only practical application of this philosophy is to verify the outer adherend thicknesses below which no special treatment is needed. None of the adhesive-bonded splices tested successfully on the PABST program were ever analyzed according to such a combined-stress failure criterion. Instead, the outermost adherend thickness was restricted to 0.030 ± 0.010 inch, as shown in Figure 10. The glue layer was not thickened until after the full-scale development component (FSDC) fuselage had been completed. However, the program personnel who performed the limited testing and fabrication with this thickening became convinced that they should incorporate such details in the shape of the extruded longeron and frame shear tee sections as well as the splice plates in any subsequent work.
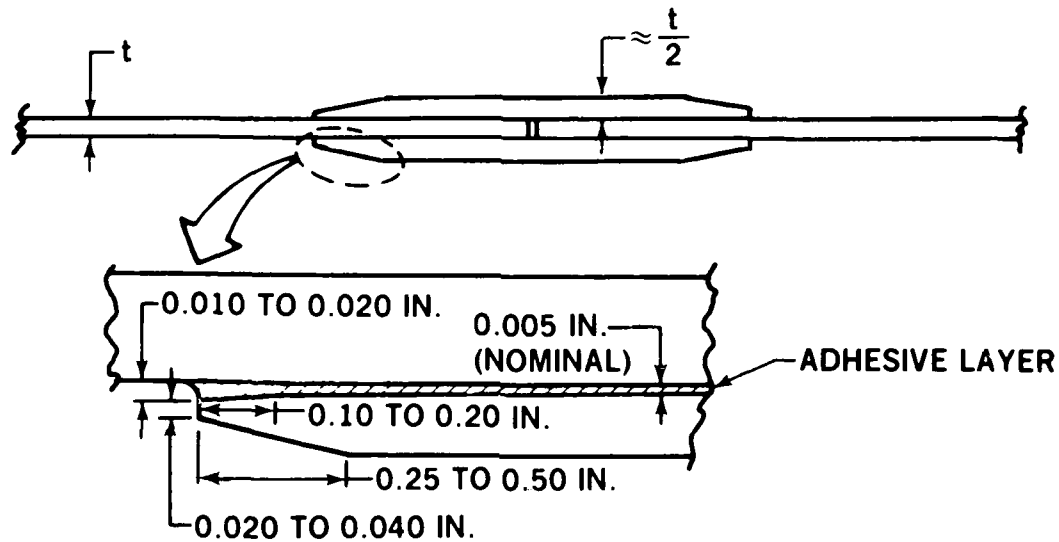
FIGURE 10. TAPERING OF EDGES OF SPLICE PLATES TO RELIEVE ADHESIVE PEEL STRESSES

With the more brittle adhesives used for higher temperature applications, it may be necessary to restrict the edge thickness more than for the ductile adhesives used on the PABST program. This should be approached with caution in view of the handling problems and damage to the extrusions that occurred early in the PABST program. That indicates a practical limit to this thinning — hence, the 0.020-inch minimum in Figure 10. Even if the combined-stress adhesive failure criteria referred to above are pursued further in the context of brittle adhesives, such prior work needs modification to account for the nonhomogenity and orthtropic properties of the adhesive layer and for nonlinear shear deformations: it will not suffice to continue to neglect the fibrous reinforcement which gives the adhesive different properties in-plane and through-the-thickness. Even the molecular structure formed during curing of the adhesive is directional and far from isotropic.

The great virtue of the design refinements shown in Figures 8 and 10 is that the improvements so obtained are extremely insensitive to the exact proportions used. The joint strength is actually established by the details at the right end of the splices shown on the left of Figure 8. The modifications on the left must be employed to a sufficient degree to ensure the transfer of the critical end of the joint from the left side to the right side. However, if they are overemployed, no harm is done because the joint strength is not changed. This is shown in Figure 11. The cor-

18

A. BASELINE JOINT — NO ADHEREND TAPER

B. SLIGHT ADHEREND TAPER

(ALL DIMENSIONS IN INCHES)

C. MODERATE ADHEREND TAPER

D. SEVERE ADHEREND TAPER

ADHESIVE STRAIN AT RIGHT I ND OF
JOINT DECREASES WITH MORE TAPER
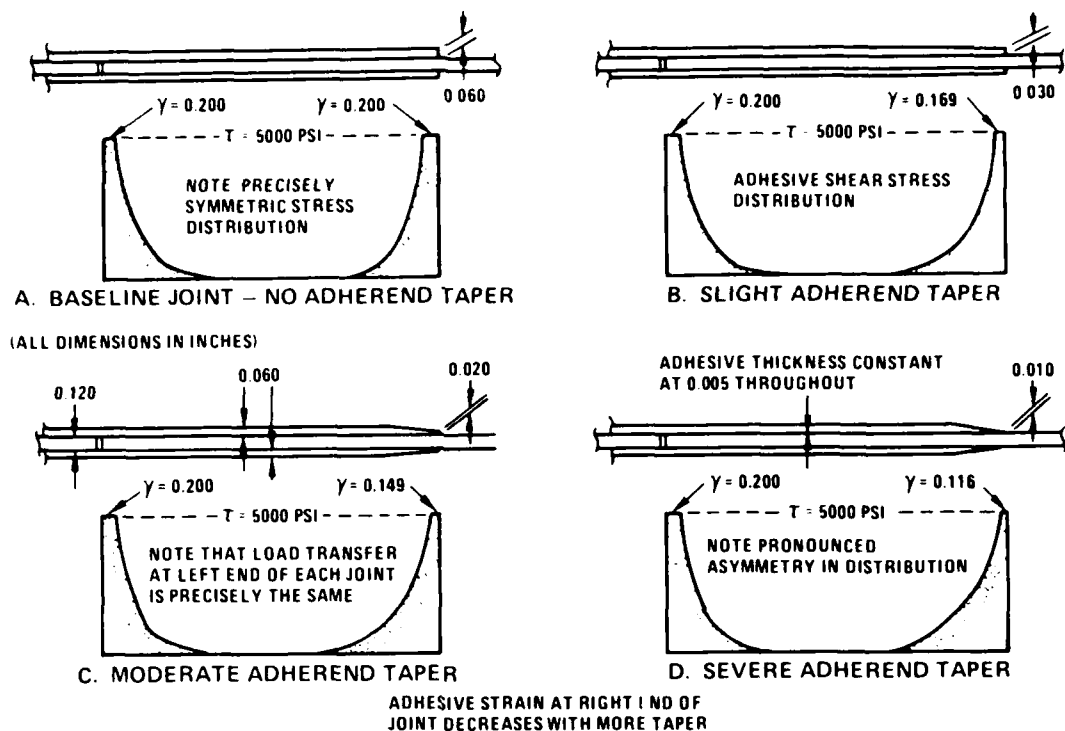
FIGURE 11. INSENSITIVITY OF ADHESIVE-BONDED JOINT STRENGTH TO MODIFICATIONS
AT ONE END OF JOINT ONLY

rect approach to the pinch-off problem shown on the right of Figure 8 is not to accept it but to eliminate it by improved manufacturing techniques or to compensate for it by employing the techniques on the left of Figure 8. However, it is still necessary to establish just how much of the problem shown on the right of Figure 8 can be tolerated. Acceptance criteria for the pinch-off problem are established below for the typical ductile and brittle adhesives discussed in this report. The methods used are explained so that they can also be applied to other situations.

19

SELECTION OF OVERLAP IN DESIGN OF BONDED JOINTS

Figure 5 indicates that, once the short-overlap region in bonded joints has been exceeded, the strength is essentially constant, regardless of overlap. The method of actually choosing the overlap is therefore based on the adhesive shear strain distribution instead. Figure 12 explains how the adhesive-bonded joints were designed for the PABST program. The method is extremely simple, resulting in a table of design overlaps corresponding with the thickness of each member being joined. The check on bond strength noted in Figure 12 results in a limit on the adherend thickness which can be bonded by the simple double-lap or double-strap splices. For aluminum adherends with the FM-73 adhesive used for the PABST program, such a table can be approximated by a simple rule-of-thumb for design — an overlap-to-thickness ratio just under 30 to 1, in double shear. The corresponding rule for single-lap joints was 80 to 1. The same dimensions could be used for high-temperature brittle adhesives. The major difference between ductile and brittle adhesives in this context is that the brittle adhesives must be restricted to use for only the thinner of the adherends that can be bonded with ductile adhesives.
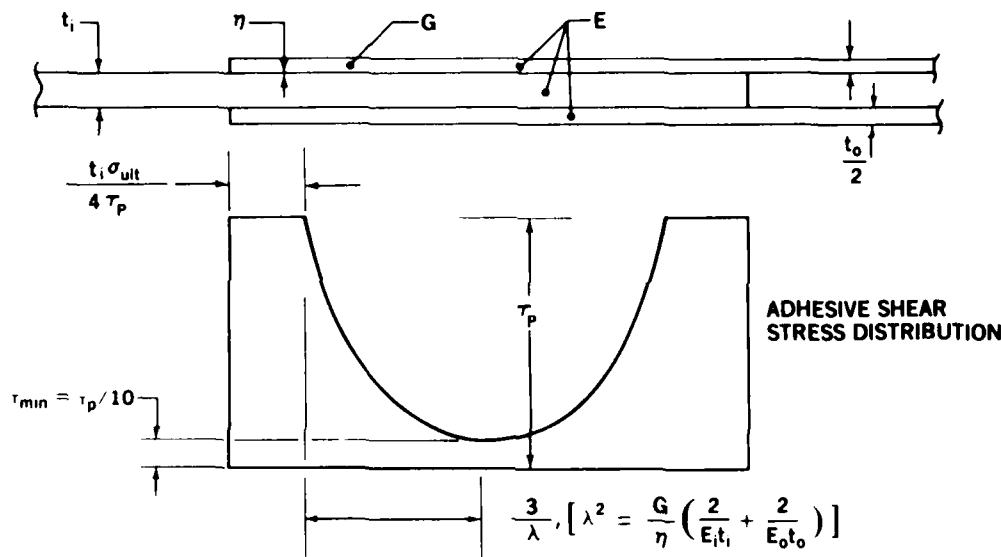
$$\frac{3}{\lambda} \cdot \left[\lambda^2 = \frac{G}{\eta} \left(\frac{2}{E_i t_i} + \frac{2}{E_o t_o} \right) \right]$$

- PLASTIC ZONES LONG ENOUGH FOR ULTIMATE LOAD

- ELASTIC TROUGH WIDE ENOUGH TO PREVENT CREEP
  AT MIDDLE

- CHECK FOR ADEQUATE STRENGTH

FIGURE 12.   DESIGN OF DOUBLE-LAP BONDED JOINTS

The key to the method presented in Figure 12 is that the minimum adhesive shear strain must be restricted in the middle of the overlap to prevent adhesive creep from accumulating at the ends of the overlap, where the maximum shear strain occurs. This topic is explained fully in Reference 8. Basically, the overlap is set at the sum of the dimensions needed to transfer the load through the plastic adhesive zones and of the dimension needed to build up the elastic adhesive trough. The determination is made for the worst environment, usually the hot, wet one. The effect of the subzero temperature on the joint proportions is to be found in details at the end of the overlap to restrict the induced adhesive peel stresses.

The fundamental difference in fatigue behavior of a structural joint, as shown in Figure 12, and of a short-overlap test coupon of the type shown in Figure 13 (l/t = 2 as opposed to 30), is that there is no mechanism with which to reverse any adhesive creep which occurs in the test coupon. There is measurable creep in the structural joint at the ends of the overlap where the adhesive strains are greatest. However, when the load is removed, that creep induces residual stresses in the adherends which are relieved only by pushing the adhesive back toward its original position. Even with long-term static loading, there is a basic difference. The rate of creep accumulation increases steadily in the coupon whereas, for the structural joint, even though the creep itself continues indefinitely, the rate decreases asymptotically because the adhesive deformations are constrained by the adherends.
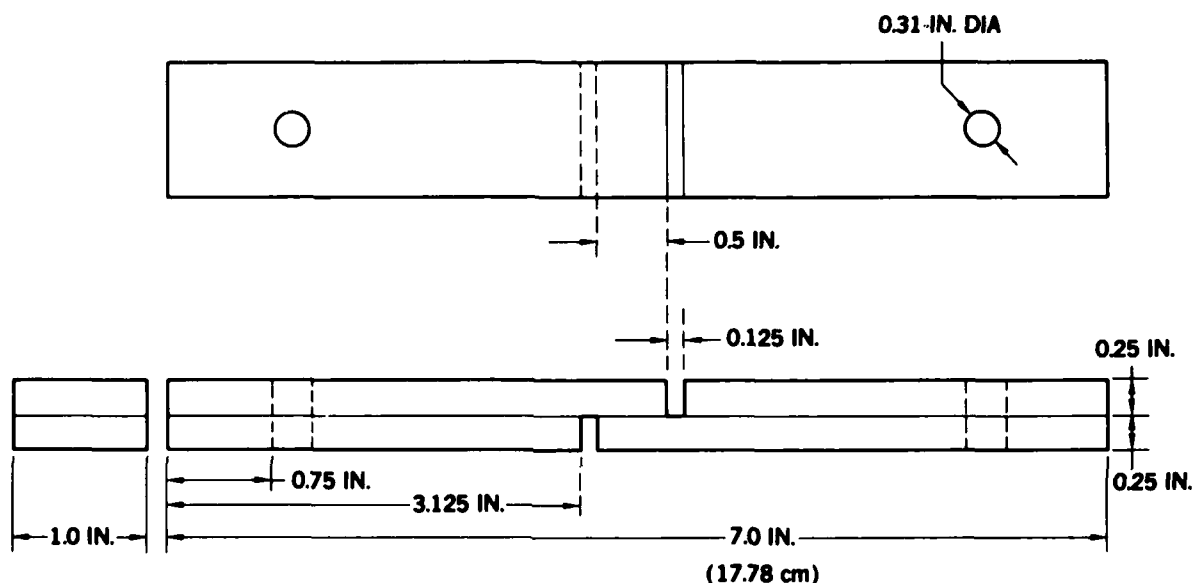
FIGURE 13.   THICK-ADHEREND SINGLE-LAP TEST COUPON

The design philosophy in Figure 12 was applied on the PABST program to overcome the doubts raised by slow-cycle testing by Bell and Boeing on short-overlap test coupons (Figure 13) just as the PABST program was getting underway at Douglas. Those tests, at about 1 load cycle per hour instead of the usual 30 cycles per second, had failed the adhesive in only a few hundred cycles instead of the many thousands needed, as discussed in Reference 8. Extensive slow-cycle testing conducted later on the PABST program proved this to be only a quirk of the test specimen geometry used. But it was an important lesson in the need to distinguish between the behavior of test coupons and real structural bonded joints. It has motivated further research into the life prediction of adhesive-bonded joints, now that the surface preparation problems have been understood and overcome.

21

EFFECT OF ADHESIVE END THICKNESS ON STRENGTH OF BONDED JOINTS

Based on the understanding of load transfer across adhesive-bonded joints described above, a series of parametric studies was performed, using the computer program A4EI. These studies are concerned with the effects of modifying the adhesive layer thickness in the immediate vicinity of the edges of the overlap. The thickness variations range from extreme pinch-off, down to 0.0005 inch, and up to 0.015 inch, as thick as can reasonably be manufactured without special techniques to prevent the adhesive from running out under capillary action. Three aluminum adherend thicknesses were considered — 0.040 inch, 0.080 inch, and 0.012 inch — in double shear. The overlaps, 1.0, 2.0, and 3.0 inches, respectively, are not critical since all joints are in the "long" overlap regime. Four adhesive characterizations are used, as described in Table 1, to cover the effects of the environment as well as the differences between ductile and brittle adhesives. The basic adhesive thickness is taken to be 0.005 inch, with the thickness modified linearly within the last 0.25 inch of overlap.

TABLE 1
MATHEMATICAL MODELS OF ADHESIVE PROPERTIES

ADHESIVE TYPE AND ENVIRONMENT	PLASTIC SHEAR STRESS τ_p (KSI)	SHEAR MODULUS G (KSI)	ULTIMATE SHEAR STRAIN $(\gamma_e + \gamma_p)$
DUCTILE ADHESIVE AT ROOM TEMPERATURE	5000	50,000	0.5
DUCTILE ADHESIVE AT -67°F	7000	70,000	0.25
DUCTILE ADHESIVE AT 140°F/100 PERCENT RELATIVE HUMIDITY	2500	40,000	1.0
BRITTLE ADHESIVE AT ROOM TEMPERATURE	9100	200,000	0.114

ELASTIC-PLASTIC ADHESIVE MODEL
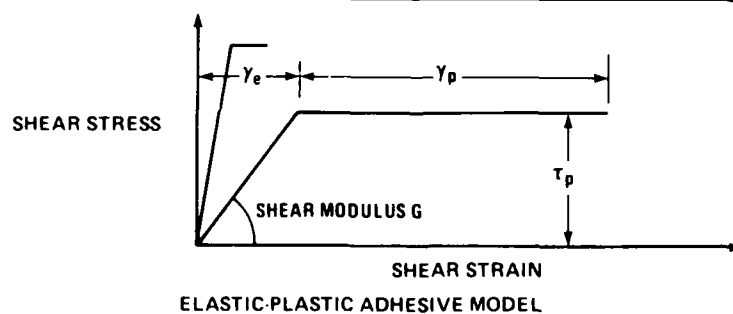
STRENGTH LOSSES DUE TO ADHESIVE PINCH-OFF AND TECHNIQUES TO ALLEVIATE THE PROBLEM

Pinch-off in the double-strap joint shown in Figure 10 can occur only at the outermost ends of the splice plates, which is equivalent to only one end of the basic double-lap joint. The interior, where the skins butt together, would tend to have a buildup rather than a decrease in adhesive thickness. For that reason, the analyses of the effects of adhesive pinch-off have been conducted for an adhesive which is pinched off at one end only. On the other hand, the benefits of deliberate local thickening could be applied to the splice plates only to reduce the induced peel stresses, or to both the splice plates and the skins to actually increase the joint shear strength above that of a perfect uniform bond. Both of these situations have been analyzed.

22

Figure 14 shows some sample adhesive shear strain distributions and joint strengths for progressively more severe pinch-off, down to a thickness of only 0.0005 inch. Figure 15 shows the corresponding results when the problem is posed in terms of a specified load, or adherend stress.
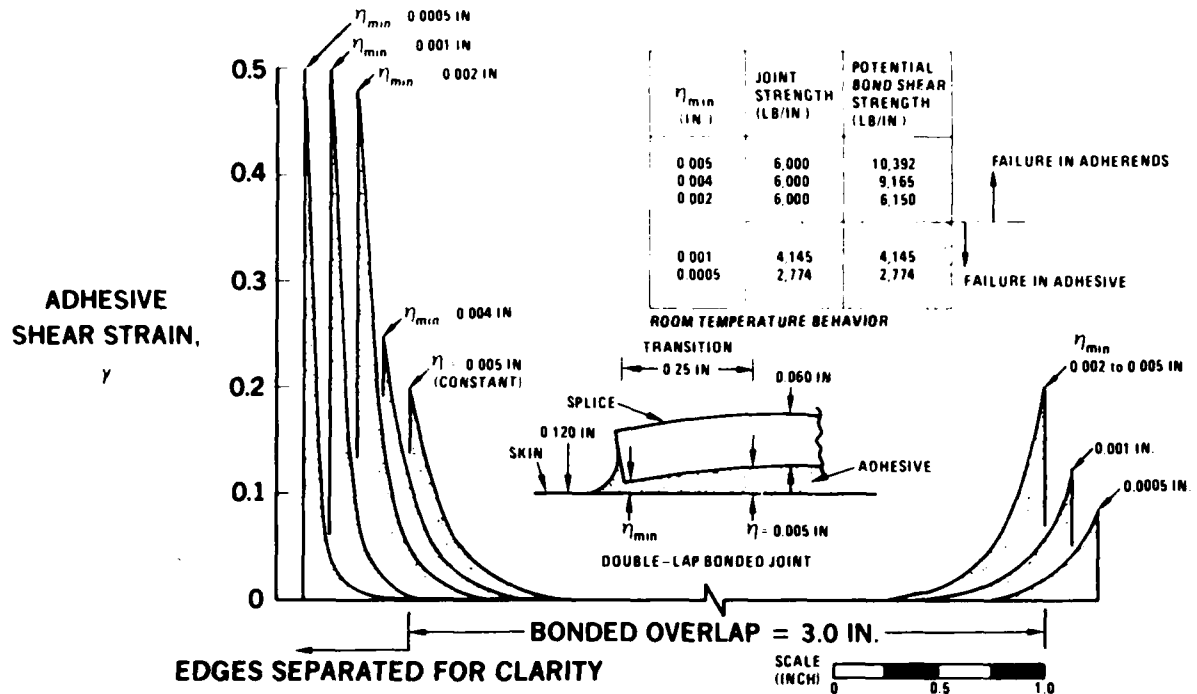
FIGURE 14. EFFECT OF PINCH-OFF ON STRENGTH OF ADHESIVE-BONDED JOINTS
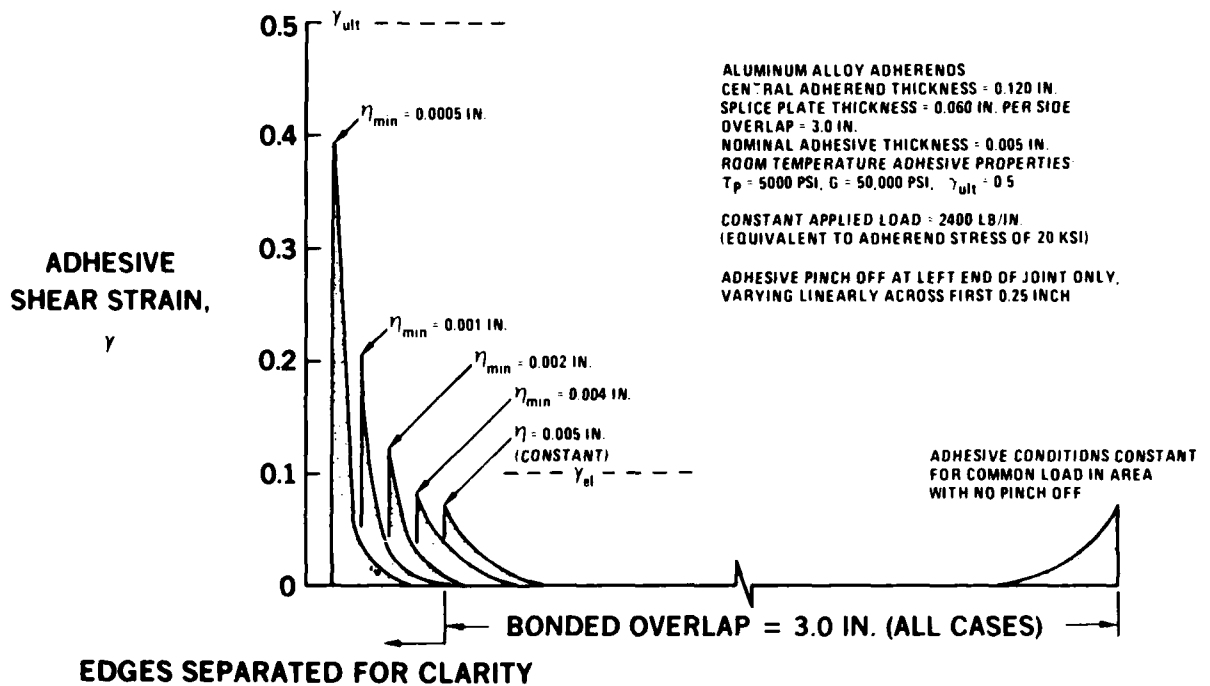
FIGURE 15. EFFECT OF PINCH-OFF ON STRAIN DISTRIBUTIONS IN ADHESIVE-BONDED JOINTS

23

Both figures show the extreme result for the maximum adherend thickness analyzed, 0.120 inch, while the greater tolerance to the pinch-off condition for the thinnest of the adherends, 0.040 inch, is shown in Figures 16 and 17. It is evident that even without the induced adhesive peel
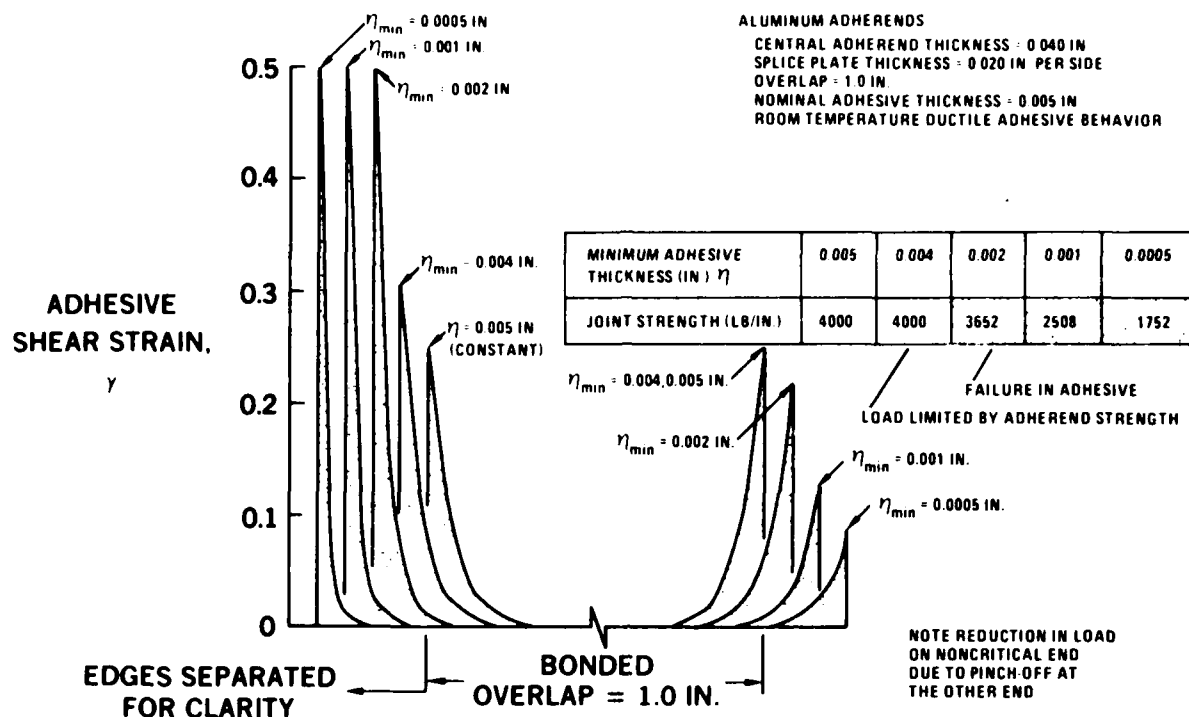
FIGURE 16.   EFFECT OF PINCH-OFF ON STRENGTH OF ADHESIVE-BONDED JOINTS
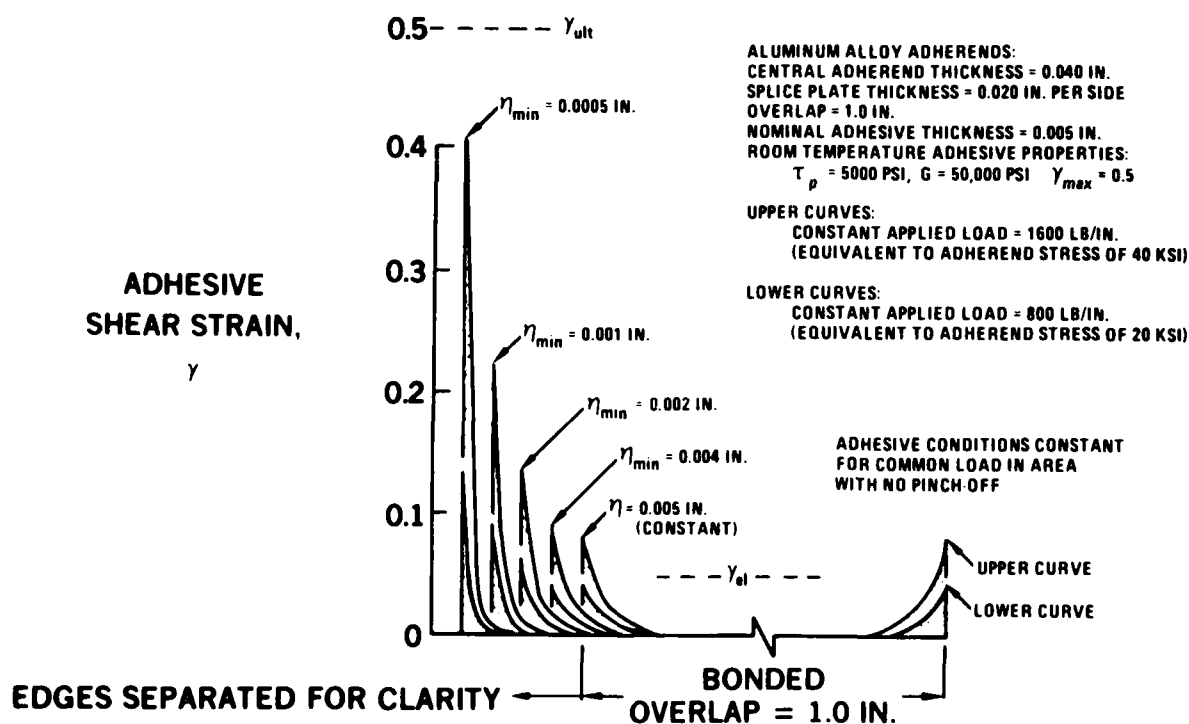
FIGURE 17.   EFFECT OF PINCH-OFF ON STRAIN DISTRIBUTIONS IN ADHESIVE-BONDED JOINTS

24

stresses which would intensify these stress concentrations, there is a very strong case for not accepting such poor-quality, weak bonded joints. One should either apply the pressure selectively to avoid the pinch-off or taper the ends of the splice plates. Yet, even so, for the thinnest skins, it can be seen that the ductile adhesives used on subsonic transport aircraft are capable of absorbing a considerable degree of pinch-off, down to about 0.001 inch, in comparison with only about a quarter as much (down to about 0.004 inch) for the thickest skins.

Equations (3) and (4) suggest a means of approximating the calculations shown in Figures 15 and 17 by replacing the yield stress F_y by a lesser applied stress σ. In fact, this proves to be quite reasonable for long-overlap structural joints, particularly for thinner gages and lighter loads, as shown in Figure 18. The effect of the pinch-off is clearly shown to be nonlinear, becoming progressively more severe as the pinch-off is accentuated. Given that the "precise" analysis relies on a stepped approximation to the adhesive pinch-off, there is little basis for preferring one method of calculation over the other. The agreement is precise for curve A in Figure 18, diverging for higher loads and more severe pinch-off. The agreement shown between the two approaches used in Figure 18 is sufficient to endorse the use of Equations (3) and (4) for variable-thickness adhesive layers also, with the adhesive characterized by its properties for some given environment and by its thickness at the ends of the bonded overlap. If the adhesive thicknesses at the ends differ, the thinner one is to be used.
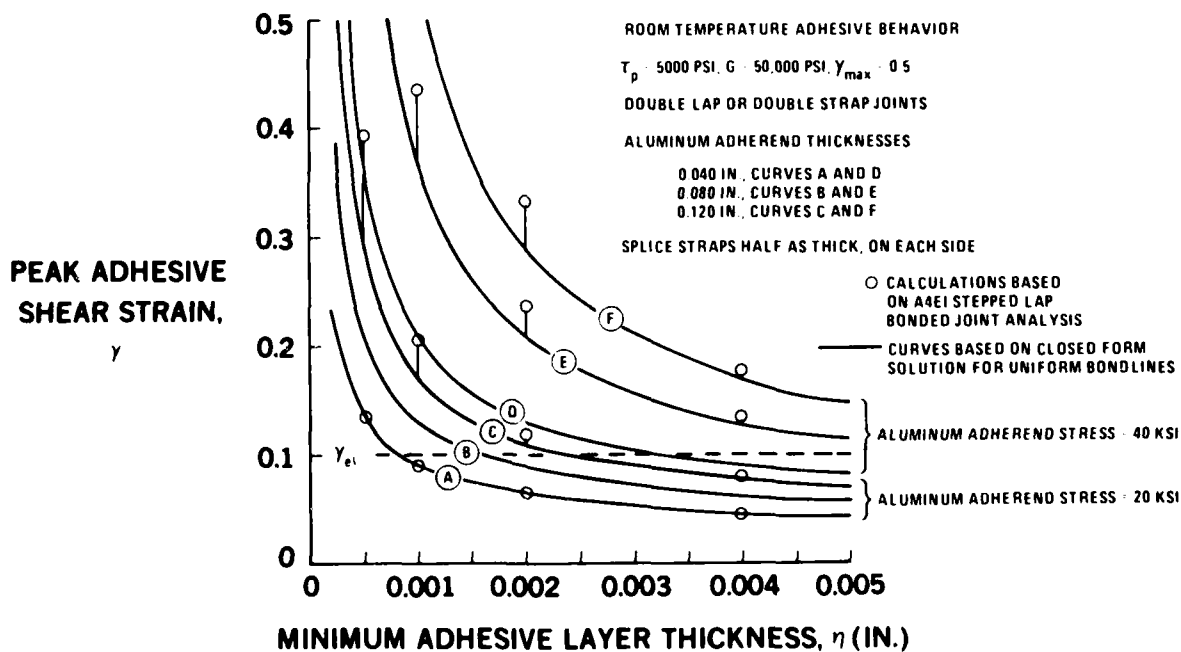
FIGURE 18. SIMPLIFIED PREDICTION OF PEAK ADHESIVE SHEAR STRAIN DUE TO PINCH-OFF

The differences between the precise solutions and the approximate analyses for a uniformly thinned bond line occur because the approximate model carries more load in the elastic trough area, which is really thicker and softer than in the approximate model. Therefore, the approximate approach is not conservative. However, the lack of conservatism will be undetectable if the load level is low enough so that no load transfer is induced except in the immediate vicinity of the ends of the overlap, as in Figure 17, for example. Likewise, if the pinch-off is not severe, the adhesive layer will be so close to uniform that a small error in the small load transferred through

25

the elastic trough will also be undetectable. This good agreement is evident at the bottom of Figure 18 where the load is low, and to the right, where the bond is uniformly thick.

Figure 18 was prepared for a ductile adhesive at room temperature. Corresponding characteristics for a brittle adhesive at room temperature and the ductile adhesive in other environments are shown in Figures 19 to 21.

FIGURE 19. SIMPLIFIED PREDICTION OF PEAK ADHESIVE SHEAR STRAIN DUE TO PINCH-OFF

FIGURE 20. SIMPLIFIED PREDICTION OF PEAK ADHESIVE SHEAR STRAIN DUE TO PINCH-OFF

26

FIGURE 21. SIMPLIFIED PREDICTION OF PEAK ADHESIVE SHEAR-STRAIN DUE TO
PINCH-OFF

In many instances, the adhesive can compensate for this strain concentration due to pinch-off. For thin adherends, the peak strain induced in the adhesive remains insufficient to fracture it because of the strength limit imposed by the adherends. When the adherends are strong enough to fracture the adhesive at the ends of the overlap, the fracture may be self-arrested as it propagates into the thicker adhesive layer away from the edge. Such crack arrest would be unlikely if the induced peel stresses in the adhesive had not been alleviated by tapering the splice straps. Tapering also decreases the peak adhesive shear stress at that end of the overlap, making the initiation of such fracture due to pinch-off remote.

The object of analysis of adhesive-bonded joints, taking into account the inevitable manufacturing imperfections, should be to establish the extent of countermeasures (as shown in Figure 10) to be taken in advance to prevent an unacceptable loss of joint strength.

Figure 11 provides quantitative support for the statements made earlier that it was impossible to overdo these refinements. Figure 11 shows how the joint strength remains constant for three different degrees of tapering of the splice strap and how the peak adhesive shear strains for common applied loads were also insensitive to the degree of tapering. However, the adhesive shear strain induced at the edge of the splice plate continues to decrease steadily, providing relief to mask the effects of any pinch-off which may be present.

This combination of effects is characterized in Figure 22, which shows that tapering can nullify substantial pinch-off. Since the other end of the joints in Figure 22 has the basic uniform adhesive layer, the behavior of such an ideal joint has been included in Figure 22 as a baseline. Figure 22 was prepared for the thickest of the skins considered, 0.120 inch, with a ductile adhesive at room temperature.

27

FIGURE 22. ALLEVIATION OF PINCH-OFF BY ADHEREND TAPERING

STRENGTH GAINS DUE TO THICKENING THE ADHESIVE AT BOTH ENDS OF THE BONDED JOINTS

Figures 14 to 17 characterize the loss of bonded joint strength due to adhesive pinch-off at the outer edges of the splice plates. One should therefore expect that deliberate thickening of the adhesive layer locally at each end of the overlap should cause a corresponding increase in strength. This is shown in Figures 23 to 25, for local thickening at both ends of the overlap. This simple procedure is all goodness — the only limit to its application is the tendency of the adhesive to flow out of the thickened areas due to capillary action during cure. This technique should be adopted as standard manufacturing practice.

However, it would be foolish to rely on these benefits in analysis to any extreme degree because of the sensitivity of the joint strength to the exact thickening actually achieved. The author would recommend that the basic analysis be performed for a nominal uniform adhesive layer, as actually produced by a manufacturer. For an adherend not so thick as to be stronger than the bond, such local thickening of the bond will serve to prolong the fatigue life. This use of thickening can be very helpful with brittle adhesives, as indicated in Figure 25. The author would recommend against relying on this technique to invert the relative strength of the adhesive and adherends. On paper, this technique could be shown theoretically to permit the bonding of up to 0.25-inch-thick aluminum adherends which could fail outside the joint area, but the slightest deficiency in adhesive thickness buildup at the ends of the overlap would convert the adhesive into a weak-link fuse. This local thickening of the adhesive should not be used to justify an increase in static strength of adhesive bonded joints for metal alloy adherends.

28

η_{max} (IN.)	JOINT STRENGTH (LB/IN.)	POTENTIAL BOND SHEAR STRENGTH (LB/IN.)
0.005	6,000*	10,392
0.008	6,000	13,416
0.010	6,000	15,099
0.015	6,000	15,391

*LIMITED BY ADHEREND STRENGTH

NOTE HOW THICKENING OF THE
ADHESIVE LAYER AT THE ENDS
REDUCES THE ADHESIVE STRAIN THERE

FIGURE 23. REDUCTION IN PEAK ADHESIVE SHEAR STRAIN DUE TO LOCAL THICKENING
OF ADHESIVE AT ENDS OF OVERLAP

DUCTILE ADHESIVE, HOT/WET ENVIRONMENT
(140°F, 100 PERCENT RELATIVE HUMIDITY)

η_{max} (IN.)	JOINT STRENGTH (LB/IN.)	POTENTIAL BOND SHEAR STRENGTH (LB/IN.)
0.005	6,000 *	10,766
0.008	6,000	12,500 †
0.010	6,000	12,500
0.015	6,000	12,500

* LIMITED BY ADHEREND STRENGTH
† STRAIN LIMITED AT 0.25 INCH FROM EDGE,
NOT AT EXTREME OUTSIDE
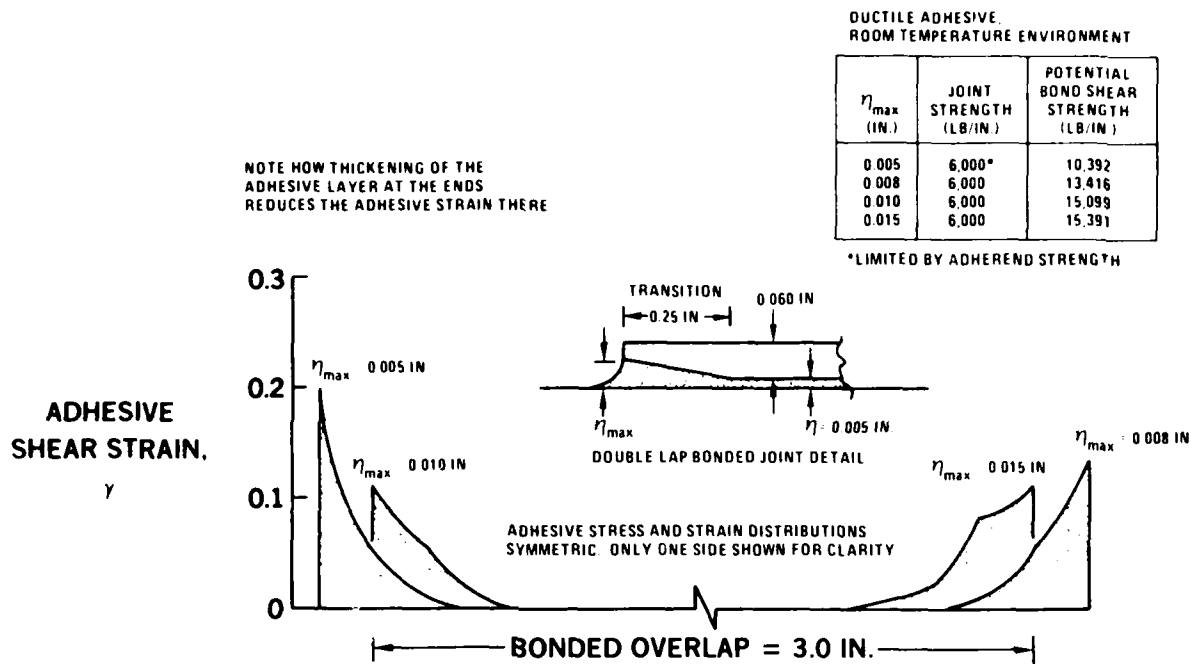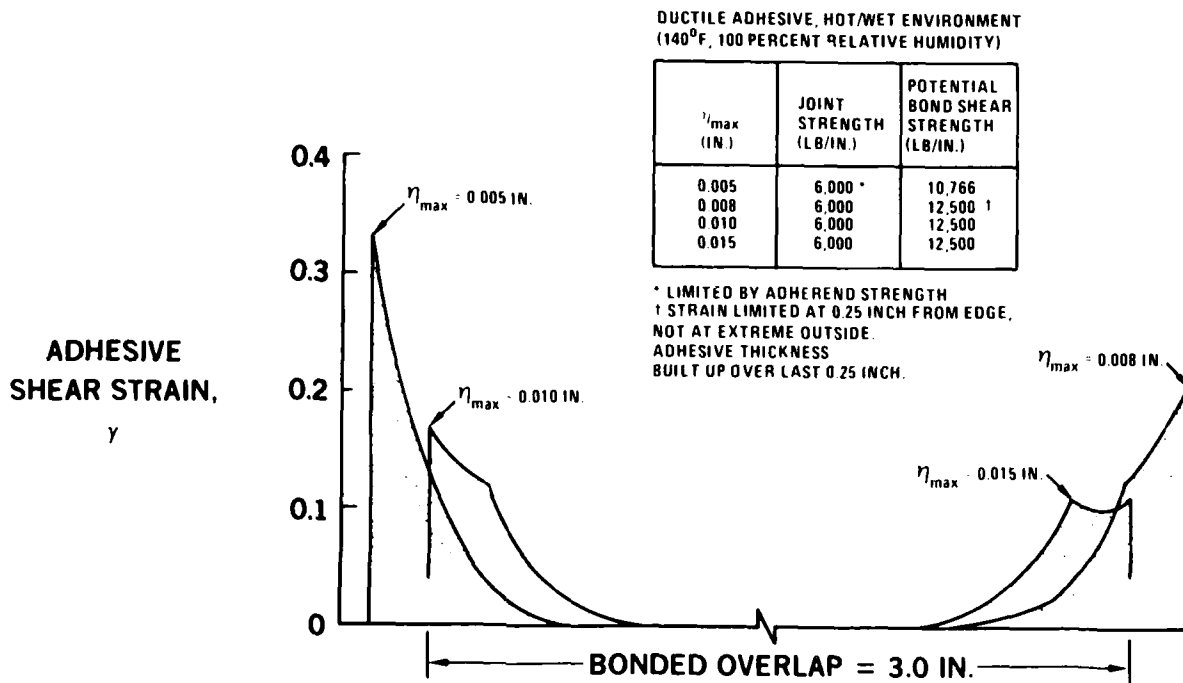ADHESIVE THICKNESS
BUILT UP OVER LAST 0.25 INCH.

FIGURE 24. REDUCTION IN PEAK ADHESIVE SHEAR STRAIN DUE TO LOCAL THICKENING
OF ADHESIVE AT ENDS OF OVERLAP

29
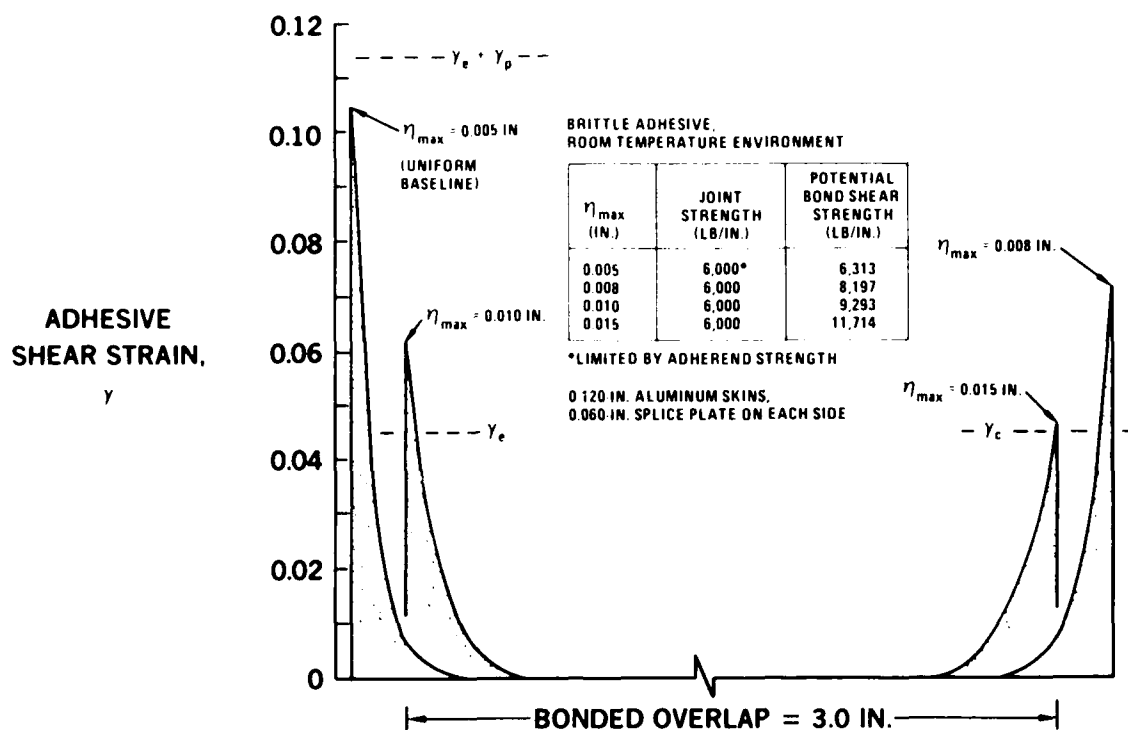
FIGURE 25. REDUCTION IN PEAK ADHESIVE SHEAR STRAIN DUE TO THICKENING OF
ADHESIVE AT ENDS OF OVERLAP

On the other hand, for fibrous composite adherends, there may well be a valid argument in favor of accepting these benefits. Because of the extreme weakness of the resins in interlaminar tension, the usual static failure mode of such joints is as shown in Figure 9. Selective thickening of the adhesive layer at the outer ends of the splice plate, as shown in Figure 10, would eliminate that weak failure mode, permitting better use to be made of the rest of the composite material in the structure. There is less need for such improvements in the middle of the splice because the induced normal stresses there are compressive rather than tensile, unless there is an eccentricity in the load path there.

There is an interesting quirk associated with excessive thickening at the ends of the overlap, for ductile adhesives in hot environments. An example of this is shown in Figure 26. First, thickening beyond 0.008 inch from the basic 0.005 inch does not contribute to the joint strength in this case. This is because the adhesive strain is then maximized at the inside of the taper, at point A, instead of at the edge of the overlap, at point B, which is the usual critical location. Second, the remaining uniform section, 2.0 inches, appears to be insufficient to prevent sustained creep of the adhesive. The minimum shear stress exceeds the elastic adhesive behavior for this potential bond strength analysis. Actually, since the adherend strength limits the load to only 6000 lb/in., the elastic trough really remains in the adhesive. The precise numbers in Figure 26 are therefore not significant but the trend in behavior is: It is far better to have the critical adhesive location at A rather than B. It is like having a controlled, more effective fillet.
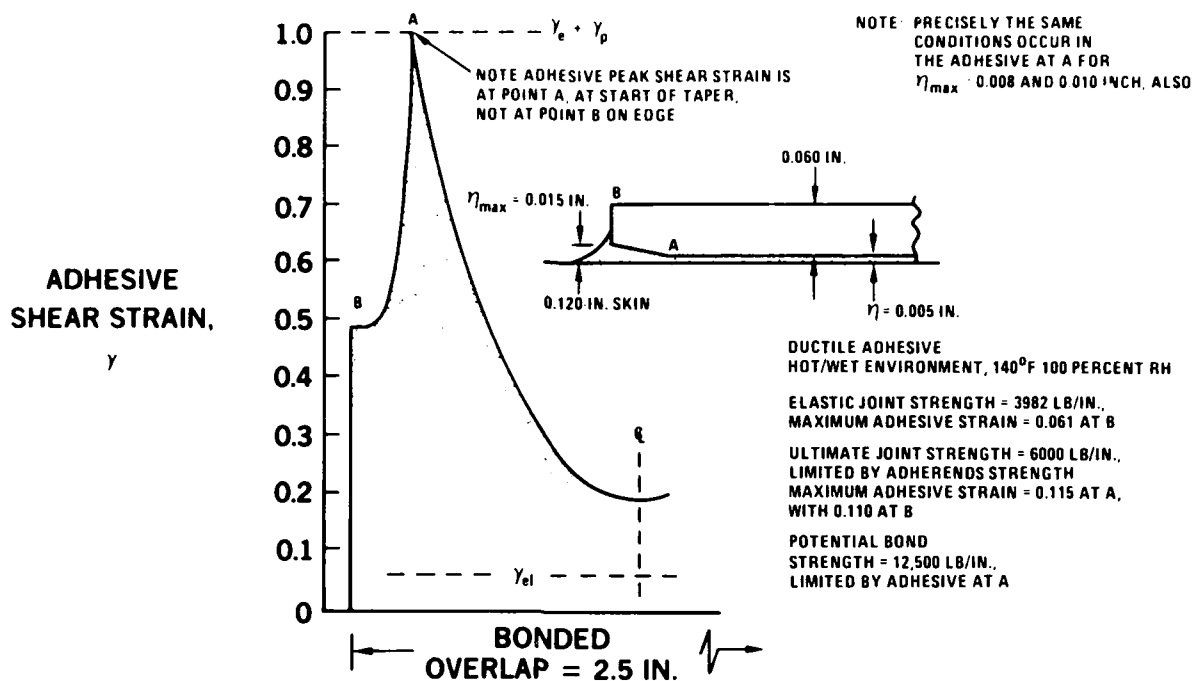
FIGURE 26. PECULIAR BEHAVIOR FOR EXCESSIVELY THICKENED ADHESIVE BOND

This sample solution in Figure 26 points to a need for clarification of the statement that excessive thickening of the adhesive can do no harm. *The conditions* shown in Figure 26 effectively reduce the joint to the shear strength of another joint having a slightly shorter total overlap than a nominally perfect joint with uniform bond thickness. Thus, while it is well protected against peel stresses by the tapered overhangs beyond the shear transfer area, its shear strength is not greater than the baseline joint. However, if the adhesive had not been as thick, the shear strength of the joint could have been enhanced without loss of peel stress protection. In that context, excessive thickness buildup is undesirable but, even so, it does not cause a reduction in bond shear strength below the baseline value — it simply fails to extract the maximum benefits possible.

Figures 23 to 25 show the benefits of thickening the adhesive at both ends of the overlap. As noted earlier, such thickening at one end only can increase the joint strength by suppressing the peel failure mode but cannot increase the shear strength with respect to an equivalent bond of uniform thickness. Figure 27 shows that the "other" end of the joint remains the critical location in determining the bonded joint strength.
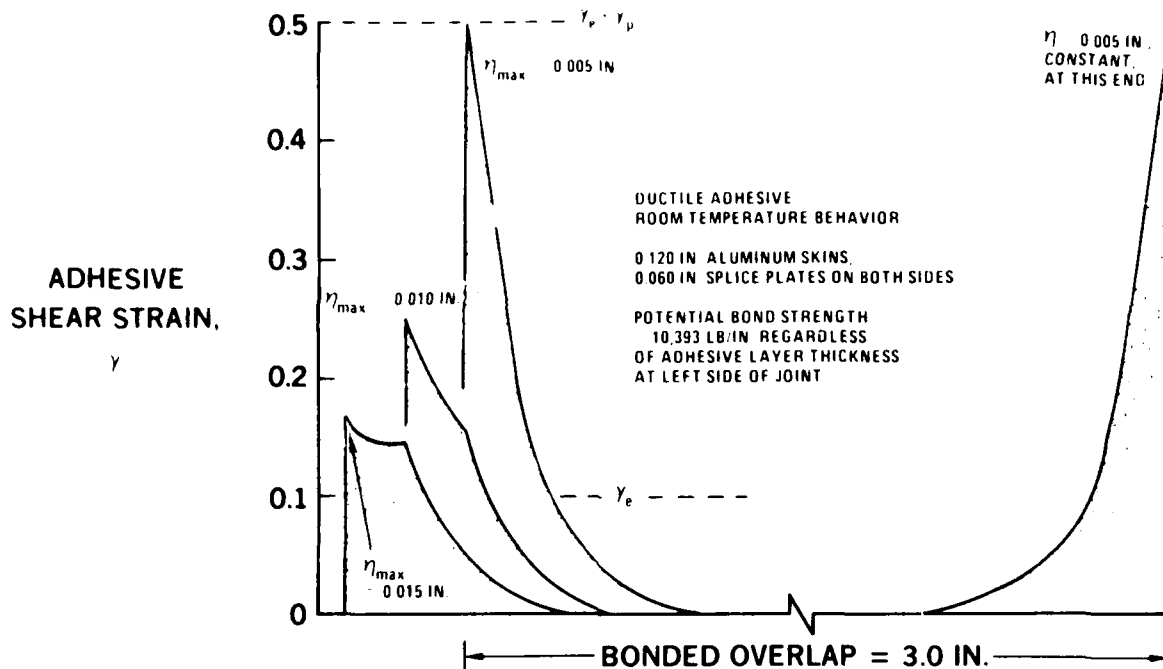
31

ADHESIVE SHEAR STRAIN, γ

$\gamma_e \cdot \gamma_p$

η_{max} 0 005 IN

η 0 005 IN CONSTANT AT THIS END

DUCTILE ADHESIVE
ROOM TEMPERATURE BEHAVIOR

0 120 IN ALUMINUM SKINS
0 060 IN SPLICE PLATES ON BOTH SIDES

POTENTIAL BOND STRENGTH
10,393 LB/IN REGARDLESS
OF ADHESIVE LAYER THICKNESS
AT LEFT SIDE OF JOINT

η_{max} 0 010 IN

γ_e

η_{max} 0 015 IN

BONDED OVERLAP = 3.0 IN.

FIGURE 27. LIMITS ON ADHESIVE STRENGTH GAIN DUE TO THICKENING ADHESIVE
LAYER AT ONLY ONE END OF BOND

The calculations used to generate the solutions described in this report have all modeled the change in adhesive thickness in four equal steps, with a total of 10 stations per joint. It would be convenient if Equations (3) and (4) could be adapted to simplify this operation. In the context of the local thickening of the adhesive, these formulas could be evaluated for a uniformly thickened adhesive layer. The predictions of joint strength should tend to be conservative because the thinner adhesive in the elastic trough would transmit more shear stress for common relative motion between the adherends. The prediction of peak shear strain at the ends, associated with a given load, would consequently also be conservative. However, since the elastic trough usually transmits only a small fraction of the total joint strength, the adhesive thickness error there is not likely to have a pronounced effect on the predictions for ductile adhesives. This is shown in Figure 28. The approximation is not as close for brittle adhesives, as shown in Figure 29. Nevertheless, it is clear that the simple formulas can be used effectively for preliminary design purposes.

The comparison between the A4EI calculations, circled in Figure 29, and the approximate solutions given by the curves shows that the simple approximate analyses are quite acceptable whenever the adhesive is critical at the ends of the overlap. Such a comparison for Figure 28 was equally good except for the hot, wet environment for the ductile adhesive, for which the critical location shifted, as in Figure 26, invalidating the comparison. That failure to achieve a gain in strength in such a case is another reason for not blindly relying on the shear strength gains shown in ˹ ures 28 and 29 from thickening the adhesive, but to accept them only as an effective cure to any induced peel-stress problem.
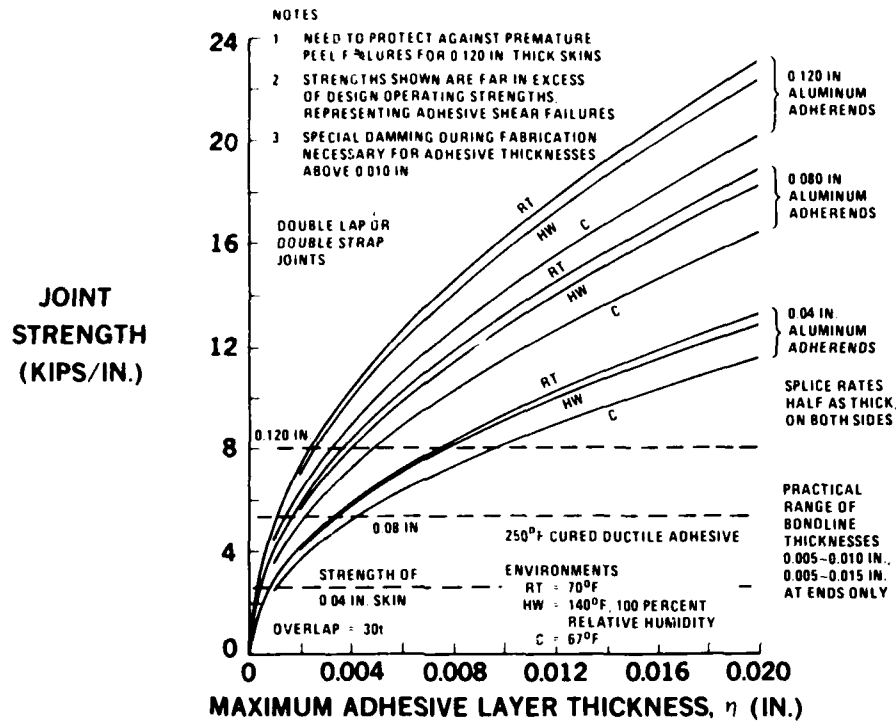
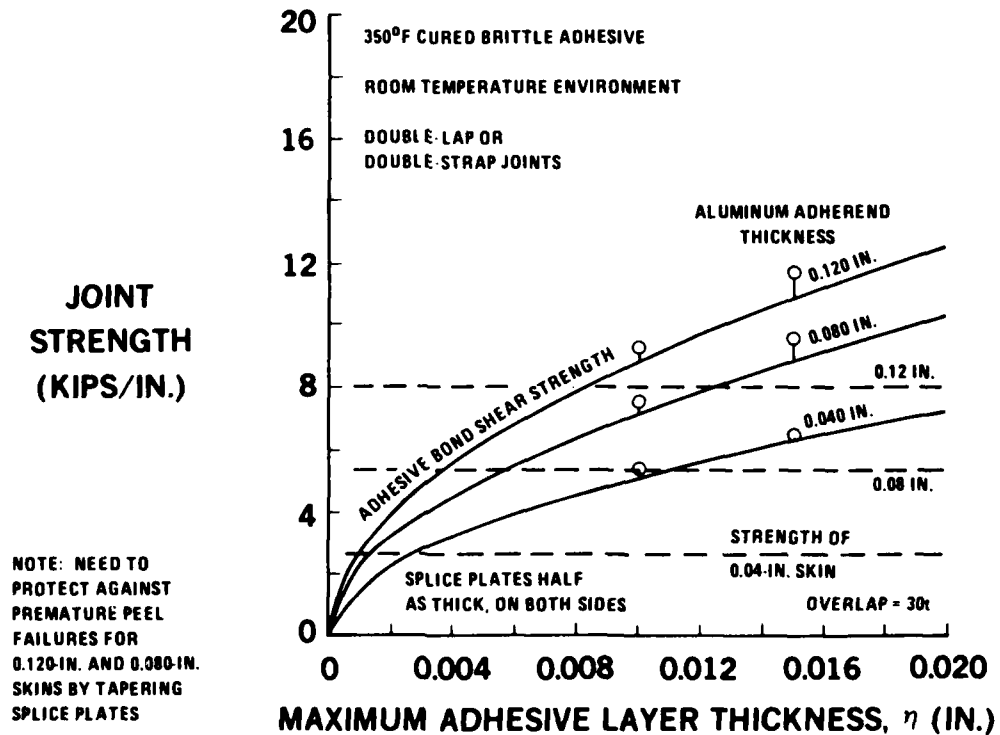FIGURE 28. SIMPLIFIED PREDICTION OF BONDED JOINT STRENGTH FOR DUCTILE ADHESIVES

FIGURE 29. SIMPLIFIED PREDICTION OF BONDED JOINT STRENGTH FOR BRITTLE (HIGH SERVICE TEMPERATURE) ADHESIVES

33

RECOMMENDED ACCEPTANCE CRITERIA FOR ADHESIVE PINCH-OFF

The analyses presented above provide a means of establishing tolerable amounts of adhesive pinch-off at the ends of the overlaps on bonded joints. Before specifying these limits, it is necessary to establish some ground rules, particularly since pinch-off is less detrimental if it is accompanied by adherend tapering to relieve both the adhesive peel and shear stresses. Also, the numbers given below are for specific adhesives and adherends, so the method of generating the numbers should be recorded for adhesives still under development or yet to be invented.

The basic rule that establishes the degree of tolerable pinch-off is easy to express. Pinch-off is excessive and unacceptable whenever it reduces the bond strength (in shear or peel) to less than the adherend strength. With brittle adhesives and thick adherends, then, no pinch-off at all can be accepted. The implications of that statement are: (1) that the manufacturing methods must be improved to prevent pinching off the adhesive layer by not applying pressure at the tip of the overlap, as described in Figure 30; or (2) the adherend must be chamfered to provide for a locally thickened glue layer to nullify any pinch-off; or (3) the joint must be redesigned into a more complex tapered or stepped-lap joint to enhance the ratio of bond strength to adherend strength. Thus, it is apparent that any hard-and-fast rules about unacceptable degrees of pinch-off are more likely to result in a design change to relieve the problem than to provide quality assurance standards.

A. PINCH-OFF UNDER VACUUM BAG

B. USE OF WIRE TO LIFT VACUUM BAG OFF TIP OF BOND
(THIS SCHEME WILL WORK ONLY WITH SIMPLE STRAIGHT EDGES)

C. RESTRICTED AREA OF PRESSURE APPLICATION IN OUT-OF-AUTOCLAVE BONDING

D. USE OF THICKER EDGE PLATE TO RELIEVE VACUUM BAG PRESSURE AT EDGE

E. ADDITION OF 1 TO 5 PERCENT OF 0.007-INCH GLASS BEADS IN ADHESIVE FILM IS A VERY EFFECTIVE TECHNIQUE FOR CONTROLLING BONDLINE THICKNESS

FIGURE 30. MANUFACTURING TECHNIQUES TO RELIEVE ADHESIVE PINCH-OFF

At the other extreme of adhesive-bonded structure — the minimum-gage skin-doubler combinations or control surfaces and fairings for subsonic aircraft bonded together with ductile adhesives —, there is no justification for spending any more effort in manufacturing to relieve the pinch-off problem than can be recouped by simplifying the inspection process. There is not likely to be any measurable structural benefit from such refinements in those cases, as indicated in Figure 31, because the adhesive is inherently so much stronger than the adherends. But the added inspection cost associated with low-quality bonds can serve as a powerful stimulant to improve the manufacturing techniques. It is important to look at the overall picture and not just at each operation alone.
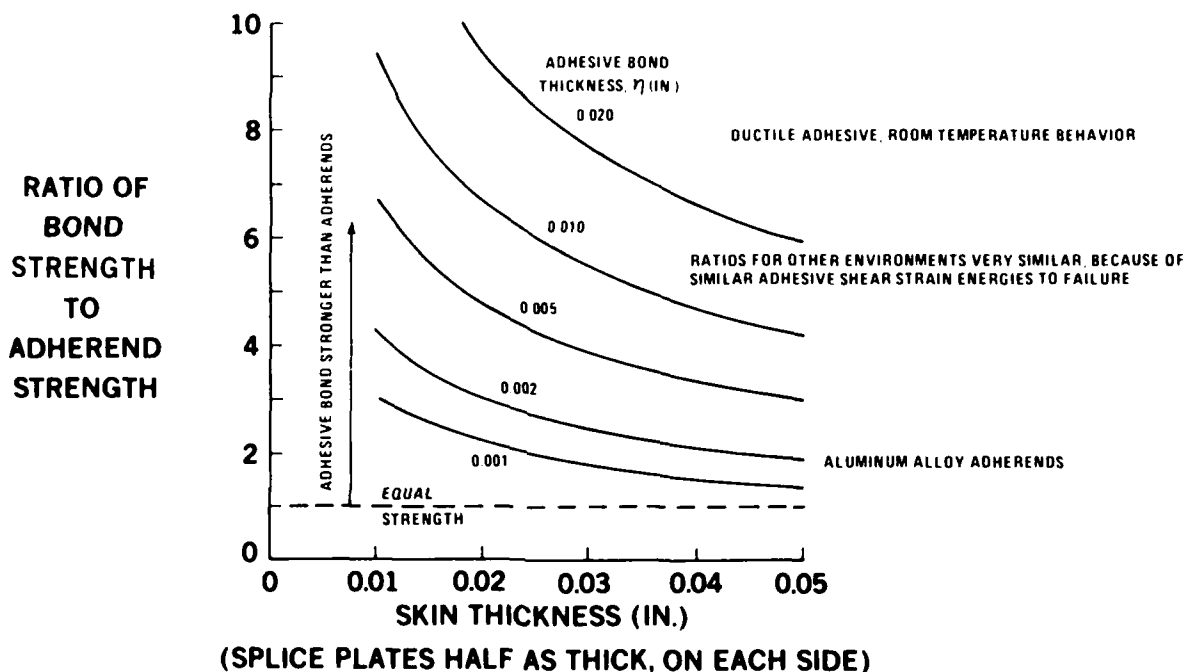
FIGURE 31. EXCESS OF BOND STRENGTH OVER ADHEREND STRENGTH FOR THIN-GAUGE ALUMINUM STRUCTURE

An assessment of the results of the approximate solutions described above, together with many solutions obtained by the A4EI program, indicates that the amount of tolerable adhesive pinch-off can be condensed to the simple form of Figure 32. The lines in Figure 32 were prepared for double-shear bonded joints between aluminum adherends but can easily be interpreted for single-shear joints (with appropriate longer overlap to alleviate the eccentricity in load path) as one side of a double-lap joint. Figure 32 presents the limits for both ductile and brittle adhesives, and it is very clear that much less pinch-off can be tolerated for the latter.
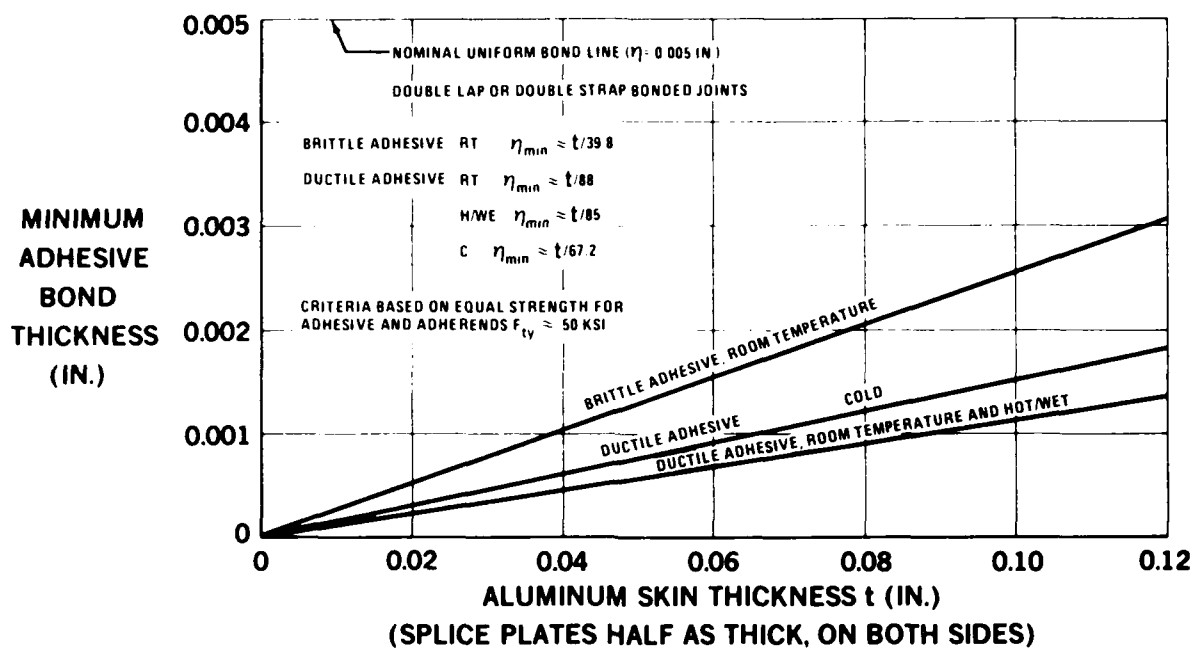
FIGURE 32. SUGGESTED CRITERIA FOR TOLERABLE ADHESIVE PINCH-OFF, BASED ON ULTIMATE LOAD CONDITIONS

Figure 32 was actually prepared on the basis of equating the adherend strength to the adhesive shear strength given by Equation (3), and checking against the A4EI predictions. From Equation (3), then

$$P = \sqrt{4\eta\tau_p(1/2\gamma_e + \gamma_p) \cdot 2Et} = \sigma t, \qquad (5)$$

whence

$$8E\tau_p(1/2\gamma_e + \gamma_p)\eta = \sigma^2 t. \qquad (6)$$

Equation (6) can be expressed as a strain energy balance since $\sigma^2 t/E$ is equivalent to $\sigma\epsilon t$. This full expression reduces to the simple relation,

$$\eta_{min} \propto t, \qquad (7)$$

whence the straight lines in Figure 32. That the task of characterizing the adhesive pinch-off problem in mathematical terms can be reduced to such a simple formula is remarkable. By omitting the plastic adhesive shear strain γp and reducing the aluminum operating stress below the yield (or ultimate) value, this same equation can also be interpreted as a fatigue condition, as has been done in Figure 33. Note how, in that context, no pinch-off can be tolerated for skin thickness above 0.08 inch for the ductile adhesive in a hot, wet environment.

36

Figure axis labels and legend:

MINIMUM ADHESIVE BOND THICKNESS (IN.)

0.005
0.004
0.003
0.002
0.001
0

SAMPLE
FATIGUE CONDITIONS
ALUMINUM STRESS – 20 KSI,
ADHESIVE NOT STRAINED
BEYOND KNEE OF
STRESS STRAIN
CURVE IN SHEAR

A $\eta_{min} = t/15.6$
B $\eta_{min} = t/41.4$
C $\eta_{min} = t/50$
D $\eta_{min} = t/70$

NO PINCH OFF
PERMITTED FOR
THIS CONDITION

DUCTILE ADHESIVE, HOT/WET ENVIRONMENT
BRITTLE ADHESIVE, ROOM TEMPERATURE ENVIRONMENT
DUCTILE ADHESIVE, ROOM TEMPERATURE ENVIRONMENT
DUCTILE ADHESIVE, SUBZERO ENVIRONMENT

0   0.02   0.04   0.06   0.08   0.10   0.12

ALUMINUM SKIN THICKNESS t (IN.)
(SPLICE PLATES HALF AS THICK, ON EACH SIDE)
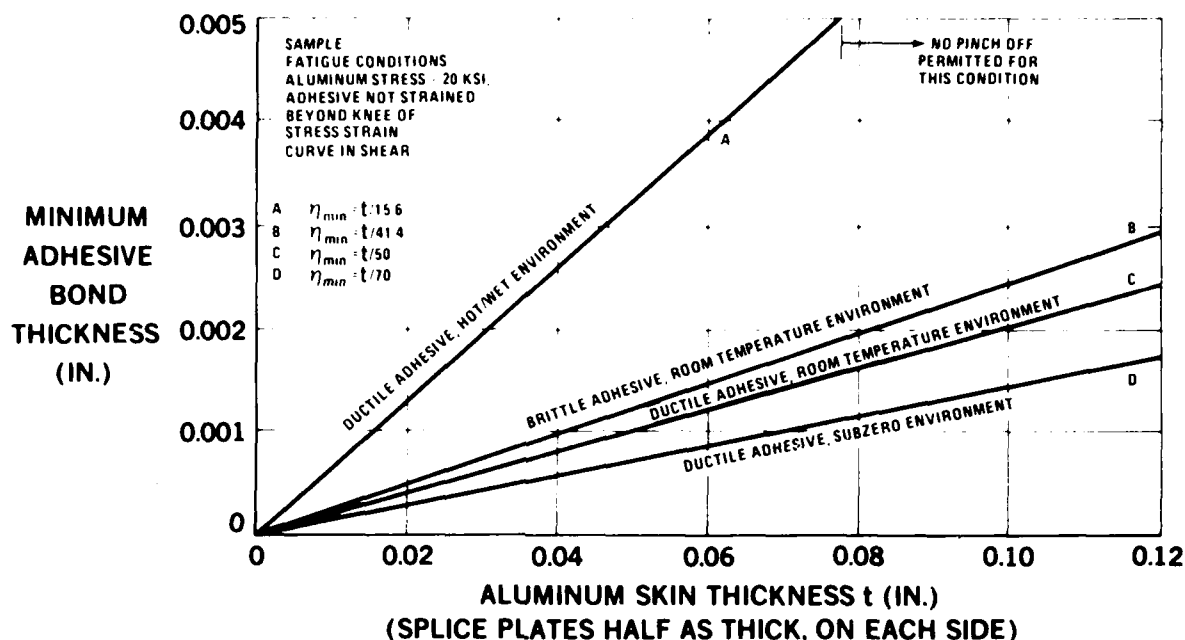
FIGURE 33. SUGGESTED CRITERIA FOR TOLERABLE ADHESIVE PINCH-OFF BASED ON
FATIGUE LOAD CONDITIONS

It should be noted that Figures 32 and 33 were prepared for adhesive shear failures. That information, on its own, would be extremely inaccurate if not supplemented by simultaneous consideration of the need to taper the splice straps, where appropriate, to prevent a premature failure due to induced peel stresses. Peel stresses are discussed fully in Section 4. It suffices to state here that it has been established that the peak induced peel stress for an adhesive-bonded joint between uniformly thick balanced adherends is given by

$$\sigma_{peel(max)} = \tau_{max}\left(\frac{3E_c'(1-\nu^2)t_0}{E_0\eta}\right)^{1/4} . \tag{8}$$

where the terminology is explained in Figure 34 (Reference 3). Now, since the failure stress of adhesives in peel is about the same order as for shear, the relative ratio E_C'/E_0 for the effective peel modulus to the adherend modulus imposes definite constraints on the ratio t_0/η of the outer adherend thickness to the adhesive layer thickness. For the ductile adhesives used on the PABST program, E_c is on the order of 10^5 psi while E_0 was on the order of 10^7 psi. Therefore, the ratio t_0/η must not be allowed to exceed about 37 to 1 under any circumstances. Actually, on the PABST program the ratio was targeted at 0.030/0.005 or 6 to 1, but manufacturing imperfections raised this to 0.040/0.002 or 20 to 1. Thus, the peak induced peel stresses in the adhesive might have been as high as 86 percent of the peak shear stresses in the thicker parts of the bonded structure. The exact numbers are not as important as the message that a balance must be kept between the adherend and adhesive thicknesses to control the peel stresses. This logic led to the justification for tapering any thicker splice plates down to 0.030 ± 0.010 inch on the
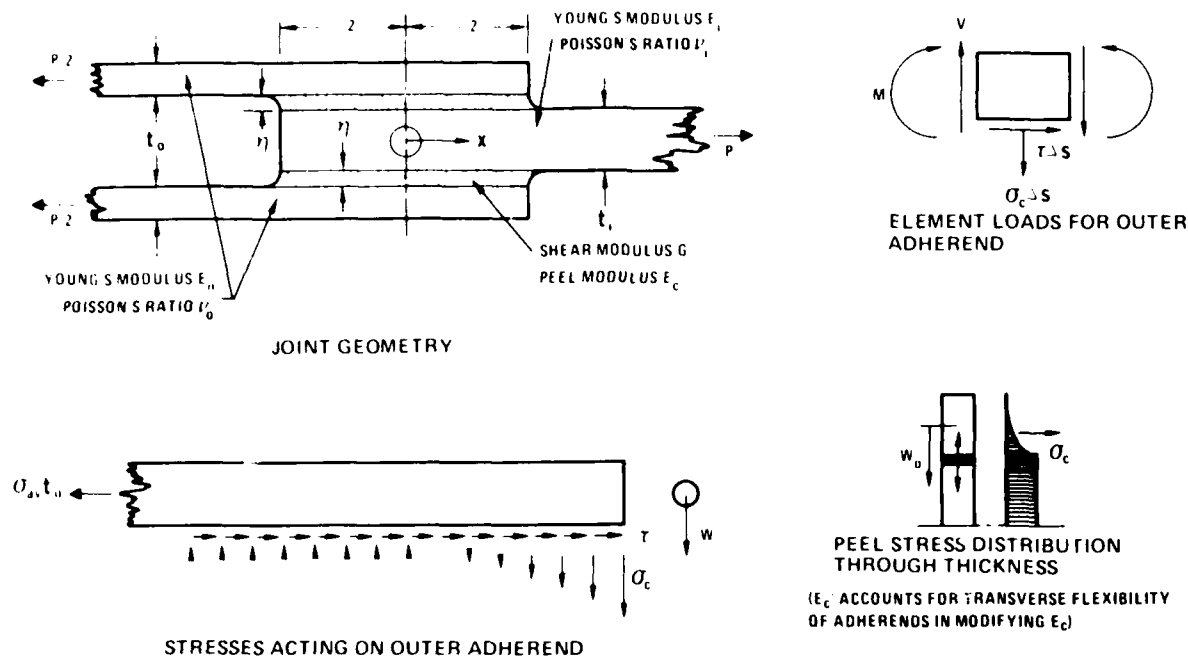
37

YOUNG'S MODULUS E_i
POISSON'S RATIO ν_i

YOUNG'S MODULUS E_o
POISSON'S RATIO ν_o

SHEAR MODULUS G
PEEL MODULUS E_c

JOINT GEOMETRY

ELEMENT LOADS FOR OUTER ADHEREND

STRESSES ACTING ON OUTER ADHEREND

PEEL STRESS DISTRIBUTION THROUGH THICKNESS

(E_c ACCOUNTS FOR TRANSVERSE FLEXIBILITY OF ADHERENDS IN MODIFYING E_c)

FIGURE 34. COORDINATE SYSTEM AND PEEL DEFORMATIONS IN DOUBLE-LAP ADHESIVE-BONDED JOINTS

PABST program. Because Equation (5) was derived for uniform adherends, it does not reflect all of the benefits of tapering. For a start, the critical value of τ_{max} would then be at the "other" end of the joint, so that the τ_{max} in Equation (5) would already reflect some margin for the adhesive which, in turn, would then be better able to tolerate the peel stresses as well. As a rough measure, the ratio t_o/η should not exceed about 10 to 1, and consequently, good design practices and the use of meaningful acceptance criteria for adhesive-bonded joints between thicker members must account for the tapering of adherends, as shown in Figure 10.

The form of the peel stress constraint has exactly the same relation as Equation (7) for the pinch-off problem, $\eta \propto t$. Thus, the same design refinements which alleviate one condition must inevitably also help the other one. This is important since it would be very difficult if the two requirements conflicted. It appears that the peel-stress problem is usually dominant, at least for the materials and applications used by the aircraft industry today.

There is a potential problem with excessive tapering to an overly thin edge. The greater flexibility will not only tend to reduce the induced peel stresses; it will also tend to aggravate the pinch-off and increase those stresses again. In this context, it is quite clear that manufacturing methods, particularly in tooling, should be guided by philosophies that permit the bonding to be effected at the minimum possible pressure needed to bring the parts into contact. The stiff details should be supported and the flexible ones allowed to deflect to improve their fit, rather than relying on massive pressure to force noncompliant parts together and squeeze out too much adhesive. This situation often affects the original design, as learned on the PABST progam and recorded in References 9 and 10.

Thus, the establishment of useful specific acceptance criteria for adhesive pinch-off in the more highly loaded bonded joints is very complex, even though the guiding rules are simple and explicit. The best possible advice is to follow the techniques described in Figure 10 to make the problem go away and simplify the inspection process as well as to improve the joint strength. The results from some such calculations are shown in Figure 35. For adherends thin enough to not need those refinements, the joint is usually stronger than the adherend by a sufficient amount so that pinch-off does not become a problem.
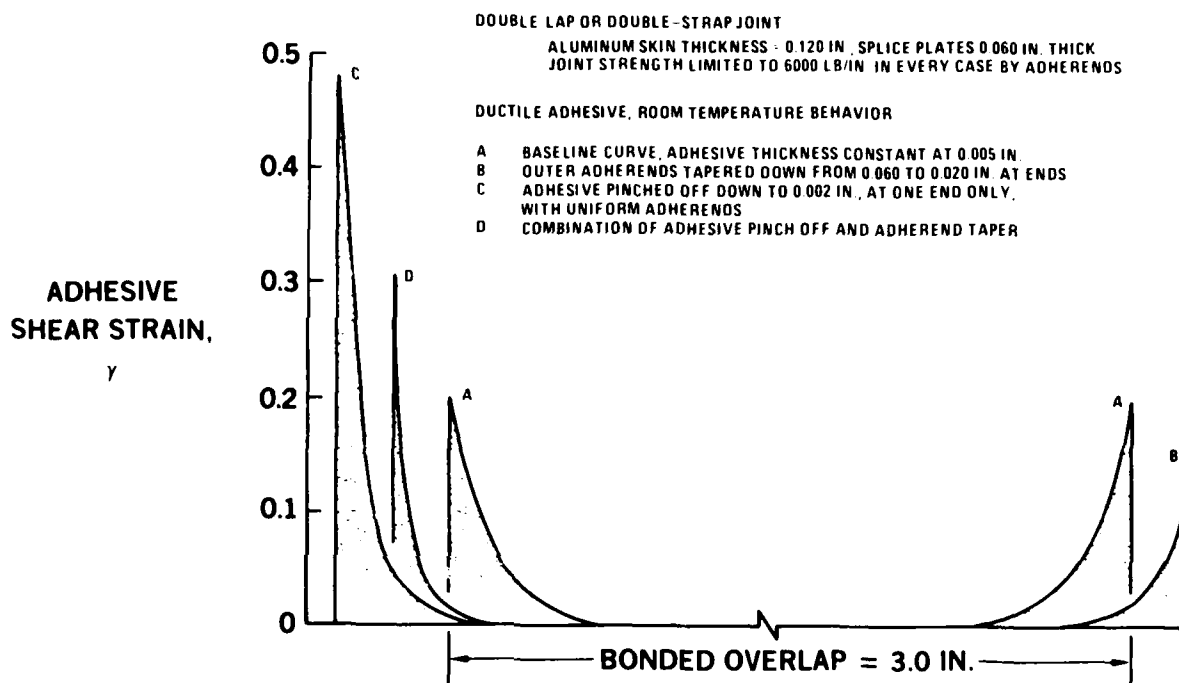

FIGURE 35.   USE OF ADHEREND TAPER TO COUNTERACT ADHESIVE PINCH-OFF

TWO-DIMENSIONAL ASPECTS OF THE PINCH-OFF PROBLEM

There is a further reason for not accepting engineering designs and manufacturing methods which result in excessive pinch-off of the adhesive layers. An additional weakness is exposed by considering the problem in its more general context — with varying pinch-off along a bonded splice. Individual one-dimensional analyses show that those areas with the greatest pinch-off are not only the weakest; they are also the stiffest and attract extra load away from the adjacent stronger bonds with less pinch-off. This problem is not as severe as it would seem at first sight because adhesive bonds are quite stiff in comparison with the extensibility of the adherends outside the joint. Nevertheless, the trend of this effect on the bonds is adverse and it provides a further reason to try and avoid the pinch-off problem by superior design and manufacturing techniques.

Since in a good bonded joint the adhesive is stronger than the adherends, this variable pinch-off effect should also be examined in the context of the adherends instead of the adhesive. It immediately becomes apparent that the variation in splice stiffness induces perturbations in the adherend stresses outside the joint. These will be quite small, but it must be remembered that very small changes in stress can produce a disproportionate change in fatigue life for long-life aircraft structure. Thus, the worst consequence of accepting severe pinch-off in the adhesive — even under circumstances in which the adhesive might very well be able to tolerate it — may well be a large weight penalty to reduce the adherend stresses in all of the structure outside the bonded joints themselves. This effect should also be remembered in establishing acceptance criteria for adhesive pinch-off. From any viewpoint whatever, it is better to eliminate the problem than to accept it in almost any case other than the most lightly loaded minimum-gage secondary structure.

CONCLUSIONS

This effort has investigated the effect on the load transfer through adhesively bonded joints of the precise joint details at the ends of the overlap. The prime interest has been in thickness of the adhesive layer here. The investigation covered both the adverse consequences of pinch-off as adhesive is squeezed out during cure and the benefits from deliberate thickening to improve the joint strength.

All of the analyses have been performed using the nonlinear continuum-mechanics based computer program A4EI, which accounts for variable adhesive properties as well as nonuniform adherend geometry. The hundreds of such cases run for the parametric studies reported here could not have been accomplished by finite-element analysis techniques.

While the A4EI program has been used to analyze joints with variable adhesive thickness or properties, some remarkably simple closed-form approximate solutions have been derived from the theory for uniform bonds. These compare well with the more precise solutions and provide a means of even simpler parametric study of these problems.

The variation in bond-line thickness has been studied in conjunction with tapering of the adherends near the ends of the overlap because of the need to reduce induced peel stresses in the adhesive to a level at which they can be ignored. Both the peak peel stresses and the peak shear stresses in the adhesive are intensified by any adhesive pinch-off in the adhesive at the ends of the overlap.

While the report characterizes the loss of strength due to pinch-off quantitatively for aluminum adherends and both ductile and brittle adhesives, several strong arguments are given as to why this problem is better eliminated than tolerated. These include the explanation of simple methods to counteract the problem before bonding occurs that require less effort than the more elaborate inspection needed afterwards if the pinch-off is not eliminated.

Even for the thin minimum-gage secondary structure in which the strength of the joint is very tolerant of severe pinch-off, the consequent redistribution of the loads outside the joint — as a function of variable stiffness bonds — is shown to possibly cause a reduction in the fatigue life of the basic structure, or to result in a weight penalty to absorb such stress concentrations in the adherends. This effect is more significant for more highly loaded structure.

41

REFERENCES

1. Volkersen, O., Die Nietkraftverteilung in Zugbeanspruchten Nietverbindungen mit Konstanten Laschenquerschnitten, Luftfahrtforschung 15, 4-47, 1938.

2. Goland, M. and Ressner, R., The Stresses in Cemented Joints, J. Appl. Mech., 11, A17-A27, 1944.

3. Hart-Smith, L. J., Adhesive-Bonded Double-Lap Joints, NASA CR-112235, January 1973.

4. Hart-Smith, L. J., Nonlinear Analysis of Adhesive-Bonded Stepped-Lap Joints and Doublers, Douglas Aircraft Company, USAF Contract Report AFWAL-TR-81-3154, February 1982, Section 2.

5. Hart-Smith, L. J., Further Developments in the Design and Analysis of Adhesive-Bonded Structural Joints, Douglas Aircraft Company Paper 6922, presented to ASTM Conference on Joining of Composite Materials, Minneapolis, Minnesota, April 1980.

6. Hart-Smith, L. J., Differences Between Adhesive Behavior in Test Coupons and Structural Joints, Douglas Aircraft Company Paper 7066, presented to ASTM Adhesives Committee D-14 Meeting, Phoenix, Arizona, March 1981.

7. Hart-Smith, L. J., Adhesive-Bonded Joints for Composites — Phenomenological Considerations, Douglas Aircraft Company Paper 6707, presented to Technology Conference Associates Conference on Advanced Composites Technology, El Segundo, California, March 1978.

8. Thrall, E. W., Jr., Failures in Adhesively Bonded Structure, Douglas Aircraft Company, Paper No. 6703, presented to AGARD-NATO Lecture Series No. 102, Bonded Joints and Preparation for Bonding, Lecture No. 5, Oslo, Norway and The Hague, Netherlands, April 1979 and Dayton, Ohio, October 1979.

9. Land, K. L., Lennert, L. B., et al, Primary Adhesively Bonded Structure Technology (PABST): Tooling, Fabrication and Quality Assurance Report, USAF Technical Report AFFDL-TR-79-3154, October 1979.

10. Hart-Smith, L. J., Basic Principles for the Tooling, Manufacture, and Design of Low-Cost Adhesive-Bonded Primary Aircraft Structures, Douglas Aircraft Company, to be published.

SECTION 3

EFFECTS OF FLAWS AND POROSITY
ON STRENGTH OF ADHESIVE-BONDED JOINTS

CONTENTS

INTRODUCTION

Most analyses of adhesively bonded structures have modeled the adhesive as being uniform and flawless throughout. The effects of flaws and porosity have historically been accounted for on the basis of coupon tests of flawed or porous bonds correlated with some form of ultrasonic nondestructive inspection, which is in turn related to the NDI of the bonded structures. This approach is itself flawed because the adhesive in short-overlap test coupons usually behaves very differently than it does in structurally proportioned, long-overlap bonded joints. In particular, the standard lap-shear test coupon (ASTM D 1002) suffers from a disproportionately severe induced peel stress in conjunction with the applied shear load, due to the relatively abrupt eccentricity in load path. That problem is aggravated by such testing of porous adhesive bonds because those bonds are necessarily thicker than unflawed bonds and that extra thickness adds to the eccentricity in load path. Furthermore, past assessments of porosity have not been able to account for the effects of variation in the adhesive bond thickness between the unflawed and porous areas within a single structural bonded joint. That variable-thickness effect is shown in this report to be of even greater significance than is the loss of bond strength in those porous areas. The effective softening of the porous bonds diverts the load elsewhere to adjacent thinner and stiffer bonds.

The prime emphasis of this report is, therefore, an analytical assessment of the influence of bond flaws and porosity as they occur naturally in structural adhesive bonded joints. The analyses are based on ideal elastic-plastic adhesive models and are either of closed form for simple joints between thin adherends, or performed by use of the Fortran computer program A4EI for complex stepped-lap joints. The mechanical behavior of porous bonds under shear loads has been determined experimentally (as part of this contract) using the thick-adherend specimen, and the results of these tests are given here. The explanation of the occurrence of adhesive porosity is related to the experimental techniques used to create it artificially for test purposes.

The aspects of the problem considered here include both thin, lightly loaded bonded structures (in which even grossly flawed adhesive bonds are stronger than the adherends outside the joint) and thick, heavily loaded joints in which even the smallest flaw could cause a catastrophic unzipping of the entire bond surface. The effects of porosity are shown to be more severe for brittle high-temperature adhesives than for ductile adhesives like those used on subsonic transport aircraft because the former have inherently less excess strength over the adherends than do the latter.

Some simple guidelines for how to cope with adhesive porosity are established here for thin adherends (for which porosity may be ignored in most cases); however, the problem is so complex for thick joints that the only universal rule that can be followed is to ensure that a fail-safe mechanical load path is available as well as the adhesive bond.

INSENSITIVITY OF THIN BONDED STRUCTURES TO FLAWS AND POROSITY

To understand the effects of flaws and porosity on the strength of adhesive-bonded joints, it is necessary first to characterize the behavior of such joints having no imperfections. Relatively thin, lightly loaded members are incapable of overloading the adhesive — the adherends break outside the joint. Much thicker members can transmit far greater loads and therefore are capable of failing any adhesive bonds between them. It follows then that, for each adhesive, there is a certain thickness of adherends for which the adherend strength precisely balances the shear strength of the adhesive (at least for a particular environment). One should infer, therefore, that relatively thin bonded structures should have considerable tolerances to bond flaws and any other imperfections or damage. Conversely, for the greater adherend thicknesses for which the adhesive is not strong enough to fail the adherends outside the joint, one would expect the bond to be very sensitive to any flaws and imperfections. Acceptance criteria for adhesive bond flaws and porosity must account for the thickness and strength of the members being joined as well as adhesive properties and the service environments. It is not possible to prescribe acceptance criteria for bond flaws based merely on the location and severity of flaws as assessed by nondestructive inspections.

The explanation above is portrayed for double-lap structural joints in Figure 1, which has been prepared on the assumption that adequate overlap has been specified to render the joint strength independent of that variable. It is evident that the prime effect of all kinds of bond
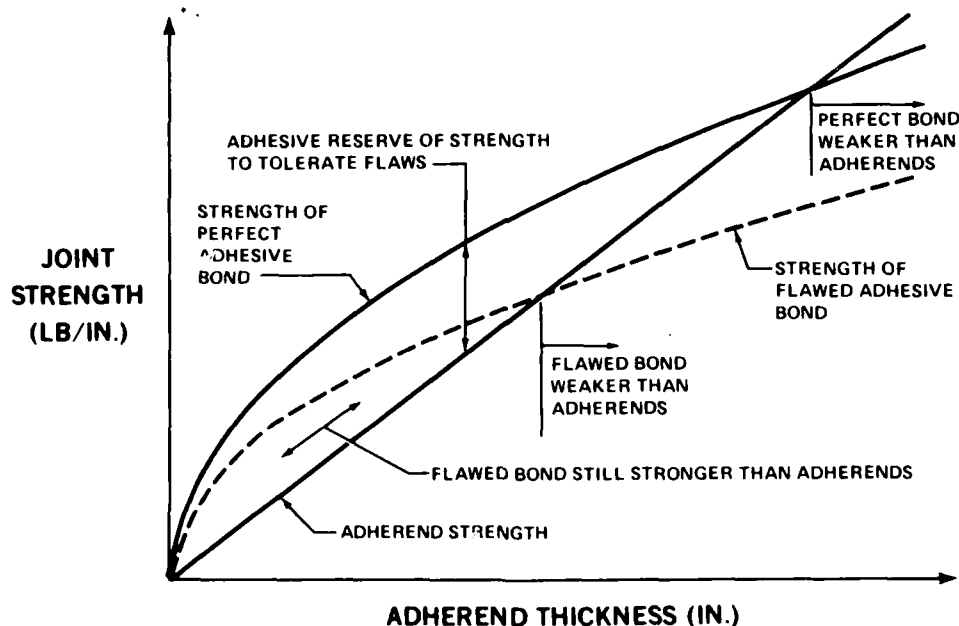

FIGURE 1. RELATIVE STRENGTH OF ADHESIVES AND ADHERENDS AS AFFECTED BY BOND FLAWS

46

flaws is a reduction in the thickness of members that can be bonded satisfactorily. For the thin adherends most suitable for bonding, even the flawed bonds are strong enough.

This insensitivity of adhesive bonds to flaws, for thin and only moderately thick structures, was explained during Douglas' PABST program work. Figures 2 to 5 show precise calculations for the three different flaws in bonded aluminum skin splices, using a 250°F cured ductile adhesive. The large areas of lightly loaded adhesive in Figure 2 provided ample reserve to rearrange the load transfer across the flaws. It is noteworthy that none of the flaws caused any increase in the peak bond stress induced by the constant load. The major effect detected is that the joint flexibilities in Figures 3 to 5 are slightly greater than shown in Figure 2 because more of the aluminum is more highly stressed. Consequently, in a real structure in which random bond flaws are surrounded by nominally perfect bonds, any flawed bonds divert some of their share of the load to the adjacent sound bonds. This two-dimensional load redistribution adds to the insensitivity shown by the one-dimensional analyses shown in Figures 2 to 5.

The benign characterization shown in the figures is typical of adhesive bonding in subsonic aircraft with a low-enough upper service temperature surface to permit the use of rubber- or nylon-modified epoxy or nitrile-phenolic adhesives. Such current and potential applications include control surfaces, fairings, fuselages, and horizontal and vertical tails for almost any size of aircraft. The wings of the general aviation aircraft also lend themselves to adhesive bonding, particularly since the bonding also provides excellent fuel tank sealing. However, the wings of larger aircraft require laminated structure to use bonding efficiently. It is not appropriate to simply replace rivets by adhesive bonding on large wing structures made from thick sheet and stiffeners.

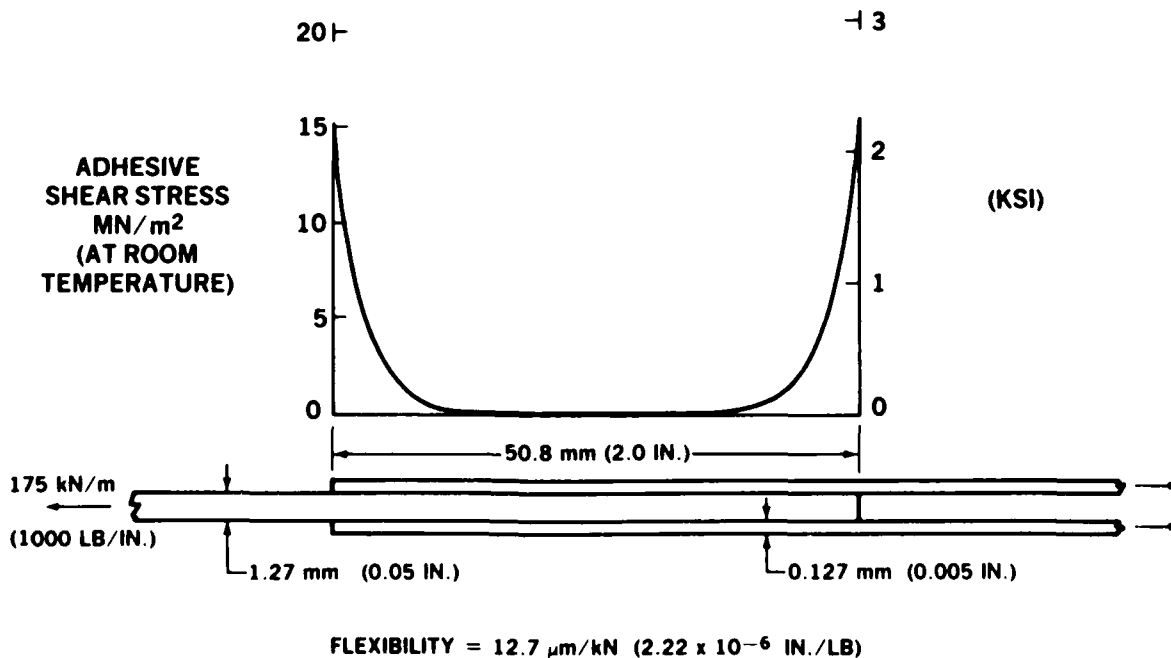FLEXIBILITY = 12.7 μm/kN (2.22 x 10⁻⁶ IN./LB)

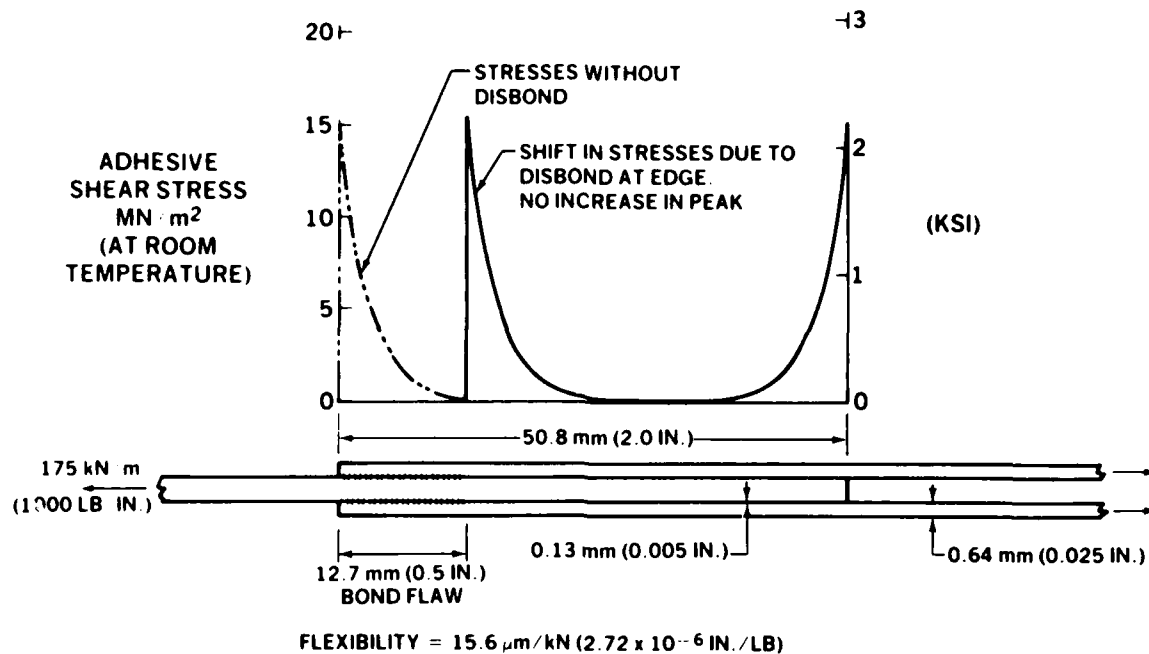FIGURE 2. ADHESIVE SHEAR STRESSES IN BONDED JOINTS

47

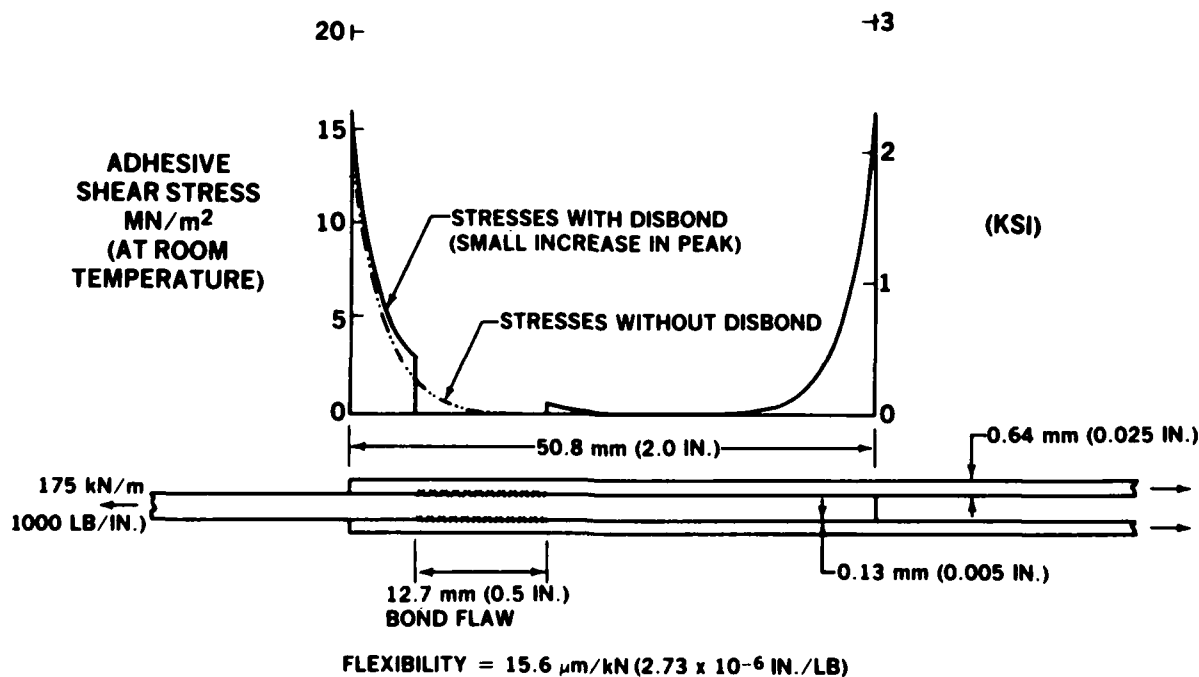FIGURE 3. ADHESIVE STRESSES IN EDGE-FLAWED BONDED JOINTS
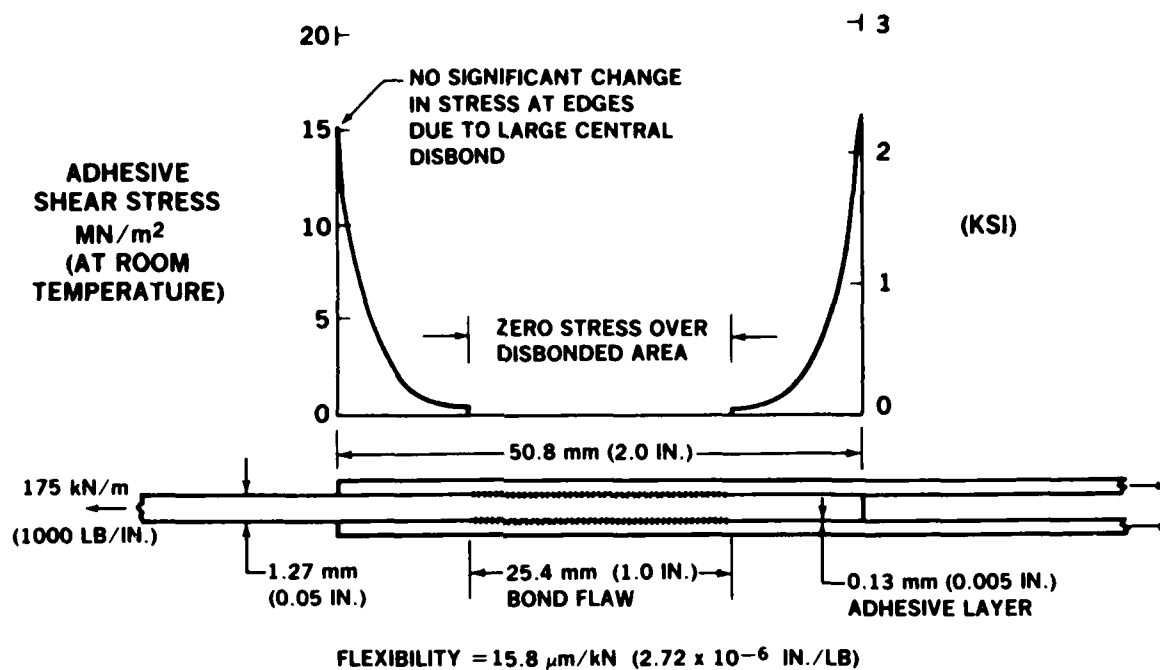

FIGURE 4. ADHESIVE STRESSES IN FLAWED BONDED JOINTS

48

FIGURE 5. ADHESIVE STRESSES IN CENTRALLY FLAWED BONDED JOINTS

EFFECT OF JOINT GEOMETRY AND SERVICE ENVIRONMENT
ON BOND STRENGTHS

One of the keys to establishing acceptance criteria for flaws and porosity in structural adhesive bonding is the determination of the transition point at which the strengths of the adhesive and adherends are equal. This balance is affected by the environment, as shown by a comparison of Figures 6 to 8. Each of these figures for double-lap joints shows how the adherend strength limits the peak adhesive shear strain in the adhesive for the lesser thicknesses but fails to do so for the thickest adherends, on the right. These same figures also show the drastic change in adhesive behavior between short-overlap test coupons and long-overlap structurally configured joints. Reference 1 contains a thorough discussion of these differences, in the context of the selection of meaningful adhesive bond test specimens and the pitfalls in the use of some of the standard coupons.

There is difficulty in associating a specific loss of bond strength with some ultrasonic assessment of a bond flaw if the data used for this correlation are based on the testing of short-overlap single-shear test coupons. Adhesive in structurally proportioned joints behaves very differently from that in short-overlap coupons, as is explained in Reference 1. The added complications from the inclusion of bond flaws exacerbates this confusion greatly and places great doubt upon many of the current practices used to assess the effects (as distinct from the presence) of all bond flaws. Therefore, the material in this section of the report is separated into discussions of flaws in structural joints, on the one hand, and test coupons on the other. It follows, however, that
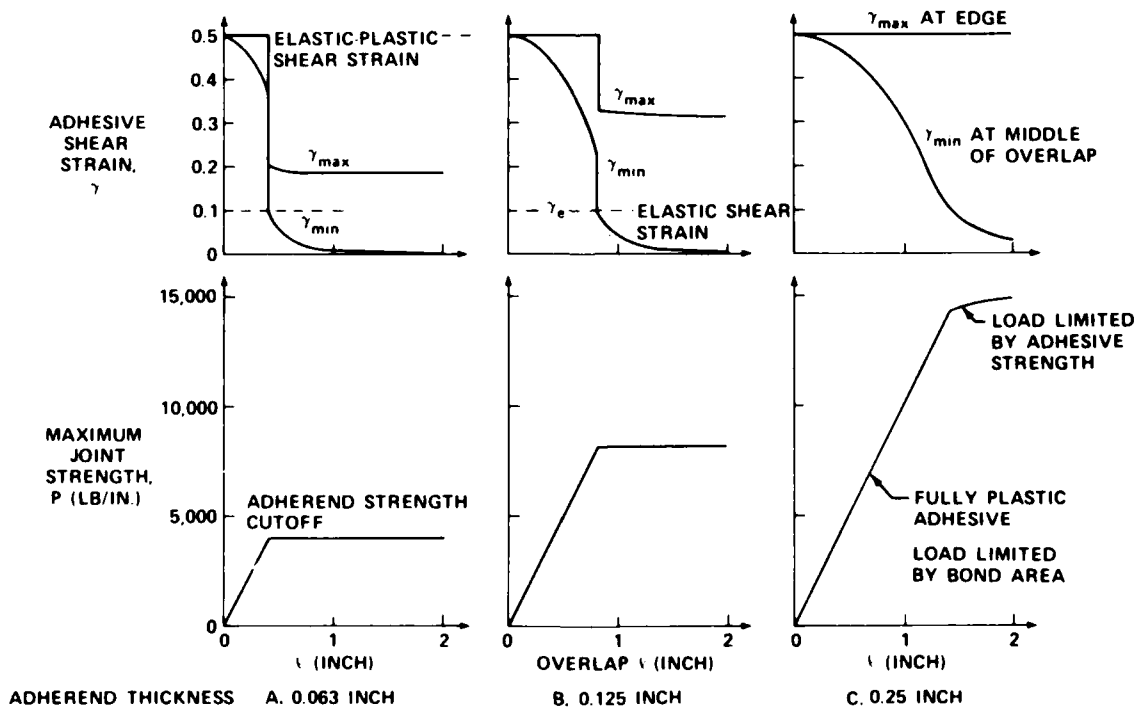
FIGURE 6. EFFECTS OF OVERLAP AND THICKNESS ON MAXIMUM AND MINIMUM ADHESIVE-BOND SHEAR STRAINS (ROOM TEMPERATURE)
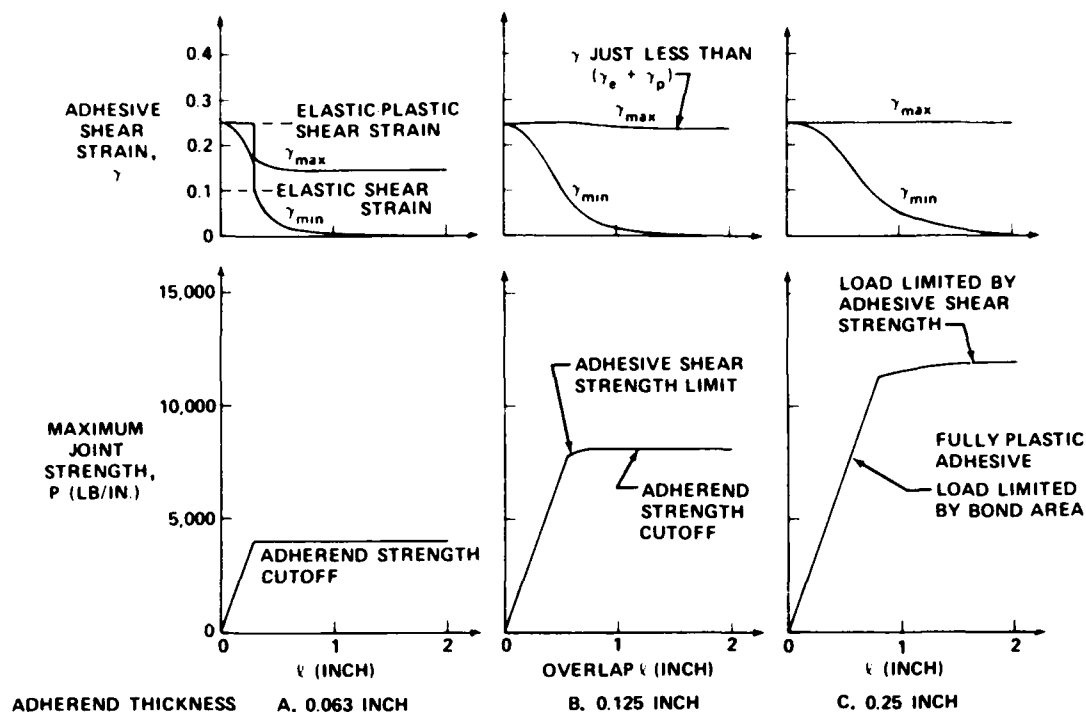
FIGURE 7. EFFECTS OF OVERLAP AND THICKNESS ON MAXIMUM AND MINIMUM ADHESIVE-BOND
SHEAR STRAINS (COLD ENVIRONMENT)

poorly designed structural joints — particularly any with high induced peel stresses — will be just as sensitive to bond flaws as the standard lap-shear test coupons are.

Within the range of long overlaps in structural joints, the bond shear strength is independent of the overlap, being given by the expression

$$P_b = 2\tau_{av}\ell = \sqrt{4\eta\tau_p\ (\frac{1}{2}\gamma_e + \gamma_p).\ 2Et} \tag{1}$$

These variables are defined in Figure 9 for a unit width strip of bond. Equation (1) has been extracted from Reference 2, which identifies the basic references for its derivation. The bond strength curves shown in Figure 1 are consistent with this equation. The strength is proportional to the square root of the adherend thickness as well as to the square root of the adhesive shear strain energy. The latter could be reduced by any flaws. The adherend strength, on the other hand, is directly proportional to its thickness:

$$P_a = F_y t \tag{2}$$

in which F_y is the adherend yield strength for sustained loading. The rapid application of loads usually gives the adhesive no opportunity to creep and, in many instances, F_y must be replaced by the ultimate strength, F_{ult}.

51
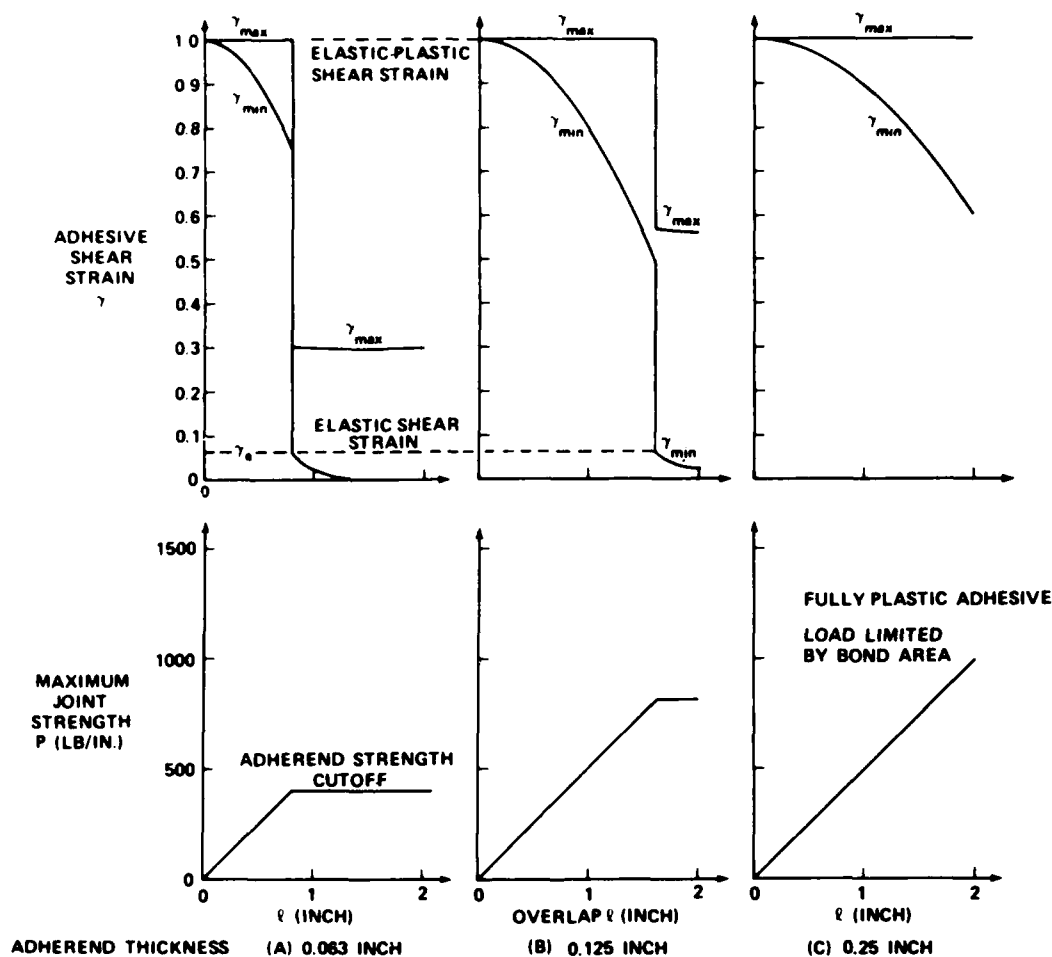
FIGURE 8. EFFECTS OF OVERLAP AND THICKNESS ON MAXIMUM AND MINIMUM ADHESIVE-BOND
SHEAR STRAINS (HOT WET ENVIRONMENT)

Those adhesives currently available that have a high enough service temperature for use around engines or on supersonic aircraft are very brittle. Therefore the strengths of joints made with such adhesives are much less than with ductile adhesives, as can be deduced from Equation (1). It should be noted that this potential bond shear strength is not sensitive to the individual adhesive properties, but to the adhesive shear strain energy explicitly. The higher shear stress τ_p of the brittle adhesives is more than offset by the much lower strain $(\gamma_e + \gamma_p)$ to failure. Consequently, brittle adhesives are far more sensitive to the effects of bond flaws and porosity. This weakness is usually accommodated by increasing the joint strength through greater geometric complexity, as with stepped-lap joints, and by cocuring and bonding composite structures directly onto metal adherends or fittings to ensure an excellent fit and minimize the occurrence of any bond flaws.

Equation (1) can be rearranged to express the maximum induced adhesive shear strain as a function of the applied load. Thus

$$\gamma_{max} = \tfrac{1}{2}\gamma_e + \frac{P^2}{8Et\eta\tau_p} \qquad (3)$$
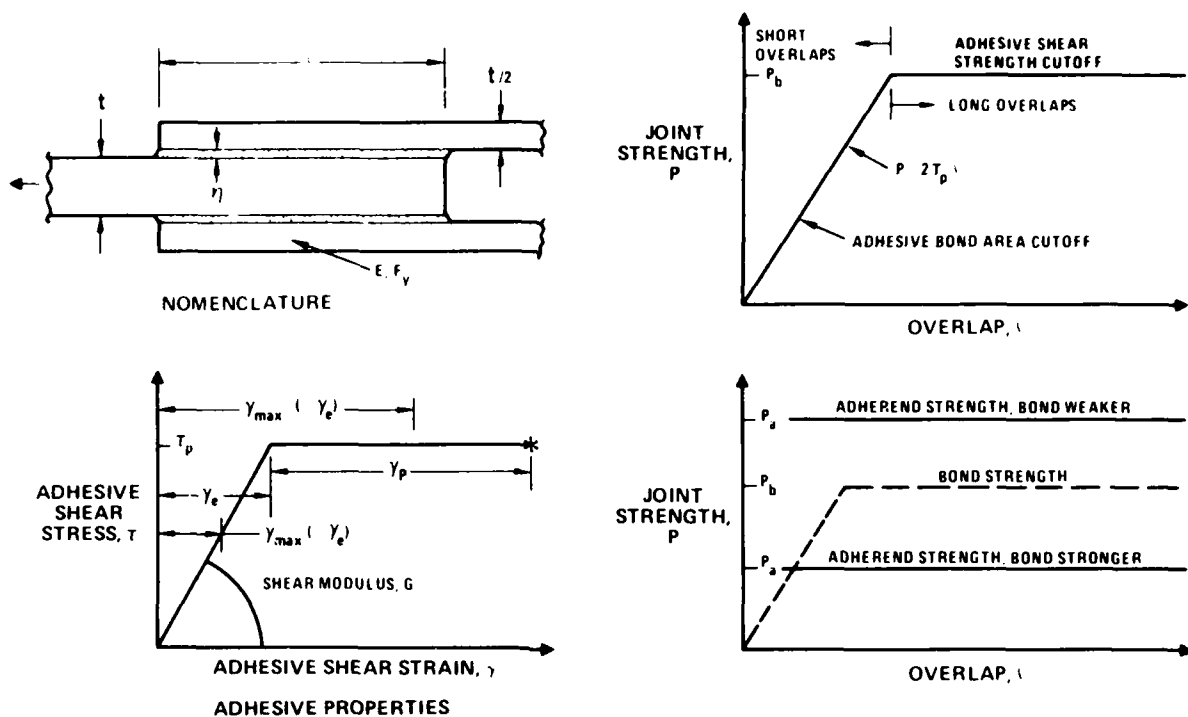
FIGURE 9. INFLUENCE OF JOINT GEOMETRY ON ADHESIVE BOND STRENGTH

and, to the right of the transitions in Figure 1,

$$\gamma_{max} = \gamma_{ult} \tag{4}$$

as the adhesive limits the load which the joint can withstand. This flaw-intolerant regime requires mechanical fastening to provide adequate fail-safety in the structure and is discussed below after the flaw-tolerant regime has been explored.

When the load transferred through the joint is limited by the adherend strength, Equation (3) is reexpressed in the form

$$\gamma_{max} = \tfrac{1}{2}\gamma_e + \frac{\sigma^2 t}{8E\eta\tau_p} \qquad (\gamma_{max} \geq \gamma_e) \tag{5}$$

or, if the load is so light as not to exceed the adhesive elastic capability,

$$\gamma_{max} = \frac{\sigma}{2}\sqrt{\frac{t}{EG\eta}} \qquad (\gamma_{max} \leq \gamma_e) \tag{6}$$

Here, σ is the adherend stress outside the bonded joint.

53

The service environment changes the adhesive properties τ_p, γ_e, γ_{ult}, and G as shown in Figure 10. Consequently, the peak adhesive shear strain induced by a given external load also changes. However, since the strain to failure also changes with environment, it is usually not possible to predetermine the most severe environment which limits a joint's design strength. Nevertheless, it is almost invariably the hot/wet upper limit on environment which is used to size the bonded overlap, as explained in Reference 2. Were adhesive porosity uniformly distributed over the bond area, the effect on bonded joint strengths could be characterized uniquely in terms of a modified stress-strain curve, just as for a change in environment. Some such stress-strain curves for porous bond lines have been generated under this contract and the peak shear stress, strain to failure, and initial modulus are all influenced by the porosity. However, porosity is not uniformly distributed over the bond area in structural joints. Furthermore, porosity is associated with slightly excessive bond layer thickness, as discussed below. So the influence of adhesive porosity on the strength of bonded joints cannot be characterized as simply as the pinchoff at the edges of bonds was in Section 2.
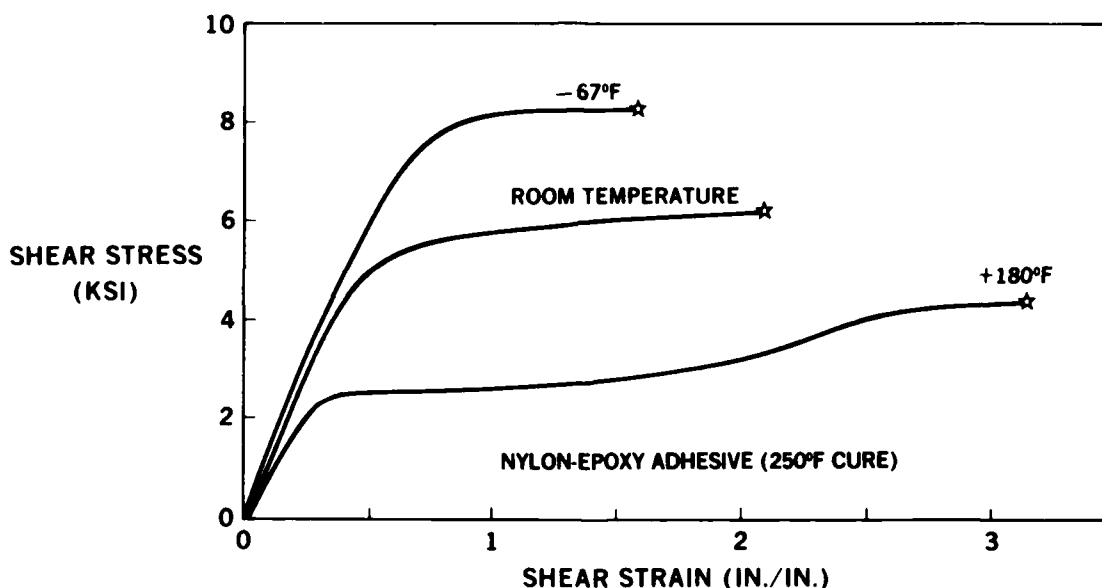
FIGURE 10. EFFECT OF TEMPERATURE ON ADHESIVE STRESS-STRAIN CURVES IN SHEAR

Returning now to the key problem in Figure 1 — the adherend thickness beyond which any bond flaw (no matter how small) will cause a loss of bond strength — Equations (1) and (2) can be rearranged in the form

$$t_{cr} = \frac{P^2}{8E\eta\tau_p\,(\tfrac{1}{2}\gamma_e + \gamma_p)}, \qquad \text{for } P = F_y\, t, \qquad (7)$$

whence

$$\frac{t_{cr}}{\eta} = \frac{8E\tau_p\,(\tfrac{1}{2}\gamma_e + \gamma_p)}{F_y^2} = 4 \times \frac{\text{ADHESIVE STRAIN ENERGY}}{\text{ADHEREND ELASTIC STRAIN ENERGY}} \qquad (8)$$

54

This formula is consistent with obvious expectations that the stronger adhesives can bond thicker adherends of a given material and that a given adhesive can bond only thinner sections of stronger adherends.

ONE-DIMENSIONAL ASSESSMENT OF ACCEPTABLE ADHESIVE BOND FLAWS

The preceding discussion of the behavior of structural bonded joints without flaws provides the framework in which to examine the effects of bond flaws. The first regime to be characterized is that of thin adherends — for which some flaws can be tolerated without loss of joint strength or durability. The simplest way of looking at this problem is to isolate a single strip while ignoring two-dimensional effects due to interactions with adjacent strips. Such more complex effects are introduced later in this report.

Figure 11 presents a qualitative description of the method for establishing acceptable bond flaws. The key to this method is the typical nonuniform adhesive shear stress distribution shown in Figure 2. The proportionally large areas of lightly loaded adhesive which ensure creep resistance can be used instead to redistribute the load transfer, as in Figures 3 to 5, with the creep resistance now depending on adjacent unflawed bonds, if necessary. It must be realized that, even with flawed adhesive bonds, it is as important to restrict the minimum adhesive shear strain as it is the maximum. Figures 6 to 8 show how the minimum adhesive shear strain in a bond is raised as the total (or effective) bonded overlap is reduced. Clearly, as the slow-cycle testing of short-overlap bonded test coupons at the start of the PABST program showed, a flaw so large as to reduce the effective bond overlap to less than that needed to transfer the entire load in a fully-plastic adhesive behavior would be unacceptable in the long term, even it it could be shown to have adequate short-term static strength. Figures 6 to 8 show that, for overlaps less than the transition and for each adherend thickness and environment, the minimum adhesive shear strain (in the middle of the overlap) is almost as high as the maximum (at the edges). The central curves in Figure 7 correspond almost precisely with the transition shown in Figure 1 in the sense that the adherend and adhesive bond strengths are almost precisely equal. In this case there is no marked transition of the type shown in the middle curves of Figure 6. Yet the middle curves in Figure 7 show how some minimum effective bond overlap must still be maintained in order to restrict the minimum adhesive shear strain and prevent further damage to the bond.
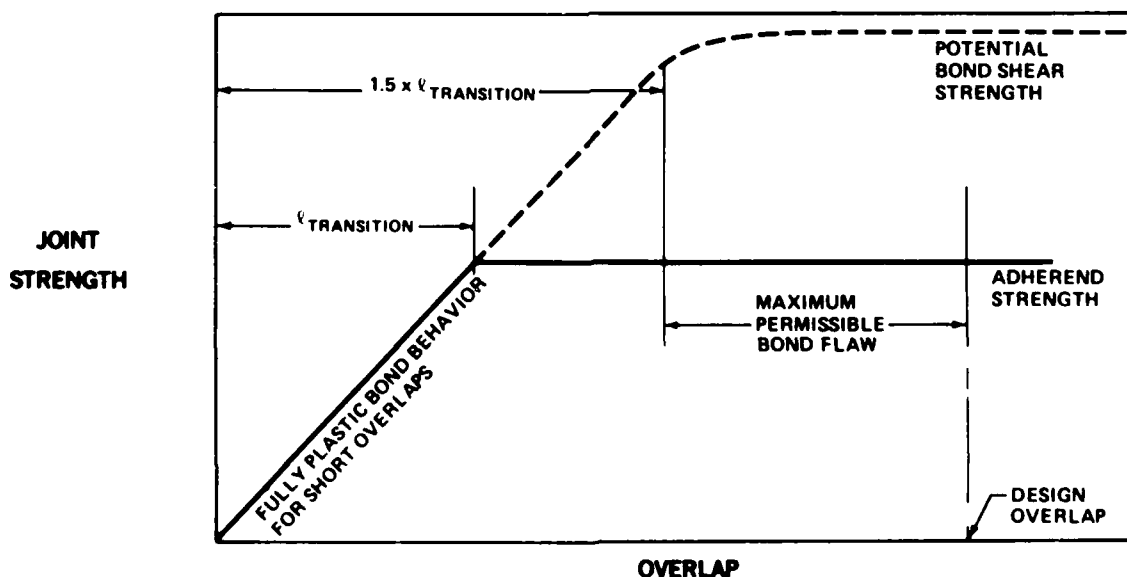

FIGURE 11. ESTABLISHMENT OF MAXIMUM PERMISSIBLE ADHESIVE BOND LOCAL FLAW SIZES
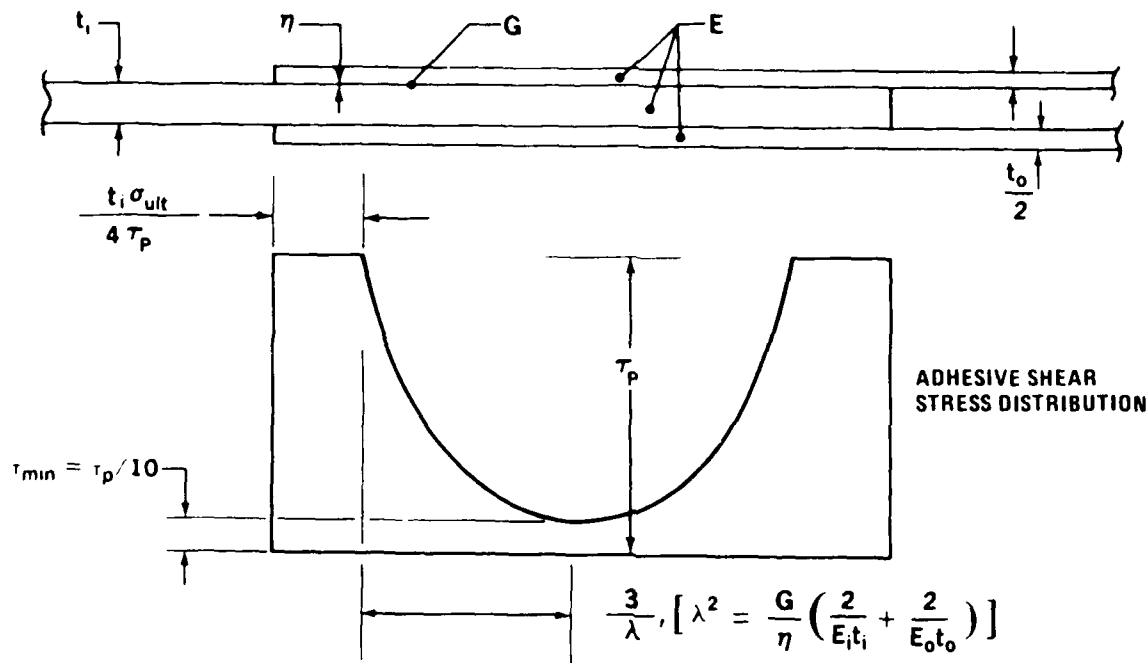
The very short overlaps at the left of each curve in Figures 6 to 8 are associated with no creep resistance, so the adhesive strains to the maximum extent possible and fails. That would not be possible in a locally grossly flawed structural adhesive bond if there were nearby areas of intact bond. The relative motion between the adherends would actually be limited by those adjacent areas with the strains reduced as at the right hand ends of the curves in Figures 6 to 8. Even with a gross local flaw, the adhesive could not creep indefinitely, but would be restricted to strains no worse than those just to the right of the transition in Figures 6 to 8. While that imposes an acceptable limit on the maximum adhesive strains, the minimum strains would be unacceptably high for sustained operation without repair. That is why the minimum acceptable effective overlap that does not need repairing (but may still need sealing) has been set in Figure 11 at 1.5 times the overlap associated with fully plastic behavior. In the short term, one could even tolerate a finite length of complete disbond without any fear that the adjacent bond would unzip, provided that the adjacent adhesive bond is stronger than the adherends. This is explained in the section below on two-dimensional load redistributions. However, there are as yet no adequate analysis methods for assessing the consequent stress concentrations in the adherends just outside the disbond. The problem is somewhat like the classical skin crack, but some of the structure is stiffened asymmetrically by the splice and the adhesive permits far more flexibility at the "crack" tip than plain metal adherends would permit.

The design overlaps in Figure 11 are established in Figure 12 as the sum of separate calculations of the plastic and elastic adhesive zones. These calculations can be approximated by the simple rule of thumb that the overlap in double shear should be about 30 times the central adherend thickness for the ductile adhesives used on subsonic transport aircraft made from aluminum alloys. More precise evaluations are given in Figure 13. Shorter overlaps could perhaps be prescribed for the stiffer, more brittle adhesives used for higher service temperatures but, remembering that the overlaps are set by the (different) highest services temperature (for which the adhesive is softest), the overlaps would not be all that much shorter. The brittle adhesives would need to be restricted to use on only the thinner adherends also, unless laminated structure or stepped-lap joints were used.

The overlaps given in Figure 13 can be approximated by the rule that the overlap in double shear should be 30 times the central adherend thickness. Also, the sum of the plastic zones is given in Figure 12 by the expression

$$\ell_p = F_{tu} t_1 / (2\tau_p) \approx 14t \tag{9}$$

Allowing for the 1.5 factor used in Figure 11 to retain some creep resistance, one can conclude that a total effective loss of about one-third of the bonded overlap can be tolerated at any one local area and that in the absence of sustained loads (as due to cabin pressure), only about half the total bond area is needed to transfer the load. It should be noted that these factors (for typical ductile adhesive used on aluminum-alloy subsonic transport aircraft) do not imply unnecessary conservation in the basic design — the total overlap is set by creep resistance, and flaws of as much as one-third or one-half the bond area can be tolerated locally only if the adjacent bond areas are intact.

ADHESIVE SHEAR STRESS DISTRIBUTION

$$\frac{3}{\lambda} \cdot \left[\lambda^2 = \frac{G}{\eta}\left(\frac{2}{E_i t_i} + \frac{2}{E_o t_o}\right)\right]$$

● PLASTIC ZONES LONG ENOUGH FOR ULTIMATE LOAD
● ELASTIC TROUGH WIDE ENOUGH TO PREVENT CREEP AT MIDDLE
● CHECK FOR ADEQUATE STRENGTH

FIGURE 12. DESIGN OF DOUBLE-LAP BONDED JOINTS

The logic above can be expressed mathematically, to cover different kinds of adhesive also. The design overlap is given in Figure 12 for double shear as

$$\ell = \ell_p + \ell_e = \frac{F_{tu} t_i}{2\tau_p} + \frac{6}{\lambda} \tag{10}$$

in which

$$\lambda^2 = \frac{G}{\eta}\left(\frac{2}{E_i t_i} + \frac{2}{E_o t_o}\right) \tag{11}$$

Based on the interpretation of tolerable flaws in Figure 11, the desired effective bond must be at least as long as

$$\ell_{min} = 1.5 \times \frac{F_{tu} t_i}{2\tau_p} \tag{12}$$

58

CENTRAL SHEET THICKNESS t_i (IN.)	0.040	0.050	0.063	0.071	0.080	0.090	0.100	0.125
SPLICE SHEET THICKNESS t_o (IN.)	0.025	0.032	0.040	0.040	0.050	0.050	0.063	0.071
RECOMMENDED OVERLAP[1] ℓ (IN.)	1.21	1.42	1.68	1.84	2.01	2.20	2.39	2.84
STRENGTH OF 2024-T3 ALUMINUM (LB/IN.)	2600	3250	4095	4615	5200	5850	6500	8125
POTENTIAL ULTIMATE BOND STRENGTH (LB/IN.)[2,3]	7699	8562	9628	10,504	10,888	11,865	12,151	13,910

[1]BASED ON 160°F DRY OR 140°F/100-PERCENT RH PROPERTIES NEEDING LONGEST OVERLAP.

VALUES APPLY FOR TENSILE OR COMPRESSIVE IN-PLANE LOADING. FOR IN-PLANE SHEAR LOADING, SLIGHTLY DIFFERENT LENGTHS APPLY.

[2]BASED ON -50°F PROPERTIES GIVING LOWEST JOINT STRENGTH AND ASSUMING TAPER OF OUTER SPLICE STRAPS THICKER THAN 0.050 IN. STRENGTH VALUES CORRECTED FOR ADHEREND STIFFNESS IMBALANCE.

[3]FOR NOMINAL ADHESIVE THICKNESS $\eta = 0.005$ IN. FOR OTHER THICKNESSES, MODIFY STRENGTHS IN RATIO $\sqrt{\eta/0.005}$.
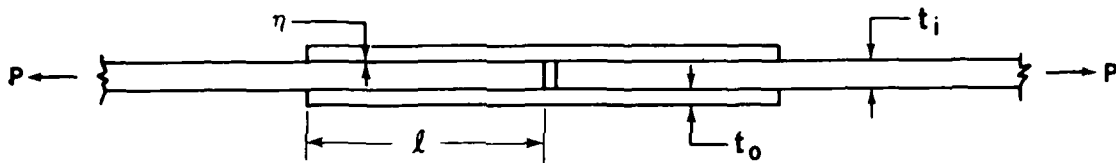
FIGURE 13. DESIGN OVERLAPS USED FOR PABST SKIN SPLICES

with the factor 1.5 being optional in the absence of sustained loads. The tolerable flaw size is expressed by the difference between equations (10) and (12). Thus

$$\ell_{flaw} = \ell - \ell_{min} = \frac{6}{\lambda} - \frac{\ell_p}{2} . \tag{13}$$

Sample evaluations of this formula for brittle adhesives give much the same order of magnitudes as for ductile adhesives. Again, the tolerable flaws amount to between one-third and one-half of the overlap.

The subject of flaws in single-lap bonded joints is much more complex than for double-lap joints due to an added sensitivity to the position of the flaws. Flaws are more tolerable in the middle of an overlap because they don't decrease the effective bond length which permits deflections to alleviate the effects of the eccentricity in load path. The analysis of single-lap bonded joints is explained in Reference 3. Any reduction in the effective overlap-to-thickness ratio imposes an immediate increase in the adhesive peel stress and the adherend bending moment at the ends of the effective bond and must, therefore, be considered unacceptable. Fortunately most flaws occur away from the edges of the overlap and, elsewhere, the single-lap bonded joints have even more

tolerance of bond flaws than do the double-lap joints because of their greater overlap. For the single-lap joints used on the PABST program, the joints were sized by the formula

$$\ell = 80t. \tag{14}$$

as a compromise between joint weight and the structural efficiency of the entire skin panel. In view of the 30:1 ratio discussed above for double-lap joints, the 80:1 in equation (13) need have been only 60:1 if adhesive shear had been the critical design condition. Figure 14 explains the mechanism of the eccentricity in load path for adhesive-bonded single-lap joints while Figure 15 quantifies the analysis for aluminium adherends. The joint strength could, in the limit, change by as much as a factor of four due to different overlaps. This is evident from the circles on the left and right scales, each pair being associated with a single curve.

The philosophy behind Figure 11 can be modified quite simply for single-lap joints. It should be assumed that there is a structurally sound area of bond, adjacent to each end of the overlap, which is sufficient to transfer the load. That extent of bond, at each end of the overlap, would be

$$\frac{\ell_p}{2} = \frac{F_{tu} t}{2\tau_p} \tag{15}$$

evaluated for that condition giving the lowest value of the adhesive plastic shear stress τ_p within the service environments. The same factor 1.5 in Figure 11 should suffice for creep resistance, but that extra bond area need not be attached to the intact end zones. Tolerable total effective flaw size for single-lap joints then follows as

$$\ell_{flaw} = \ell - 3F_{tu} t/\tau_p \tag{16}$$

LOW LOAD LEVEL

MAXIMUM STRESS CONCENTRATION

DEFORMATION OF ADHERENDS UNDER MODERATE LOAD

"INTERLAMINAR" FAILURE OF FILAMENTARY COMPOSITE ADHERENDS

PLASTIC HINGES

HIGH LOAD LEVEL (METAL ADHERENDS)

PERMANENTLY DEFORMED (METAL) ADHERENDS AFTER FAILURE OF ADHESIVE
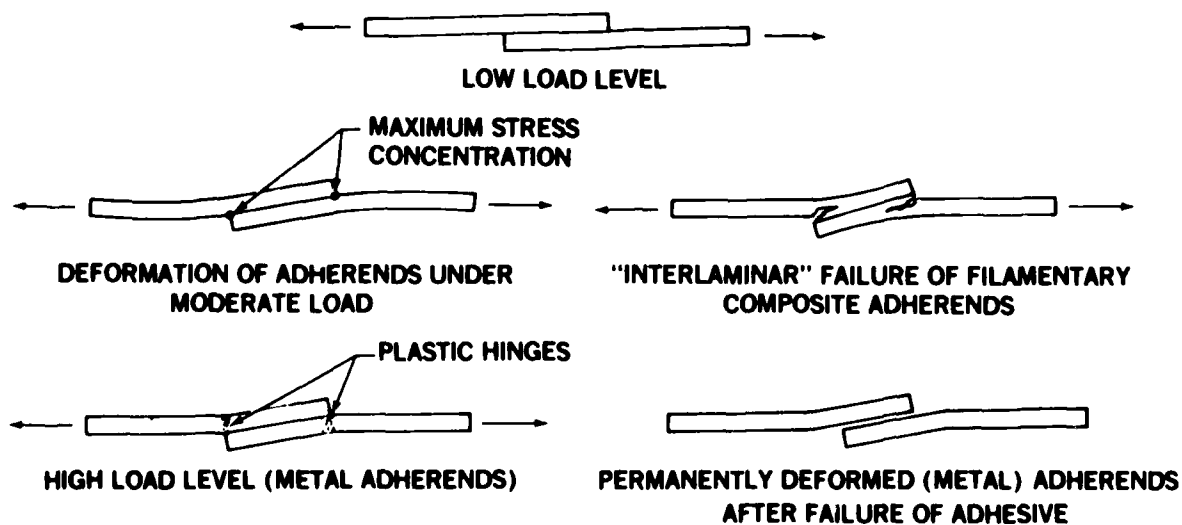
FIGURE 14. SINGLE-LAP BONDED JOINTS WITH ECCENTRIC LOAD PATH (BRITTLE AND DUCTILE ADHERENDS)
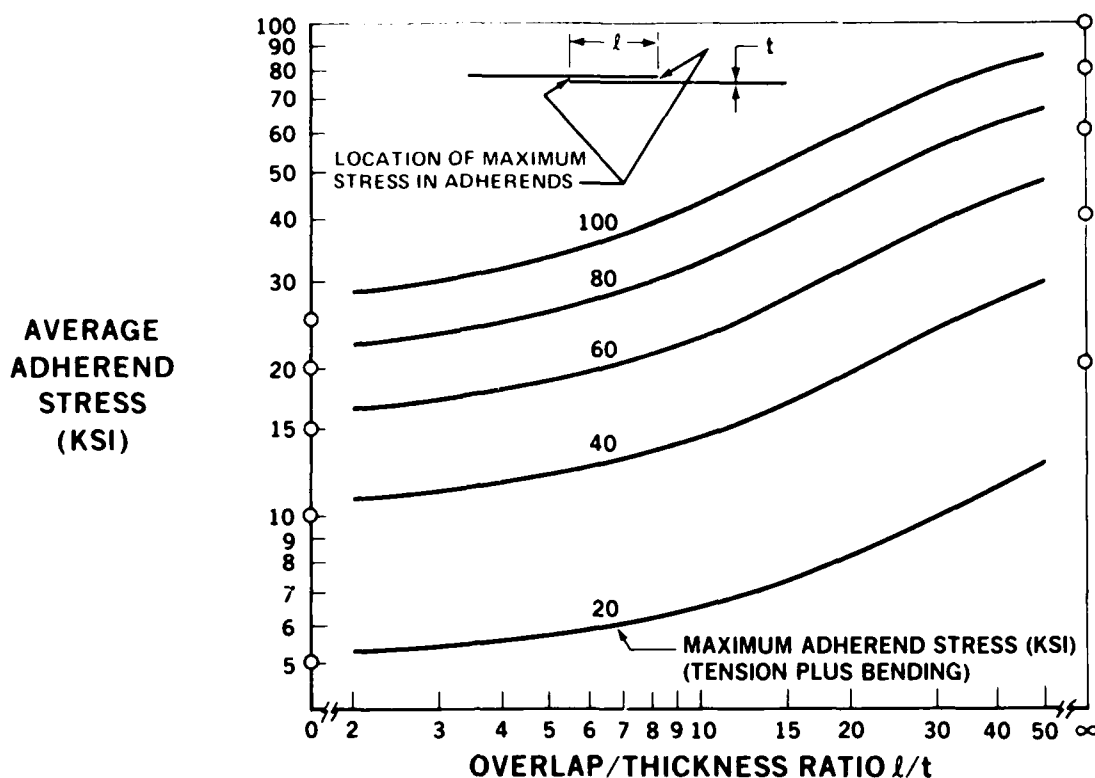
FIGURE 15. STRESS AMPLIFICATION OF SINGLE-LAP JOINTS DUE TO ECCENTRICITY IN LOAD PATH

and must not be closer to an end of the overlap than $\ell_p/2$, as given in equation (15). Since for the double-lap joint some half of the total overlap was needed to transfer the load (in double shear), as per equation (9), that would amount to about 30t in single shear out of a total of between 80t and 100t, so the interior of single-lap bonded joints can tolerate proportionally greater flaws than even the remarkable tolerance demonstrated by the double-lap joints tested during the PABST program.

This somewhat benign assessment of flaws and porosity in long-overlap (structural) single-lap joints does not extend to short-overlap lap-shear test coupons. Bond flaws and porosity are associated with thicker than normal bonds and that results in an increased eccentricity in the load path. That, in turn, weakens such short-overlap bonds even more than the loss in the mechanical properties alone.

It is perhaps appropriate to point out here that the prime interests in assessing the effects of bond flaws extend beyond the obvious one of safety. Structurally unnecessary bond repairs often *reduce* the life of bonded structure because the repair frequently breaks the anodize which protects the bonded surfaces. For the same reason, trimming edges on assembly and drilling fastener holes in bonded panels should always be avoided by performing those operations before anodizing wherever possible. When that cannot be done, such areas should be alodined and protected by sealant.

61

TWO-DIMENSIONAL ASSESSMENT OF ADHESIVE BOND FLAWS

The one-dimensional, or local, bond flaws discussed above can often be tolerated indefinitely. This is because they rely on adjacent intact bonds to prevent any load redistribution. In such cases it is preferable to not repair the flaws at all, but to only seal them against ingress of moisture, if necessary. Some much larger flaws can be tolerated for a short time on the basis of there being no possibility of any catastrophic unzipping of adjacent previously intact bond areas. However, the associated two-dimensional redistribution of the load transfer increases the load locally in the adherends and that can reduce the life of the structure if it is not repaired.

In the extreme, a large enough bond flaw can cause a catastrophic failure not of the adhesive but of the adherends adjacent to the flaw. This phenomenon is explained in Figure 16. The behavior is closely akin to that of a finite-length crack in a metal sheet. Provided that the adhesive bond adjacent to the large flaw is intact and that the joint has been properly proportioned, the flaw in the bond cannot grow because the adherends in Figure 16 are simply not strong enough to over-load the bond anywhere. This can be understood by considering the thinner adherends in Figures 6 to 8. The consequences of such large bond flaws cannot be predicted on the basis of any analysis of the flaw alone. It is probable that the appropriate analysis is that of a cracked sheet, modified somehow to account for the added flexibility of the adhesive-bonded joint and for the added stiffness of the splice area. Thus, the analysis of the adhesive bond in such a situation would serve only as the generation of input data for the more general problem. As such, it is considered beyond the scope of this report.
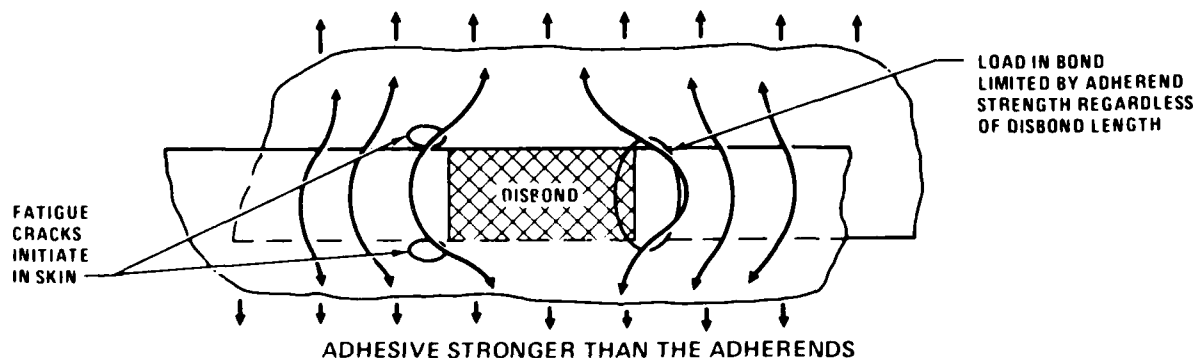
FIGURE 16. LOAD REDISTRIBUTION AROUND TWO-DIMENSIONAL ADHESIVE-BOND FLAWS

A large disbond can be made to spread if the adhesive rather than the adherends is the weak link. This behavior can be prevented, or contained, only by an alternative mechanical load path, as shown in Figure 17. Without the fasteners, the disbond growth would be unlimited and potentially instantaneously catastrophic. Two effects result from the incorporation of the fasteners in such a design. The first is that, as the disbond grows and the fasteners in the middle of the disbond are then able to accept load (due to the additional relative deformation between the sheets), the load intensity around the edges of the disbond decreases progressively until the disbond growth is arrested. Those fasteners in the areas of intact bond never transfer any load because their flexibility is so much greater than that of the adhesive. The second effect is that the

62

DISBOND GROWTH
ARRESTED ONCE
FASTENERS ACCEPT
LOAD IN DISBOND AREA

LIFE LIMITED BY CRACK
INITIATION AT MOST
HIGHLY LOADED FASTENER

DISBOND

ADHESIVE
BOND

ADHESIVE WEAKER THAN THE ADHERENDS
(FASTENERS NECESSARY TO PROVIDE FAIL SAFETY AND
PREVENT CATASTROPHIC UNZIPPING OF BOND)
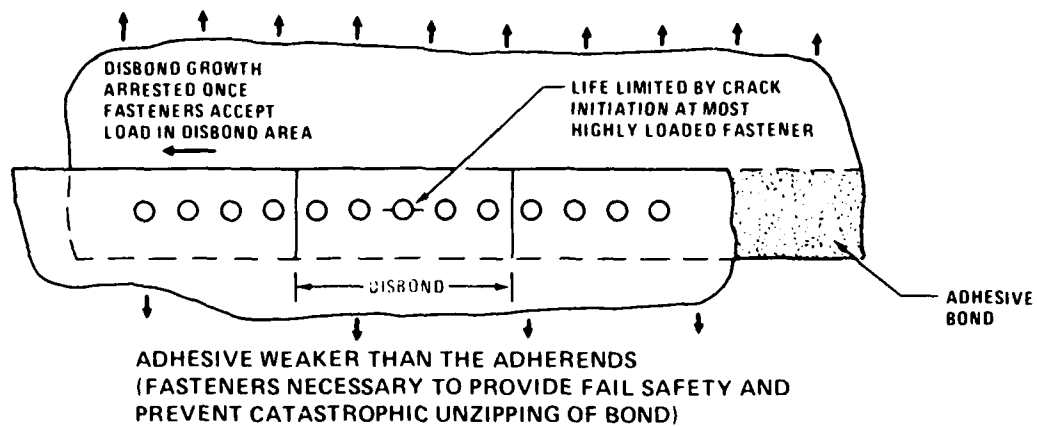
FIGURE 17. LOAD TRANSFER THROUGH RIVETS IN DISBOND AREA

maximum load transfer through the fasteners will occur at the middle of the disbond and will probably eventually result in the initiation of cracks from such fasteners, as shown in Figure 17. At that stage, the appropriate analysis is that for unbonded structure since there are no critical conditions in any of the intact adhesive.

While flaws of the type shown in Figures 16 and 17 are tolerable from certain viewpoints, they obviously would need prompt repair to prevent corrosion and any flaw propagation by the freeze/thaw cycle associated with water in the disbond.

THE NATURE AND OCCURRENCE OF POROSITY IN ADHESIVE BONDS

The discussions above have been illustrated in terms of complete local flaws. However, there is nothing inherent in the logic which prevents partial flaws, or porosity, from being considered from the same viewpoints. Indeed, the techniques needed to artificially create porosity in test coupons make it clear that porosity is just one of a family of adhesive bond flaws. Porosity can be created by bonding plates together while they are separated by spacer shims, as shown in Figure 18. The thickness of the shims is critical as is evident from the ultrasonic inspection records in Figure 19. Even thicker shims — 0.020 inch, for example — would result in all of the adhesive being attached to only one sheet. Thus porosity is created throughout a range of gaps which are slightly too great for the adhesive to fill. The exact range of gaps will vary with the adhesive type, the presence or absence of any multiple adhesive films, the minimum adhesive viscosity during cure, and other factors such as the presence or absence of edge dams. Porosity is inevitably associated with glue-layer thicknesses greater than those which produce flawless bonds.

The characterization of the load transfer through porous adhesive bonds requires a stress-strain curve in shear. Such tests have been conducted as part of this program and several such curves are shown in Figures 20 to 31, for the ductile FM-73 adhesive and the brittle FM-400 adhesive, both with and without porosity and for a range of service environments.

The precise degrees of porosity have yet to be estimated. Some effects of the porosity are clear while others are somewhat ambiguous. There is a consistent loss of adhesive shear stress, both at the knee and at failure, due to the presence of porosity. There is some indication of a loss of
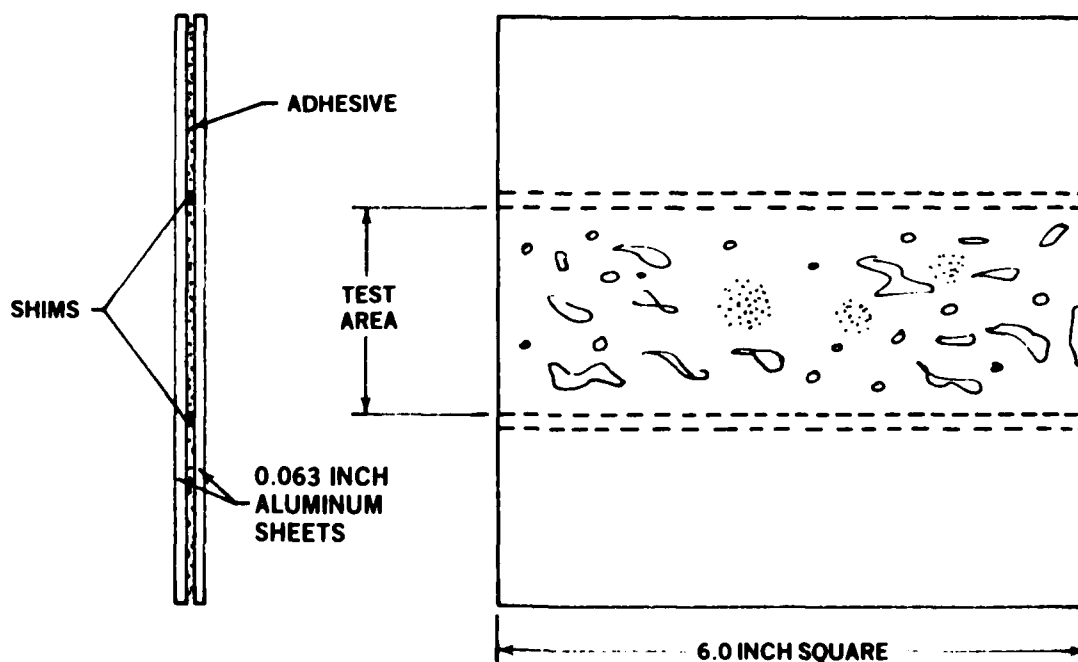
FIGURE 18. TEST SPECIMEN FOR CREATING POROSITY IN ADHESIVE-BONDED JOINTS

64

FM-73 ADHESIVE, SINGLE LAYER
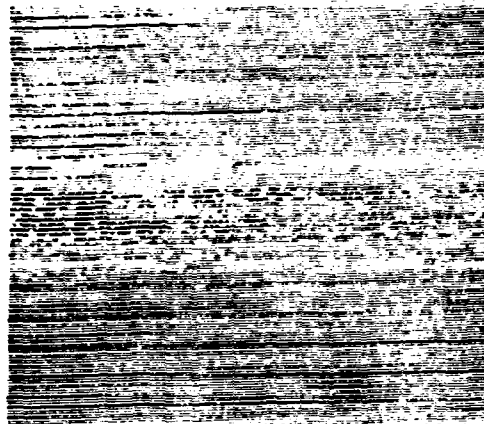
0.010 INCH SHIMS
UNIFORM POROSITY
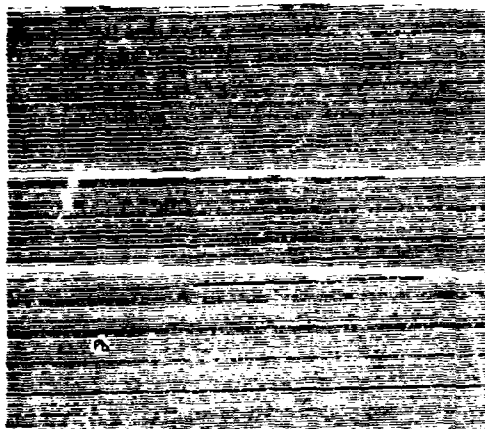
0.005 INCH SHIMS
NEGLIGIBLE POROSITY

0.015 INCH SHIMS
EXCESSIVE POROSITY

ULTRASONIC THROUGH TRANSMISSION
0.063 INCH ALUMINUM SHEETS

SCALE: (INCHES)

FIGURE 19. C-SCAN RECORDS OF POROSITY IN ADHESIVE BONDS

FM-73 ADHESIVE, BR-127 PRIMER, BOND THICKNESS = 0.0067 INCH,
TESTED AT ROOM TEMPERATURE

INITIAL SHEAR MODULUS = 72,500 PSI (AVERAGE OF BOTH READINGS)
INITIAL SHEAR MODULUS = 72,000 PSI (THIS CURVE)
SECANT MODULUS AT KNEE = 45,300 PSI
SHEAR STRESS AT KNEE = 4,764 PSI
ULTIMATE SHEAR STRESS = 5,585 PSI
ULTIMATE SHEAR STRAIN = 0.72
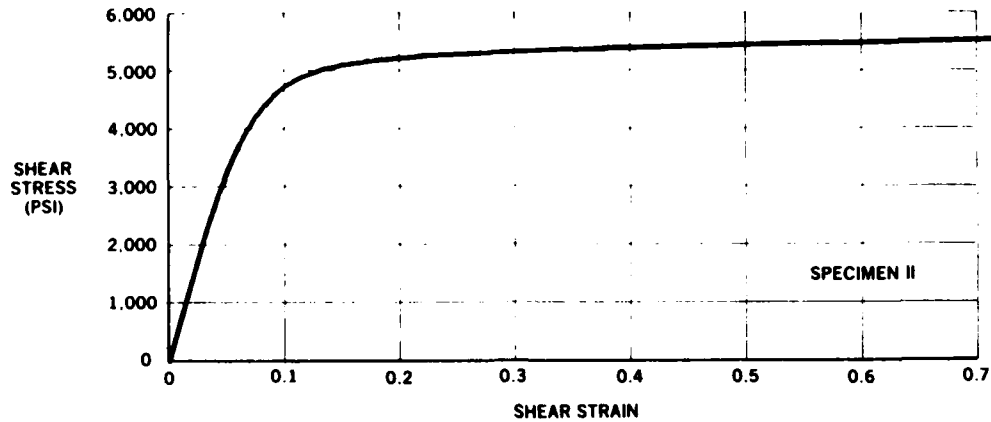
FIGURE 20. ADHESIVE STRESS-STRAIN CURVE IN SHEAR
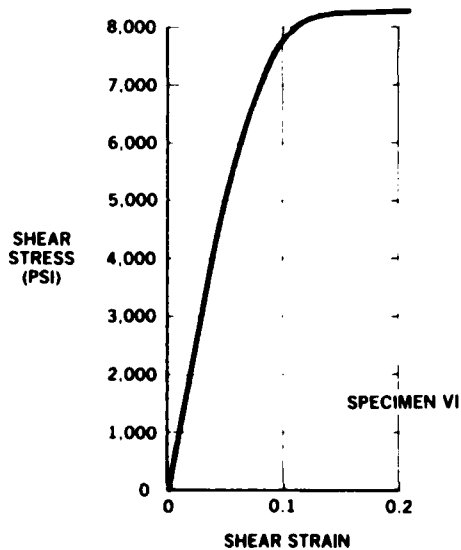
FM-73 ADHESIVE, BR-127 PRIMER, BOND THICKNESS = 0.0067 INCH,
TESTED AT —67°F

INITIAL SHEAR MODULUS = 113,200 PSI (AVERAGE OF BOTH READINGS)
INITIAL SHEAR MODULUS = 104,500 PSI (THIS CURVE)
SECANT MODULUS AT KNEE = 72,500 PSI
SHEAR STRESS AT KNEE = 8,057 PSI
ULTIMATE SHEAR STRESS = 8,264 PSI
ULTIMATE SHEAR STRAIN = 0.21

FIGURE 21. ADHESIVE STRESS-STRAIN CURVE IN SHEAR

initial shear stiffness (modulus) for the ductile adhesive but not for the brittle adhesive. However, the picture with regard to the strain to failure is very unclear. There are some dramatic reductions but other equally pronounced increases. Perhaps the discrete ligaments of the porous bond inhibit the propagation of the single failure surface that would occur for an intact bond. In any event, each of the porous bonds tested still retained a considerable shear strength, even though the degree of porosity was quite visible, as shown in Figure 32.

FM-73 ADHESIVE, BR-127 PRIMER, BOND THICKNESS = 0.0050 INCH,
TESTED AT 140°F AND 100% RELATIVE HUMIDITY

INITIAL SHEAR MODULUS = 52,400 PSI (AVERAGE OF BOTH READINGS)
INITIAL SHEAR MODULUS = 51,100 PSI (THIS CURVE)
SECANT MODULUS AT KNEE = 32,600 PSI
SHEAR STRESS AT KNEE = 2,704 PSI
ULTIMATE SHEAR STRESS = 4,455 PSI
ULTIMATE SHEAR STRAIN = 1.26

FIGURE 22. ADHESIVE STRESS-STRAIN CURVE IN SHEAR

FM-73 ADHESIVE, BR-127 PRIMER, POROUS BOND LINE, THICKNESS = 0.0109 INCH,
TESTED AT ROOM TEMPERATURE

INITIAL SHEAR MODULUS = 83,200 PSI (AVERAGE OF BOTH READINGS)
INITIAL SHEAR MODULUS = 79,900 PSI (THIS CURVE)
SECANT MODULUS AT KNEE = 48,100 PSI
SHEAR STRESS AT KNEE = 3,707 PSI
ULTIMATE SHEAR STRESS = 4,415 PSI
ULTIMATE SHEAR STRAIN = 0.42

FIGURE 23. ADHESIVE STRESS-STRAIN CURVE IN SHEAR

67

FM-73 ADHESIVE, BR-127 PRIMER, POROUS BOND LINE, THICKNESS = 0.0109 INCH,
TESTED AT —67°F

INITIAL SHEAR MODULUS = 94,300 PSI (AVERAGE OF BOTH READINGS)
INITIAL SHEAR MODULUS = 86,300 PSI (THIS CURVE)
SECANT MODULUS AT KNEE = 52,200 PSI
SHEAR STRESS AT KNEE = 5,698 PSI
ULTIMATE SHEAR STRESS = 6,642 PSI
ULTIMATE SHEAR STRAIN = 0.35

FIGURE 24. ADHESIVE STRESS-STRAIN CURVE IN SHEAR

FM-73 ADHESIVE, BR-127 PRIMER, POROUS BOND LINE, THICKNESS = 0.0105 INCH,
TESTED AT 140°F AND 100% RELATIVE HUMIDITY

INITIAL SHEAR MODULUS = 33,000 PSI (AVERAGE OF BOTH READINGS)
INITIAL SHEAR MODULUS = 36,000 PSI (THIS CURVE)
SECANT MODULUS AT KNEE = 19,900 PSI
SHEAR STRESS AT KNEE = 1,243 PSI
ULTIMATE SHEAR STRESS = 2,858 PSI
ULTIMATE SHEAR STRAIN = 1.92
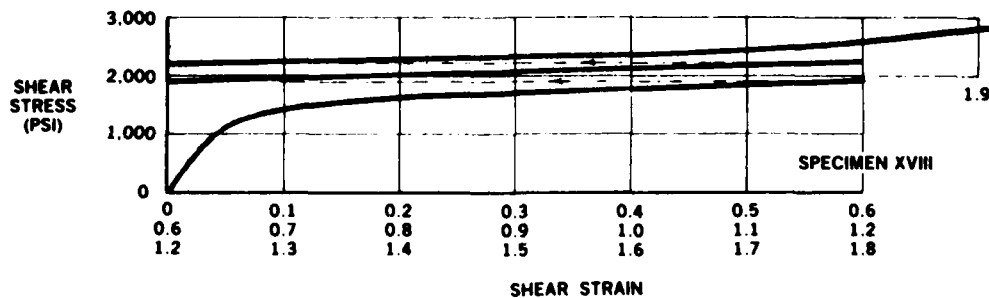
FIGURE 25. ADHESIVE STRESS-STRAIN CURVE IN SHEAR

68
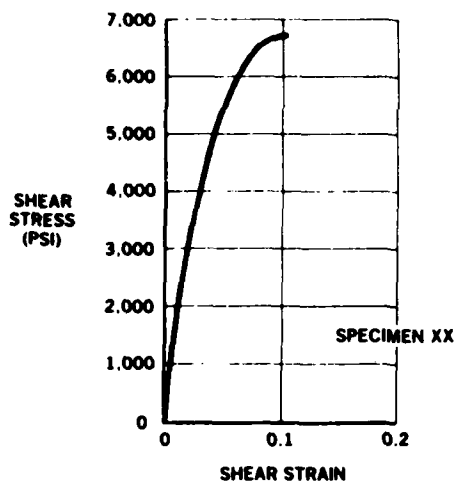
FM-400 ADHESIVE, BR-140 PRIMER, BOND THICKNESS = 0.0105 INCH, TESTED AT ROOM TEMPERATURE

INITIAL SHEAR MODULUS = 229,500 PSI (AVERAGE OF BOTH READINGS)
INITIAL SHEAR MODULUS = 202,200 PSI (THIS CURVE)
ULTIMATE SHEAR STRESS = 6,745 PSI
ULTIMATE SHEAR STRAIN = 0.10

SPECIMEN XX

FIGURE 26. ADHESIVE STRESS-STRAIN CURVE IN SHEAR
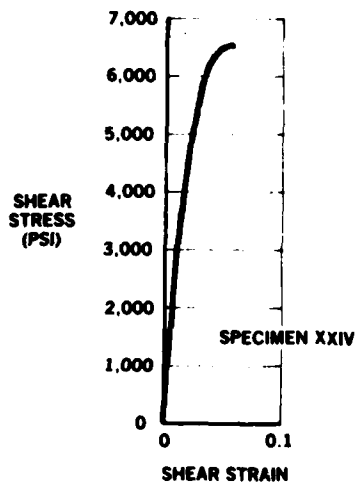
FM-400 ADHESIVE, BR-400 PRIMER, BOND THICKNESS = 0.0118 INCH, TESTED AT −67°F

INITIAL SHEAR MODULUS = 314,400 PSI (AVERAGE OF BOTH READINGS)
INITIAL SHEAR MODULUS = 324,100 PSI (THIS CURVE)
ULTIMATE SHEAR STRESS = 6,557 PSI
ULTIMATE SHEAR STRAIN = 0.06

SPECIMEN XXIV

FIGURE 27. ADHESIVE STRESS-STRAIN CURVE IN SHEAR
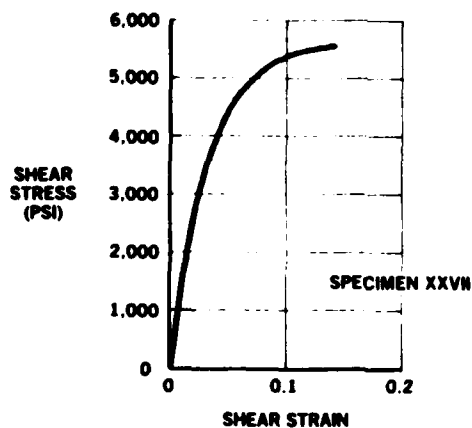
FM-400 ADHESIVE, BR-400 PRIMER, BOND THICKNESS = 0.0105 INCH, TESTED AT 140°F AND 100% RELATIVE HUMIDITY

INITIAL SHEAR MODULUS = 182,600 PSI (AVERAGE OF BOTH READINGS)
INITIAL SHEAR MODULUS = 141,300 PSI (THIS CURVE)
ULTIMATE SHEAR STRESS = 5,578 PSI
ULTIMATE SHEAR STRAIN = 0.14

SPECIMEN XXVII

FIGURE 28. ADHESIVE STRESS-STRAIN CURVE IN SHEAR

69
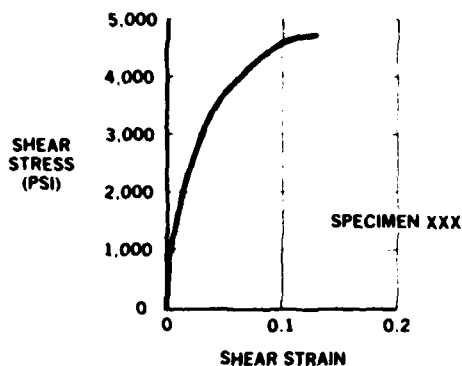
FM-400 ADHESIVE, BR-400 PRIMER, POROUS BOND, THICKNESS = 0.0155 INCH,
TESTED AT ROOM TEMPERATURE

INITIAL SHEAR MODULUS = 186,000 PSI (AVERAGE OF BOTH READINGS)
INITIAL SHEAR MODULUS = 202,200 PSI (THIS CURVE)
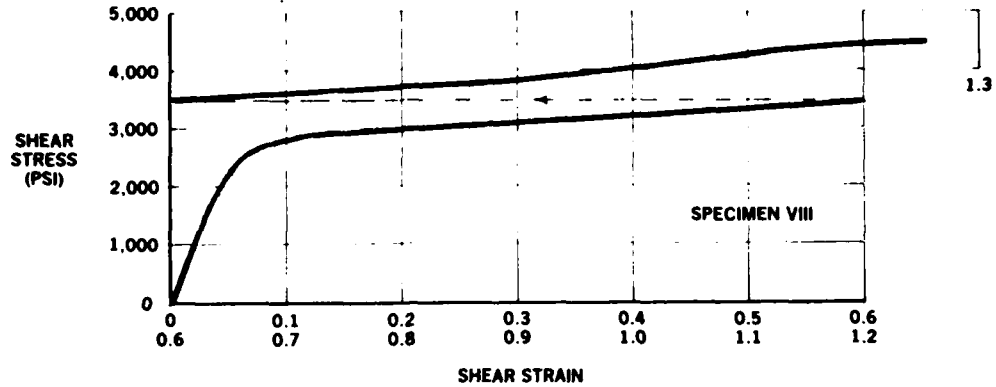ULTIMATE SHEAR STRESS = 4,734 PSI
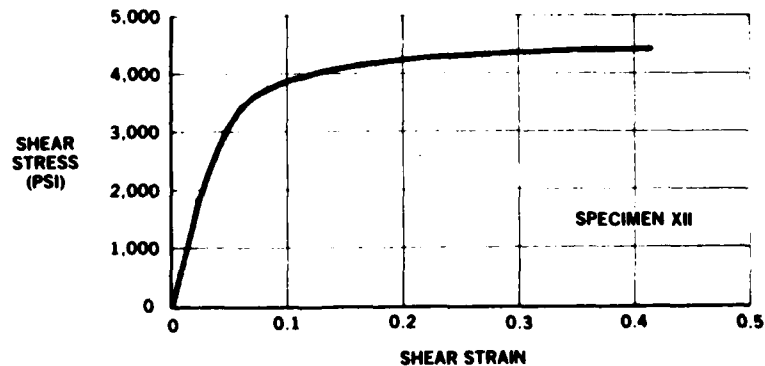STRAIN TO FAILURE = 0.13

FIGURE 29. ADHESIVE STRESS-STRAIN CURVE IN SHEAR
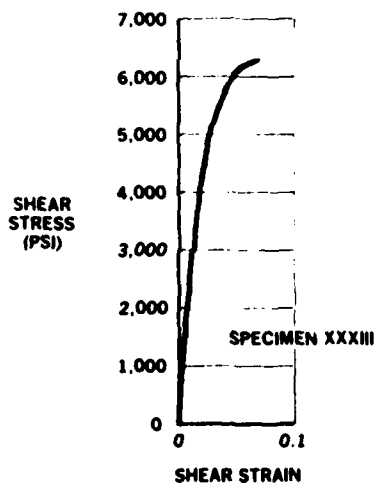
FM-400 ADHESIVE, BR-400 PRIMER, POROUS BOND LINE, THICKNESS = 0.0151 INCH,
TESTED AT −67°F

INITIAL SHEAR MODULUS = 321,900 PSI (AVERAGE OF BOTH READINGS)
INITIAL SHEAR MODULUS = 280,600 PSI (THIS CURVE)
ULTIMATE SHEAR STRESS = 6,296 PSI
STRAIN TO FAILURE = 0.07

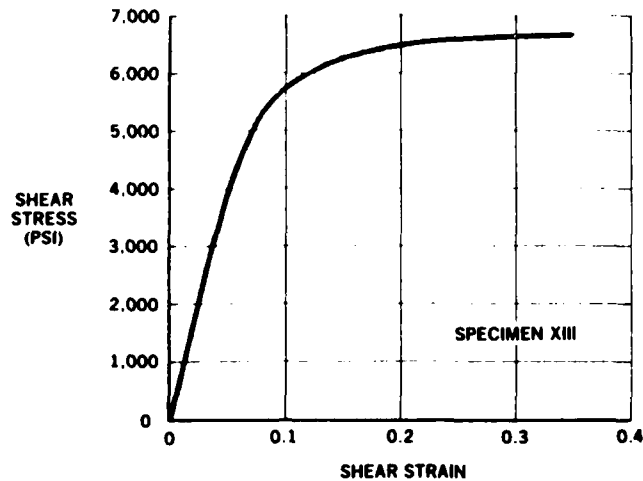**FIGURE 30. ADHESIVE STRESS-STRAIN CURVE IN SHEAR**
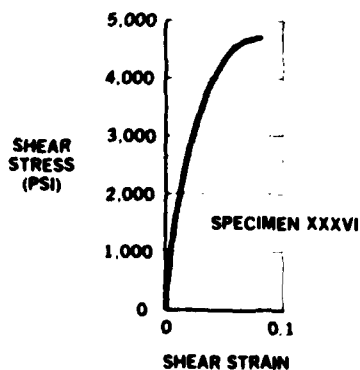
FM-400 ADHESIVE, BR-400 PRIMER, POROUS BOND, THICKNESS = 0.0134 INCH,
TESTED AT 140°F AND 100% RELATIVE HUMIDITY

INITIAL SHEAR MODULUS = 203,700 PSI (AVERAGE OF BOTH READINGS)
INITIAL SHEAR MODULUS = 187,700 PSI (THIS CURVE)
ULTIMATE SHEAR STRESS = 4,717 PSI
ULTIMATE SHEAR STRAIN = 0.08

FIGURE 31. ADHESIVE STRESS-STRAIN CURVE IN SHEAR
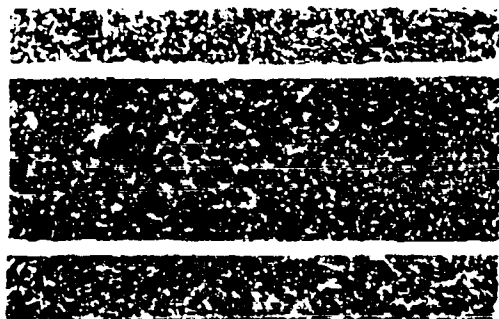
FM-73M ADHESIVE, 0.012 INCH SHIMS
PANEL NUMBER 1

FM-400 ADHESIVE, 0.012 INCH SHIMS
PANEL NUMBER 1

FIGURE 32. C-SCAN RECORDS OF POROUS BONDED PANELS

Figures 33 to 38 are enlargements of the fractured porous bonds which are nominally 1.0-inch wide and 0.5-inch long. The FM-400 specimens failed mainly in the primer, as is typical for that adhesive. There was obviously more porosity for the FM-400 adhesive than for the FM-73, due probably to different flow characteristics during the cure of the adhesive. However, the ultrasonic inspection records in Figure 19 make it clear that the degree of porosity is extremely sensitive to the precise spacer shims used during the adhesive cure. Even a further 0.001 inch on the FM-73 shims might have caused excessive porosity.

FM-73M ADHESIVE, BR-127 PRIMER, POROUS BONDS, TESTED AT ROOM TEMPERATURE

2X ENLARGEMENTS OF FRACTURE OF TEST AREA (BOTH BOND SURFACES)

FIGURE 33. ADHESIVE BOND FAILURES UNDER SHEAR LOADING

71

FM-73 ADHESIVE, BR-127 PRIMER, POROUS BONDS, TESTED AT 67°F

2X ENLARGEMENTS OF FRACTURE OF TEST AREA (BOTH BOND SURFACES)

FIGURE 34. ADHESIVE BOND FAILURES UNDER SHEAR LOADING

FM-73M ADHESIVE, BR-127 PRIMER, POROUS BONDS, TESTED AT 140°F & 100% RELATIVE HUMIDITY

2X ENLARGEMENTS OF FRACTURE OF TEST AREA (BOTH BOND SURFACES)

FIGURE 35. ADHESIVE BOND FAILURES UNDER SHEAR LOADING

FM-400 ADHESIVE, BR-400 PRIMER, POROUS BONDS, TESTED AT ROOM TEMPERATURE
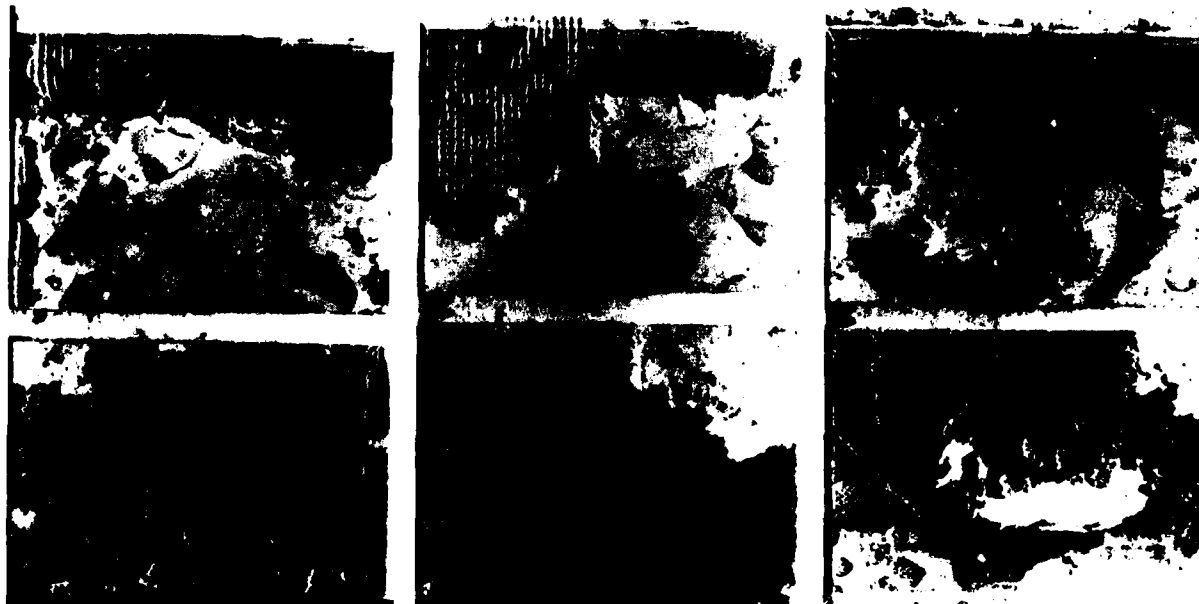
2X ENLARGEMENTS OF FRACTURE OF TEST AREA (BOTH SURFACES)

FIGURE 36. ADHESIVE BOND FAILURES UNDER SHEAR LOADING

FM-400 ADHESIVE, BR-400 PRIMER, POROUS BONDS, TESTED AT −67°F
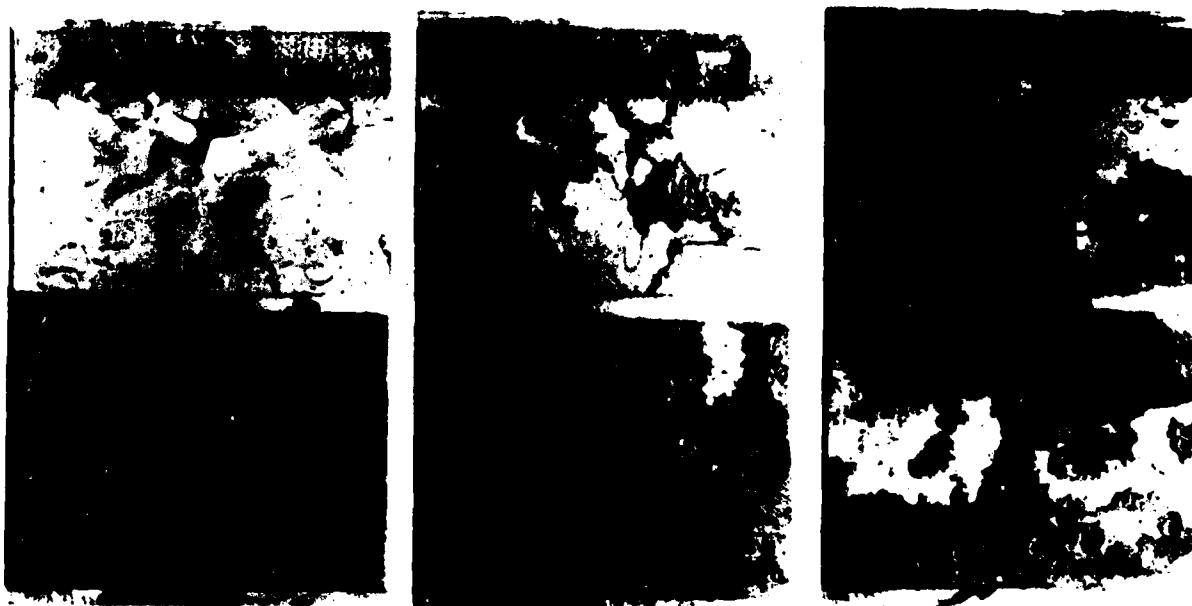
2X ENLARGEMENTS OF FRACTURE OF TEST AREA (BOTH SURFACES)

FIGURE 37. ADHESIVE BOND FAILURES UNDER SHEAR LOADING

2X ENLARGEMENTS OF FRACTURE OF TEST AREA (BOTH SURFACES)

FIGURE 38. ADHESIVE BOND FAILURES UNDER SHEAR LOADING

Now, the stress-strain curves in Figures 20 to 31 do not convey the entire effect of any porosity on the strength of a structurally proportioned (long overlap) joint. Equation (1) shows that, all other things being equal, double-lap joints are strengthened by thickening the bond layer. For instance, since the bond thickness would be increased from a nominal 0.005 inch to 0.012 inch, if the area under the stress-strain curve was decreased by less than 50 percent due to the porosity, the porous bond would be stronger than the intact bond. This would usually be the case for relatively small degrees of porosity, as in Figures 33 to 35. (The holes in Figures 35 and 38 were for moisture conditioning and had no effect on the strength.)

Another effect which ameliorates any loss of joint strength due to adhesive porosity is the natural location of porosity within the joint. Most natural porosity occurs in the interior of a joint, where virtually no load is transferred, rather than at the edges of the overlap where a good bond is needed because of the characteristic load transfer, as in Figure 2. Porosity in those interior locations cannot possibly have the effects of the same porosity created artificially, in short-overlap test coupons, with the intent to correlate ultrasonic flaw measurements with a loss in measured shear strength of the bonded joints. Regrettably, it is common practice to use such an approach, as the cross-reference in Figure 39 indicates. Such an assessment is, at least, conservative, but usually unnecessarily so.

LAP-SHEAR STRENGTH (KSI)

BONDTESTER MODEL: 70
PROBE: 3814
FRONT SHEET: 7075-T6 (0.060)
BACK SHEET: 2024-T3 (0.050)
ADHESIVE: FM73
PRIMER: BR127

FOKKER BONDTESTER QUALITY UNITS

FIGURE 39. LAP-SHEAR STRENGTH VERSUS FOKKER BONDTESTER QUALITY UNITS

FLAWS AND POROSITY IN COMPLEX BONDED JOINTS

The discussion above has concentrated on adhesive-bonded joints between relatively thin adherends of essentially uniform thickness. However, porosity and flaws can also occur in thick stepped-lap joints. The computer program A4EI permits the analysis of such joints, but it does not seem possible to draw such simple and general conclusions as has been done above for the simpler joints.

Figure 40 describes a typical stepped-lap joint. The adherends are much stronger than the adhesive in this case, so the effects of any imperfections anywhere in the bond would be noticeable. Figure 41 shows the adhesive shear stress distributions for this joint under tensile shear loads for the case of a nominally perfect bond with a uniform thickness of 0.005 inch. [For compressive shear loads, the stress and strain distributions would be mirror images (end-for-end) and of the opposite sign.] The lesser adherend strength is 48,000 pounds per inch while the adhesive shear strengths are only 13,749 pounds per inch under both tensile and compressive shear loads, because of the precise adherend stiffness balance.

Figure 42 shows what happens as the result of a misfit whereby the central step has been given a complete void because the adhesive is set there at 0.015-inch thick. The intermediate steps are modelled as having a 50-percent loss of shear strength due to a less severe thickening of the bond layer, to 0.010 inch. The adhesive bond strength is predicted to be reduced to 13,350 pounds per inch, which is clearly far less severe than the proportional effective loss of bond area. That is

A. SPECIMEN GEOMETRY

B. ADHESIVE PROPERTIES

C. ADHEREND PROPERTIES
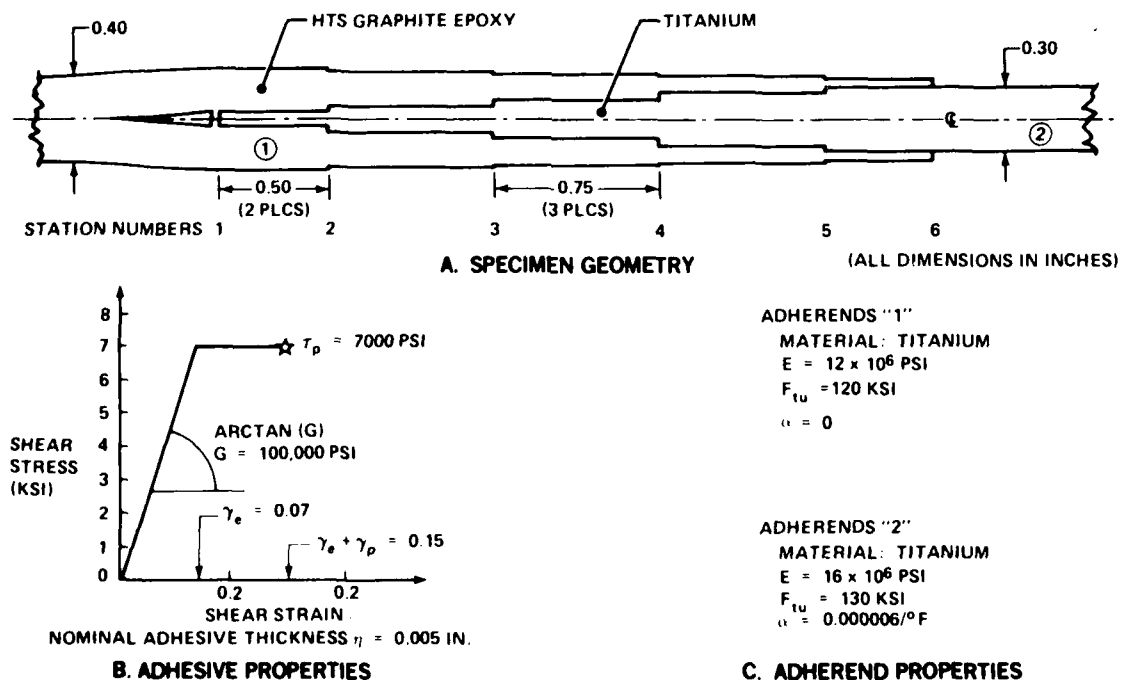
FIGURE 40. TYPICAL STEPPED-LAP ADHESIVE BONDED JOINT

76

TENSILE LOADING

($\Delta T = -250°F$)

STRENGTH = 13,749 LB/IN.
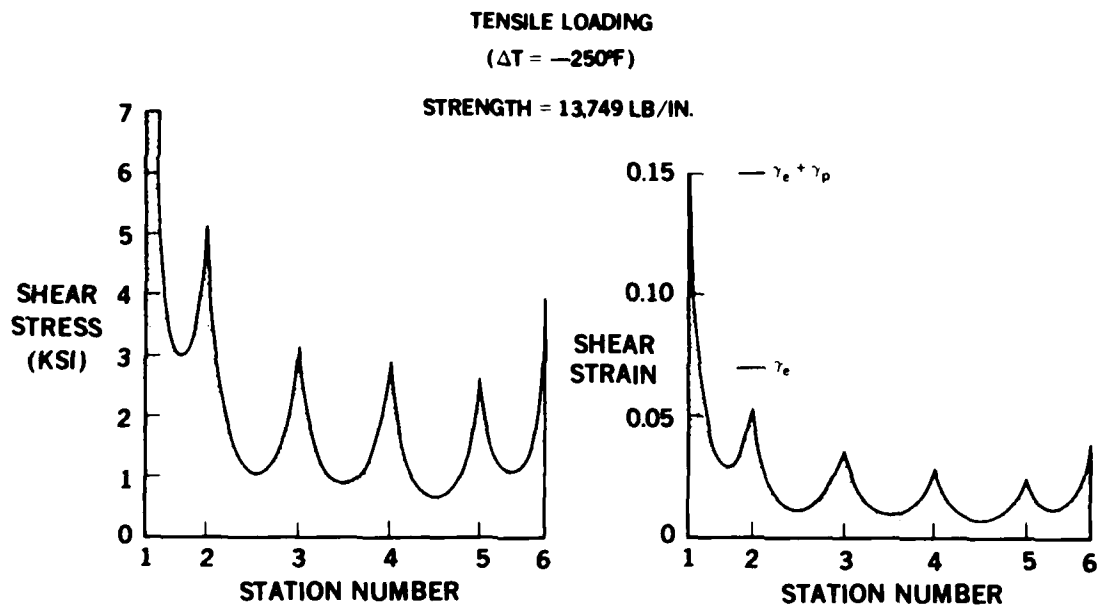
FIGURE 41. ADHESIVE SHEAR STRESSES AND STRAINS IN UNFLAWED JOINT

TENSILE LOAD

($\Delta T = -250°F$)

STRENGTH = 13,35? LB/IN.
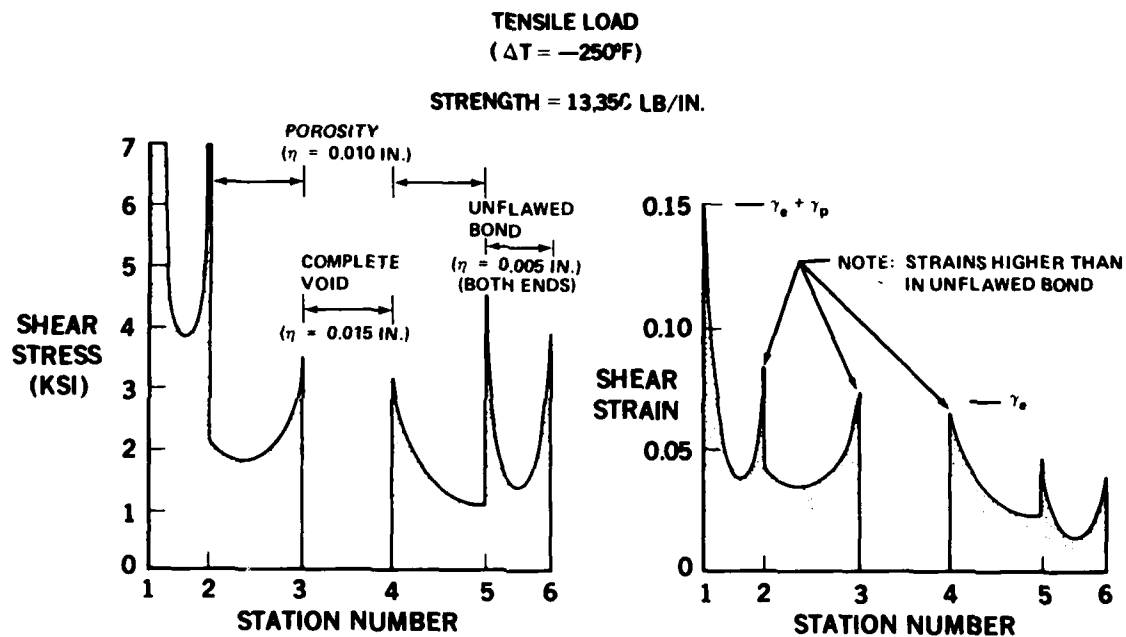
FIGURE 42. SHEAR STRESSES AND STRAINS IN FLAWED, POROUS BONDED JOINT

because the critical condition remains in the outermost steps. The added adhesive strains in the porous bond steps, with respect to the same steps in Figure 41, are caused by the loss of load transferred by the central step.

Figure 43 depicts the further losses of strength due to a complete void throughout all of the bond except the outermost steps. The strength would be further reduced to 8,350 pounds per inch. That represents a strength retention of 61 percent even though the effective bond area had been

77

TENSILE LOADING

($\Delta T = -250°F$)

STRENGTH = 8350 LB/IN.
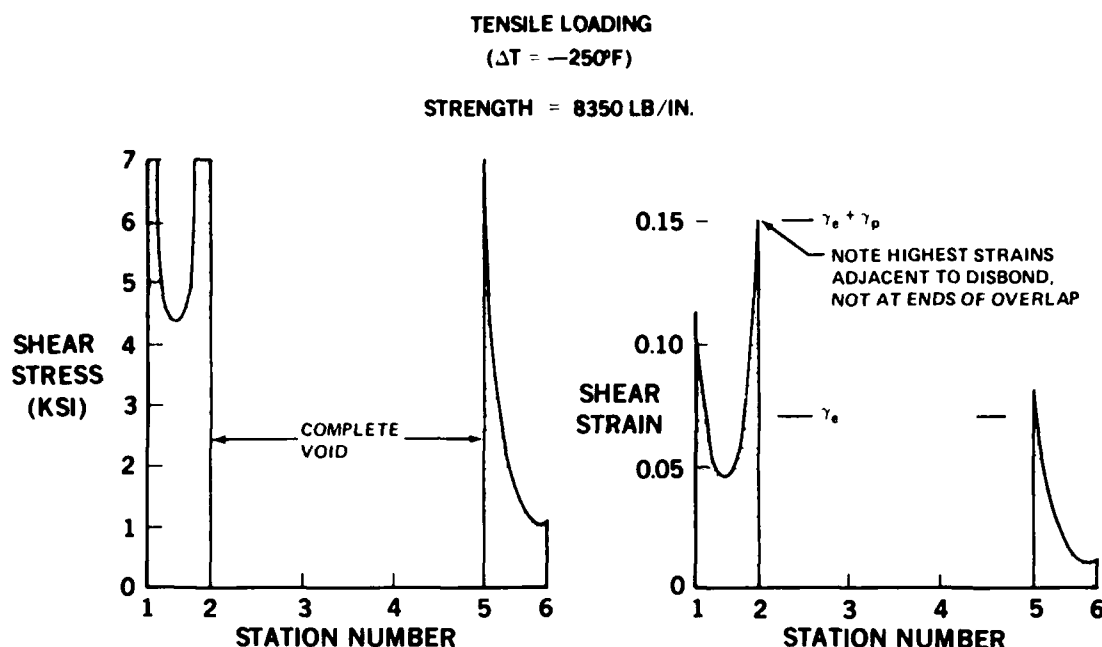
FIGURE 43. SHEAR STRESSES AND STRAINS IN FLAWED ADHESIVE-BONDED JOINT

reduced to only 31 percent of the original extent. It is significant that this large loss of strength *is associated with a shift of the critical location from the left end of the overlap to the left side of the complete bond flaw.* It is precisely because such a shift did not occur in the data of Figure 42 that here was so much less strength loss associated with the less severe bond flaw.

These predictions for this typical stepped-lap joint between titanium and graphite epoxy indicate the difficulty of reaching specific conclusions about the effects of bond flaws and porosity in complex joints. However, it is reasonable to infer that any loss of shear strength would be significantly less than predicted merely by the proportional loss of bond area in the absence of a precise analysis. The most significant characteristic of bond flaws in such joints is that discussed above in the context of two-dimensional load transfer redistributions. Any bond flaw in such a joint has the potential of being propagated into adjacent sound bonds. That behavior is very different than that for bonded joints between thin adherends.

ACCEPTANCE CRITERIA FOR ADHESIVE POROSITY

It must be recognized from the various factors discussed above that the effects of adhesive porosity on the strength of bonded joints can be quite complex. The most severe effects would occur in conjunction with high induced peel stresses in the adhesive. Those peel stresses should be removed from any structural joint by the use of a little design finesse. However, such peel stresses seem to be almost inherent in some test coupons for which, as yet, there is no satisfactory analysis. Peel-stress problems are not considered in this section, but are discussed thoroughly in Section 4. It is these induced peel stresses that complicate the application of data of the type shown in Figure 39 to the prediction of loss of strength in structural joints under shear loads.

Setting aside these peel-stress effects, the consequences of shear-dominated loadings are still complex. Figure 42 illustrates the quite common condition of the critical condition remaining in the sound adhesive at the ends of the overlap — the porous bond is protected from being critically strained by the compatibility of deformations throughout the joint. Only 42 percent of the load was predicted to be transferred through the porous bond areas, even though their area was 50-percent greater than that for the nominally perfect bonds in that joint. The greater adhesive layer thickness necessarily associated with the bond porosity is largely responsible for the lack of criticality in the porous areas. Indeed, the load diversion due to the thicker, and hence softer bonds associated with the porosity is often more significant than the actual loss of mechanical properties of that bond. Even a flawless thicker bond in the same area could seldom transfer much load.

This tendency of natural porosity to be associated with low load transfer means that the porosity must be accounted for realistically in thick complex joints. However, in bonded joints between thin uniform adherends, the critical location will be predicted to still be outside the joint, even for large-area natural flaws since only such a small area of unflawed bond is needed at the ends of the overlap.

For thin bonded adherends, porosity can be treated as if it were a complete flaw, using the logic of Figure 11. Porosity is, after all, just one form of bond flaws. This approach won't usually be unduly conservative, and is due more to the increased flexibility of thick porous bonds than to the loss of strength.

Porosity, as with any flaw in bonded joints between thick adherends, is more critical because of the possibility that quite local imperfections could have a widespread effect. If the bond is weaker than the adherends and there are no fail-safe mechanical load paths as shown in Figure 17, the load that can be transferred safely is reduced drastically, as explained in Figure 44. Otherwise, any such bond flaw could be catastrophic. This is in stark contrast with the consequences of adhesive flaws in thin bonded structures. However, as has been stated, it is unwise to ever design or build a purely bonded joint which is weaker than the members themselves. Mechanical fasteners should be used in such a joint, even if the bond is flawless. The fasteners alone should be designed to carry limit load. While there is no analysis method to characterize the

79

FLAW

BOND   BOND

τ_p

σ_∞

ADHESIVE
STRESS   SKIN STRESSES

τ_p

- LOW STRESS IN BOND AND SKIN SO AS   - IF METAL YIELDS PRIOR TO BOND
  NOT TO PROPAGATE DISBOND   FAILURE, FLAW PROPAGATES.

                                       - IF BOND DOES NOT FAIL, FATIGUE
                                         CRACK IN METAL IS LIKELY
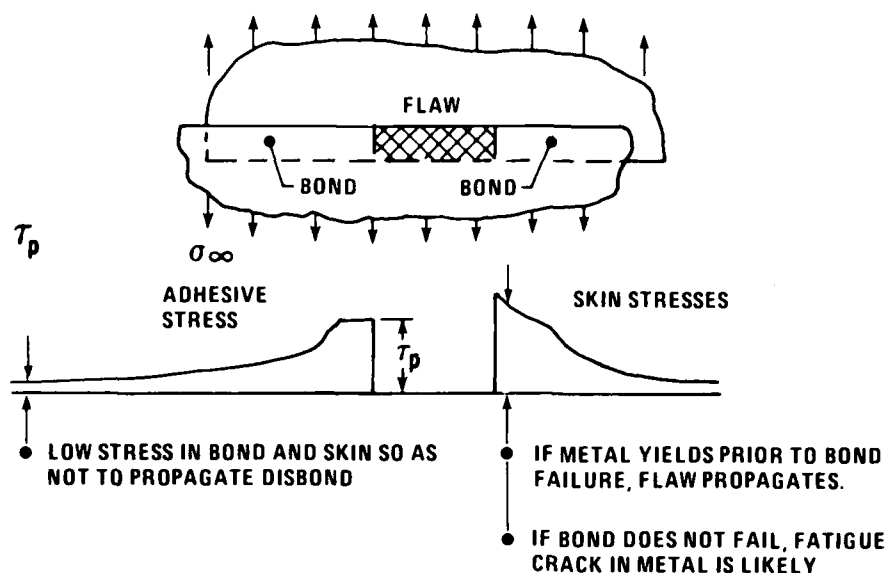
FIGURE 44. REDISTRIBUTION OF LOAD AROUND FLAWS IN BOND

growth of any bond flaw in such a situation, the knowledge that the growth will soon be arrested as the fasteners pick up the load permits the use of a conservative analysis based on the presence of the fasteners alone. The variable-adhesive analysis program A4EI can be used to solve for any one-dimensional load transfer redistribution, as in Figure 42. Nonlinear finite-element analyses may also be used, but linear analysis is not appropriate for even the most brittle of real structural adhesives.

In two respects, porosity cannot be regarded as one special case of adhesive bond flaws. Obviously, they are a manufacturing problem only — they cannot occur in service — although they may not always be detected before service. Essentially though, they will all be repaired by the manufacturer rather than the user, and such repairs can be made before any contamination or corrosion has occurred. Unfortunately, any necessary repairs to porosity cannot be effected by simply drilling a couple of small holes and injecting adhesive, as is commonly done for large discrete flaws. It can be seen from Figures 33 to 38 that each and every little void would have to be filled separately if there really were a need to rely on the load that should have been transferred through that area of bond. That is obviously impractical, so any necessary repairs for adhesive bond flaws are inevitably difficult if they extend beyond the addition of fasteners and sealant. It should be noted that none of the numerous bond flaws or porosity which occurred on the PABST program required repairs.

Adhesive porosity is likely to be of concern only in the bonding of thick structures, particularly in fibrous composites. A porous bond in a composite to titanium stepped-lap joint, for example, cannot be opened up by a wedge to convert it into a more repairable single large void; the composite would be delaminated in the process. If mechanical repairs are insufficient, and the part is too valuable to scrap or rebuild, the porosity must be removed by cutting some of the structure

80

away and repairing it along the lines used for battle damage. In principle, though, this differs little from the in-service repairs of many large bond flaws in thin bonded metal structures. The corrosion and contamination of the bond surface which is usually present by then leaves the same alternatives — use sealant and rivets, or cut away enough of the structure to reclean the surfaces to be bonded. This prospect explains why it is best to restrict the use of adhesive bonding to those applications and designs in which there is no possibility of any local bond flaw growing during the life of the aircraft.

CONCLUSIONS

This effort has investigated the effects of the shear load transfer through adhesively-bonded joints of any flaws or porosity which may be present. These effects have been explained both for thin adherends (for which the adhesive is so much stronger than the adherends that there is great tolerance for bond flaws) and for thick adherends (for which there is the likelihood that any small bond flaw could cause a widespread problem).

The effect of bond flaws and porosity on adhesive joints with a high peel-stress has been described only briefly and is considered to be beyond the scope of this report. There is no reason for such a condition to occur in well-designed structural bonded joints, even though the standard lap-shear test coupon is strongly influenced by induced peel stresses.

The interpretation of any loss of bond strength due to porosity on the basis of ultrasonic measurements and coupon tests is, therefore, questionable for structural joints.

Furthermore, the greater bond thickness necessarily associated with porous bonds than with adjacent structurally sound areas makes the porous bonds less stiff so that they usually transfer load to the sound areas rather than become overloaded and fail themselves.

It is recommended therefore that, for thin bonded structures, any porosity be regarded as a complete flaw, and simple analysis methods and equations have been prepared for this task. This will usually not cause any noticeable loss of strength because porosity is usually confined to the interior of bonded joints where there is virtually no load transferred anyway. The load is transferred through the unflawed bonds near the ends of the overlap.

Thicker bonded structures usually require fail-safe mechanical joints in conjunction with the adhesive bond. The rivets or bolts then stop the unlimited growth of any disbonds or flaws, regardless of the original source of the problem. At that stage the most critical condition is no longer in the adhesive but at the most heavily loaded fastener in the middle of the disbond.

The loss of strength due to local porosity in complex bonded joints can be examined for a unit width of joint by the nonlinear analysis program A4EI. No specialized analysis program is yet available to explain the two-dimensional aspects of the problem, so a large nonlinear finite-element analysis progam would be needed.

It should be noted that structural bonded joints in most typical lightly-loaded structures have very considerable tolerance for all bond flaws and do not need structural repairs. Usually all that is needed is to seal the edges with a rubber-base material to prevent ingress of moisture and corrosion. Indeed, any attempt to perform a structural repair in such a case usually ensures only a decrease in life of the structure by breaking the adherend surface protection.

The key to understanding the tolerance or sensitivity of adhesive bonds to flaws or porosity is that there is almost complete insensitivity to even quite large defects provided that the defect is located somewhere other than at the critical location (usually at the ends of the overlap). Bond defects become really significant only when they are large enough to alter the distribution of the load transfer through the bond so that they cause a shift in the critical location (usually to an edge of that defect).

REFERENCES

1. Hart-Smith, L. J., Differences Between Adhesive Behavior in Test Coupons and Structural Joints. Douglas Aircraft Company Paper No. 7066, presented to ASTM Adhesives Committee D-14 Meeting, Phoenix, Arizona, March 1981.

2. Hart-Smith, L. J., Effects of Adhesive Layer Edge Thickness on Strength of Adhesive-Bonded Joints. Douglas Aircraft Company Technical Report MDC-J4675, May 1981 (Section 2 of this report).

3. Hart-Smith, L. J., Adhesive-Bonded Single-Lap Joints. Douglas Aircraft Company, NASA CR-112236, January 1973.

SECTION 4

INDUCED PEEL STRESSES
IN ADHESIVE-BONDED JOINTS

CONTENTS

SYMBOLS

A,B,C,F = Integration constants
c = Half length of overlap (in.)
D = Flexural rigidity of adherends (lb in.^{2})
E = Young's modulus of adherend (psi)
E_c = Adhesive elastic modulus in peel (psi)
G = Adhesive shear modulus (psi)
i = Location of point of inflexion (in.)
k = Eccentricity factor
ℓ = Length of adherend outside joint (in.)
ℓ = Overlap (length of bond) ($\approx$ 2c) (in.)
M = Bending moment in adherend (lb in./in.)
P = Applied load on joint (lb/in.)
s = Coordinate aligned along load path (different origin from x) (in.)
T = Direct stress resultants in adherend(s) (lb/in.)
t = Thickness of adherend (in.)
V = Transverse shear force in adherend (lb/in.)
w = Transverse displacement of adherend under eccentric load (in.)
x = Axial (longitudinal) coordinate aligned along load path (in.)

γ = Adhesive shear strain (in./in.)
δ = Lateral deflection (in.)
η = Adhesive layer thickness (in.)
η = Joint efficiency
Θ = Coefficient
ν = Poisson's ratio
ξ = Exponent of bending stress distribution in adherend (in.$^{-1}$)
σ = Adherend stress (psi)
σ_c = Peel stress in adhesive (psi'
τ = Adhesive shear stress (psi)
χ = Peel stress distribution exponent (in.$^{-1}$)

SUBSCRIPTS

c = Adhesive (cement)
d = Doubler (splice plate)
e = Location at outer edge of splice plate
f = Stiffener flange
i = Inner adherend
i = Location of point of inflexion in bending of adherends
m = Middle of splice plate, where skins butt together
o = Outer adherends
0 = Remote location, away from joint, at load introduction
1,2,3,4 = Different regions of the adherends (see figures)

INTRODUCTION

This effort is designed to provide an understanding of peel stresses induced in the adhesive by shear loads applied to adhesive-bonded joints of various configurations, including both structural joints and test coupons. This assessment builds on work done under an earlier USAF contract, F33615-75-C-5209 (Reference 1), in which the criticality of adhesive bond-line flaws was investigated under three levels of severity of the induced peel stresses for a common shear load. It was found that the double-lap and double strap joints, having the least peel stresses, and the single-lap joints with moderate peel stresses were quite insensitive to initial flaws. Only the single-strap flush joints had sufficiently severe peel stresses to cause initial flaws to grow or fatigue failure of the bond before the aluminum adherends failed.

The analyses available for these peel stresses at the time of the earlier contract convered only the double-lap and single-lap joints. This earlier work is supplemented here by analyses for the more critical single-strap joints. In addition, the current contract has permitted an experimental investigation of simple techniques to alleviate the peel-stress problem by tapering the ends of the adherends to make them more flexible in order to destroy the resistance to bending which was causing the peel stresses in the first place. Further benefits are derived from locally thickening the adhesive as well. Apart from some inconclusive results because of premature failure caused by poor surface preparation, rather than by mechanical fatigue, the new testing has shown the local modifications to be very effective in suppressing the peel failures, even on flush joints. Full details of this testing are given in this portion of the report.

The results will provide the designer with quantified solutions which show how to reduce any induced peel stresses to insignificance by selecting appropriate joint geometry. These analyses include the standard half-inch-overlap single-lap test coupon, which has both high shear stresses and high peel stresses in the adhesive. In structural bonded joints, the peel stresses have been greatly diminished to enable the adhesive to develop its full potential shear strength. The report includes comparisons between the peel stresses in short-overlap test coupons, proportioned so as to force a failure in the adhesive, and those in long-overlap structural joints, proportioned so as not to fail the adhesive until the adherends outside the joint have been overloaded. The differences in intensity of the peel stresses are dramatic. The adherend tapering (thinning at the ends) is shown to further reduce those peel stresses.

SINGLE-LAP JOINTS BETWEEN IDENTICAL ADHERENDS

The first investigation of peel stresses in adhesive-bonded joints was the classic analysis by Goland and Reissner in 1944 (Reference 2). Their estimate of the adherend bending moment at the ends of the overlap was unnecessarily conservative, being refined by the present author in 1973 (Reference 3), and that poorly evaluated boundary condition affected all of their subsequent calculations. However, their basic approach was otherwise sound; they recognized the need to allow for relief of the bending moments due to structural deformations under load, and they established that quite high peel stresses were developed at the ends of the overlap. Considering that they overestimated both the peak adhesive peel stress and the severity of the maximum adherend bending moment, it is surprising that their work did not inspire more immediate attention to that problem, since it clearly indicated a structural inefficiency in need of alleviation. Because this problem is the best known of induced peel stresses in adhesive-bonded joints, it makes an excellent starting point for this report, to explain the techniques used in subsequent analyses. Figure 1 depicts some of the key characteristics of the behavior of single-lap bonded joints. The methods developed in References 2 and 3 are used here.

LOW LOAD LEVEL

MAXIMUM STRESS CONCENTRATION

DEFORMATION OF ADHERENDS UNDER MODERATE LOAD

"INTERLAMINAR" FAILURE OF FILAMENTARY COMPOSITE ADHERENDS

PLASTIC HINGES

HIGH LOAD LEVEL (METAL ADHERENDS)

PERMANENTLY DEFORMED (METAL) ADHERENDS AFTER FAILURE OF ADHESIVE
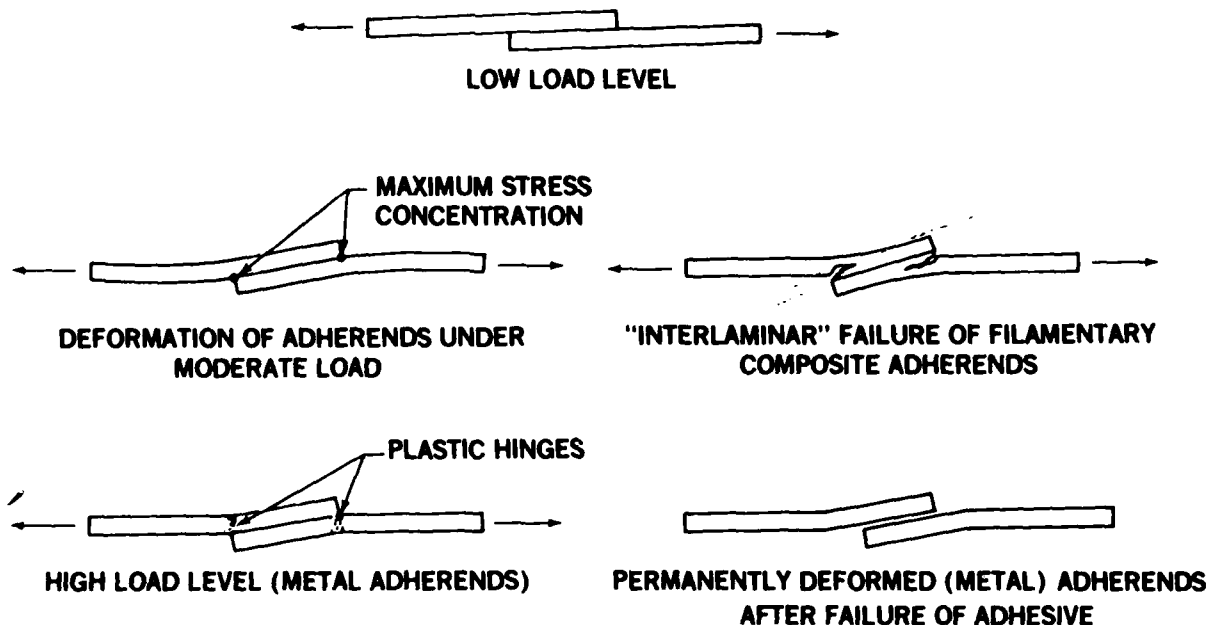
FIGURE 1. SINGLE-LAP BONDED JOINTS WITH ECCENTRIC LOAD PATH – BRITTLE AND DUCTILE ADHERENDS

Figure 2 depicts geometry and nomenclature for the analysis of a precisely antisymmetric single-lap bonded joint between identical adherends. For purposes of analysis, the joint is divided into the four sections shown.
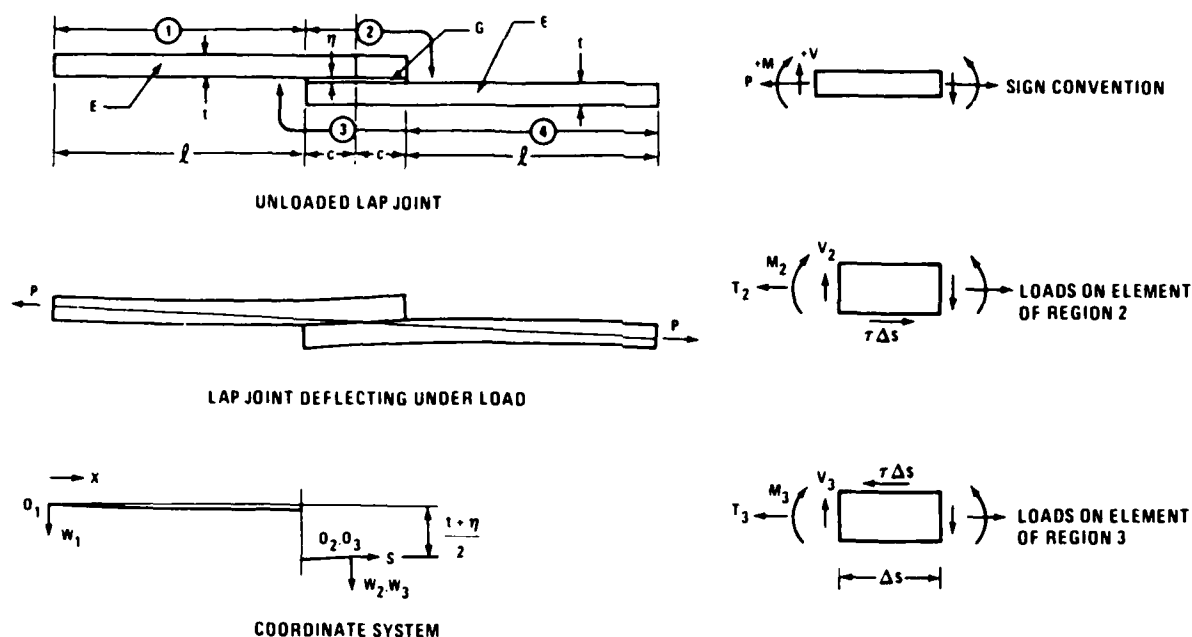
FIGURE 2. COORDINATE SYSTEM AND DEFORMATIONS IN BALANCED SINGLE-LAP BONDED JOINTS

Throughout the adherend 1, the longitudinal stress resultant is uniform, at the value of P of the applied load. The stress couple M_1 is then given by the equilibrium equation

$$M_1 = -M_o + P\left[\left(\frac{t+\eta}{\ell+c}\right)\frac{x}{2} - w_1\right] \text{ for } 0 \leqslant x \leqslant \ell \tag{1}$$

The moment M_o at the points of load introduction would be zero for simply supported ends. According to the classical theory for the infinitesimal bending of thin cylindrically deformed plates,

$$\frac{d^2 w_1}{dx^2} = -\frac{M_1}{D} = \frac{M_o}{D} - \frac{P}{D}\left[\left(\frac{t+\eta}{\ell+c}\right)\frac{x}{2} - w_1\right] \tag{2}$$

the solution of which is

$$w_1 = A_1 \cosh(\xi x) + B_1 \sinh(\xi x) + \left(\frac{t+\eta}{\ell+c}\right)\frac{x}{2} - \frac{M_o}{P} \tag{3}$$

where

$$\xi^2 = P/D \tag{4}$$

90

The condition of zero lateral displacement at the point of load introduction requires that

$$A_1 = M_o / P \qquad (5)$$

Therefore,

$$w_1 = \frac{M_o}{P}\left[\cosh(\xi x) - 1\right] + B_1 \sinh(\xi x) + \left(\frac{t + \eta}{\ell + c}\right)\frac{x}{2} \qquad (6)$$

Both simply supported and built-in edge supports, at $x = 0$, could be considered here. Provided that the length outside the joint is large in comparison with the overlap ($\ell \gg c$), it will be found that both conditions lead to approximately the same displacement and bending moment at the ends of the overlap.

For simple support at $x = 0$,

$$M_o = 0 \qquad (7)$$

and the displacement at $x = \ell$ is

$$w_1 \bigg|_{x=\ell} = B_1 \sinh(\xi\ell) + \left(\frac{t + \eta}{\ell + c}\right)\frac{\ell}{2} \qquad (8)$$

while the adherend bending moment at $x = \ell$ is

$$M_c = -D\frac{d^2 w_1}{dx^2}\bigg|_{x=\ell} = -B_1 P \sinh(\xi\ell) \approx -\frac{B_1 P e^{\xi\ell}}{2} \qquad (9)$$

For built-in supports at $x = 0$, $dw_1/dx = 0$ at $x = 0$, so

$$B_1 = -\left(\frac{t + \eta}{\ell + c}\right)\frac{1}{2\xi} \qquad (10)$$

so

$$w_1 = \frac{M_o}{P}\left[\cosh(\xi x) - 1\right] + \frac{1}{2}\left(\frac{t + \eta}{\ell + c}\right)\left[\ell - \frac{1}{\xi}\sinh(\xi x)\right] \qquad (11)$$

Thus, the displacement at $x = \ell$ would then be

$$w_1 \bigg|_{x=\ell} = \frac{M_o}{P}\left[\cosh(\xi x) - 1\right] + \frac{1}{2}\left(\frac{t + \eta}{\ell + c}\right)\left[\ell - \frac{1}{\xi}\sinh(\xi\ell)\right] \qquad (12)$$

while the associated bending moment would be

$$M_e = -D \frac{d^2 w_1}{dx^2}\bigg|_{x=\ell} = -M_0 \cosh(\xi\ell) + \frac{D\xi}{2}\left(\frac{t+\eta}{\ell+c}\right) \sinh(\xi\ell) \tag{13}$$

From Equations (10) and (13), then, for $\ell \gg t$,

$$M_e \approx \frac{1}{2}\left(B_1 P - M_0\right) e^{\xi\ell} \tag{14}$$

so that, provided M_0 is small due to a large ℓ /t ratio outside the bonded overlap, the boundary conditions at the end of the overlap are not sensitive to the precise nature of the support conditions remote from the joint. This difference might be significant for some test coupons, however, so the distinction should be remembered even though it will not be considered further in this report.

Returning to the simply supported case,

$$w_1 = \left(\frac{t+\eta}{\ell+c}\right)\frac{x}{2} + B_1 \sinh(\xi x) \tag{15}$$

$$\frac{dw_1}{dx} = \frac{1}{2}\left(\frac{t+\eta}{\ell+c}\right) + B_1 \xi \cosh(\xi x) \tag{16}$$

and

$$\frac{d^2 w_1}{dx^2} = B_1 \xi^2 \sinh(\xi x) \tag{17}$$

Therefore,

$$w_1\bigg|_{x=\ell} \approx \left(\frac{t+\eta}{\ell+c}\right)\frac{\ell}{2} + \frac{1}{2}B_1 e^{\xi\ell} \tag{18}$$

$$\frac{dw_1}{dx}\bigg|_{x=\ell} \approx \frac{1}{2}\left(\frac{t+\eta}{\ell+c}\right) + \frac{1}{2}B_1 \xi e^{\xi\ell} \tag{19}$$

and

$$\frac{d^2 w_1}{dx^2}\bigg|_{x=\ell} \approx \frac{1}{2}B_1 \xi^2 e^{\xi\ell} = -\frac{M_e}{D} \tag{20}$$

Turning attention now to regions 2 and 3 in Figure 2, moment equilibrium requires that

$$
\left.
\begin{aligned}
\frac{dM_2}{ds} \quad V_2 + \tau \left(\frac{t + \eta}{2} \right) &= 0 \\[2em]
\frac{dM_3}{ds} \quad V_3 + \tau \left(\frac{t + \eta}{2} \right) &= 0
\end{aligned}
\right\}
\tag{21}
$$

while longitudinal force equilibrium requires that

$$
\left.
\begin{aligned}
\frac{dT_2}{ds} + \tau &= 0 \\[2em]
\frac{dT_3}{ds} - \tau &= 0
\end{aligned}
\right\}
\tag{22}
$$

and transverse force equilibrium requires that

$$
\left.
\begin{aligned}
\frac{dV_2}{ds} + \sigma_c &= 0 \\[2em]
\frac{dV_3}{ds} - \sigma_c &= 0
\end{aligned}
\right\}
\tag{23}
$$

From plate theory, with the sign convention depicted in Figure 2,

$$
\left.
\begin{aligned}
\frac{d^2 w_2}{ds^2} &= -\frac{M_2}{D} \\[2em]
\frac{d^2 w_3}{ds^2} &= -\frac{M_3}{D}
\end{aligned}
\right\}
\tag{24}
$$

Assuming that the adhesive properties are linearly elastic in transverse tension,

$$
\frac{\sigma_c}{E_c} = \frac{(w_3 - w_2)}{\eta}
\tag{25}
$$

Based on the analyses developed in Reference 3, it is possible to proceed directly with an approximate solution of these equations. The precisely antisymmetric average adherend displacement throughout the bonded area is taken to be

93

$$\frac{1}{2}(w_2 + w_3) = As^3 + Cs \approx w_2 \approx w_3 \tag{26}$$

The similarity of the slopes dw_2/ds and dw_3/ds is also assumed, but the distinction between the higher derivatives must be maintained since, at the ends of the joint $(s = \pm c)$,

$$\frac{d^2 w_3}{ds^2} = \frac{d^3 w_3}{ds^3} \equiv 0 \text{ at } s = \quad c \text{ and } \frac{d^2 w_2}{ds^2} = \frac{d^3 w_2}{ds^3} \equiv 0 \text{ at } s = +c \tag{27}$$

Therefore, it is sometimes necessary to set

$$w_2 = \left[\left(w_2 + w_3 \right) + \left(w_2 \quad w_3 \right) \right] /2 \tag{28}$$

to complete the solution.

The displacement at the edge of the overlap $(x = \ell , s = -c)$ is given by

$$w_1 \Big|_{x=\ell} = \left(\frac{t + \eta}{\ell + c} \right) \frac{\ell}{2} + \frac{1}{2} B_1 e^{\xi \ell} = \frac{1}{2}(w_2 + w_3) \Big|_{s=-c} = -Ac^3 - Cc \tag{29}$$

Matching the slopes at the same location leads to the results

$$\frac{dw_1}{dx} \Big|_{x=\ell} = \frac{1}{2} \left(\frac{t + \eta}{\ell + c} \right) + \frac{1}{2} B_1 \xi e^{\xi \ell} \approx \frac{1}{2} \frac{d(w_2 + w_3)}{ds} \Big|_{s=-c} = 3Ac^2 + C \tag{30}$$

The continuity of the bending moment at that location requires that

$$\frac{d^2 w_1}{dx^2} \Big|_{x=c} = \frac{1}{2} B_1 \xi^2 e^{\xi \ell}$$

$$= \frac{1}{2} \left[\frac{d^2(w_2 + w_3)}{ds^2} + \frac{d^2(w_2 \quad w_3)}{ds^2} \right]_{s=\quad c} = -6Ac \quad \frac{M_c}{2D} \tag{31}$$

so that

$$\frac{M_c}{D} = -\frac{1}{2} B_1 \xi^2 e^{\xi \ell} = 12Ac \tag{32}$$

The equations above can be solved simultaneously. Thus,

94

$$\left(\frac{t+\eta}{\ell+c}\right)\frac{\ell}{2}+\frac{1}{2}B_1e^{\xi\ell} = -Ac^3 \quad Cc$$

$$\frac{1}{2}\left(\frac{t+\eta}{\ell+c}\right)+\frac{1}{2}B_1\xi e^{\xi\ell} = 3Ac^2 + C$$

$$\frac{1}{2}B_1\xi^2 e^{\xi\ell} = 12Ac$$

(33)

These are easily solved to yield

$$\frac{1}{2}\left(\frac{t+\eta}{\ell+c}\right)(\ell+c)+\frac{1}{2}B_1e^{\xi\ell}(1+\xi c) = 2Ac^3 = -\frac{1}{2}B_1e^{\xi\ell}\left(\frac{\xi^2c^2}{6}\right)$$

(34)

whence the bending moment at the ends of the bonded overlap ($x = \ell$, $s = -c$) is given by

$$M_c = \frac{P(t+\eta)/2}{[1+\xi c+\frac{1}{6}\xi^2c^2]}$$

(35)

as given in Equation (39) of Reference 3. The relation is plotted in Figure 3 for aluminum alloys of various overlap-to-thickness ratios and for a range of nominal average adherend stresses outside the joint area. Increases in the bonded overlap (2c) are shown to be a very powerful means of increasing the joint efficiency because the entire adherend outside the joint area can then be operated safely at a higher stress.

The primary consequence of the bending moment M_e, due to the eccentricity in load path, is a reduction in the remote adherend stress for a given maximum allowable stress. The ratio of this average to maximum stress represents the structural efficiency of the panel and is expressible in the form

$$\eta = \frac{\sigma_{avg}}{\sigma_{max}} = \frac{\sigma_{avg}}{\sigma_{avg}+6M/t^2} = \frac{1}{1+3/[1+\xi c+\frac{1}{6}\xi^2c^2]}$$

(36)

as plotted in the lower portion of Figure 4. The upper portion is the inverse of this quantity and represents the severity of stress concentration.

Now that the bending moment M_e at the ends of the overlap has been established, it is possible to solve for the distribution of the adhesive peel stresses σ_c. From Equations (24) and (25),

$$\frac{d^2(w_3 - w_2)}{ds^2} = \frac{1}{D}(M_3 - M_2) = \left(\frac{\eta}{E_c}\right)\frac{d^2\sigma_c}{ds^2}$$

(37)

95
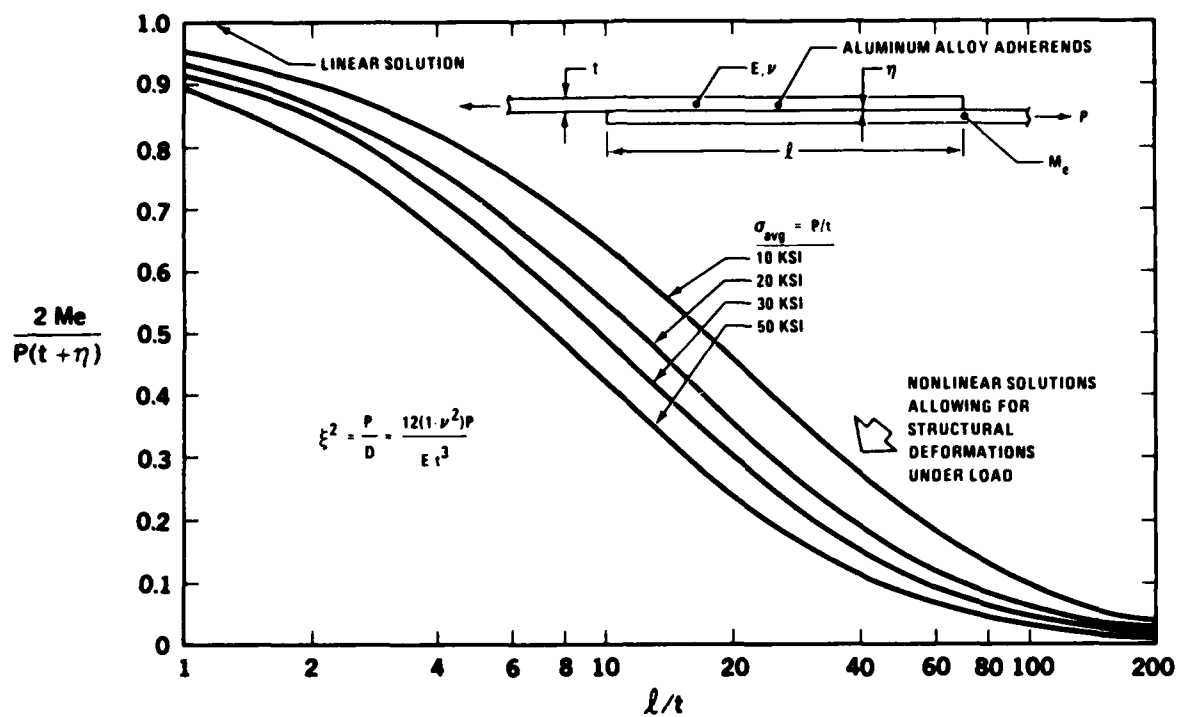
FIGURE 3. NONDIMENSIONALIZED ADHEREND BENDING MOMENT IN SINGLE-LAP JOINTS
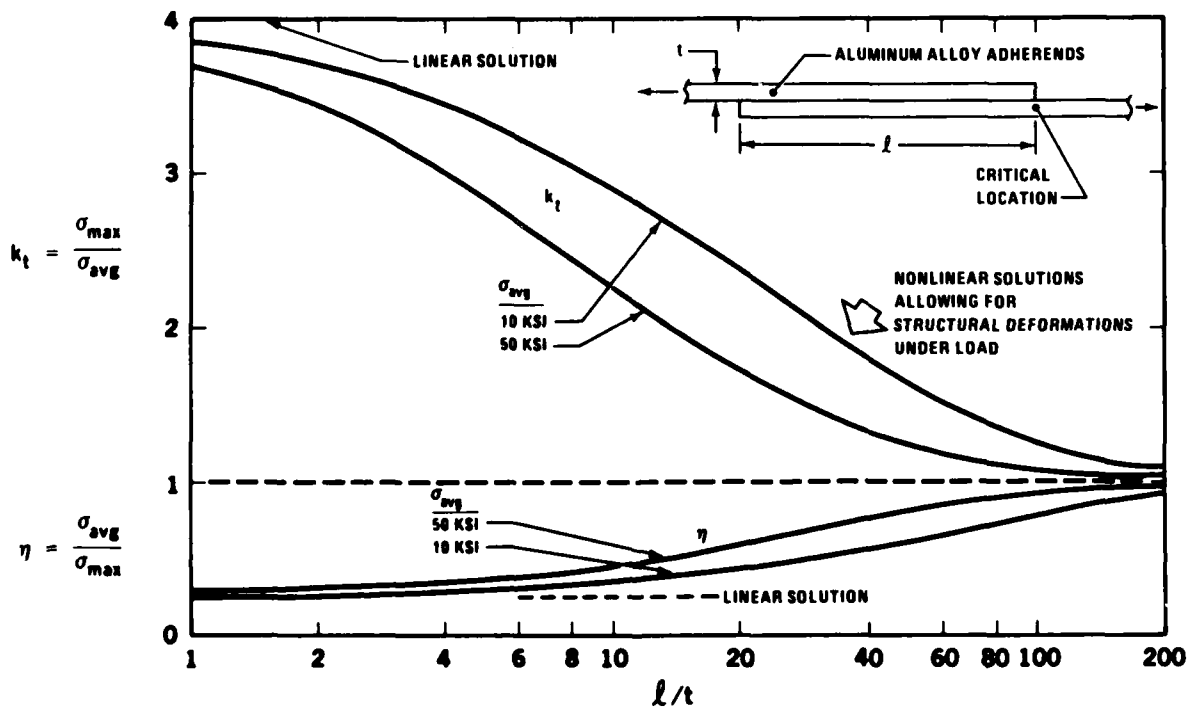
FIGURE 4. ADHEREND STRESS CONCENTRATION AND JOINT EFFICIENCY OF SINGLE-LAP JOINTS

96

Differentiating twice, and substituting from Equations (21) and (23), it follows that

$$\left(\frac{\eta}{E_c}\right)\frac{d^3\sigma_c}{ds^3} = -\frac{1}{D}(V_3 - V_2) \tag{38}$$

and

$$\left(\frac{\eta}{E_c}\right)\frac{d^4\sigma_c}{ds^4} = -\frac{2\sigma_c}{D} \tag{39}$$

or

$$\frac{d^4\sigma_c}{ds^4} + 4\chi^4\sigma_c = 0 \tag{40}$$

where

$$\chi^4 = \frac{E_c}{2\eta D} \tag{41}$$

Given that the adhesive peel stresses must be symmetric about the middle of the overlap (s = 0), the appropriate solution of Equation (40) is

$$\sigma_c = A\cos(\chi s)\cosh(\chi s) + B\sin(\chi s)\sinh(\chi s) \tag{42}$$

The boundary conditions are the value of the adherend bending moment, M_e, at the ends of the overlap and the absence of net transverse force across the bond line: that is

$$\int_{-c}^{+c}\sigma_c\,ds \equiv 0, \text{ or } \int_{o}^{c}\sigma_c\,ds \equiv 0 \tag{43}$$

Thus,

$$A[\sin(\chi c)\cosh(\chi c) + \cos(\chi c)\sinh(\chi c)]$$
$$+ B[\sin(\chi c)\cosh(\chi c) - \cos(\chi c)\sinh(\chi c)] = 0 \tag{44}$$

so that, for all but very short overlaps,

$$A[\cos(\chi c) + \sin(\chi c)] = B[\cos(\chi c) - \sin(\chi c)] \tag{45}$$

The preceding simplification follows from the approximation

97

$$\sinh(\chi c) \cong \cosh(\chi c) \to \frac{1}{2}e^{\chi c} \qquad (46)$$

for moderately long, or longer, overlaps. The incorporation of the bending moment boundary condition can be understood from Figure 2. At $s = -c$,

$$M_2 \equiv M_e \text{ and } M_3 \equiv 0 \qquad (47)$$

with M_e being given by Equation (35). From Equations (37) and (47), then,

$$\frac{E_c M_e}{\eta D} = \frac{d^2 \sigma_c}{ds^2}\bigg|_{s = -c} = -2A\chi^2 \sin(\chi c)\sinh(\chi c) + 2B\chi^2 \cos(\chi c)\cosh(\chi c) \qquad (48)$$

$$\approx -\chi^2 e^{\chi c} [A \sin(\chi c) - B \cos(\chi c)] \qquad (49)$$

Now, from Equation (45),

$$A \sin(\chi c) - B \cos(\chi c) = A/[\sin(\chi c) - \cos(\chi c)] \qquad (50)$$

and

$$A \cos(\chi c) + B \sin(\chi c) = A/[\cos(\chi c) - \sin(\chi c)] \qquad (51)$$

From Equations (50) and (49),

$$A = \frac{E_c M_e}{\eta D \chi^2 e^{\chi c}} [\cos(\chi c) - \sin(\chi c)] \qquad (52)$$

whence,

$$B = \frac{E_c M_e}{\eta D \chi^2 e^{\chi c}} [\cos(\chi c) + \sin(\chi c)] \qquad (53)$$

From Equations (42) and (51), the peak peel stress at $s = \pm c$ is given by

$$\sigma_{c\,max} = \frac{E_c M_e}{2\eta D \chi^2} = M_e\sqrt{\frac{E_c}{2\eta D}} \qquad (54)$$

Thus, the peak peel stress in the adhesive is directly proportional to the adherend bending moment M_e induced by the eccentricity in load path. This explains why it is so important to design in an adequate overlap for single-lap joints, to reduce that bending moment. Equation

(54) is also the key to understanding the reason why the adhesive in test coupons behaves so differently from the adhesive in structural joints — the test coupons are proportioned to force a failure within the adhesive instead of outside the joint.

Equation (53) can be reexpressed in a slightly different form

$$\frac{\sigma_{c\ max}}{\sigma_{avg}} \propto k\sqrt{\left(\frac{E_c}{E}\right)\left(\frac{t}{\eta}\right)} \tag{55}$$

showing that, for a given adherend operating stress σ_{avg}, the maximum induced adhesive peel stress $\sigma_{c_{max}}$ can be minimized by the use of low-modulus (E_c) adhesives, by thick adhesive layers (η), and by thin ends of the adherends (t), as well as by increasing the overlap   decrease the eccentricity coefficient (k).

Figure 5 presents a comparison between the adhesive peel stresses in short- :   long-overlap joints which are otherwise identical. The difference is dramatic. Since the   :esive shear stresses would show much less difference between these cases — that derivatic .· e found in Equation (85) of Reference 3 — the adhesive peel stresses would obviously be   .y significant for the short-overlap test coupon in Figure 5 and negligible for the long-overlap structural joint.
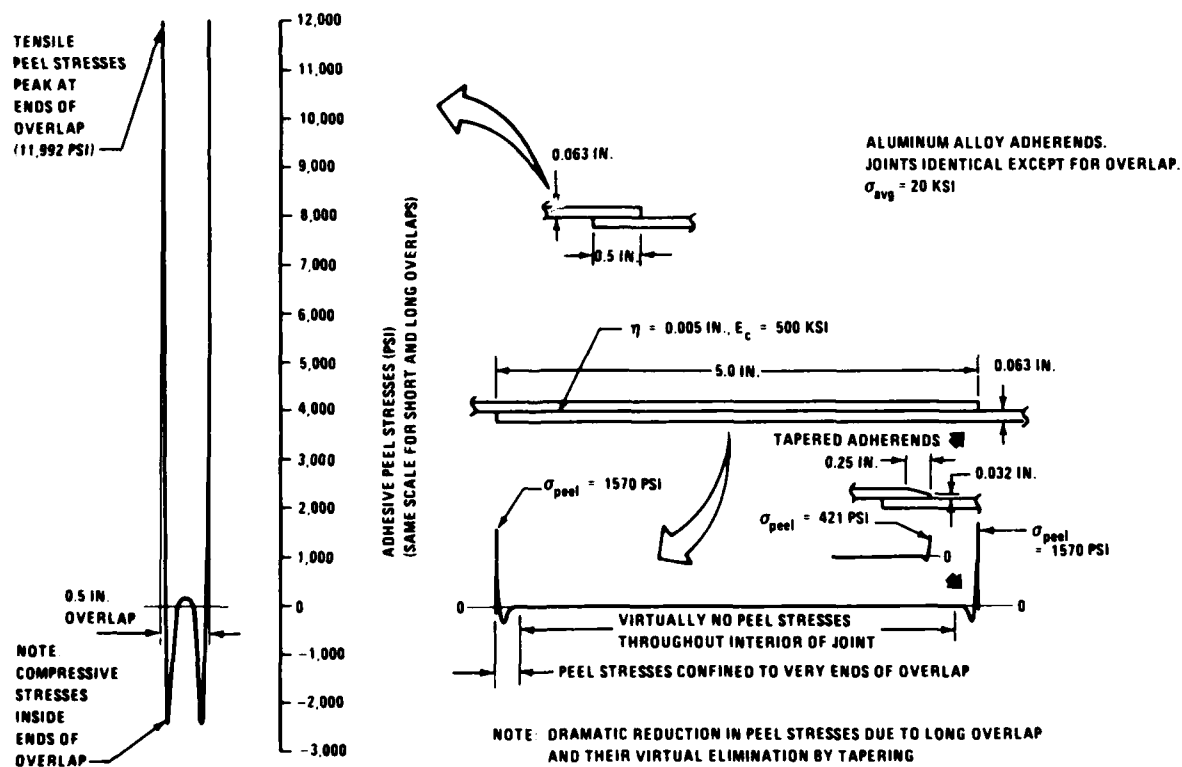
FIGURE 5. ADHESIVE PEEL STRESSES IN SHORT- AND LONG-OVERLAP SINGLE-LAP BONDED JOINTS

The peel stress distributions shown in Figure 5 also indicate that much of the bond area is subject to normal compressive stresses. This amplifies the peel stresses tremendously — indeed, almost half of the adhesive is trying to push the other half apart. This is why it is so important to minimize any induced peel stresses.

Figure 5 also illustrates a technique to restrict the peel stresses even further. The reduction in thickness of the adherends at the ends of the overlap decreases the resistance of the adherends to bending precisely where the peel stresses would be maximized. That, in turn, reduces the peel stresses, by a factor of 4 in the case shown. It should be noted that the adhesive peel stresses are confined to the very ends of the overlap, suggesting that the precise form of the thickness reduction — by stepping or tapering — is not critical. This thickness modification to minimize the peel stresses has a small benign effect on the adhesive shear stress distribution provided that the thickness of the adhesive layer is maintained. Actually, this tapering is prone to be associated with a pinch-off of the adhesive and a reduction in strength, as explained in Reference 4, if poor tooling and bagging techniques are used in manufacture. The end thickness of 0.020 inch shown in Figure 5 is representative of proper design practice, 0.030 ± 0.010 inch for aluminum alloys and 0.020 ± 0.010 inch for fibrous composites, the latter being thinner because the resin matrices are weaker in peel than are structural adhesives.

The modification of Equations (52) and (53) upon which the insert in Figure 5 is based is derived as follows. The local modification at the ends of the overlap has no effect on the value of the bending moment M_e at the ends of the overlap — at least to the level of accuracy implied by the approximation in Equation (26). Therefore, in the modified area, Equation (37) is replaced by

$$\frac{d^2(w_2 - w_3)}{ds^2} = \left(\frac{\eta}{E_c}\right) \frac{d^2\sigma_c}{ds^2} = -\frac{M_3}{D_t} + \frac{M_2}{D} \tag{56}$$

with D_t representing the thin tip on the adherend. Assuming that the effects of the adhesive shear stress distribution are small, as shown in Reference 3 by the identical solutions for linearly elastic and perfectly plastic adhesives, it then follows that

$$\frac{d^4\sigma_c}{ds^4} + 4(\chi')^4 \sigma_c = 0 \tag{57}$$

where

$$(\chi')^4 = \frac{E_c}{4\eta}\left(\frac{1}{D} + \frac{1}{D_t}\right) \tag{58}$$

The solution of Equation (57) is

$$\sigma_c = A' \cos(\chi's)\cosh(\chi's) + B' \sin(\chi's)\sinh(\chi's) \tag{59}$$

100

where

$$A' = \frac{F_c M_e}{\eta D(\chi')^2 e^{\chi' c}} [\cos(\chi' c) - \sin(\chi' c)] \tag{60}$$

and

$$B' = \frac{F_c M_e}{\eta D(\chi')^2 e^{\chi' c}} [\cos(\chi' c) + \sin(\chi' c)] \tag{61}$$

The peak peel stress at s = ±c is now given by

$$\sigma_{c\ max} = \frac{F_c M_e}{2\eta D(\chi')^2} = M_e \sqrt{\frac{F_c}{\eta D\left[1 + \left(\frac{t}{t_e}\right)^3\right]}} \tag{62}$$

and can be much less than given by Equation (54) without the tapering. The ratio of peak induced peel stress with and without thinning the ends of the adherends is thus

$$\frac{(\sigma_{c\ max})\ tapered}{(\sigma_{c\ max})\ uniform} = \sqrt{\frac{2}{1 + \left(\frac{t}{t_e}\right)^3}} \tag{63}$$

The single-lap joints between identical adherends which have been analyzed here have the same adhesive and adherend stresses at each end of the joint. If one of the members were to be thicker than the other, the thinner member would be subject to a proportionally greater bending moment at the end of the overlap because of both the increased eccentricity in load path and the greater flexibility at that end of the joint. The adhesive peel stresses would be aggravated there also. These additional stress concentrations are analyzed in Reference 3, albeit not always to the depth covered here. The key conclusion from those analyses is that any adherend imbalance induces even greater stress concentrations than does the basic eccentricity in load path. The techniques used to minimize those stress concentrations — increased overlaps and tapering the ends of the adherends — remain effective for unbalanced joints also but are even more necessary.

SINGLE-STRAP (FLUSH) BONDED JOINTS

The use of a long bonded overlap was shown above to improve the strength of single-lap bonded joints because the eccentricity in load path could be alleviated by gentle deflections. In the case of the flush bonded joint, shown in Figure 6, there must inevitably be an abrupt discontinuity precisely where the skins butt together. Consequently, the single-strap (flush) bonded joint has more severe induced peel stresses in the adhesive than any other kind of skin splice. This was the only form of bonded joint to exhibit any flaw growth in the series of tests reported in Reference 1. Tests conducted during the present investigation, on unflawed flush bonded joints, have also confirmed the tendency of such joints to disbond. However, parallel tests have demonstrated that simple modifications can considerably increase the fatigue life. It must be noted, however, that the fatigue life should be increased to infinity because, once such a disbond starts, it spreads quite rapidly.
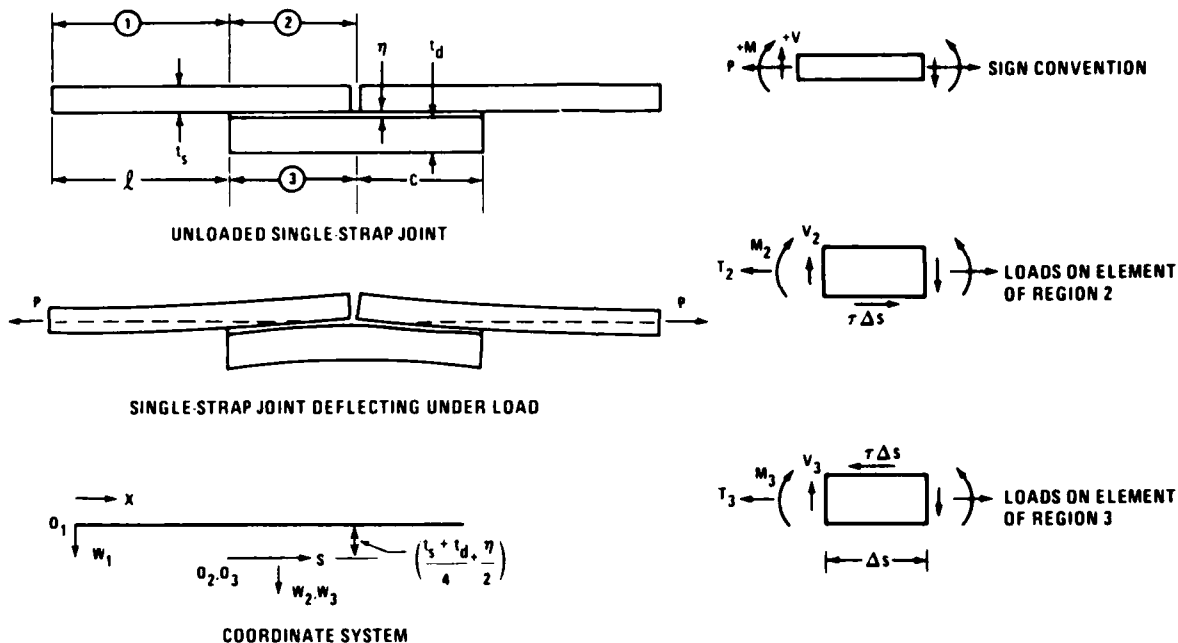
FIGURE 6. COORDINATE SYSTEM AND DEFORMATIONS IN SINGLE-STRAP BONDED JOINTS

The analysis of such a single-strap bonded joint should include provision for a splice strap which is thicker than the skin because the bending moment induced in the splice plate where the skins butt together is frequently the most critical condition in the joint. Using the terminology defined in Figure 6, the governing equations derived are as follows.

Throughout the adherend 1, outside the joint, the longitudinal stress resultant is uniform, at the value P of the applied load. The associated bending moment is then given by the equilibrium equation

$$M_1 = Pw_1 \text{ for } 0 \leqslant x \leqslant \ell$$

(64)

102

Since

$$\frac{d^2 w_1}{dx^2} = + \frac{M_1}{D_s} \qquad (65)$$

the equation defining the deflection of the skin outside the joint is

$$\frac{d^2 w_1}{dx^2} = \frac{P}{D_s} w_1 = \xi_s^2 w_1 \qquad (66)$$

and the solution is

$$w_1 = A_1 \left[\cosh(\xi_s x) \ 1 \right] + B_1 \sinh(\xi_s x) \qquad (67)$$

The values of A_1 and B_1 depend on the precise nature of the boundary conditions at $x = 0$ but, in the area adjacent to the joint, the solution can be approximated by the result

$$w_1 \approx C_1 e^{\xi_s x} \qquad (68)$$

regardless of whether the ends are simply supported or built-in. The deflection at the edge of the splice plate is thus

$$\delta_e = C_1 e^{\xi_s \ell} \qquad (69)$$

and the slope there is

$$\left. \frac{dw_1}{dx} \right|_{x=\ell} = C_1 \xi_s e^{\xi_s \ell} \qquad (70)$$

while the bending moment is given by

$$M_e = D_s \left. \frac{d^2 w_1}{dx^2} \right|_{x=\ell} = C_1 D_s \xi_s^2 e^{\xi_s \ell} \qquad (71)$$

Within the bonded joint area, the deflection is approximated by the simplest possible expression,

$$\frac{1}{2}(w_2 + w_3) = A_{23} s^3 + B_{23} s^2 + C_{23} s + F_{23} \qquad (72)$$

The matching of the various boundary conditions then yields

103

$$w_1 \bigg|_{x=c} = C_1 e^{\xi_s x} = \frac{1}{2}(w_2 + w_3)\bigg|_{s=0} = F_{23} \tag{73}$$

$$\frac{dw_1}{dx}\bigg|_{x=c} = C_1 \xi_s e^{\xi_s x} \approx \frac{1}{2}\frac{d(w_2 + w_3)}{ds}\bigg|_{s=0} = C_{23} \tag{74}$$

$$M_c = D_s \frac{d^2 w_1}{dx^2}\bigg|_{x=c} = C_1 D_s \xi_s^2 e^{\xi_s x} = \frac{1}{2}D_s\left[\frac{d^2(w_2 + w_3)}{ds^2} + \frac{d^2(w_2 - w_3)}{ds^2}\right]_{s=0}$$

$$= 2B_{23}D_s + \frac{1}{2}M_c \tag{75}$$

$$\frac{1}{2}\frac{d(w_2 + w_3)}{ds}\bigg|_{s=c} \equiv 0 = 3A_{23}c^2 + 2B_{23}c + C_{23} \tag{76}$$

The bending moment in the middle of the splice plate, at $s = c$, is determined as follows

$$M_m = D_d \frac{d^2 w_3}{ds^2}\bigg|_{s=c} = \frac{D_d}{2}\left[\frac{d^2(w_2 + w_3)}{ds^2} - \frac{d^2(w_2 - w_3)}{ds^2}\right]_{s=c}$$

$$= D_d\left[6A_{23}c + 2B_{23}\right] + \frac{1}{2}M_m \tag{77}$$

whence

$$M_m = 2D_d(6A_{23}c + 2B_{23}) \tag{78}$$

and M_m will have the opposite sign to that of the bending moment M_e at the outer edge of the bond — M_m will be negative for the sign convention adopted in Figure 6.

An explicit algebraic solution of these equations can be achieved for all of these quantities by solving first for the deflection δ_e at the outer edge of the bonded area. An alternative expression for the bending moment M_m is given by

$$M_m = P\left[\frac{t_s + t_d}{2} + \eta \quad w_3\bigg|_{s=c}\right] = P\left[\frac{t_s + t_d}{2} + \eta \quad A_{23}c^3 \quad B_{23}c^2 \quad C_{23}c \quad F_{23}\right] \tag{79}$$

104

so that

$$\frac{t_s + t_d}{2} + \eta = A_{23} c \left(c^2 - 12 \frac{D_d}{P} \right) + B_{23} \left(c^2 - 4 \frac{D_d}{P} \right) + C_{23} c + F_{23} \tag{80}$$

Now,

$$F_{23} = \delta_c \tag{81}$$

$$C_{23} = \xi_s \delta_c \tag{82}$$

$$B_{23} = \frac{1}{4} \xi_s^2 \delta_c \tag{83}$$

and

$$A_{23} = -\frac{C_{23}}{3c^2} - \frac{2 B_{23} c}{3c^2} = -\frac{\xi_s \delta_c}{3c^2} \left(\frac{\xi_s c}{2} + 1 \right) \tag{84}$$

Substituting Equations (81) through (84) into Equation (80) then yields, after some algebraic manipulation,

$$\delta_c = \frac{\left(\frac{t_s + t_d}{2} + \eta \right)}{\left[1 + \frac{2}{3} \xi_s c + \frac{1}{12} \xi_s^2 c^2 + \frac{\xi_s^2}{\xi_d^2} \left(1 + \frac{4}{\xi_s c} \right) \right]} \tag{85}$$

in which

$$\xi_d^2 = P/D_d \tag{86}$$

is related to the splice plate (or doubler).

The coefficients A_{23}, B_{23}, C_{23}, and F_{23} can then be evaluated in turn. The deflection δ_m at the middle of the splice plate, where the skins butt together, then follows from Equations (72), (84), (83), (82), and (81) as

$$\delta_m = \delta_c \left[-\frac{\xi_s c}{3} \left(\frac{\xi_s c}{2} + 1 \right) + \frac{1}{4} \xi_s^2 c^2 + \xi_s c + 1 \right] \tag{87}$$

105

whence

$$\delta_m = \frac{\left(\dfrac{t_s + t_d}{2} + \eta\right)}{\left[1 + \dfrac{\xi_s^2 \left(1 + 4/\xi_s c\right)}{\xi_d^2 \left(1 + \dfrac{2}{3}\xi_s c + \dfrac{1}{12}\xi_s^2 c^2\right)}\right]} \tag{88}$$

Since

$$\delta_m < \left(\frac{t_s + t_d}{2} + \eta\right) \tag{89}$$

it can be concluded that the centroid of the splice plate never crosses over to the other side of the line of action of the load. It can never deflect quite that far, anyway, because the bending moment would then be zero. The deflection δ_m is important because it represents the relief with respect to the original undeflected position.

The most severe bending moments in the adherends are at the ends of the bonded overlap. The peak bending moment in the skin is

$$M_e = P\delta_e \tag{90}$$

and the associated bending stresses can be combined with the direct membrane stresses to produce a maximum stress (adjacent to the adhesive) of

$$\left(\sigma_{max}\right)_{skin} = \frac{P}{t_s} \left(1 + 6\frac{\delta_e}{t_s}\right) \tag{91}$$

Likewise, in the middle of the splice plate, the maximum stress is

$$\left(\sigma_{max}\right)_{doubler} = \frac{P}{t_d} \left[1 + \frac{6}{t_d}\left(\frac{t_s + t_d}{2} + \eta \quad \delta_m\right)\right] \tag{92}$$

An alternate expression for the bending moment M_m follows from Equations (78), (83), and (84).

$$M_m = D_d \xi_s^2 \delta_e \left(1 + \frac{4}{\xi_s c}\right) \tag{93}$$

This bending moment, being intrinsically negative, reflects curvature in the opposite direction to that in the skin immediately outside the joint.

106

Equation (93) can be reexpressed in nondimensional form as

$$\frac{M_m}{P\left(\dfrac{t_s + t_d}{2} + \eta\right)} = \frac{1}{\left[1 + \dfrac{\left(1 + \dfrac{2}{3}\xi_s c + \dfrac{1}{12}\xi_s^2 c^2\right)}{\left(\dfrac{t_d}{t_s}\right)^3 \left(1 + \dfrac{4}{\xi_s c}\right)}\right]} \tag{94}$$

and this expression is plotted at the bottom of Figure 7 for aluminum alloys. Again, the structural deformations under load impart a substantial relief with respect to what would be predicted by the first-order linear analysis. The bending Moment M_e, at the outside end of the load, cannot be expressed in such a simple form because the linear analysis would not predict that there was a bending moment there. However, the same denominator as in the left side of Equation (94) could be used as a reference value, whence

$$\frac{M_e}{P\left(\dfrac{t_s + t_d}{2} + \eta\right)} = \frac{1}{\left[1 + \dfrac{2}{3}\xi_s c + \dfrac{1}{12}\xi_s^2 c^2 + \left(\dfrac{t_d}{t_s}\right)^3 \left(1 + \dfrac{4}{\xi_s c}\right)\right]} \tag{95}$$
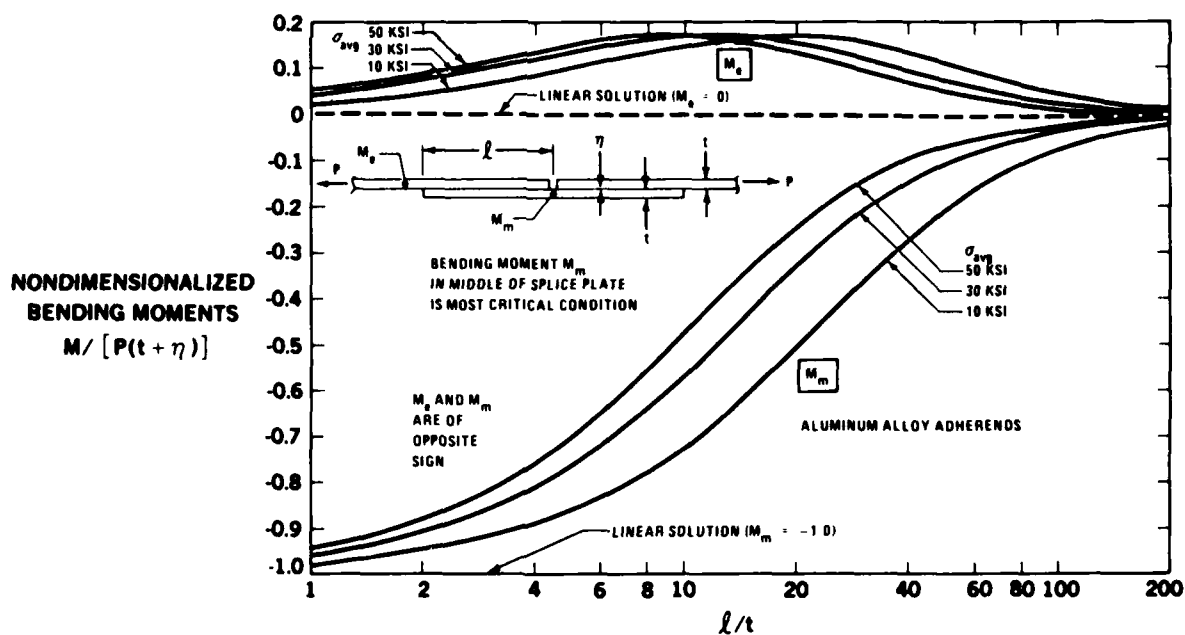
FIGURE 7. NONDIMENSIONALIZED ADHEREND BENDING MOMENTS IN SINGLE-STRAP (FLUSH) JOINTS

This relation is plotted at the top of Figure 7, and comparison with the lower curves in Figure 7 for the nondimensionalized bending moment M_m at the middle of the splice plate indicates that the conditions at the outer edge are less severe. It is also informative to compare

107

Figures 3 and 7, which show how much more rapidly the bending stresses decay for the unsupported single-lap joint which can more easily deflect out of the way. Nevertheless, long bonded overlaps are still very beneficial for single-strap (flush) bonded joints.

Equations (94) and (95) permit the splice plate to be thicker than the skin, to alleviate the bending moment in the middle of the splice plate, where the skins butt together. Replotting the curves from Equations (94) and (95) for values of the ratio t_d/t_s other than unity, however, would indicate only the harm from the increase in eccentricity in load path. This can be noted from a comparison between Figures 7 and 8. A more meaningful comparison would be the combination of the peak bending stresses with the membrane stresses since they will also be reduced in the splice plate. From plate-bending theory,

$$\sigma_{max} = \frac{P}{t_d} + \frac{6M_m}{t_d^2} = \sigma_{remote} \left(\frac{t_s}{t_d}\right) \left(1 + \frac{6M_m}{Pt_d}\right) \tag{96}$$

in which σ_{remote} is the average skin stress far away from the splice. Neglecting the small contribution from the thin adhesive layer, Equation (96) can be reexpressed by means of Equation (94) as

$$\frac{\sigma_{max}}{\sigma_{remote}} = \left(\frac{t_s}{t_d}\right) \left[1 + \frac{3\left(1 + \frac{t_s}{t_d}\right)}{1 + \frac{\left(1 + \frac{2}{3}\xi_s c + \frac{1}{12}\xi_s^2 c^2\right)}{\left(\frac{t_s}{t_d}\right)^3 \left(1 + \frac{4}{\xi_s c}\right)}}\right] \tag{97}$$

NONDIMENSIONALIZED BENDING MOMENTS

$$M / \left[P\left(\frac{t_s + t_d}{2} + \eta\right)\right]$$

BENDING MOMENT M_s IN SKIN DECREASED DUE TO STIFFER SPLICE PLATE

BENDING MOMENT M_m IN SPLICE PLATE INCREASED DUE TO INCREASED ECCENTRICITY IN LOAD PATH, BUT NOT AS MUCH AS BENDING STRENGTH IS INCREASED

FIGURE 8. EFFECT OF THICKENED DOUBLER ON BENDING MOMENTS IN SINGLE-STRAP (FLUSH) JOINTS

108
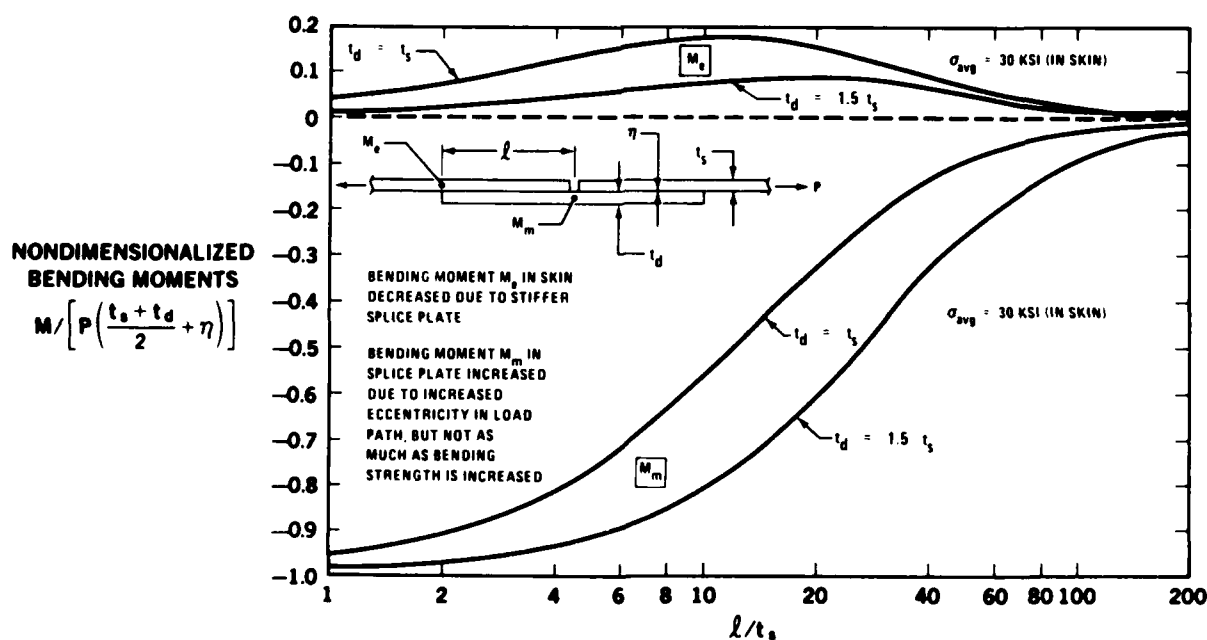
In Equation (97), which is plotted in Figure 9,

$$\xi_c = \left(\frac{c}{t_s}\right)\sqrt{12(1-\nu^2)\left(\frac{\sigma_{remote}}{t}\right)}$$

(98)
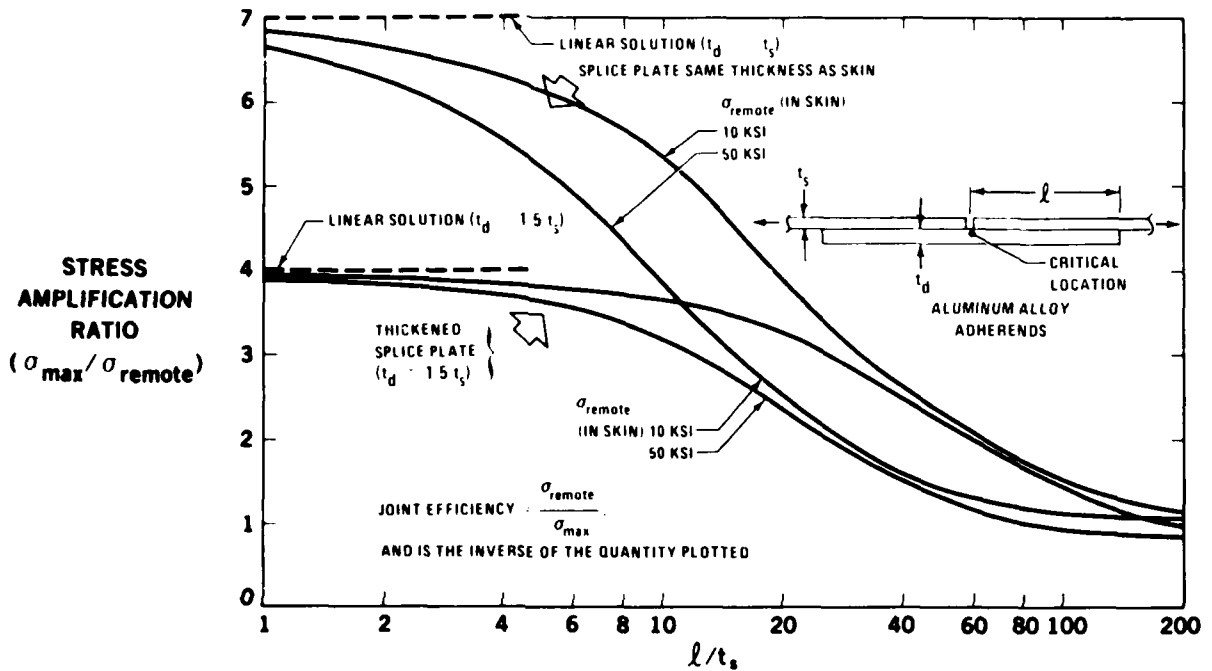
FIGURE 9. REDUCTION IN MAXIMUM ADHEREND STRESS IN SINGLE-STRAP JOINTS DUE TO
THICKENED SPLICE PLATE

The curves in Figure 9 show all the effects of increasing the thickness of the splice plate.
Whereas the effect of the c/t_s ratio is monotonic and always beneficial, as shown in Figure 7, the
effects of the t_d/t_s ratio on the bending moment M_m are complex, as can be noted from Figures 8
and 9. In Figure 8, the peak bending moment M_m at the middle of the splice plate is increased by
thicker splice plates because of the increase in eccentricity, while the peak bending moment M_e
in the skin is decreased by the thicker splice plate which bends less. Figure 9, however, shows
that the overall effect on the peak stress in the thickened splice plates is beneficial. It is
necessary that the doubler be thicker than the skin if these two stress concentration areas are to
be equally severe.

The peaks in the adhesive panel stress distribution also occur at the same two locations, at $s = 0$
and $s = c$, and usually differ in intensity. The method of determining these stress distributions is
as follows. Within regions 2 and 3 in Figure 6, moment equilibrium requires that

$$\left.\begin{array}{c} \dfrac{dM_2}{ds} - V_2 + \tau\left(\dfrac{t_s + \eta}{2}\right) = 0 \\[2ex] \dfrac{dM_3}{ds} - V_3 + \tau\left(\dfrac{t_d + \eta}{2}\right) = 0 \end{array}\right\}$$

(99)

109

while longitudinal force equilibrium requires that

$$\left.\begin{array}{l} \dfrac{dl_2}{ds} + \tau = 0 \\[4mm] \dfrac{dl_3}{ds} \quad \tau = 0 \end{array}\right\} \tag{100}$$

and transverse force equilibrium requires that

$$\left.\begin{array}{l} \dfrac{dV_2}{ds} + \sigma_c = 0 \\[4mm] \dfrac{dV_3}{ds} \quad \sigma_c = 0 \end{array}\right\} \tag{101}$$

From the classical theory of the plate bending,

$$\left.\begin{array}{l} \dfrac{d^2 w_2}{ds^2} = +\dfrac{M_2}{D_s} \\[4mm] \dfrac{d^2 w_3}{ds^2} = +\dfrac{M_3}{D_d} \end{array}\right\} \tag{102}$$

and, assuming that the adhesive properties are linearly elastic in peel (transverse tension),

$$\frac{\sigma_c}{E_c} = \frac{(w_2 \quad w_3)}{\eta} \tag{103}$$

Now, from Equations (102) and (103),

$$\left(\frac{\eta}{E_c}\right) \frac{d^2 \sigma_c}{ds^2} = \frac{d^2 (w_2 \quad w_3)}{ds^2} = +\frac{M_2}{D_s} \quad \frac{M_3}{D_d} \tag{104}$$

whence

$$\left(\frac{\eta}{E_c}\right) \frac{d^4 \sigma_c}{ds^4} = \left(\frac{1}{D_s} + \frac{1}{D_d}\right) \sigma_c \quad \frac{1}{2} \left[\frac{(t_s + \eta)}{D_s} \quad \frac{(t_d + \eta)}{D_d}\right] \frac{d\tau}{ds} \tag{105}$$

110

Assuming that the shear stress terms can be neglected, as due to plastic adhesive behavior at the ends of the overlap, for instance,

$$\frac{d^4\sigma_c}{ds^4} + 4\chi^4\sigma_c = 0 \tag{106}$$

where

$$\chi^4 = \frac{4F_c}{\eta}\left(\frac{1}{D_c} + \frac{1}{D_d}\right) \tag{107}$$

The solution of Equation (106) in this case can be asymmetric and requires all possible terms. Thus,

$$\sigma_c = A\cos(\chi s)\cosh(\chi s) + B\sin(\chi s)\sinh(\chi s)$$
$$\tag{108}$$
$$+ C\cos(\chi s)\sinh(\chi s) + D\sin(\chi s)\cosh(\chi s)$$

The key to evaluating coefficients A, B, C, and D is that, at some location within the bond area,

$$M_2 + M_3 \equiv 0 \text{ at } s = i \tag{109}$$

because of the opposite signs of M_m and M_e. At the point where the line of action of the load passes through the combined centroid, there must be a point of inflexion in both the adherends. Therefore,

$$\frac{d^2 w_2}{ds^2} = \frac{d^2 w_3}{ds^2} = \frac{1}{2}\frac{d^2(w_2 + w_3)}{ds^2} = 0 \text{ at } s = i \tag{110}$$

Since this point of inflexion is remote from the edges of the overlap (at s = 0 and s = c), there can be no high peel stresses at s = i, so

$$\frac{d^2(w_2 \quad w_3)}{ds^2} \approx 0 \text{ at } s = i \tag{111}$$

From Equations (72) and (110), then,

$$\frac{1}{2}\left.\frac{d^2(w_2 + w_3)}{ds^2}\right|_{s=i} = 0 = 6A_{23}i + 2B_{23} \tag{112}$$

whence, from Equations (83) and (84),

$$\iota = \frac{B_{23}}{3A_{23}} = \frac{\xi_s c^2}{(2 + \xi_s c)} = \frac{c}{\left(2 + \frac{1}{\xi_s c}\right)} \leqslant \frac{c}{2} \tag{113}$$

The point of inflexion thus shifts from near the outer edge (s = 0) at very low load toward the middle of the bond (s = c/2) at high loads. The significance of the location of this inflexion point is that it provides two of the "boundary" conditions to evaluate the constants A, B, C, and D in Equation (108). Overall vertical equilibrium requires that

$$\int_0^c \sigma_c \, ds \equiv 0 = \frac{A}{2\chi} \left| \sin(\chi c) \cosh(\chi c) + \cos(\chi c) \sinh(\chi c) \right|$$

$$+ \frac{B}{2\chi} \left| \sin(\chi c) \cosh(\chi c) - \cos(\chi c) \sinh(\chi c) \right| \tag{114}$$

so that, for all but very short overlaps,

$$A \left| \cos(\chi c) + \sin(\chi c) \right| = B \left| \cos(\chi c) - \sin(\chi c) \right| \tag{115}$$

since

$$\sinh(\chi c) \approx \cosh(\chi c) \approx \frac{1}{2} e^{\chi c} \text{ for large } \chi c \tag{116}$$

The other boundary conditions are that

$$M_2 = M_c \text{ and } M_3 = 0 \text{ at } s = 0 \tag{117}$$

$$M_2 = 0 \text{ and } M_3 = 0 \text{ at } s = \iota \tag{118}$$

and

$$M_2 = 0 \text{ and } M_3 = M_m \text{ at } s = c \tag{119}$$

Equation (106) is reexpressed in the form

$$\frac{d^4(w_2 - w_3)}{ds^4} + 4\chi^4(w_2 - w_3) = 0 \tag{120}$$

to express these three conditions. Now,

$$\frac{d^2(w_2 - w_3)}{ds^2} = \left(\frac{\eta}{E_c}\right) \frac{d^2\sigma_c}{ds^2} \tag{121}$$

$$= \frac{2\eta\chi^2}{E_c} \left[\text{A sin} (\chi s) \sinh (\chi s) + \text{B cos} (\chi s) \cosh (\chi s) \right.$$

$$\left. \text{C sin} (\chi s) \cosh (\chi s) + \text{D cos} (\chi s) \sinh (\chi s) \right] \tag{122}$$

So, from Equations (117) to (119) and (121) and (122), together with Equations (102),

$$\frac{M_e}{D_s} = \frac{2\eta\chi^2}{E_c} \, B \tag{123}$$

$$\text{A sin} (\chi) \sinh (\chi i) + \text{B cos} (\chi i) \cosh (\chi i) \quad \text{C sin} (\chi i) \cosh (\chi i)$$

$$+ \text{D cos} (\chi i) \sinh (\chi i) = 0 \tag{124}$$

and

$$\frac{M_m}{D_d} = \frac{2\eta\chi^2}{E_c} \left[\text{A sin} (\chi c) \sinh (\chi c) + \text{B cos} (\chi c) \cosh (\chi c) \right.$$

$$\left. \text{C sin} (\chi c) \cosh (\chi c) + \text{D cos} (\chi c) \sinh (\chi c) \right] \tag{125}$$

On introducing the approximations in Equation (116) and, for all but small loads, that

$$\sinh (\chi i) \approx \cosh (\chi i) \approx \frac{1}{2} e^{\chi i} \tag{126}$$

these conditions can be simplified further, to read

$$\text{A sin} (\chi i) + \text{B cos} (\chi i) \quad \text{C sin} (\chi i) + \text{D cos} (\chi i) = 0 \tag{127}$$

and

$$\frac{M_m}{D_d} = \left(\frac{\eta\chi^2}{E_c} \right) e^{\chi c} \left[- (A + C) \sin (\chi c) + (B + D) \cos (\chi c) \right] \tag{128}$$

The solution of these equations proceeds as follows. From Equation (123),

$$B = \frac{M_e}{D_s} \left(\frac{E_c}{2\eta\chi^2} \right) \tag{129}$$

113

Then, from Equation (115),

$$A = B \left[\frac{\cos(\chi c) \quad \sin(\chi c)}{\cos(\chi c) + \sin(\chi c)} \right] \qquad (130)$$

Now, from Equations (128) and (127),

$$(A + C)\sin(\chi c) \quad (B + D)\cos(\chi c) = \frac{M_m E_c}{D_d \eta \chi^2 e^{\chi c}} \qquad (131)$$

$$(A + C)\sin(\chi i) \quad (B + D)\cos(\chi i) = 0 \qquad (132)$$

whence

$$(A + C)\left[\tan(\chi c) \quad \tan(\chi i) \right] = \frac{M_m}{D_d}\left(\frac{E_c}{\eta \chi^2 e^{\chi c} \cos(\chi c)} \right) \qquad (133)$$

and

$$(B + D)\left[\frac{1}{\tan(\chi i)} \quad \frac{1}{\tan(\chi c)} \right] = \frac{M_m}{D_d}\left(\frac{E_c}{\eta \chi^2 e^{\chi c} \sin(\chi c)} \right) \qquad (134)$$

Therefore,

$$C = \frac{M_m}{D_d}\left(\frac{E_c}{\eta \chi^2 e^{\chi c} \cos(\chi c)} \right)\left[\frac{1}{\tan(\chi c) \quad \tan(\chi i)} \right] \qquad (135)$$

and

$$D = \frac{M_m}{D_d}\left(\frac{E_c}{\eta \chi^2 e^{\chi c} \sin(\chi c)} \right)\left[\frac{\tan(\chi c)\tan(\chi i)}{\tan(\chi c) \quad \tan(\chi i)} \right] \qquad (136)$$

The adhesive peel stress distribution then follows from Equations (108), (113), (129), (130), (135), and (136).

The peak peel stress at the edge of the splice plate is thus

$$\sigma_{c\ max}\bigg|_{s=0} = A = \frac{M_c}{D_s}\left(\frac{E_c}{2\eta \chi^2} \right)\left[\frac{\cos(\chi c) \quad \sin(\chi i)}{\cos(\chi c) + \sin(\chi i)} \right] \qquad (137)$$

114

while, at the middle of the splice plate,

$$\sigma_{c \, max} \Big|_{x \, c} \approx \frac{1}{2} e^{\chi c} \left[(A + C) \cos(\chi c) + (B + D) \sin(\chi c) \right]$$

$$= \frac{M_m}{D_d} \left(\frac{E_c}{2\eta\chi^2} \right) \left[\frac{1 + \tan(\chi c)\tan(\chi i)}{\tan(\chi c) \quad \tan(\chi i)} \right] \tag{138}$$

with each peak peel stress being proportional to the associated local peak adherend bending moment.

The explicit solution above, for large values of χc and χi, would be replaced by numerical solutions not relying on the approximations in Equations (116) and (126) for very short overlaps. The calculations for the examples presented have indicated some further useful approximate solutions. For short overlap joints, particularly at low load intensities, Equation (116) is often still valid, but Equation (126) is not. In such a case, the further solution of Equations (124) and (125) proceeds as follows.

$$\Theta = \frac{M_m E_c}{2\eta\chi^2 D_d} = A \sin(\chi c) \sinh(\chi c) \quad B \cos(\chi c) \cosh(\chi c)$$

$$+ C \sin(\chi c) \cosh(\chi c) \quad D \cos(\chi c) \sinh(\chi c) \tag{139}$$

$$\Theta = A \sin(\chi i) \sinh(\chi i) \quad B \cos(\chi i) \cosh(\chi i) + C \sin(\chi i) \cosh(\chi i)$$

$$D \cos(\chi i) \sinh(\chi i) \tag{140}$$

Then, by eliminating D between these equations,

$$\frac{\Theta}{\cos(\chi c)\sinh(\chi c)} = A \left[\tan(\chi c) \quad \tan(\chi i) \right] + B \left[\frac{1}{\tanh(\chi i)} \quad \frac{1}{\tanh(\chi c)} \right]$$

$$+ C \left[\frac{\tan(\chi c)}{\tanh(\chi c)} \quad \frac{\tan(\chi i)}{\tanh(\chi i)} \right] \tag{141}$$

when C can be determined on the basis of expressions from A and B in Equations (130) and (129). Likewise, by eliminating C,

$$\frac{\Theta}{\sin(\chi c)\cosh(\chi c)} = A \left[\tanh(\chi c) \quad \tanh(\chi i) \right] + B \left[\frac{1}{\tan(\chi i)} \quad \frac{1}{\tan(\chi c)} \right]$$

$$+ D \left[\frac{\tanh(\chi i)}{\tan(\chi i)} \quad \frac{\tanh(\chi c)}{\tan(\chi c)} \right] \tag{142}$$

115

which permits the determination of D. For long overlaps, the peel stress distributions at each end can be evaluated separately. Thus, for the outer end (s ≈ 0),

$$\sigma_c \approx A \cos(\chi s) \cosh(\chi s) + B \sin(\chi s) \sinh(\chi s) \tag{143}$$

while, at the other end of the joint (s ≈ c),

$$\sigma_c \approx \frac{1}{2} e^{\chi s} \left[(A + C) \cos(\chi s) + (B + D) \sin(\chi s) \right] \tag{144}$$

The accuracy of Equation (144) can be improved by the elimination of the coefficients (A + C) and (B + D) by Equations (133) and (134). This eliminates the need to compute the ratio of the very large quantities $e^{\chi c}$ and $e^{\chi s}$. Thus,

$$\sigma_c \approx \frac{M_m F_c}{2D_d \eta \chi^2 e^{\chi(c-s)}} \left\{ \frac{1}{[\tan(\chi c) - \tan(\chi i)]} \cdot \frac{\cos(\chi s)}{\cos(\chi c)} \right.$$

$$\left. + \frac{\tan(\chi c)\tan(\chi i)}{[\tan(\chi c) - \tan(\chi i)]} \cdot \frac{\sin(\chi s)}{\sin(\chi c)} \right\} \tag{145}$$

Since there are virtually no peel stresses inbetween the widely separated zones characterized by Equations (143) and (145), these equations can be used to calculate the peel stresses for all long-overlap joints, obviating the need to calculate the products of extremely large and extremely small quantities in the direct evaluation of Equation (108).

The actual adhesive peel stress distributions in single-strap (flush) bonded joints are not symmetric, as they are for single-lap joints. Figure 10 compares adhesive peel stress distributions for short- and long-overlap splices. Again, the benefits due to the long overlap is very evident. The reason for the compressive normal stresses at the outside ends of the splice plates appears to be that the splice plate moves toward the original position of the skin over its entire length. Because the bending moment in the middle of the splice plate is typically more severe than at the ends of the overlap of a single-lap joint [as can be seen by comparing Equations (36) and (97)], the associated peel stresses are also more severe. There is therefore a greater need for still longer overlaps or for the adherend tapering described in Figure 5. A sample of the benefit of such tapering is shown as an insert in Figure 10. In the case of a flush joint, it is aesthetically better to taper the bonded side of the skin, as shown in Figure 10, than the other side. Such modifications have been tested as part of this program. The tests have so far confirmed that the tapering is very effective in greatly delaying the failure of the adhesive caused by the induced peel stresses.

116
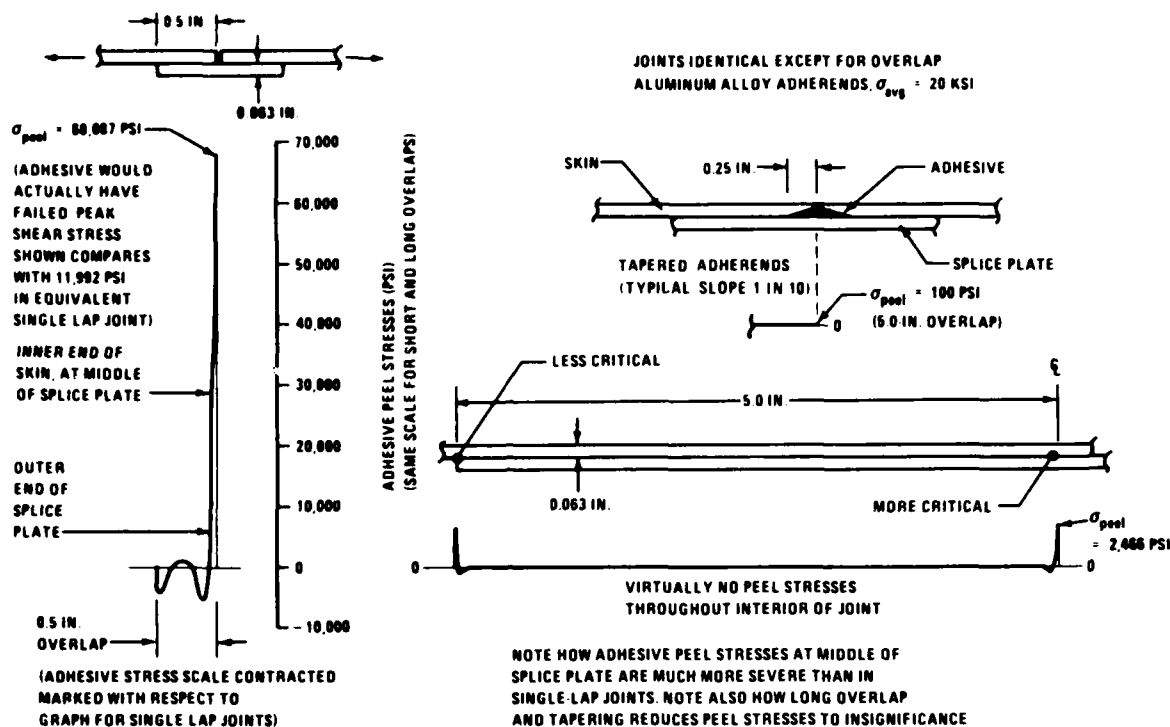
FIGURE 10. ADHESIVE PEEL STRESSES IN SHORT- AND LONG-OVERLAP SINGLE-STRAP BONDED JOINTS

IMPROVED FLUSH BONDED JOINTS

The analysis in the preceding section has indicated that the conventional single-strap flush bonded joint has a potential critical location in the splice plate and in the adhesive where the skins butt together. The severity of this condition can be alleviated by increasing the bonded overlap to about 100 times the skin thickness, or by thickening the splice plate an extra 20 to 50 percent with respect to the skin. The modifications to the end of the adherends which can be thinned down by tapering, in conjunction with local thickening of the adhesive layer, are particularly effective in minimizing the adhesive peel stresses. However, those local modifications have only a negligible effect on the bending moments in the adherends because the bending moments are dominated by the basic eccentricity in the load path.

Two other techniques for dealing with the problems inherent in flush bonded joints are worthy of discussion here. The first is described in Figure 11 and is based on a simultaneous decrease in the eccentricity and increase in the bending stiffness of the splice plate. The thinned step in the skin does not represent a major weakness because roughly half of the load has already been transferred by the adhesive bond at the outer end of the joint before the thickness has been reduced. The splice plate can be made either by laminating at the time the bonded joint is made or by chem-milling ahead of time. The former method is preferable, but the differences are so small they do not influence the analysis to the depth covered here.

It is not necessary to repeat the entire analysis for the uniform single-strap (flush) bonded joints since the dominant effect is a reduction in eccentricity load path. The numerator in Equation (85) would be reduced from $[(t_s + t_d)/2 + \eta]$ to $[(t_d/2) + \eta]$, with a consequent reduction in the deflection δ_e at the edge of the splice to

$$\delta_e = \frac{\left(\frac{t_d}{2} + \eta\right)}{\left[1 + \frac{2}{3}\xi_s c + \frac{1}{12}\left(\xi_s c\right)^2 + \frac{\xi_s^2}{\xi_d^2}\left(1 + \frac{4}{\xi_s c}\right)\right]} \tag{146}$$

In Equation (146), the exponent ξ_s is evaluated for the skin just outside the bonded overlap (at s = 0 in Figure 6) while ξ_d is evaluated for the full splice plate thickness (at s = c in Figure 6). These distinctions are needed in this and related equations because of the variation in skin and splice thickness throughout the bonded area (Figure 11).

Likewise the deflection at the middle of the splice, where the skins butt together, would be reduced in the same ratio to less than that given by Equation (88):

$$R = \left(\frac{t_d}{2} + \eta\right) \bigg/ \left(\frac{t_s + t_d}{2} + \eta\right) \tag{147}$$

The bending moments M_m and M_e, given by Equations (94) and (95) respectively, would also be reduced by this same factor.

118
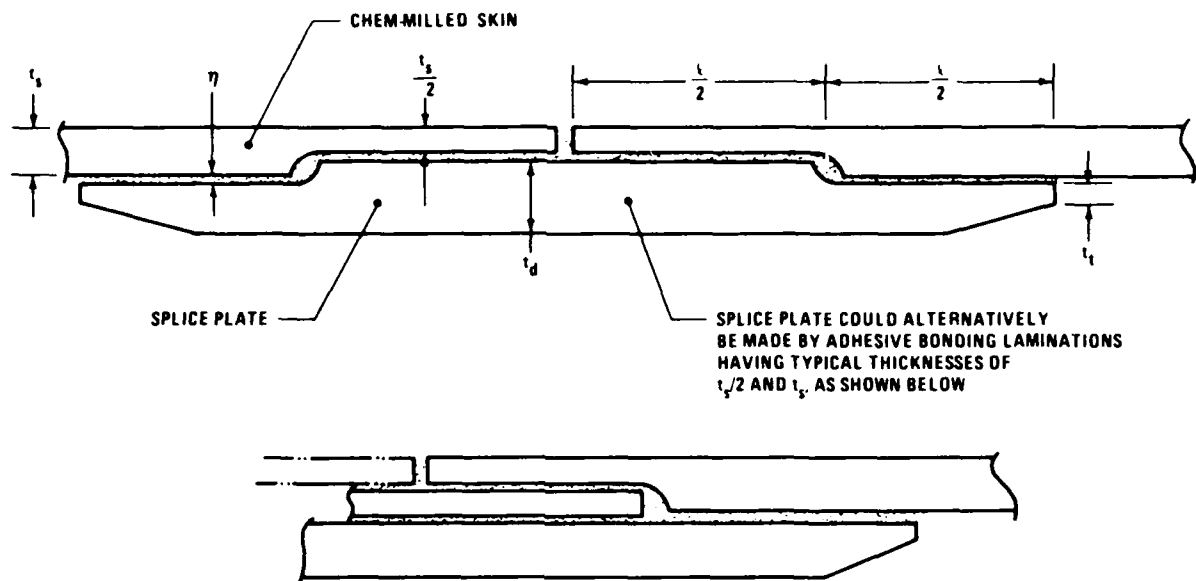
FIGURE 11. FLUSH BONDED JOINT WITH REDUCED ECCENTRICITY IN LOAD PATH

Since the induced peel stresses in the adhesives are proportional to these same adherend bending moments, they would be reduced in the same ratio from their values given by Equations (137) and (138). However, there is a further reduction in these peel stresses because of the increased flexibility of the thinned skin at the middle of the splice plate. In addition, the value of the exponent χ in Equation (107) is altered by the changes in skin and splice plate thicknesses. There would now be a different value of χ for each end of the bonded overlap, identified by the subscripts e and n.

Consider first the outer ends of the splice plate, as at $s = 0$. The adhesive peel stresses are still given by Equation (106)

$$\frac{d^4 \sigma_c}{ds^4} + 4\chi_e^4 \sigma_c = 0 \tag{148}$$

where, now, the value of χ_e is not given by Equation (107) but by

$$\chi_e^4 = \frac{E_c}{4\eta} \left(\frac{1}{D_s} + \frac{1}{D_d} \right) \quad or \quad \frac{E_c}{4\eta} \left(\frac{1}{D_s} + \frac{1}{D_t} \right) \tag{149}$$

Based on the knowledge from the analysis above that the peel stresses decay to zero quite rapidly (Figure 10), the appropriate solution of Equation (148) is

$$\sigma_c = e^{-\chi_e s} \left[A \cos (\chi_e s) + B \sin (\chi_e s) \right] \tag{150}$$

119

The condition that

$$\int_{0}^{\infty} \sigma_c \, ds = 0 = \frac{e^{-\chi_e s}}{2\chi_e} \left[(A + B) \cos (\chi_e s) - (A - B) \sin (\chi_e s) \right] \Big|_{0}^{\infty} \tag{151}$$

is easily seen to require that

$$B = - A \tag{152}$$

The other boundary condition is that

$$\frac{d^2 \sigma_c}{ds^2} = 2\chi_e^2 e^{-\chi_e s} \left[A \sin (\chi_e s) - B \cos (\chi_e s) \right] = \left(\frac{E_c}{\eta} \right) \left(\frac{M_2}{D_s} - \frac{M_3}{D_d} \right) \tag{153}$$

If s = 0, this equation yields

$$B = -\frac{1}{2\chi_e^2} \left(\frac{E_c}{\eta} \right) \left(\frac{M_e}{D_s} \right) \tag{154}$$

just as in Equation (123). The adhesive peel stresses in the vicinity of the ends of the splice plate are thus given by

$$\sigma_c = \left(\frac{E_c}{\eta} \right) \left(\frac{M_e}{D_s} \right) \frac{e^{-\chi_e s}}{2\chi_e^2} \left[\cos (\chi_e s) - \sin (\chi_e s) \right] \tag{155}$$

Equation (155) is likely to be intrinsically free from the very large number problems encounterd in the evaluation of Equation (108) which are discussed above after Equation (138). Except for relatively short overlap joints, which would invalidate the use of Equation (150), the more precise solutions in the preceding section can be replaced by Equations (155) and (160) by appropriate substitutions for M_e, M_m, D_s, D_d, D_t, χ_e and χ_d.

A similar simple solution can be found for the peel stresses in the middle of the splice plate by the introduction of a new coordinate r, starting where the skins butt together and having the same sense as the coordinates x and s in Figure 6. The induced peel stresses are still governed by an equation of the same form as Equation (148), but the exponent χ_e would be replaced by χ_m, where

$$\chi_m^4 = \frac{4 E_c}{\eta} \left(\frac{8}{D_s} + \frac{1}{D_d} \right) \tag{156}$$

in which D_s still refers to the bending stiffness of the entire skin outside the joint. A coefficient different from the 8 would be used if the thinning down were to something other than 50 percent

120

of the basic thickness. Equation (152) can be incorporated directly into Equation (150) so that, in this case,

$$\sigma_c = e^{-\chi_m r} A \left[\cos (\chi_m r) - \sin (\chi_m r) \right] \tag{157}$$

The other boundary condition relies on the value of the bending moment M_m in the middle of the splice plate. Thus, as in Equation (153),

$$\frac{d^2 \sigma_c}{ds^2} = 2\chi_m^2 e^{-\chi_m r} A \left[\sin (\chi_m r) + \cos (\chi_m r) \right] = \left(\frac{E_c}{\eta} \right) \left(\frac{8M_2}{D_s} - \frac{M_3}{D_d} \right) \tag{158}$$

Hence

$$A = \frac{1}{2\chi_m^2} \left(\frac{E_c}{\eta} \right) \left(\frac{M_m}{D_d} \right) \tag{159}$$

with the minus sign disappearing because the bending moment M_m has the opposite sense to that of M_e. Thus, in the immediate vicinity of where the thinned skins butt together, the adhesive peel stresses are given by

$$\sigma_c = - \left(\frac{E_c}{\eta} \right) \left(\frac{M_m}{D_d} \right) \frac{e^{-\chi_m r}}{2\chi_m^2} \left[\cos (\chi_m r) - \sin (\chi_m r) \right] \tag{160}$$

The reduction in σ_c, with respect to the peak value given by Equation (138) is due both to a reduction in the bending moment M_m by the ratio R given in Equation (147) and to an increase in χ_m in accordance with Equation (156). The benefits from using the technique shown in Figure 11 are characterized in Figure 12 by comparing the reduced induced peel stresses with those of the basic long-overlap joint in Figure 10. There is a reduction at both ends of the joint because both M_e and M_m are reduced, but by far the larger reduction is at the middle of the splice plate which had been the more critical location in the unmodified joint.

A slightly heavier but less expensive way of improving the design of flush bonded splices is shown in Figure 13. The total overlap may need to be increased because of the reduced effective bond area for shear load transfer. However, there is no need for the chem-milling to reduce the skin thickness as in Figure 11. Furthermore, the overlap needed for the basic joint shown in Figure 6 exceeds that needed for shear bond transfer and is actually set to minimize the adhesive peel or adherend bending stresses. Therefore the total overlap used in Figure 13 may not be all that much greater than that for Figure 6. Whereas the basic uniform joint had an overlap of 100 times the skin thickness per side, the modification in Figure 13 would need no more than 120 times that thickness, based on the adequacy of a 30t overlap for double-lap bonded joints (Reference 5).

σ_avg = 20,000 PSI

1,250 LB/IN

5.0 IN

0.063 IN

0.063 IN.

σ_b = 6,099 PSI

η = 0.005 IN.

E_c = 500,000 PSI

E = 10,300,000 PSI

ν = 0.3

σ_b = 8,129 PSI

σ_{peel} = 1,885 PSI

σ_{peel} = 2,466 PSI

0

A. ADHESIVE AND ADHEREND STRESSES IN BASIC FLUSH JOINT

1,250 LB/IN

0.063 IN.

0.032 IN.

σ_b = 3,250 PSI

σ_{avg} = 4,444 PSI

σ_b = 4,635 PSI

σ_{peel} = 465 PSI

0

σ_{peel} = 624 PSI

B. ADHESIVE AND ADHEREND STRESSES IN IMPROVED FLUSH JOINT

FIGURE 12. RELIEF OF ADHESIVE PEEL STRESSES IN FLUSH (SINGLE-STRAP) BONDED JOINTS

t_s

t_0

$(t_s + t_d + \eta)$

t_d

ℓ_i

POSITIVE BENDING MOMENTS

POINT OF INFLECTION IN THIS VICINITY REDUCES ADHESIVE PEEL STRESSES

NEGATIVE BENDING MOMENTS

REDUCED BOND AREA FOR SHEAR LOAD TRANSFER

SPLICE PLATE REINFORCED TO MINIMIZE BENDING STRESSES

FIGURE 13. FLUSH BONDED JOINT REINFORCED AT CRITICAL LOCATION

122

The key features of the scheme in Figure 13 are: (1) the eccentricity in overlap at the middle of the splice is reduced from $[(t_s + t_d)/2 + \eta]$ to $[(t_s + t_d)/2 + \eta]/[2 + (t_s/t_d)]$, (2) the splice member is reinforced throughout its middle area in which it had previously been critically loaded, and (3) the intense peel stresses in the adhesive where the skins butt together (Figure 6) have been reduced virtually to zero by relocating them to the vicinity of the point of inflexion in the adherends as they bend under load. That leaves the adhesive most severely loaded at the ends of the splice plate in Figure 13, but less severely than in Figure 6 because of the reduction in eccentricity in load path. Therefore the skin filler strap in Figure 13 could be reduced in width to save weight by increasing the adhesive peel stresses at the edge of that strip while keeping them lower than at the edge of the splice plate.

Much of the basic analysis of Equations (64) to (98) remains applicable, with minor modifications due to the reduction in eccentricity in load path. Thus the bending moment M_e in Equation (95) can be reduced to read

$$M_e = \frac{P\left(\dfrac{t_s + t_d}{2} + \eta\right) \Big/ \left(1 + \dfrac{t_s}{t_d}\right)}{\left[1 + \dfrac{2}{3}\xi_s(\ell_i + \ell_o) + \dfrac{1}{12}\xi_s^2(\ell_i + \ell_o)^2 + \left(\dfrac{t_d}{t_s}\right)^3\left(1 + \dfrac{4}{\xi_s(\ell_i + \ell_o)}\right)\right]} \tag{161}$$

A similar reduction by the factor $(1 + t_s/t_d)$ would apply to the bending moment M_m given in Equation (94). However, the interest in that moment would largely disappear since there is a simultaneous increase in the bending strength due to the lamination. The associated reduction in bending stress would be of the order $(1 + t_s/t_d)^3$ or about 8, with a simultaneous reduction in direct stress in the ratio $(1 + t_s/t_d)$ or about 2.

For the modified bonded splice shown in Figure 13, it is necessary to evaluate the bending moment in the splice member at the new position where the skins butt together. Identifying this location $(s = \ell_o)$ by the subscript n, Equation (72) would give the local deflection as

$$\delta_n = A_{23}\ell_o^3 + B_{23}\ell_o^2 + C_{23}\ell_o + F_{23} \tag{162}$$

with the coefficients A_{23}, B_{23}, C_{23}, and F_{23} still given by Equations (81) to (84). These coefficients are evaluated in terms of the deflection δ_e in Equation (85) which is here reduced by the factor $(1 + t_s/t_d)$. After these coefficients have been evaluated, the bending moment M_m can be deduced as follows. Since $M_2 \equiv 0$ at $s = \ell_o$,

$$M_n = 2 D_d \frac{d^2}{ds^2}\left[\frac{w_2 + w_3}{2}\right]\Bigg|_{s=\ell_o} = 2 D_d\left[6 A_{23}\ell_o + 2 B_{23}\right] \tag{163}$$

From Equations (83), (84), and (163), then

$$M_n = D_d \xi_s^2 \left[1 - \frac{4\ell_o}{\xi_s (\ell_i + \ell_o)^2} \left(\frac{\xi_s (\ell_i + \ell_o)}{2} + 1 \right) \right] \delta_e \qquad (164)$$

and it is quite evident that a value of ℓ_o can be found to render M_m equal to zero. Specifically,

$$\ell_o = \left(\frac{\ell_i + \ell_o}{2} \right) \Bigg/ \left[1 + \frac{2}{\xi_s (\ell_i + \ell_o)} \right] \qquad (165)$$

and is less than half the sum $\ell_o + \ell_i$, putting the point of inflexion nearer the outer edge of the splice plate than the middle. For any value of the overlaps ℓ_o and ℓ_i, the bending moment can be determined from Equations (163) and (85), with δ_e reduced by the factor $(1 + t_s/t_d)$.

The peak adhesive peel stresses would now be given by an equation of the form of Equation (160):

$$\sigma_c = \left(\frac{E_c}{\eta} \right) \left(\frac{M_n}{D_d} \right) \frac{e^{-X_n r}}{2X_n^2} |\cos (X_n r) - \sin (X_n r)| \qquad (166)$$

Figure 14 presents a comparison between the peel stresses in a basic flush splice, as in Figure 6, and in the modified form shown in Figure 13, having the same overlap and weight in each case. The reduction in peak stresses is dramatic and the adhesive peel stresses where the skins butt together have been replaced by small interlaminar stresses of no concern.

In concluding this section on modified flush bonded joints, it should be acknowledged that either modification can be effective in reducing the severity of the stress concentrations in the joint but that only the reduction of the eccentricity by the stepped joint shown in Figure 11 gives a major weight saving. The local thickening of the adhesive layer and tapering of the ends of the adherends should still be used even with these other modifications.
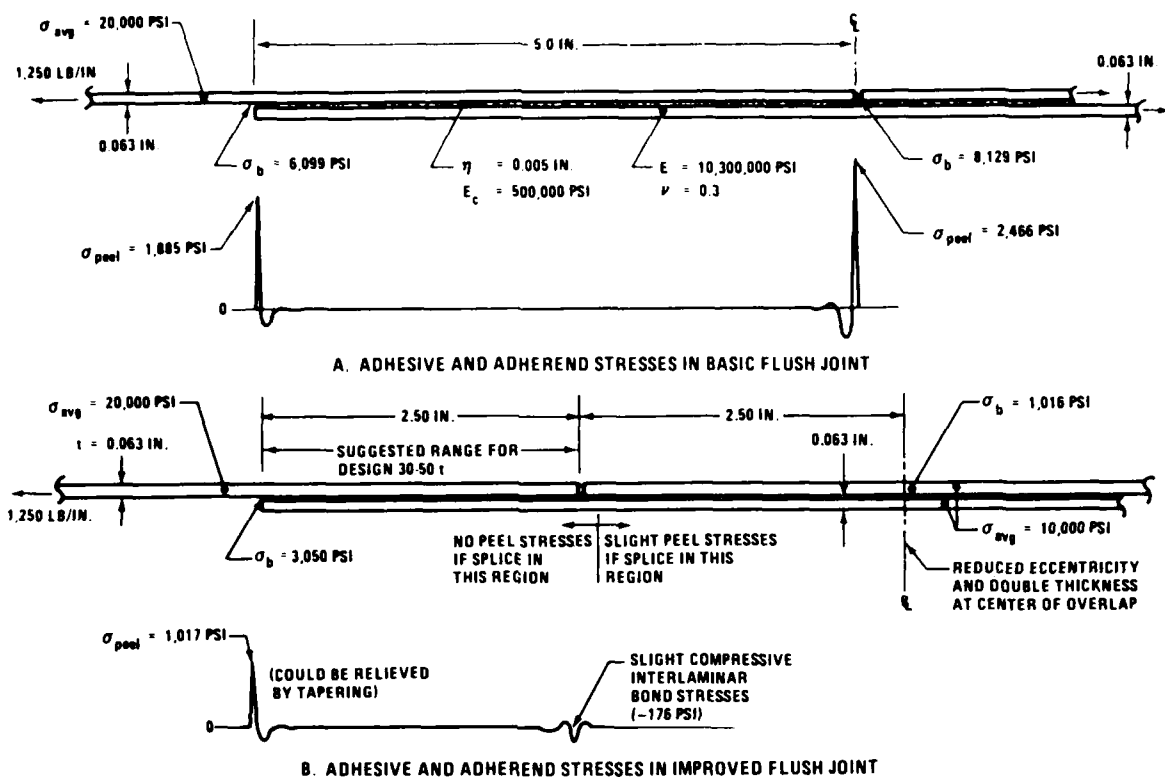
A. ADHESIVE AND ADHEREND STRESSES IN BASIC FLUSH JOINT

B. ADHESIVE AND ADHEREND STRESSES IN IMPROVED FLUSH JOINT

FIGURE 14. BASIC AND IMPROVED DESIGNS OF SINGLE-STRAP ADHESIVE-BONDED JOINTS

125

TENSION-TEE SKIN-TO-STIFFENER BONDED JOINTS

All of the bonded joints discussed earlier have had a basically pure-shear applied load which has induced secondary peel stresses in the adhesive due to some eccentricity in load path. The severity of these peel stresses has been shown to be directly proportional to some adherend bending moment associated with structural deformations under load. The magnitude of those bending moments has, in turn, been shown to be quite sensitive to the geometric proportions of the joints. Another class of adhesive bonded joints of interest to aircraft and missile designers is the bond between the skin and the frames or longerons. In such a case there is a directly applied adhesive peel load in addition to any that is induced by the bending of the members. This peel load is not distributed uniformly across the bonded area but is described by an exponentially damped sinusoid, with intense peaks at the ends of the overlaps as was the case in the preceding analyses. The reason for this stress amplification is that almost half of the bonded area is not transmitting the applied load but is trying to push the other half apart, as shown in Figure 15.

This direct peel load situation exists in two basic configurations in pressurized aircraft fuselages. In one case, the pressurized skin is pinched in locally by the frames and, to a lesser exten*, by the longerons. The junction load between the skin and the stiffeners is limited by the continuity of the skin as a cylinder. The skin tries to grow radially by a typical amount of 0.05 to 0.10 inch away from the frames and by about half as much over the frames. This particular problem is analyzed in Reference 6 in which a digital computer program A4EP is developed. That analysis does not address the distribution of the adhesive peel stresses, but the output from that program provides the input data for the analysis developed here. The other case of the peel loads between pressurized skins and stiffeners is found in flat bulkheads,* where the skin deflection has no definite limit due to hoop strain limitations. Nevertheless, the skin deflections are constrained by the diaphragm action of the induced membrane stresses in the skin to something far less than a linear bending analysis would predict. Analysis of this latter problem will be documented in Reference 7 to a greater depth than has been done before. There are several other available references on the diaphragm action of pressurized flat rectangular plates which could provide the necessary boundary conditions for the problem under investigation here.

These two situations can be approximated by the test specimen shown in Figure 16. The stiff spreader bar needed to induce the membrane stress in the skin is of particular importance since, without it, there would be no diaphragm action of the skin and the bonded joint would fail prematurely due to excessive deflection and bending of the skin. The stiffness of the spreader bar and the attachment to the skin should be sufficient to restrict the vertical deflection of the bonded tees to something representative of the actual complete structure. A precise match usually will not be possible but experience with such coupons on the PABST (Primary Adhesively Bonded Structure Technology) program indicated that relatively massive steel plates would suffice to reduce the deflection by a factor of four or more. Actually, the most critical detail was found to be the fit of the holes through which the specimen was bolted to the fixture — the use of oversize holes to achieve an interchangeable predrilled pattern was completely unacceptable.

---

*It might seem that the problem of the cabin pressure trying to push the bulkhead panels off the stiffeners could be avoided by simply putting the stiffeners on the back side of the panels so that the pressure pushes the panel sheet against the stiffeners instead of away from them. However, the junction load between the flat sheet and stiffeners is usually no more than about 100 pounds per inch, while the shear load to be transmitted to the ends of the stiffeners (where they tie to a major frame, for example) is of the order of 5000 pounds. The ends of the stiffeners obviously must be mechanically attached, because the loads there are too high for bonding. Even so, it is often better to optimize the joint details at the ends, to permit that high shear load to be taken by compressive bearing instead of by tensile loads on the fasteners, rather than to compromise that area to improve the less critical flat-sheet-to-stiffener joint. In any case, each design will be constrained also by adjacent structure and by efforts to simplify manufacturing.
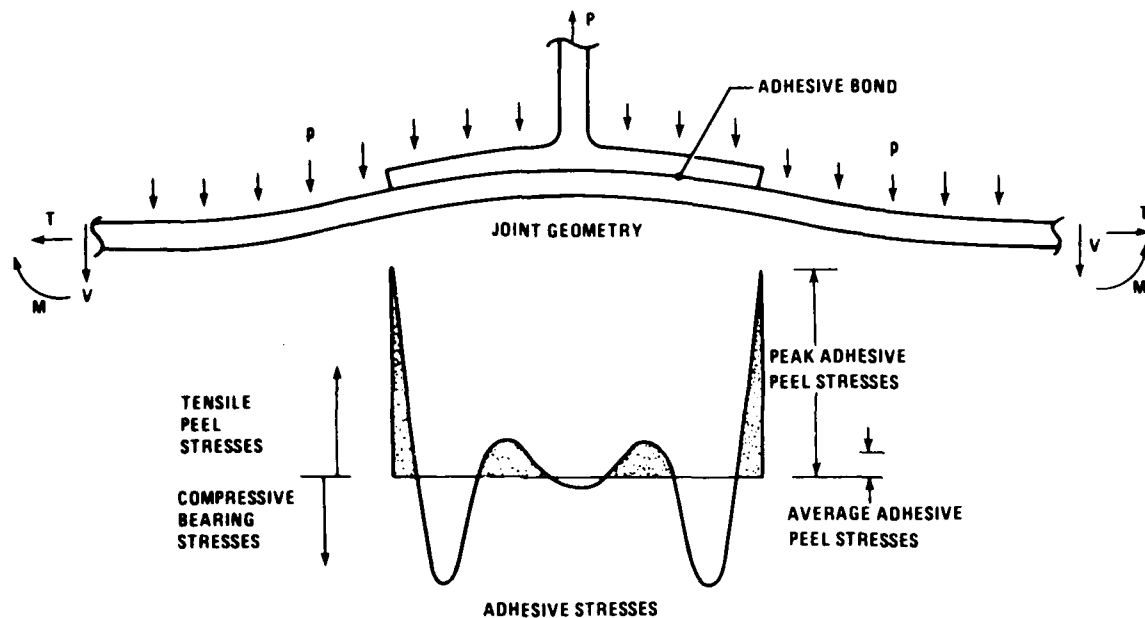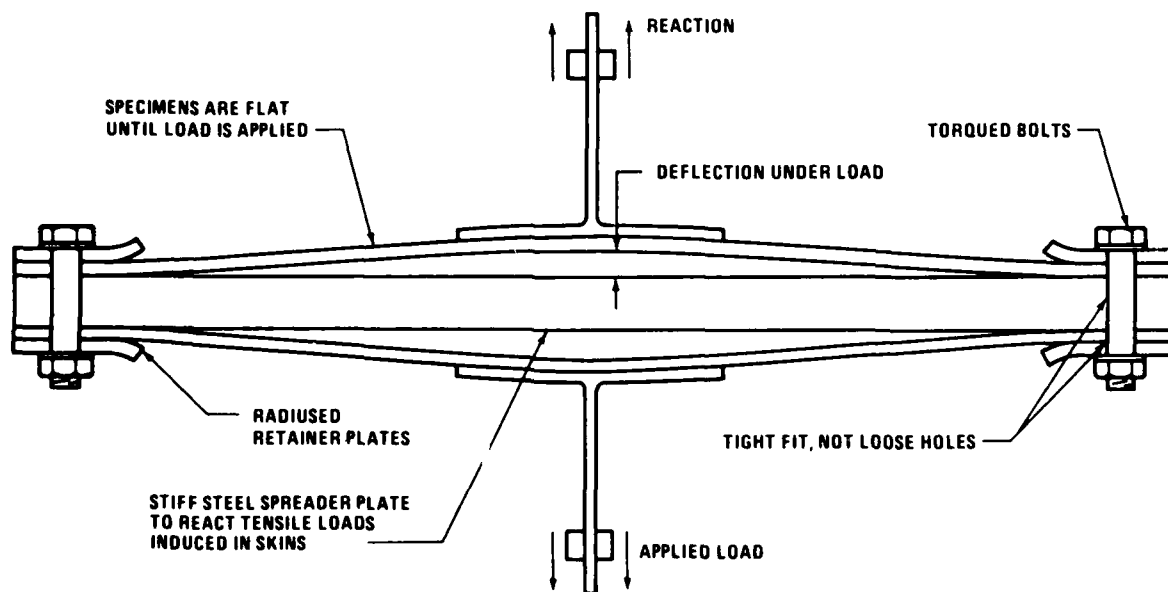
FIGURE 15. PEEL STRESS DISTRIBUTION BETWEEN STIFFENER AND SKIN

NOTE: USE OF BACK-TO-BACK SPECIMEN TESTING SIMPLIFIES SPREADER BAR WITH RESPECT TO PABST DESIGN AND ACCUMULATES FATIGUE CYCLES MORE RAPIDLY. BUT DOES REQUIRE COUNTERBALANCING AND SUPPORT TO PREVENT POST-FAILURE DAMAGE TO LOWER SPECIMEN.

FIGURE 16. BONDED TENSION-TEE TEST SPECIMEN AND FIXTURE

127

The test fixture actually used in the PABST program tested only one specimen at a time and therefore did not need counterbalance weights which the scheme in Figure 16 would require. Reference 8 contains a detailed description of the test fixture used in the PABST program, along with the test results which showed considerable margins over the requirements. While no analysis exists yet to characterize the peel stresses induced by wrinkling of the skin panels under shear loading, the tests of large panels in the PABST program showed that the designs used were adequate.

Figure 17 defines the effects included in the analysis of the test specimen shown in Figure 16. The purpose of this initial analysis is to relate the forces P and T to the central deflection Δ. The semispan ℓ should be about 3 inches or so to represent a skin-to-frame joint based on pressure-pillowing (quilting) analyses of typical fuselages, and be adjusted to other values representative of skin-to-longeron or flat panel structures. There is no distributed pressure load because of the difficulty of including such loads in the test fixture. However, were it possible to do so it would be found that the central deflection and skin bending moments would be less than those calculated here. Some of the load P in Figure 17 could be reacted directly by the pressure rather than all the load having to be sheared across to the outer supports. Thus the analysis here is conservative in that regard.

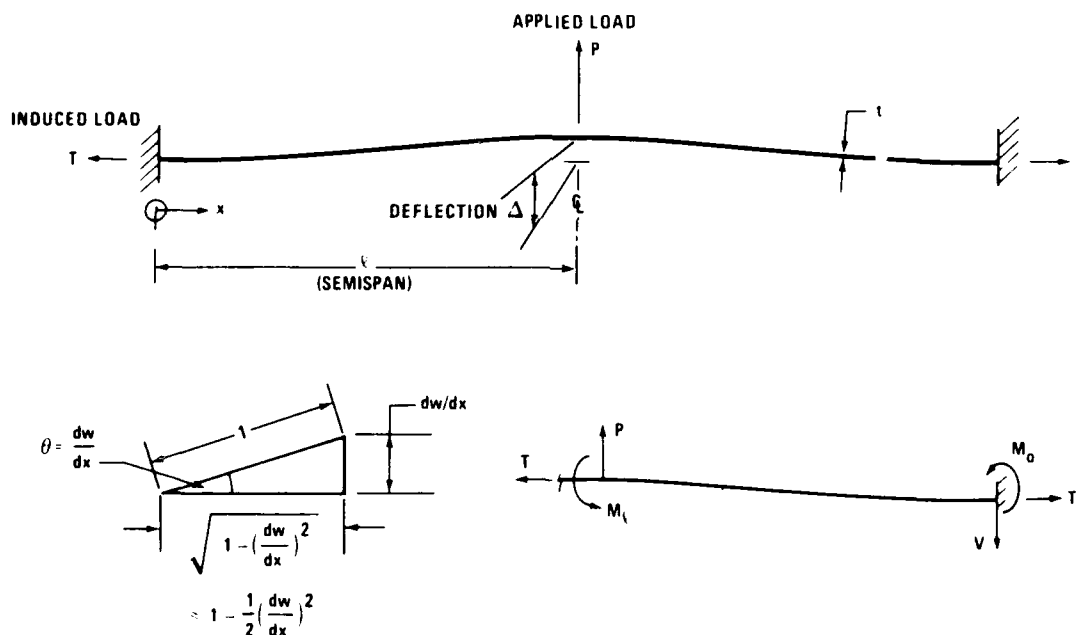**FIGURE 17. IDEALIZATION OF BONDED TENSION TEE AS DIAPHRAGM PLATE**

The work of Timoshenko (Reference 9) shows that a precise deflected shape is not necessary to achieve a reasonably accurate solution. Therefore, a simple shape having the necessary curves and inflexion is used to characterize the skin deflection. The assumption that

$$w = \frac{\Delta}{2}\left[1 - \cos\left(\frac{\pi x}{\ell}\right)\right] \tag{167}$$

128

implies that the bending moments at the ends and middle of the skin are equal and opposite.

$$M_\ell = M_0 \tag{168}$$

since

$$\left.\frac{d^2 w}{dx^2}\right|_{x=0} = \left.\frac{d^2 w}{dx^2}\right|_{x=\ell} \tag{169}$$

This relation would be strictly true in the absence of the membrane load T, and the neglect of the distributed pressure load also makes it true in the presence of the membrane load.

Now, assuming that the ends of the spreader bar are immovable, the membrane strain induced in the skin is given by the nonlinear theory of elasticity as

$$\epsilon = \frac{1}{2\ell} \int_0^\ell \left(\frac{dw}{dx}\right)^2 dx \tag{170}$$

and, since

$$\frac{dw}{dx} = \frac{\Delta}{2}\left(\frac{\pi}{\ell}\right) \sin\left(\frac{\pi x}{\ell}\right) \tag{171}$$

$$\epsilon = \left(\frac{\pi \Delta}{4\ell}\right)^2 \tag{172}$$

The membrane load per unit width then follows as

$$T = E t \epsilon = \frac{\pi^2 E t}{16 \ell^2} \Delta^2 \tag{173}$$

The bending moment M_ℓ in the middle of the skin can be expressed in two forms:

$$M_0 = M_\ell = D_s \left.\frac{d^2 w}{dx^2}\right|_{x=\ell} = \frac{\Delta}{2}\left(\frac{\pi}{\ell}\right)^2 D_s = \frac{\pi^2 E t^3}{24(1-\nu^2)\ell^2} \Delta \tag{174}$$

where

$$D_s = E t^3 / [12(1-\nu^2)] \tag{175}$$

129

is the bending stiffness of the skin. From static equilibrium,

$$M_\ell = \frac{P\ell}{2} - T\Delta - M_0 \tag{176}$$

whence

$$M_\ell = \frac{P\ell}{4} - \frac{T\Delta}{2} \tag{177}$$

Elimination of M_ℓ between Equations (174) and (177) yields as an expression for the normal force P per unit width

$$P = \frac{2T\Delta}{\ell} + \frac{2\Delta}{\ell}\left(\frac{\pi}{\ell}\right)^2 D_s \tag{178}$$

and, on eliminating the membrane stress resultant T between Equations (178) and (173),

$$P = \frac{\pi^2 Et^3 \Delta}{6(1-\nu^2)\ell^3}\left[1 + \frac{3(1-\nu^2)}{4}\left(\frac{\Delta}{t}\right)^2\right] \tag{179}$$

Equation (179) has the characteristic form of the diaphragm plate analysis

$$P = A\Delta + B\Delta^3 \tag{180}$$

The strong influence of the ℓ^3 term in the denominator of Equation (179) is the reason why the span ℓ must be set in the test specimen to be representative of the specific structure. Clearly, an excessive value of ℓ would result in a gross increase in the deflection Δ, for a given applied load P, with a consequent premature failure.

Once the deflection Δ has been specified, or assumed, the other quantities P, T, and M_0 follow from Equations (179), (173), and (174). Sample solutions are shown in Figure 18 for aluminum alloy sheets.

Figure 18 can be read either starting from Δ to deduce P and T or from P by deducing Δ and then T. A linear bending solution for this problem can be obtained by setting the membrane force equal to zero. The straight line shown in Figure 18 for the linear solution indicates much larger deflections for a given load P, governed by Equation (179) after deletion of the nonlinear term in the square brackets.

The analysis above is needed to deduce the induced boundary conditions T and M_0, as distinct from the applied condition P, with which to solve for the adhesive peel stresses in the joint in Figure 15. No account has been taken yet of the effect of the finite width of the stiffener flange. A simple, approximate treatment of this detail is shown in Figure 19. It is assumed here that the skin/flange combination is so much stiffer in bending than the skin alone that the reinforced area
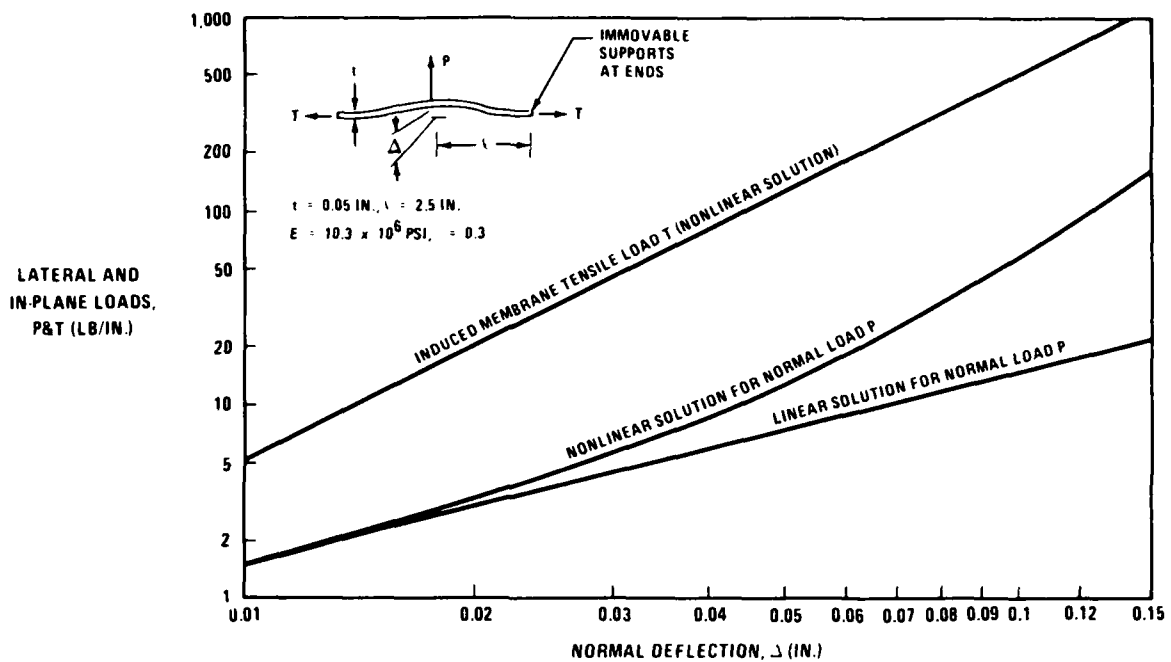
130

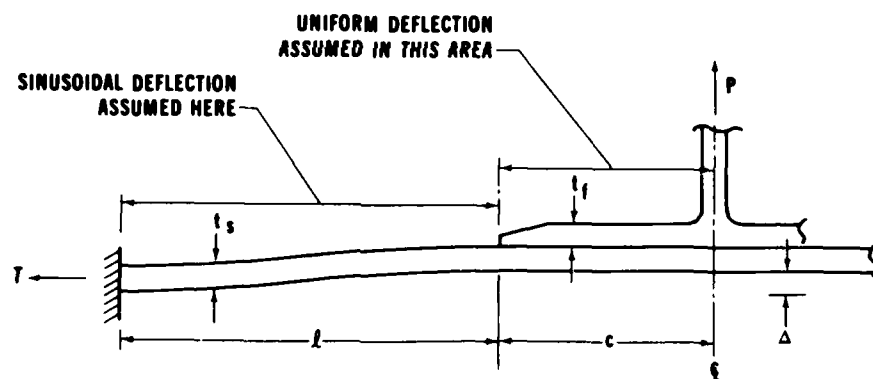**FIGURE 18. DIAPHRAGM PLATE BEHAVIOR (SAMPLE SOLUTION)**

FIGURE 19. APPROXIMATE ANALYSIS OF SKIN BONDED TO TENSION TEE

remains flat. The total elongation of the skin and skin/flange combination is still that given by Equation (172). Thus,

$$\left(\frac{\pi \Delta}{4\ell}\right)^2 \ell = T\left(\frac{\ell}{E_s t_s} + \frac{c}{E_s t_s + E_f t_f}\right) \qquad (181)$$

whence

131

$$T = \frac{\pi^2 E_s t_s}{16 \ell^2} \Delta^2 \Big/ \left[1 + \frac{c/\ell}{\left(1 + \dfrac{E_f t_f}{E_s t_s}\right)} \right] \tag{182}$$

Equation (174) would still define the bending moments at each end of the unreinforced skin.

$$M_e = M_0 = \frac{\pi^2 E_s t_s^3}{24(1-\nu^2)\ell^2} \Delta \tag{183}$$

and the vertical load P would still be expressed by Equation (178) but not by Equation (179). This estimate of the bending moment M_e, which defines the peak adhesive peel stress, can be improved upon by allowing for bending of the skin/flange combination, as is done below. However, the greatest contribution to the accuracy of M_e comes from the inclusion of the relief due to the diaphragm load T in the skin, as indicated by Equation (177). A linear solution for that bending moment would suggest that

$$M_{e_{linear}} = \frac{P\ell}{4} = \frac{\pi^2 E_s t_s^3}{6(1-\nu^2)\ell^2} \Delta \tag{184}$$

which not only neglects the relief from the diaphragm load in the skin but also involves a gross overestimate of the deflection Δ, as can be seen in Figure 18.

The simple nonlinear analysis above would probably suffice for most calculations, but a more precise solution may be needed in some cases to account for the effects of bending of the stiffener flange. This more complicated problem is defined in Figure 20. It is evident that the bending moments M_0 and M_m will no longer be equal and opposite. A new value is to be computed for the bending moment M_e at the edge of the flange on the tee on the assumption that the estimate above for the bending moment M_0 remains reasonably accurate. For the skin-to-frame bond in a pressurized circular fuselage, a precise value of that bending moment M_0 can be derived from the pressure-pillowing program A4EP.

Throughout the adherend 1 in Figure 20, the deflected shape can be taken to be

$$w_1 = Be^{\xi x} + \frac{M_0}{D_s} \frac{x^2}{2} - \frac{P}{D_s} \frac{x^3}{12} \tag{185}$$

in which the exponent ξ is given by

$$\xi^2 = T/D_s \tag{186}$$

It is assumed that the skin length in Figure 20 is great enough that all terms and derivatives associated with the exponential sum in Equation (185) can be neglected at the remote part of the
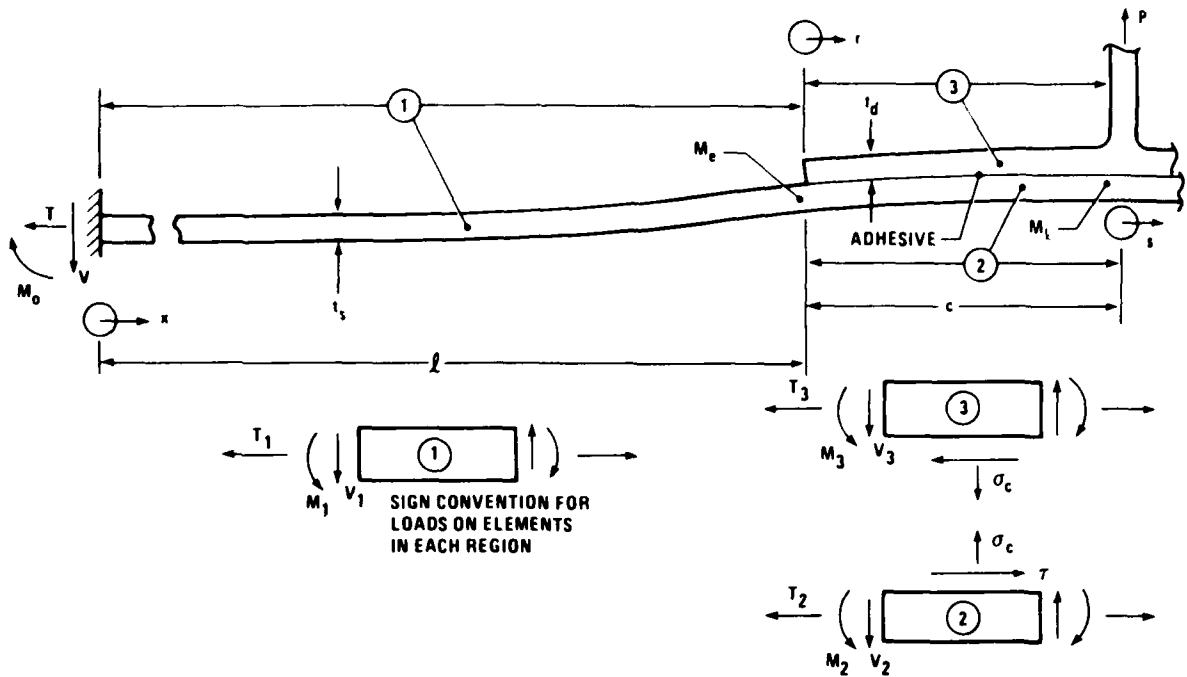
FIGURE 20. COORDINATE SYSTEM AND DEFORMATIONS IN TENSION-TEE BONDED JOINT

joint $(x = 0)$ while being included at the edge of the tee $(x = \ell)$. The adequacy of Equation (185) can then be established from known boundary conditions. Throughout Region 1,

$$\frac{dw_1}{dx} = B\xi e^{\xi x} + \frac{M_0}{D_s}x - \frac{P}{D_s}\frac{x^2}{4} \tag{187}$$

which satisfies the condition

$$\frac{dw_1}{dx}\bigg|_{x=0} \approx 0 \tag{188}$$

Differentiating again,

$$\frac{d^2 w_1}{dx^2} = B\xi^2 e^{\xi x} + \frac{M_0}{D_s} - \frac{P}{D_s}\frac{x}{2} \tag{189}$$

and

$$\frac{d^3 w_1}{dx^3} = B\xi^3 e^{\xi x} - \frac{P}{2D_s} \tag{190}$$

133

Equations (189) and (190) are consistent with the boundary conditions

$$\frac{d^2 w_1}{dx^2}\bigg|_{x=0} = \frac{M}{D_s}\bigg|_{x=0} \quad \text{and} \quad \frac{d^3 w_1}{dx^3}\bigg|_{x=0} = -\frac{V}{D_s}\bigg|_{x=0} \tag{191}$$

Throughout the bonded area ($s = -c$ to $s = 0$), the deflected shape can be approximated as

$$\frac{1}{2}(w_2 + w_3) = \Delta \quad \frac{M_m}{D_{sf}} \frac{s^2}{2} \quad \frac{P}{D_{sf}} \frac{s^3}{12} + As^4 + Cs^5 \tag{192}$$

in which D_{sf} refers to the bending stiffness of the combined skin and flange. The various derivatives needed for the subsequent analysis are

$$\frac{1}{2}\frac{d(w_2 + w_3)}{ds} = \frac{M_m}{D_{sf}} s - \frac{P}{D_{sf}} \frac{s^2}{4} + 4As^3 + 5Cs^4 \tag{193}$$

$$\frac{1}{2}\frac{d^2(w_2 + w_3)}{ds^2} = \frac{M_m}{D_{sf}} - \frac{P}{D_{sf}} \frac{s}{2} + 12As^2 + 20Cs^3 \tag{194}$$

and

$$\frac{1}{2}\frac{d^3(w_2 + w_3)}{ds^3} = \frac{P}{2D_{sf}} + 24As + 60Cs^2 \tag{195}$$

Equations (194) and (195) can easily be seen to be consistent with the boundary conditions at the middle of the tee. That is

$$\frac{1}{2}\frac{d^2(w_2 + w_3)}{ds^2}\bigg|_{s=0} = \frac{M}{D_{sf}}\bigg|_{s=0} \quad \text{and} \quad \frac{1}{2}\frac{d^3(w_2 + w_3)}{ds^3}\bigg|_{s=0} = \frac{V}{D_{sf}}\bigg|_{s=0} \tag{196}$$

The remaining coefficients A, B, and C in Equations (185) and (192) can be determined by matching the displacement, slope, and curvature at the transition between Zones 1 and 2 in Figure 20. Displacement compatibility requires that

$$w_c = w_1\bigg|_{x = c} = Be^{\xi c} + \frac{M_0 \ell^2}{2D_s} \quad \frac{P\ell^3}{12D_s}$$

$$= \frac{1}{2}(w_2 + w_3)\bigg|_{s = c} = \Delta \quad \frac{M_m c^2}{2D_{sf}} + \frac{Pc^3}{12D_{sf}} + Ac^4 \quad Cc^5 \tag{197}$$

134

The matching of the slopes then requires that

$$\frac{dw_1}{dx}\bigg|_{x=\ell} = B\xi e^{\xi\ell} + \frac{M_0\ell}{D_s} \quad \frac{P\ell^2}{4D_s}$$

$$= \frac{1}{2}\frac{d(w_2+w_3)}{ds}\bigg|_{s=\ell} = \frac{M_m c}{D_{sf}} \quad \frac{Pc^2}{4D_{sf}} \quad 4Ac^3 + 5Cc^4 \tag{198}$$

The curvature matching relation relies on the free edge condition that

$$M_3\bigg|_{s=\pm c} \equiv 0 \tag{199}$$

whence

$$\frac{d^2w_2}{ds^2}\bigg|_{s=\ell} = 2\frac{d^2}{ds^2}\left[\frac{1}{2}(w_2 + \dot w_3)\right]\bigg|_{s=\cdot c} \tag{200}$$

Thus

$$\frac{d^2w_1}{dx^2}\bigg|_{x=\ell} = B\xi^2 e^{\xi\ell} + \frac{M_0}{D_s} - \frac{P\ell}{2D_s} = \frac{d^2w_2}{ds^2}\bigg|_{s=-c}$$

$$= -\frac{2M_m}{D_{sf}} + 24Ac^2 - 40Cc^3 + \frac{Pc}{D_{sf}} + 24Ac^2 - 40Cc^3 \tag{201}$$

The central bending moment M_m can be expressed separately as

$$M_m = \frac{P(\ell + c)}{2} - M_0 - T\Delta \tag{202}$$

in terms of quantities which must be considered known at the start of this analysis.

The unknowns A and C in Equations (198) and (199) can be separated into the expressions

$$B\xi e^{\xi\ell}(8 + \xi c) + \frac{M_0}{D_s}(8\ell + c) \quad \frac{P\ell}{2D_s}(4\ell + c) - \frac{6M_m c}{D_{sf}} + \frac{Pc^2}{D_{sf}} = 8Ac^3 \tag{203}$$

and

$$B\xi c^{\xi\kappa}(b+\xi c) + \frac{M_0}{D_s}(6\ell+c) - \frac{P\ell}{2D_s}(3\ell+c) - \frac{4M_m c}{D_{sf}} + \frac{Pc^2}{2D_{sf}} = 10Cc^4 \qquad (204)$$

The elimination of the unknowns A and C from Equation (197) using Equations (203) and (204) results in a single expression for B as a function of Δ. That is

$$Bc^{\xi\kappa}\left(1 + \frac{2}{5}\xi c + \frac{1}{40}\xi^2 c^2\right) = \Delta - \frac{M_0\ell^2}{2D_s}\left(1 - \frac{4}{5}\frac{c}{\ell} - \frac{1}{20}\frac{c^2}{\ell^2}\right)$$

$$+ \frac{P\ell^3}{12D_s}\left(1 - \frac{6}{5}\frac{c}{\ell} - \frac{3}{20}\frac{c^2}{\ell^2}\right) - \frac{3M_m c^2}{20D_{sf}} + \frac{1}{48}\frac{Pc^3}{D_{sf}} \qquad (205)$$

The deflection w_e of the skin at the edge of the stiffener then follows from Equation (197), with the unknown $Bc^{\xi l}$ coming from Equation (205) and the other unknowns A and C being given by Equations (203) and (204). The bending moment M_m is expressed by Equation (202).

At this stage it is now possible to solve for the crucial bending moment M_e. Moment equilibrium in terms of Figure 20 gives

$$M_e = \frac{P\ell}{2} - M_0 - Tw_e \qquad (206)$$

The algebra is too complex for a direct expression of M_e and, in any case, some of the intermediate calculations are of interest in their own right.

Sample solutions calculated from this set of equations indicate that their use requires a well-matched set of boundary conditions — P, M_0, T, and Δ — to obtain realistic solutions for the deflection w_e and bending moment M_e. The simple nonlinear solution in Equation (183) is preferred, even though it is always slightly nonconservative, whenever there is doubt about the self-consistency of the boundary conditions for the more precise analysis.

Now that the bending moment M_e in the skin has been derived, it is possible to proceed with the analysis of the adhesive peel stresses between the skin and stiffener. The terms involved in this particular analysis are defined in Figure 20. Moment equilbruim requires that

$$\left.\begin{array}{l} \dfrac{dM_2}{ds} - v_2 + \tau\left(\dfrac{t_s}{2}\right) = 0 \\[4mm] \dfrac{dM_3}{ds} - v_3 + \tau\left(\dfrac{t_f}{2}\right) = 0 \end{array}\right\} \qquad (207)$$

136

while longitudinal equilibrium requires that

$$\left.\begin{array}{l} \dfrac{dT_2}{ds} + \tau = 0 \\[3mm] \dfrac{dT_3}{ds} - \tau = 0 \end{array}\right\} \tag{208}$$

and transverse force equilibrium requires that

$$\left.\begin{array}{l} \dfrac{dV_2}{ds} + \sigma_c = 0 \\[3mm] \dfrac{dV_3}{ds} - \sigma_c = 0 \end{array}\right\} \tag{209}$$

From plate bending theory, with the sign convention depicted in Figure 20,

$$\frac{d^2 w_2}{ds^2} = - \frac{M_2}{D_s} \quad \text{and} \quad \frac{d^2 w_3}{ds^2} = - \frac{M_3}{D_f} \tag{210}$$

Assuming that adhesive properties are linearly elastic in transverse tension,

$$\frac{\sigma_c}{E_c} = \frac{(w_3 - w_2)}{\eta} \tag{211}$$

It follows that

$$\frac{d^2 (w_3 - w_2)}{ds^2} = \frac{M_3}{D_f} + \frac{M_2}{D_s} = \left(\frac{\eta}{E_c}\right) \frac{d^2 \sigma_c}{ds^2} \tag{212}$$

$$\frac{d^3 (w_3 - w_2)}{ds^3} = - \frac{V_3}{D_f} + \tau\left(\frac{t_f}{2D_f}\right) + \frac{V_2}{D_s} - \tau\left(\frac{t_s}{2D_s}\right) = \left(\frac{\eta}{E_c}\right) \frac{d^3 \sigma_c}{ds^3} \tag{213}$$

and

$$\frac{d^4 (w_3 - w_2)}{ds^4} = - \left(\frac{1}{D_f} + \frac{1}{D_s}\right) \sigma_c + \left(\frac{t_f}{2D_f} - \frac{t_s}{2D_s}\right) \frac{d\tau}{ds} = \left(\frac{\eta}{E_c}\right) \frac{d^4 \sigma_c}{ds^4} \tag{214}$$

137

The second term on the right of Equation (214) may be discarded using the following logic. The term would always be zero if $t_d = t_s$. Also, if the loads are sufficiently high for the membrane skin load T to yield the adhesive in shear, then $d\tau/ds \equiv 0$ and the term would disappear again. It stands to reason that an effect that can be justifiably neglected at high load levels need not be considered at lower loads. Thus Equation (214) can be reduced to the approximate result

$$\frac{d^4 \sigma_c}{ds^4} + 4(\chi')^4 \sigma_c = 0 \tag{215}$$

where

$$(\chi')^4 = \frac{E_c}{4\eta}\left(\frac{1}{D_d} + \frac{1}{D_s}\right) \tag{216}$$

Based on these analyses, it is appropriate to seek the solution of Equation (215) in two forms. For narrow stiffener flanges, the symmetric peel stress distributions require that

$$\sigma_c = A \cos(\chi's) \cosh(\chi's) + B \sin(\chi's) \sinh(\chi's) \tag{217}$$

The boundary conditions are that the resultant peel force is

$$\int_0^c \sigma_c \, ds = \frac{P}{2} \tag{218}$$

and that, at the tip of the flange,

$$\left(\frac{\eta}{E_c}\right) \frac{d^2 \sigma_c}{ds^2} = \frac{d^2 w_2}{ds^2} = \frac{M_2}{D_2} \tag{219}$$

Equations (218) and (217) can be combined to yield the result

$$
\begin{aligned}
&A\ [\sin(\chi'c)\cosh(\chi'c) + \cos(\chi'c)\sinh(\chi'c)] \\
&+ B\ [\sin(\chi'c)\cosh(\chi'c)\quad \cos(\chi'c)\sinh(\chi'c)] = \chi'P
\end{aligned}
\tag{220}
$$

For all but very short overlaps then,

$$A\,[\cos(\chi'c) + \sin(\chi'c)]\quad B\,[\cos(\chi'c)\quad \sin(\chi'c)] \approx \chi'P \left/ \left[\frac{1}{2}e^{(\chi'c)}\right]\right. \tag{221}$$

From Equations (219) and (217),

138

$$\frac{d^2\sigma_c}{ds^2}\bigg|_{s=c} = 2(\chi')^2 \left[A \sin(\chi'c) \sinh(\chi'c) + B \cos(\chi') \cosh(\chi'c)\right] = \frac{E_c}{\eta} \frac{M_c}{D_s} \quad (222)$$

Again, for all but very short overlaps,

$$A \sin(\chi'c) + B \cos(\chi'c) \approx \left(\frac{E_c}{\eta}\right)\left(\frac{M_c}{D_s}\right)\frac{1}{(\chi')^2 \, e^{(\chi'c)}} \quad (223)$$

The solution of Equations (221) and (222) proceeds as follows:

$$A \left[\frac{\sin(\chi'c) + \cos(\chi'c)}{\sin(\chi'c) - \cos(\chi'c)} + \frac{\sin(\chi'c)}{\cos(\chi'c)}\right]$$

$$= \frac{1}{e^{(\chi'c)}}\left[\frac{2\chi'P}{\sin(\chi'c) - \cos(\chi'c)} - \frac{E_c M_c}{\eta D_s (\chi')^2 \cos(\chi'c)}\right] \quad (224)$$

$$B \left[\frac{\sin(\chi'c) - \cos(\chi'c)}{\sin(\chi'c) + \cos(\chi'c)} + \frac{\cos(\chi'c)}{\sin(\chi'c)}\right]$$

$$= \frac{1}{e^{(\chi'c)}}\left[\frac{2\chi'P}{\sin(\chi'c) + \cos(\chi'c)} + \frac{E_c M_c}{\eta D_s (\chi')^2 \sin(\chi'c)}\right] \quad (225)$$

Thence

$$A = \frac{1}{e^{(\chi'c)}}\left\{2\chi'P \cos(\chi'c) - \frac{E_c M_c}{\eta D_s (\chi')^2} \left[\sin(\chi'c) - \cos(\chi'c)\right]\right\} \quad (226)$$

and

$$B = \frac{1}{e^{(\chi'c)}}\left\{2\chi'P \sin(\chi'c) + \frac{E_c M_c}{\eta D_s (\chi')^2} \left[\sin(\chi'c) + \cos(\chi'c)\right]\right\} \quad (227)$$

Since, to the same level of accuracy,

$$\sigma_c = \left[A \cos(\chi's) + B \sin(\chi's)\right]\frac{e^{(\chi's)}}{2} \quad (228)$$

the peak value of σ_c, at the edges of the bonded stiffener, is

139

$$\sigma_{c_{max}} = \chi'P + \frac{E_c M_c}{2\eta D_c (\chi')^2} \qquad (229)$$

involving contributions from both the directly applied load P and the induced bending moment M_c. The contribution from the bending moment could even be negative if the overlaps C were wide enough compared with the skin expanse ℓ.

Equation (228) might seem to suggest the desirability of a small value for the amplifying factor χ' on P. However, a larger value of χ' is associated with thinner, more flexible members and a far lower value of the structural load P.

In order to avoid numerical accuracy problems in the evaluation of the large exponential functions in Equations (225), (226), (227), and (228) for bonded stiffeners with large flange widths, a different solution of Equation (215) is preferable. Introducing a new coordinate starting at the edge of the stiffener instead of the middle, as shown in Figure 20, the appropriate solution of Equation (215) is

$$\sigma_c = e^{-(\chi'r)} [A \cos(\chi'r) + B \sin(\chi'r)] \qquad (230)$$

Equation (218) then requires that

$$\chi'P = e^{-(\chi'r)} [(A + B) \cos(\chi'r) - (A - B) \sin(\chi'r)] \Big|_0^\infty \qquad (231)$$

whence

$$A + B = \chi'P \qquad (232)$$

Equation (219) would require that

$$\frac{d^2\sigma_c}{dr^2} = 2(\chi')^2 e^{-(\chi'r)} [A \sin(\chi'r) - B \cos(\chi'r)] = \left(\frac{E_c}{\eta}\right)\left(\frac{M_2}{D_s} - \frac{M_3}{D_d}\right) \qquad (233)$$

or that

$$B = \frac{1}{2(\chi')^2}\left(\frac{E_c}{\eta}\right) \frac{M_c}{D_c} \qquad (234)$$

Thus, from Equations (232) and (234),

$$A = \chi'P + \frac{1}{2(\chi')^2}\left(\frac{E_c}{\eta}\right)\frac{M_c}{D_s} \qquad (235)$$

140

The peak adhesive peel stress, at r = 0, is then

$$\sigma_{c_{max}} = \chi' P + \frac{F_v M_c}{2\eta D_v (\chi')^2}$$

(236)

just as in Equation (229).

Figure 21 shows a sample solution for the adhesive peel stresses in a typical bonded skin and stiffener joint. The inclusion of the geometric nonlinearities in the analyses above makes these peel stresses seem far more tolerable than any simple linear analysis would have predicted. Also worthy of note is the tremendous amplification of the average adhesive peel stress to the peak value developed right at the edge of the stiffener flange.

Another important aspect of this problem cannot be deduced from the single example analyzed in Figure 21 but can be anticipated on the basis of Figure 18. While the peak adhesive peel stresses in Figure 21 seem to be very large in view of the extremely low applied load P, it must be realized that as the deflection Δ increases prior to failure P will increase at a far more rapid rate that Δ or M_e, or consequently $\sigma_{c\ max}$. Indeed, PABST program testing (Reference 8) revealed failure loads P of the order of 2,000 pounds per inch — at deflections far in excess of what would be encountered in actual aircraft structures.

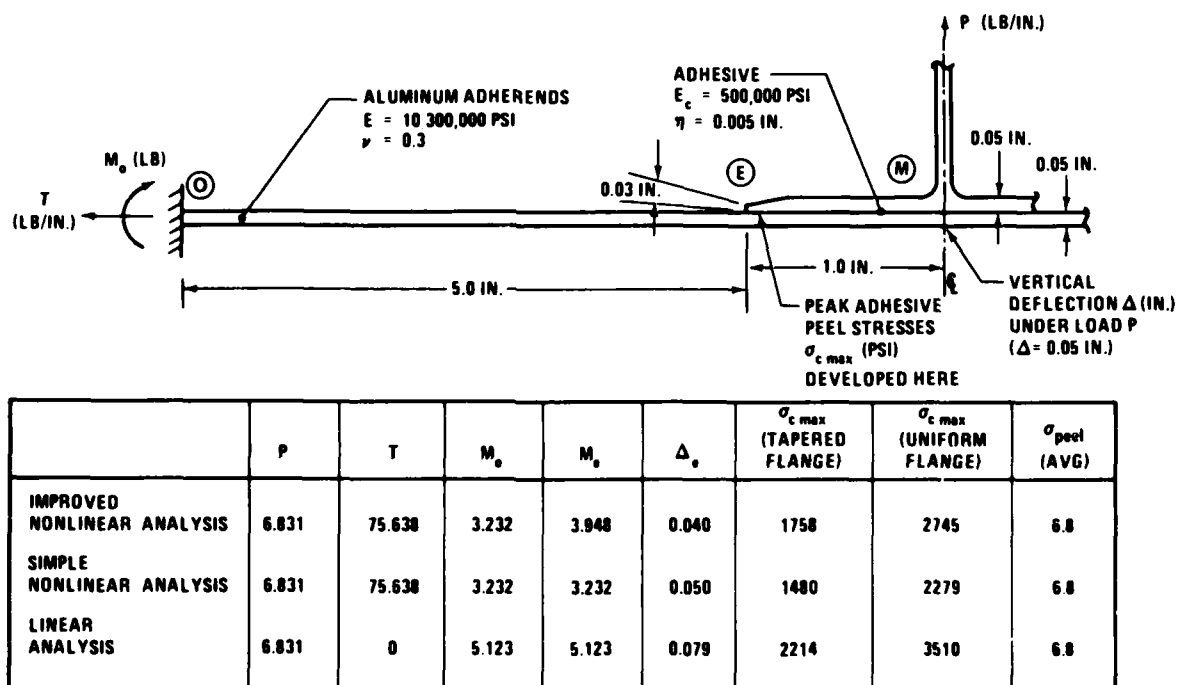|	P	T	M_o	M_e	Δ_e	σ_c max (TAPERED FLANGE)	σ_c max (UNIFORM FLANGE)	σ_peel (AVG)
IMPROVED NONLINEAR ANALYSIS	6.831	75.638	3.232	3.948	0.040	1758	2745	6.8
SIMPLE NONLINEAR ANALYSIS	6.831	75.638	3.232	3.232	0.050	1480	2279	6.8
LINEAR ANALYSIS	6.831	0	5.123	5.123	0.079	2214	3510	6.8

FIGURE 21. SAMPLE SOLUTION FOR ADHESIVE-BONDED TENSION-TEE PROBLEM

PEEL STRESSES IN DOUBLE-LAP AND DOUBLE-STRAP BONDED JOINTS

Because there is no primary eccentricity in load path in double-lap and double-strap bonded joints, it is not always recognized that the shear load transfer through the bond induces adhesive peel stresses as well. That such is indeed the case can be seen from Figure 22. It should be acknowledged that the peel stresses associated with these basically noneccentric joints are much less severe than in the case of the single-lap or single-strap joints analyzed above. Nevertheless, the analysis in Reference 11, which is summarized here, indicates that these peel stresses can be significant for thicker members, particularly for fibrous composite joints which are weaker in interlaminar tension than adhesives are under peel loads.
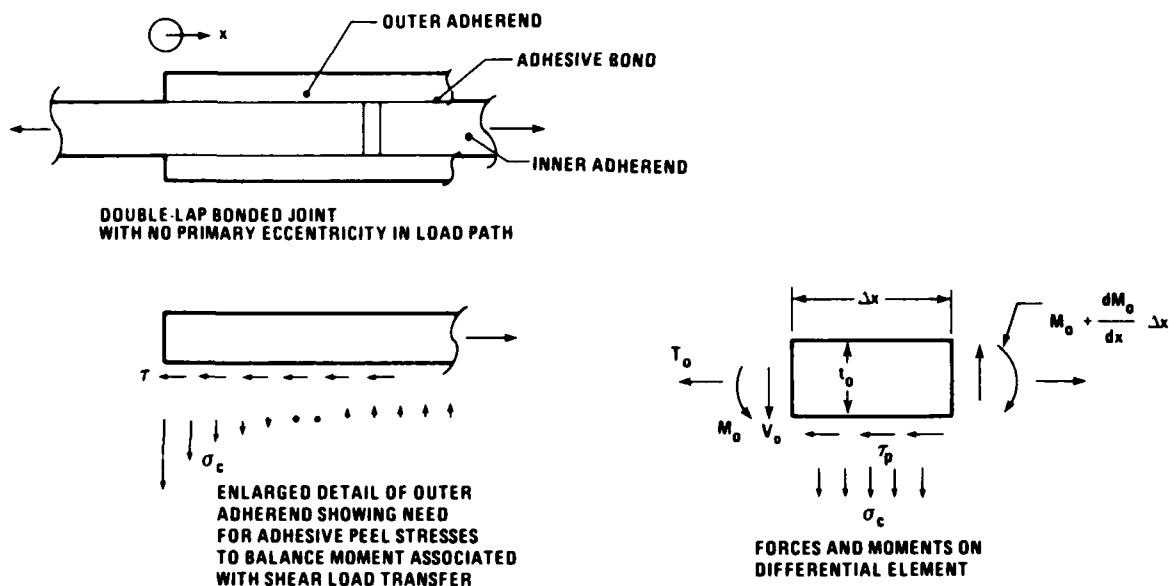
FIGURE 22. INDUCED PEEL STRESSES IN DOUBLE-LAP ADHESIVE-BONDED JOINTS

The geometry and nomenclature for this analysis are illustrated in Figure 22. The extensional stiffness of the inner adherend of the double-lap joint shown need not be twice that of each outer adherend. This peel failure mode is governed essentially by the outer adherend(s) alone, even though the observed failure mode is in the inner adherend for composite structures. The differential equilibrium equations for the element of outer adherend are

$$\frac{dM}{dx} = V \quad \tau_p \frac{t_o}{2} \tag{237}$$

and

$$\frac{dV}{dx} = \sigma_c \tag{238}$$

The characteristic equation of the outer adherend undergoing elastic plate bending is

142

$$\frac{d^2 w_o}{dx^2} = \frac{M}{D_o} \qquad (239)$$

while the assumed elastic peel stress is defined as

$$\frac{\sigma_c}{E_c} = \frac{w_o}{\eta} \qquad (240)$$

In order to proceed with the analysis, it is convenient to assume that the bonded joint is not so weak in peel that it would fail before the adhesive yields in shear throughout the small area at the ends of the joint where significant peel stresses might develop. Such an assumption is reasonable when the objective of the analysis is to identify those designs or detailed improvements which ensure that the induced peel stresses will be small in comparison with the adhesive shear stresses. However, the approximate analysis derived here would not suffice to predict the premature failure of a thick untapered bonded joint in which the adhesive shear stresses remained elastic. In any event, it also would probably be necessary to include allowance for transverse shear deformations of the adherends in any more precise analysis and to account also for the decay of the peel stresses across the thickness. Subject to this assumption, the governing differential equation for the deflection of an outer adherend is

$$\frac{d^4 w_o}{dx^4} - \frac{E_c}{D_o \eta} w_o = 0 \qquad (241)$$

and, introducing the notation

$$\chi^4 = E_c/(4 D_o \eta) \qquad (242)$$

the relevant solution is

$$w_o = e^{-\chi x} [A \cos(\chi x) + B \sin(\chi x)] \qquad (243)$$

It is assumed also that the bonded overlap is not so short as to require the inclusion of the additional terms in Equation (243). Now, since there can be no bending moment at the free edge of the splice or doubler,

$$\frac{d^2 w_o}{dx^2} = 0 \qquad \text{at} \qquad x = 0 \qquad (244)$$

Therefore, in Equation (243),

$$B = 0 \qquad (245)$$

It follows than that

143

$$w_o = Ae^{-\chi x} \cos(\chi x) \tag{246}$$

$$\frac{dw_o}{dx} = A\chi e^{-\chi x} [\cos(\chi x) + \sin(\chi x)] \tag{247}$$

$$\frac{d^2 w_o}{dx^2} = 2A\chi^2 e^{-\chi x} \sin(\chi x) \tag{248}$$

and

$$\frac{d^3 w_o}{dx^3} = 2A\chi^3 e^{-\chi x} [\cos(\chi x) - \sin(\chi x)] \tag{249}$$

The remaining boundary condition follows from Equation (237).

$$\left. \frac{dM_1}{dx} \right|_{x=0} = -D_o \left. \frac{d^3 w_o}{dx^3} \right|_{x=0} = -\tau_p \frac{t_o}{2} \tag{250}$$

Hence

$$A = \frac{\tau_p t_o}{4\chi^3 D_o} \tag{251}$$

and, from Equations (240), (241), and (246),

$$\sigma_c = \frac{\tau_p t_o E_c}{4\chi^3 D_o \eta} e^{-\chi x} \cos(\chi x) = \tau_p \chi e^{-\chi x} \cos(\chi x) \tag{252}$$

so the peak adhesive peel stress is

$$\sigma_{c_{max}} = \tau_p \chi t_o \tag{253}$$

or, in nondimensional form,

$$\frac{\sigma_c}{\tau_p} = \left[\frac{3(1-\nu^2) E_c}{E} \right]^{\frac{1}{4}} \left(\frac{t_o}{\eta} \right)^{\frac{1}{4}} \tag{254}$$

144

Thus the peak induced adhesive peel stress is proportional to the quarter power of the outer adherend thickness. The peak adhesive shear stress, on the other hand, is proportional to the half power of the adherend thickness, as demonstrated in Reference 11. One concludes from this that as joints become thicker (and larger), the relative severity of adhesive peel stresses and shear stresses is altered. This issue is explained in Figure 23 in which it is shown that, for very thin uniform adherends with square-cut ends, the adhesive is not critical in either failure mode because the adherends limit the load which can be applied to the adhesive.
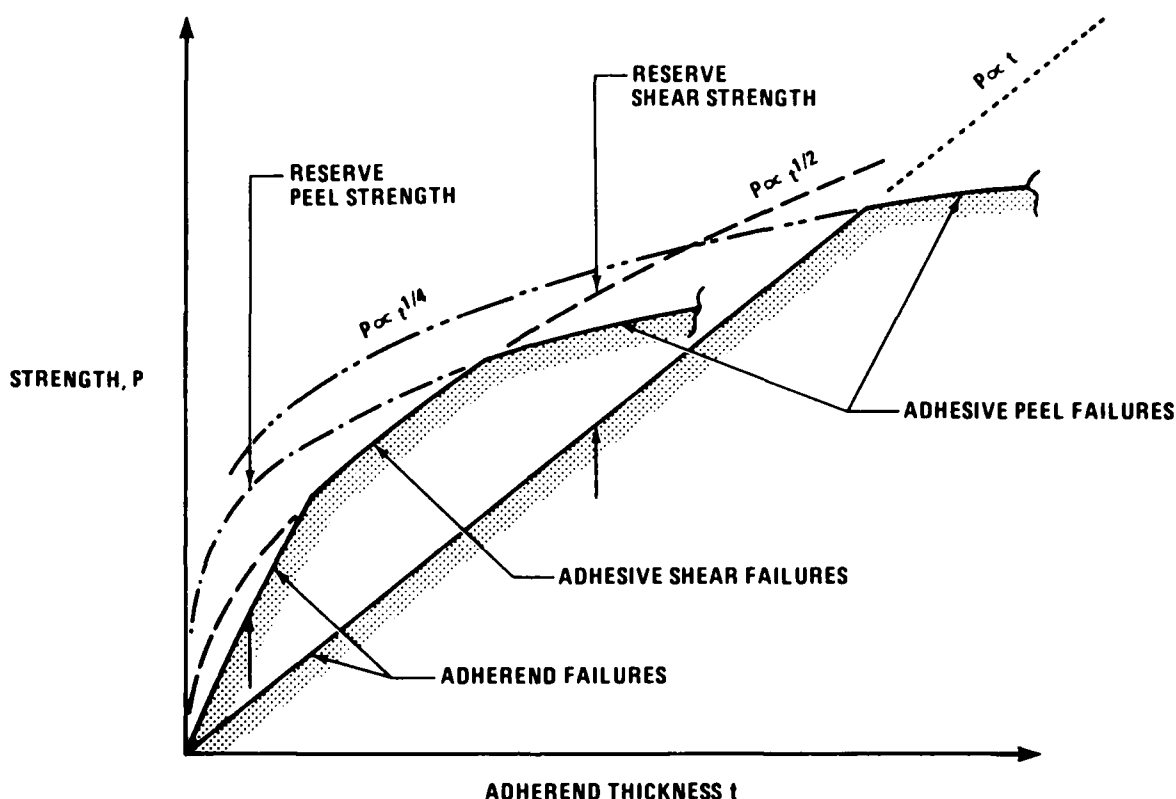

FIGURE 23. RELATIVE SEVERITY OF ADHESIVE SHEAR AND PEEL STRESSES

For these thin adherends, the resistance of the adhesive to peel failure must be greater than its resistance to overloading by shear. For some thick adherends, however, the peel strength falls below the shear strength. Furthermore, neither bond strength increases as fast as the adherend strength. Eventually, beyond some adherend thickness, the failure mode shifts from the adherend to the adhesive. Depending on the various material properties, that first weakness may show up in shear or in peel — the two straight lines in Figure 23 illustrate this point — but ultimately the weakest failure mode will always be in peel stresses for sufficiently thick adherends. This distinction between failure modes is important in intepreting failures of test coupons to deduce material properties since the properties involved are dependent on the failure mode.

If the adhesive peel stresses implied by Equation (252) are integrated along the length of the bond, it will appear that there is a net tensile force pulling the adherends together. This, of course, would violate overall equilibrium. The explanation is as follows. The plastic adhesive

145

shear stress τ_p does not extend indefinitely throughout the adhesive, but is limited by the total applied load to some length $\ell = P/(2\tau_p)$. The integral of the peel stresses throughout that zone ℓ then provides the boundary condition, on the transverse shear force V, for the remaining bond area throughout which τ is zero and there is a small net compressive normal bond stress. The peak peel stress is thus limited by the plastic adhesive shear stress τ_p beyond those loads sufficient to strain the adhesive that much. For lower loads, not analyzed here, the peak peel stress would be a function of the applied load P. For the higher loads analyzed here, the load P influences only the interior distribution of the adhesive peel stresses and not their peak value.

146

DESIGN TECHNIQUES FOR ALLEVIATING INDUCED ADHESIVE PEEL STRESSES

The analyses described earlier for induced peel stresses contain two common threads. Thin ends on the adherends increase the local flexibility in bending so there is less resistance, therefore less cause for peel stresses to develop. The recommended design for the tips of aluminum alloy adherends is tapered ends down to a thickness of 0.030 ± 0.010 inch with a slope of 1 in 10, as shown in Figure 24. Simultaneous thickening of the adhesive layer is also beneficial, but care must be exercised to avoid having the adhesive flow out of the thickened area. In any joint having a direct eccentricity in load path, it is vital to use a large ℓ/t ratio and allow gentle deflections to minimize the peel stresses in the adhesive and the bending moments in the adherends. The associated bonded overlaps are typically far greater than would be needed for shear transfer alone. There still are benefits to be obtained from ℓ/t ratios in excess of 100, despite the apparently heavy joint detail. The entire skin panel can be lighter if the joint is more efficient. There are also opportunities for design finesse to minimize the eccentricities or to relocate the discontinuities, and some of these have been illustrated in the body of this report.

There are practical limits to the ℓ/t ratios of the flanges of extruded stiffeners. Consequently, despite the desire to maximize those ratios to minimize the peel stresses, the overall design process is one of compromise. The factors involved in the proportioning of adhesively bonded stiffeners are described in Figure 25. Specific sizes can be obtained from various reports published about the PABST program.
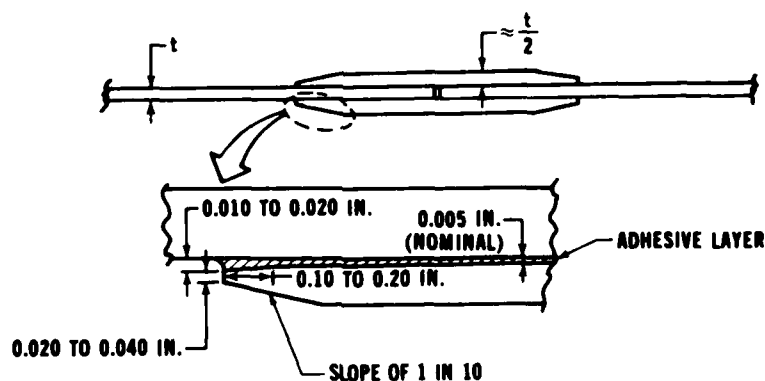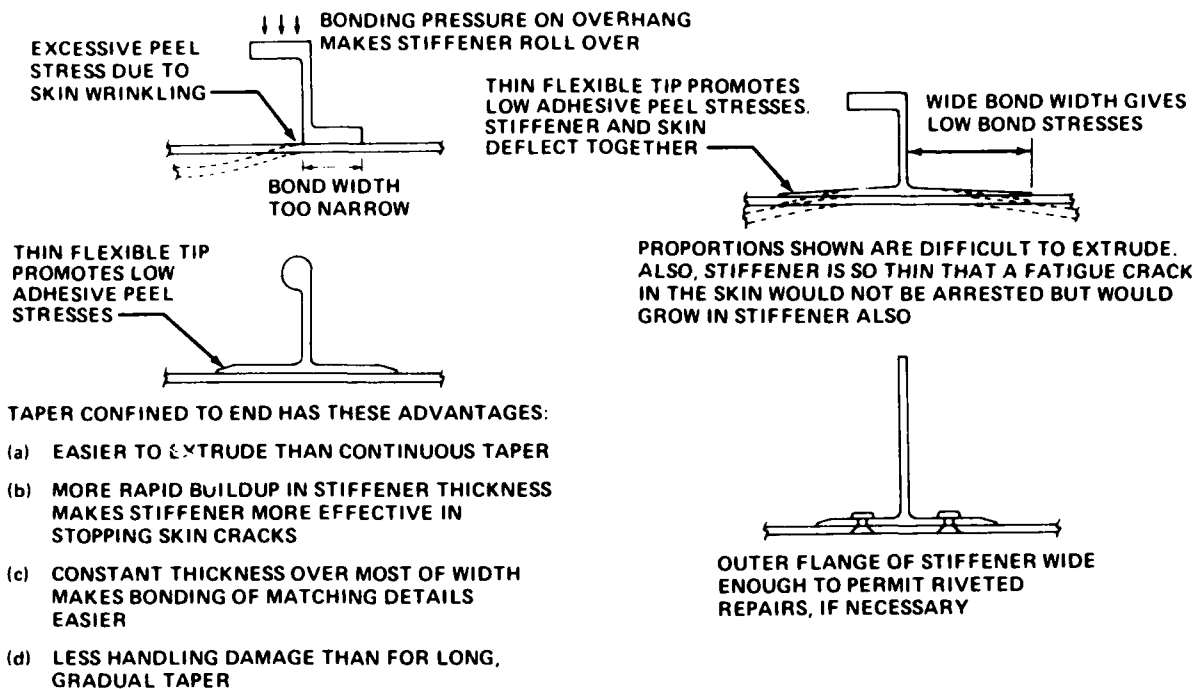
FIGURE 24. TAPERING OF EDGES OF SPLICE PLATES TO RELIEVE ADHESIVE PEEL STRESSES

BONDING PRESSURE ON OVERHANG
MAKES STIFFENER ROLL OVER

EXCESSIVE PEEL
STRESS DUE TO
SKIN WRINKLING

THIN FLEXIBLE TIP PROMOTES
LOW ADHESIVE PEEL STRESSES.
STIFFENER AND SKIN
DEFLECT TOGETHER

WIDE BOND WIDTH GIVES
LOW BOND STRESSES

BOND WIDTH
TOO NARROW

THIN FLEXIBLE TIP
PROMOTES LOW
ADHESIVE PEEL
STRESSES

PROPORTIONS SHOWN ARE DIFFICULT TO EXTRUDE.
ALSO, STIFFENER IS SO THIN THAT A FATIGUE CRACK
IN THE SKIN WOULD NOT BE ARRESTED BUT WOULD
GROW IN STIFFENER ALSO

TAPER CONFINED TO END HAS THESE ADVANTAGES:

(a) EASIER TO EXTRUDE THAN CONTINUOUS TAPER

(b) MORE RAPID BUILDUP IN STIFFENER THICKNESS
    MAKES STIFFENER MORE EFFECTIVE IN
    STOPPING SKIN CRACKS

(c) CONSTANT THICKNESS OVER MOST OF WIDTH
    MAKES BONDING OF MATCHING DETAILS
    EASIER

OUTER FLANGE OF STIFFENER WIDE
ENOUGH TO PERMIT RIVETED
REPAIRS, IF NECESSARY

(d) LESS HANDLING DAMAGE THAN FOR LONG,
    GRADUAL TAPER

A FURTHER CONSIDERATION FOR DAMAGE TOLERANCE WITH RESPECT TO CRACKS IN SKIN
OR STIFFENERS IS THAT THE STIFFENER BOND WIDTH MUST BE LARGE ENOUGH, IN
COMPARISON WITH STIFFENER AREA AND SPACING, TO PREVENT UNZIPPING OF THE
BONDS. THE ADHESIVE MUST NEVER BE THE WEAK LINK.

FIGURE 25. CONSIDERATIONS IN THE PROPORTIONING OF BONDED STRUCTURES

148

EXPERIMENTAL INVESTIGATION

Testing the growth of flaws and defects in adhesive-bonded joints during the contract work reported in Reference 1 showed that for typical aircraft bonded structures flaw growth would not occur unless there was a substantial peel stress in the adhesive as well as the applied shear load. Likewise, disbonds could not be made to initiate under cold, or hot and wet environments in the absence of such a stress component. Given that history of testing, which showed no reason for concern about double-lap joints or long-overlap single-lap joints, it was appropriate to assess experimentally the benefits of tapering the ends of the adherends in single-strap joints as part of this investigation. The specimen used is illustrated in Figure 26, which also shows how this specimen bends under the applied axial load.

The design of this specimen is very much a compromise. There is 100-percent load transfer through the adhesive bond because of the need to generate sufficient eccentricity to induce the peel stresses. The overall length is limited by the environmental test chamber — a longer overlap would have permitted more prolonged study of any disbond growth, but the overlap used was sufficient to prevent instantaneous failure following crack initiation. The load is limited by the test fixture and the adherend thickness had to be somewhat representative of aircraft construction yet thick enough to ensure that any failure of the adhesive would not be precluded by premature fatigue failure of the metal adherends. The coupon testing conducted as part of the PABST program showed that the results can be misleading if the testing were done on inappropriate specimens. Indeed, great care must be exercised in interpreting test results on any bonded joint that is not a one-for-one replica of some structural joint loaded with real loads under real-time testing in the real environment. Considerable judgement is still needed for adhesive-
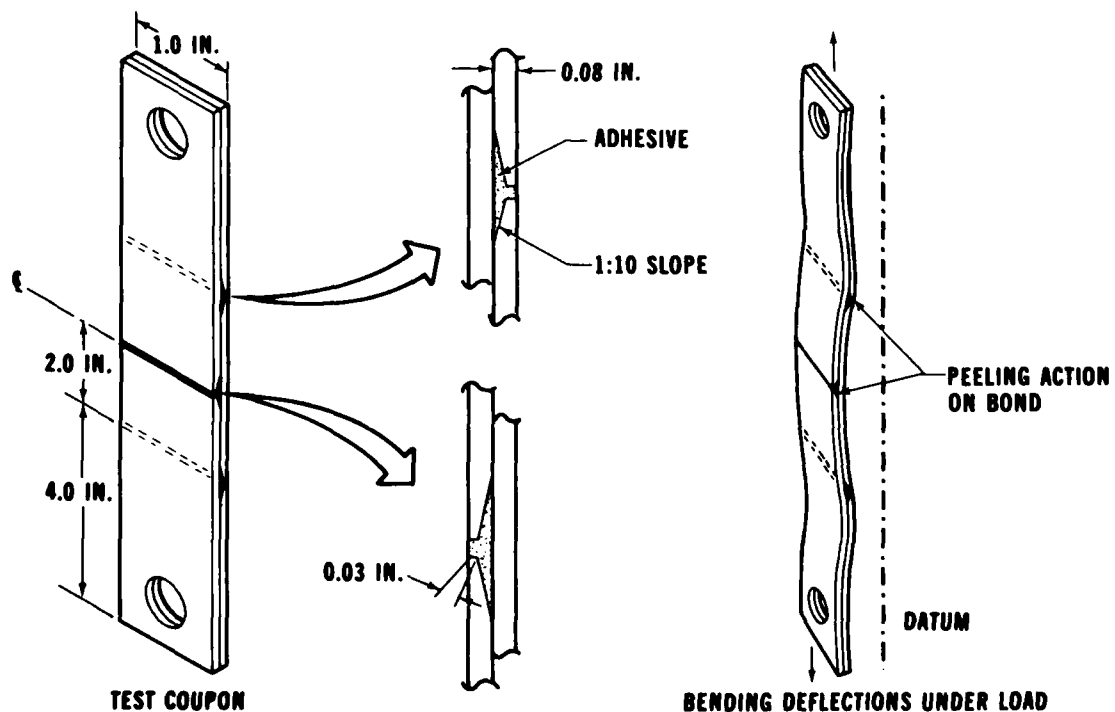

FIGURE 26. FLUSH BONDED JOINT WITH TAPERED ADHERENDS TO REDUCE ADHESIVE PEEL STRESSES

149

bonded joint testing because of the grossly dissimilar behavior of the adhesive in most test coupons as contrasted with real structure. This point is clarified in Reference 12.

Slow cycle tests were run in environments of severe cold (−65°F) and extreme heat and humidity (140°F, 100% relative humidity). The reason for the long load cycles is that testing during the PABST program had repeatedly shown that high-frequency (30-Hz) testing of adhesive bonds led to misleading results because the adhesive would never fail since the load was always being *removed before the adhesive had time to creep.*

The results of this test program are summarized below, specimen by specimen. It is significant that no failures have occurred with the tapered specimens in the cold environment in which the adhesive is brittle and most likely to fail. The specimens for which the PABST surface treatment had inadvertently not been used failed prematurely under the hot and wet environment − in adhesion at the bond-to-adherend interface followed by surface corrosion − but showed no signs of degradation when tested in the sub-zero environment. Some of the early specimens with tapered adherends were made without additional adhesive to fill the gap. The resultant porosity did not weaken the joint because the adhesive was inevitably of high quality in the adjacent thin bond where the peak peel stresses would be developed. However, the exposed porosity would have caused failure of those bonds in service due to the freeze/thaw cycle. At the time this report was prepared, the tapered bonded specimen being cycled in the hot/wet environment had no cracks in the adhesive but the band of adhesive between the skin segments was visibly milky.

All Specimens Loaded by 1,500 Pounds on 1-inch Width Corresponding to a Nominal Aluminum Stress of 19,000 PSI.

Cold Tests, Tapered Edges, FM-73 Adhesive, BR-127 Primer, FPL Etch:

- Temperature −65°F, 4 Cycles per Hour
- Two Specimens, No Failures at 6,620 and 6,561 Cycles

Hot/Wet Tests, Tapered Edges, FM-73 Adhesive, BR-127 Primer, FPL Etch

- Temperature 140°F, Relative Humidity 95%, 2 Cycles per Hour
- Four Specimens, All Failed at Primer-to-Metal Interface After 4,172, 4,272, 4,437, and 6,524 cycles

Hot/Wet Tests, Square-cut Edges, FM-731 Adhesive, BR-127 Primer, Phosphoric Acid Anodize

- Temperature 140°F, Relative Humidity 95%, 2 Cycles per Hour
- Two Specimens, Both Failed Cohesively in Adhesive After 1,747 and 1,257 Cycles

Hot/Wet Tests, Tapered Edges, FM-73 Adhesive, BR-127 Primer, Phosphoric Acid Anodize

- Temperature 140°F, Relative Humidity 95%
- One Specimen Loaded at 2 Cycles per Hour With No Failure After 2,732 Cycles (Test Continuing)
- One Specimen Under Sustained Load With Visible Cohesive Crack Initiation at 2,000 Cycles, Crack Grown 3/8 Inch While Still Sustaining Full Load After 2,914 Hours (Test Continuing)

150

Hot/Wet Tests, Tapered Edges, FM-400 Adhesive, BR-400 Primer, FPL Etch

• Three Specimens, All Failed at the Primer-to-Metal Interface After 3, 5, and 235 Cycles

While complete conclusions must await the accumulation of more test cycles data, certain facts are already evident. The testing has borne out the analytical prediction that tapering would reduce the adhesive peel stresses. While a one-to-one comparison with the half-inch overlap single-shear RAAB specimens tested as part of the PABST program is not possible, it should be noted that the aluminum stress is much higher in the present tests while the number of cycles, either to failure or without failure, has been much greater. This can be deduced from the test results on Page 273 of Reference 8. Comparisons on the basis of average adhesive shear stress are not meaningful. While the incidence of failures with flush joints has been reduced from that of the earlier tests (Reference 1), the failure here under sustained load serves as a reminder that peel stresses in adhesives are to be avoided if long structural lives are to be attained. The results of these tests have confirmed again the improvements associated with replacing the FPL etch surface preparation for bonding by phosphoric acid anodize.

CONCLUSIONS

The analyses of the peel stresses induced in adhesive-bonded joints has shown that:

1. The peel stresses are very severe in the short-overlaps used in test coupons designed specifically to force a failure in the adhesive.

2. The peel stresses associated with properly proportioned structural bonded joints are far less severe because of the much longer overlaps which permit the eccentricities in load path to be alleviated by gentle deflections under load.

3. The peel stresses can be reduced to insignificance by thinning the ends of the adherends or by local thickening of the adhesive layer. This is confirmed by test results on single-strap joints.

The analyses have confirmed the greater severity of the induced peel stresses in the single-strap (flush) joints than in the single-lap joints, as found by tests in an earlier investigation.

Whereas the peel stresses can be significant or even greater than the shear stresses in bonded test coupons, there should be no significant peel stresses in structural joints. Therefore, there is no need to account for peel stresses in the analysis of structural joints loaded primarily by shear. If they need to be accounted for, they imply a deficiency in the design and an easily corrected weakness in either static strength or fatigue life.

REFERENCES

1. Clark, H. T., Definition and Non-Destructive Detection of Critical Adhesive Bond-Line Flaws, USAF Technical Report AFML-TR-78-108, July 1978.

2. Goland, M. and Reissner, E., The Stresses in Cemented Joints, J. Appl. Mech. 11, A17-A27 (1944).

3. Hart-Smith, L. J., Adhesive-Bonded Single-Lap Joints, NASA CR 112236, January 1973.

4. Hart-Smith, L. J., Effects of Adhesive Layer Edge Thickness on Strength of Adhesive-Bonded Joints, Douglas Aircraft Company, McDonnell Douglas Corporation, Report MDC-J4675, May 1981.

5. Hart-Smith, L. J., Design and Analysis of Bonded Repairs for Metal Aircraft Structures, Douglas Aircraft Company, McDonnell Douglas Corporation Paper DP 7089 presented to International Workshop on Defense Applications of Advanced Repair Technology for Metal and Composite Structures, Naval Research Laboratory, Washington, D. C., July 1981.

6. Hart-Smith, L. J., Pressure-Induced Stresses in Axially-Loaded Frame-and Longeron-Stiffened Circular Cylindrical Shells, Douglas Aircraft Company, McDonnell Douglas Corporation, Report MDC-J6079, to be published.

7. Hart-Smith, L. J., Deflections of Flat Plates and Beams under Lateral Pressure and Simultaneous In-Plane Loading, Douglas Aircraft Company, McDonnell Douglas Corporation, Report MDC-J8729, to be published.

8. Thrall, E. W. Jr. et al, Primary Adhesively Bonded Structure Technology, Phase Ib: Preliminary Design Report, (Douglas Aircraft Company Report MDC-J6070), Air Force Flight Dynamics Laboratory Technical Report No. AFFDL-TR-76-141, pp. 159-160, December 1986.

9. Timoshenko, S. P. and Woinowski-Krieger, S., Theory of Plates and Shell, McGraw Hill, New York, 2nd edition, pp. 24-27, 1959.

10. Hart-Smith, L. J., Structural Details of Adhesive -Bonded Joints for Pressurized Aircraft Fuselages, Douglas Aircraft Company, McDonnell Douglas Corporation, Report MDC-J8858, December 1980.

11. Hart-Smith, L. J., Adhesive-Bonded Dougle-Lap Joints, NASA CR 112235, January 1973.

12. Hart-Smith, L. J., Differences Between Adhesive Behavior in Test Coupons and Structural Joints, Douglas Aircraft Company, McDonnell Douglas Corporation, Paper DP 7066, presented to American Society for Testing and Materials, Adhesives Committee D-14 Meeting, Phoenix, Arizona, March 1981.

SECTION 5

CONCLUDING REMARKS

Most prior analyses of the load transfer through adhesive-bonded joints have considered the adhesive layer to be of uniform thickness and of uniform properties throughout. This report has been prepared because it is recognized that real structural joints frequently lack that uniformity. The concern here has been with two specific variations — layer thickness and porosity (as a special case of flaws) — which cause a redistribution of the load transfer with respect to nominally perfect bonds. There are other sources of nonuniformity in the adhesive layer besides those discussed here. For example, the load transfer and peak adhesive strains in the adhesive are affected by a nonuniform moisture level within the adhesive — the extremities of the bond may be drying out with respect to the interior, or vice versa, depending on the differences between current and previous environments. This effect has been discussed elsewhere, relying on the same analysis program A4EI used here.

One might expect that real structural bonded joints would exhibit the same sensitivity to these various imperfections that can be demonstrated on short-overlap test coupons. However, the analyses reported here and elsewhere have shown that structurally configured joints behave in a manner that is almost independent of the apparent behavior of standard test coupons. It is important to select test coupons which can generate data needed to characterize the adhesive in structurally-configured joints, while recognizing that the effects of any variable will inevitably be different. The adhesive in the test coupon should be under as uniform a state of stress and strain as possible, while the adhesive in a structural joint is not (and should not be) uniformly strained. That nonuniformity is the key to long-life durable bonded structures and provides alternative areas through which the load can be transferred — sometimes with no loss of joint strength!

The load transfer in real structural joints is actually effected through a small fraction of the total bond area, leaving the remainder inevitably lightly loaded to resist failure by creep rupture. Some of the analyses performed here have shown how to take advantage of that characteristic to simplify the problem. Whenever the critical location in the adhesive can be identified a priori — and that is usually very easy because it is almost always at one or both ends of the overlap — the adhesive can be modeled as being uniform throughout and having the thickness and properties of the critical location. In several such cases, explicit closed-form solutions were obtained which agreed well with the more precise analyses. Obviously, a coarse approximation of the load transfer in an area of the joint which does not transfer a significant load anyway will not invalidate the accuracy of the overall assessment. However, it is appropriate to add the reminder that gross variations in adhesive layer thickness and disproportionately large flaws were each able to move the critical location elsewhere, invalidating the simplified approach. In the case of pinch-off, at the ends of the overlap, both the peak shear and peel stresses could be predicted accurately by this simplified approach. Both stresses were aggravated in such a case, pointing to the need for improved manufacturing methods to eliminate the problem. Alternatively, the analysis of the pinch-off points to the desirability of design modifications, such as the locally tapered ends of the adherends, which were tested here and demonstrated substantial improvements in fatigue life with respect to unmodified joints having inherently higher peel stresses in the adhesive.

The analyses of the effects of flaws and porosity which are reported here indicate a deficiency in the assessment of such flaws in practice. The problem is that many of the bond flaws which can be detected by nondestructive inspection are better left unrepaired — the repair often decreases the remaining life of the structure by breaking the surface protection on the metal adherends. Furthermore, the repair is usually incapable of adding to the joint strength because most natural flaws tend to occur in the interior of bonded joints where no load can be transferred anyway.

Voids or porosity at the edges of the overlap (where most of the load is transferred) are rare — the problem there is pinch-off, which is difficult to detect by nondestructive inspection. The key to understanding the effect of flaws in bonded joints is that, unless they cause a shift in the location of the critical condition within the adhesive layer, the flaws are incapable of changing the joint strength significantly. And, if a flaw merely shifts some critical condition to an adjacent previously lightly-loaded area, without changing the intensity of that condition, the joint strength will not be changed by that flaw either.

The discussion above implies that there will always be some lightly-loaded areas within the adhesive which can accept a certain amount of loaded redistribution. Obviously this would not be the case for some foolish design in which the adhesive had been allowed to become the weak link in the structure. While mechanical fasteners can be obtained in all sizes and strengths from 1/16th-inch soft aluminum rivets to heat-treated steel bolts several inches in diameter, good adhesive bonds are difficult to produce outside the thickness range of 0.005 to 0.010 inch. Furthermore, the variation in adhesive mechanical properties is small and becomes even less when it is recognized that the properties are almost identical at the (different) upper temperature limit for which each adhesive is used. The implication of all this is that most simple adhesive-bonded joints are limited to thin and moderately thick structures, as in large transport aircraft control surfaces, fairings, fuselage primary structure and all empennage structure. Also, bonded wings have been shown to be superior for small aircraft. However, adhesive bonding in thick, highly-loaded, primary wing box structure for large aircraft requires the use of laminated structure and the more complex stepped-lap joints. Such thick bonded structures have distinct advantages over conventional riveted or integrally-stiffened structures in regard to the initiation and retardation of fatigue cracks. However, it is very difficult to provide comparable residual strengths after relatively large damage, without relying on mechanical attachments (which would transmit no load until the bonded structure had been damaged). The bonding of thick structures should be considered largely beyond the scope of this report.

The best use that can be made of the information in this report is not the characterization of the effects of some tolerable level of imperfections in the context of a reduction in strength or life. Rather it should be used to improve designs and manufacturing or tooling techniques to reduce the in-service maintenance costs of adhesively-bonded structure. It costs no more to bond a structure properly than poorly — and it certainly costs much less to inspect flawless structures. On the other hand, if there are some flaws in the first few bonded panels made in a production run, the contents of this report can be invaluable in preventing any further damage to those structures as the result of unnecessary repairs to at least many of the flaws, even if not to all. A further function of analyses of the type reported here is illustrated by the improved joint designs which were generated to overcome the inherently high peel stresses in standard single-strap (flush) bonded joints.